IDENTIFICATION
OF
WASTEWATER PROCESSES

Jacob Carstensen

LYNGBY 1996
Ph.D. THESIS
NO. 73

ISSN 0107–525X

Jacob Carstensen
IMSOR & I.Krüger Systems AS

Printed by IMSOR, Technical University of Denmark

Some of the work in this thesis has previously been published in:

Carstensen, J., Madsen, H., Poulsen, N.K. & Nielsen, M.K. (1994). Identification of Wastewater Treatment Processes for Nutrient Removal on a Full-scale WWTP by Statistical Methods. *Water Research, 28(10)*, 2055-2066.

Carstensen, J., Madsen, H., Poulsen, N.K. & Nielsen, M.K. (1993). Grey Box Modelling in two Time Domains of a Wastewater Pilot Scale Plant. *Environmetrics, 4(2)*, 187-208.

Carstensen, J., Madsen, H., Poulsen, N.K. & Nielsen, M.K. (1992). *Identification of Wastewater Processes using Non-linear Grey Box Models*. Institute of Mathematical Statistics and Operations Research, Technical University of Denmark.

Carstensen, J. (1992). *Wastewater Processes - Controlling a Sewage Treatment Plant*. Institute of Mathematical Statistics and Operations Research, Technical University of Denmark.

Preface

The present thesis has been prepared at the Institute of Mathematical Statistics and Operations Research (IMSOR), Technical University of Denmark and I. Krüger Systems AS, in partial fulfillment of the requirements for the degree of Ph.D. in engineering.

The thesis is concerned with the modelling of wastewater processes with the objective of using the models for control of wastewater treatment plant with nutrient removal. The general framework of the thesis is applied time series analysis and wastewater treatment. Prior knowledge of these areas will be beneficial to the understanding of the thesis, but not crucial.

The treatment of the subjects is by no means exhaustive, but it is intended to show the aspects of time series analysis applied to wastewater treatment technology.

This version of the thesis is for the World Wide Web and includes some minor corrections of the published version.

Lyngby, January 1994

Jacob Carstensen

Acknowledgements

The author would like to thank the supervisors, Assoc. Prof., Ph.D. Henrik Madsen (IMSOR), Assoc. Prof., Ph.D. Niels Kjølstad Poulsen (IMSOR), and Senior Engineer, Ph.D. Marinus K. Nielsen (I. Krüger Systems AS), for guidance and encouragement during the course of this work. Their constructive criticism and lasting enthusiasm have been a great help for me.

I wish to thank my colleagues of the time series analysis group at IMSOR, Ken Sejling, Henning T. Søgaard, Ólafur P. Pálsson, and Henrik Melgaard for inspiring discussions and social environment. Programming routines of Henrik Madsen and Henrik Melgaard have been greatly appreciated in this research project. Furthermore, for the last two and a half years I have shared my office at IMSOR with many students. These students are acknowledged for their broadening of my views on many different issues during coffee-breaks.

I also wish to thank my colleagues of the 'Styring & proces'-group of the Research and Development Department at I. Krüger Systems AS, Dines E. Thornberg, Jan Pedersen, Tine B. Önnerth, Henrik A. Thomsen, Kenneth Kisbye, and Henrik Bechmann, who have helped me with the data acquisition and interpretation of the results. I am grateful to their remembrance of my existence for social activities during the periods of work at IMSOR.

Dr.Ing. Steven H. Isaacs, Department of Chemical Engineering, Technical University of Denmark, is acknowledged for his help in providing data from the Lundtofte pilot scale plant and answering questions regarding the pilot plant.

Finally, I am indebted to my brother, Ph.D. Jens Michael Carstensen, for reading proofs of the manuscript and helping me with UNIX- and LaTeX-related problems, and my fiancée Lotte Kristiansen, for her patience and support in my preparations of the present thesis.

This research was sponsored by the The Danish Academy for Technical Sciences (In Danish: ATV) and I. Krüger Systems AS. I would like to express my gratitude for this support.

Summary

The introduction of on-line sensors for monitoring of nutrient salts concentrations on wastewater treatment plants with nutrient removal, opens a wide new area of modelling wastewater processes. The subject of this thesis is the formulation of operational dynamic models based on time series of ammonia, nitrate, and phosphate concentrations, which are measured in the aeration tanks of the biological nutrient removal system. The alternating operation modes of the BIO-DENITRO and BIO-DENIPHO processes are of particular interest. Time series models of the hydraulic and biological processes are very useful for gaining insight in real time operation of wastewater treatment systems with variable influent flows and pollution loads, and for the design of plant operation control.

In the present context non-linear structural time series models are proposed, which are identified by combining the well-known theory of the processes with the significant effects found in data. These models are called grey box models, and they contain rate expressions for the processes of influent load of nutrients, transport of nutrients between the aeration tanks, hydrolysis and growth of biomass, nitrification, denitrification, biological phosphate uptake in biomass, and stripping of phosphate. Several of the rate expressions for the biological processes are formulated on the assumption of Monod-kinetics. The formulation of models for time-varying parameters in a new time domain divides the variations of the processes into fast dynamics and slower dynamics. In addition, this modelling in two

time domains increases the interpretability of the parameters. The models are put into state space form and the parameters are estimated by the maximum likelihood method, where a Kalman filter is used in calculating the likelihood function.

The grey box models are estimated on data sets from the Lundtofte pilot scale plant and the Aalborg West wastewater treatment plant. Estimation of Monod-kinetic expressions is made possible through the application of large data sets. Parameter estimates from the two plants show a reasonable consistency with suggested kinetic parameter values of the literature. A large amount of information about the two plants and their performances is obtained from the models, of which the variations of the influent ammonia load, and the autotrophic and heterotrophic biomass activity have particular interest. The models are appropriate for control, because the present states of the plants are reflected in the parameter estimates.

The grey box models may be applied to control of wastewater treatment plants in many ways. In this thesis off-line simulations of control strategies and on-line model-based predictive control are discussed. Both methods include the evaluation of a cost function incorporating the cost of operation and discharge of nutrients to the recipient. The concept of prediction based control is demonstrated in a simulation study.

Resumé

Med indførslen af on-line sensorer til overvågning af næringssalts koncentrationer på rensningsanlæg med næringssalts-fjernelse er et helt nyt område indenfor modellering af spildevands-processer blevet åbnet. Nærværende afhandling omhandler formuleringen af operationelle dynamiske modeller baseret på tidsrækker af ammoniak-, nitrat- og fosfat-koncentrationer målt i luftningstankene i den biologiske del af et rensningsanlæg. Den alternerende drift af BIO-DENITRO og BIO-DENIPHO processerne har speciel interesse. Tidsrækkemodeller, som beskriver de hydrauliske og biologiske processer, er meget anvendelige til at opnå indsigt i real-tids styring af systemer til spildevandsrensning med varierende strømningshastigheder og stofbelastninger, og som fundament for udviklingen af forbedred styringsmetoder.

I denne sammenhæng foreslås ikke-lineære strukturelle tidsrækkemodeller, som identificeres ved at kombinere den kendte teori fra processerne med de væsentlige effekter, som kan findes i data. Disse modeller kaldes grey box-modeller, og de indeholder hastighedsudtryk for følgende processer: belastning af næringssalte, stoftransport mellem luftningstanke, hydrolyse and biomasse-vækst, nitrifikation, denitrifikation, biologisk fosfat-optagelse og fosfat-stripning. Flere af de anvendte hastighedsudtryk for de biologiske processer er formuleret på basis af Monod-kinetikken. Ved formulering af modeller for tids-varierende parametre i et nyt tids-domæne opdeles procesvariationerne i hurtig og langsom dynamik. Denne formulering i to tidsdomæner giver en forbedret fortolkning af parametrene. Modellerne bringes

på en tilstandsform, hvor parametrene estimeres ved hjælp af maximum likelihood metoden, idet et Kalman filter bruges til at beregne likelihood funktionen.

Grey box-modellerne er estimeret på datasæt fra pilotanlægget i Lundtofte og Ålborg Vest renseanlæg. Ved anvendelse af store datasæt er en estimation af Monod-kinetiske udtryk mulig. Parameter estimaterne fra de to anlæg viser en rimelig overensstemmelse med anvendte kinetiske parameter værdier fra litteraturen. En stor mængde information om de to anlæg er udtrykt i parametrene fra modellerne, hvoraf variationerne i ammoniakbelastningen og den autotrofe og heterotrofe biomasse aktivitet er speciel interessant. Modellerne er egnede til styring, fordi anlæggets nuværende tilstand er afspejlet i parameter estimaterne.

Grey box-modellerne kan umiddelbart anvendes som fundament for en forbedret styring. I nærværende afhandling foreslås: off-line simuleringer af styringsstrategier og on-line model-baseret prædiktiv styring. Begge metoder indeholder en vurdering af en kriterie-funktion, som bygger på omkostningerne ved driften og udledning af næringssalte til recipienten. Fremgangsmåden ved prediktionsbaseret styring er vist vha. simuleringer.

Contents

Chapter 1

Introduction

The discharge of wastewater from urbanized areas has a major impact on the receiving body of water. Insufficient wastewater treatment potentially devastate the ecological balance of nature, and environmental and health problems associated with eutrophic conditions in receiving waters requires greater removals in many areas. Thus, removal of organic matter and nutrients (mainly nitrogen and phosphorus) from the wastewater is an important cause for the society of today.

Historically, wastewater treatment requirements were determined by the need to maintain the oxygen content of the receiving water, and this was accomplished primarily through the removal of settle-able solids and dissolved organic materials from the wastewater before discharge. However, discharge of nutrients stimulate growth of algae and other photo-synthetic aquatic life, which lead to accelerated eutrophication, excessive loss of oxygen resources, and undesirable changes in aquatic populations. Biological nutrient removal systems are relative new technologies with the potential of high quality effluents. Furthermore, they have shown to be the most operation cost-effective systems at present time.

In the last decade reliable on-line sensors for monitoring of nutrient salt concentrations (ammonia, nitrate, and phosphate) on activated sludge wastewater treatment plants (WWTP) have been developed. Though, the main objective of these sensors so far has been surveillance of plant performance and alarm handling, the use of these sensors for on-line control of operations of WWTP's has a large potential and still needs to be investigated.

Many WWTP's are presently operated according to predetermined schemes with very little considerations to the variations of the material loads. Using on-line sensors in on-line control of the operation of the plants may enhance the ability to comply with the assigned effluent standards. In general, a better understanding of the dynamic behaviour of the WWTP's and an on-line identification of loads with the use of control systems have significant potential for solving operational problems as well as reducing operational costs. In addition, this knowledge may be used to reduce volume holdings in the design of the plants to be constructed in the future.

The understanding of the dynamic behaviour of a WWTP is often described in the form of a model. However, the dynamics of a WWTP can be expressed in a multitude of ways, and the objective of a given type of model should agree with the employment of the model (i.e. some models are developed to yield a very detailed understanding of the processes, while other models are developed to be operational). The purpose of this thesis is to develop operational models based on the information obtained from on-line sensors with the objective of controlling the plant operation. The most important physical and biochemical laws of the WWTP are sought captured in the formulation of the models.

1.1 State of the art

For modelling of wastewater processes, most effort in the last decade has been placed in detailed and complex deterministic models. Especially the IAWPRC (International Association on Water Pollution, Research, and Control) Activated Sludge Model No.1 (Henze et al. (1987)) has gained

much attention. The model expresses a very detailed theoretically relation of all the processes in activated sludge using Monod-kinetic expressions. However, the model contains a huge number of parameters which implies that an identification of all the parameters by statistical methods is very difficult or in fact impossible, and that the model is unsuitable for an on-line control.

Great emphasis has also been placed in modelling reduced-order forms of the IAWPRC model, for instance models for the process of aerobic degradation of organic materials have been published frequently. Kabouris & Georgakakos (1991) suggest using a deterministic model with stochastic input for optimal control. The control method minimizes the expected deviations of effluent substrate from its steady-state values. In Parkum (1992) a non-linear adaptive controller for the nitrification process is considered.

Some authors have proposed more inductive methods for the modelling of wastewater processes. These are developed from input and output monitoring data series. Hiraoka et al. (1990) have used a multivariate autoregressive model with exogenous input and a PI-controller to suppress fluctuations in treated wastewater quality. Novotny et al. (1991) suggest using time series ARMA (AutoRegressive Moving Average)-models to processes, that are mathematically linear or can be linearized and neural network models for highly non-linear processes. It is furthermore recommended that the ARMA- and neural network-models are self-learning, i.e. the performance can be periodically improved as new information is collected by monitoring. In Capodaglio et al. (1992) ARMA- and transfer function-models are shown to have a better performance than simplified deterministic models for characterization of the activated sludge process. ARMAX-models (ARMA with eXogenous input) with an on-line estimation of the parameters using a Kalman filter or a recursive parameter estimation method are proposed by Olsson et al. (1989). Some parameter variations are assumed to be considerable slower than the process variable rate of change.

Applications of neural network models to wastewater processes including nutrient removal have been employed by Bhat & McAvoy (1990). Comparing feed-forward networks with recurrent networks they found, that recurrent networks are more appropriate for the application of model predictive control. Enbutsu et al. (1993) suggest using neural networks on on-line data to provide operation guidance for a fuzzy logic system, which incorporates operators' heuristic as fuzzy rules. Couillard & Zhu (1992) propose fuzzy logic for control of the concentration of dissolved oxygen and the height of the sludge blanket at the bottom of the clarifier under shock loading, while on-line microorganism image information from a high resolution submerged microscope is combined with heuristic on a full scale plant using fuzzy logic in Watanabe et al. (1993).

The applied models for control of a WWTP tend to be either purely deterministic (white box) or of the black box type. In this thesis stochastic models incorporating physical knowledge are reported.

1.2 Outline of the thesis and reading guide

Chapter 2 gives an overview of the essential biological processes for nutrient removal in an activated sludge WWTP. The use of Monod-kinetic expressions in modelling the rates of these processes is described, and rate expressions for the different processes are derived. Finally, environmental factors influencing the biological processes are mentioned.

The performance of a WWTP is mainly determined by the composition of the wastewater and the design and operation of the plant. Chapter 3 lists some of the important characteristics of the incoming wastewater, and a description of biological nutrient removal plants is given with the most emphasis on the BIO-DENITRO and BIO-DENIPHO processes. The modelling of the activated sludge reaction vessels is also explained.

Chapter 4 is the central part of the thesis, where operational models describing the hydraulic and biological processes of the WWTP are derived.

The modelling methodology and the components of which the models are built, are described before the modelling of the WWTP can be properly explained. These models which incorporates physical knowledge of the biological and hydraulic processes are called grey box models. An introduction to the identifiability concept of model parameters is also given. The last part of the chapter deals with the technicalities of getting the grey box models into a form such that the parameters of the models can be estimated. Statistics of the model performance and parameter significance are described. Readers with less interest in statistics and stochastic modelling may skip some of the sections in this chapter.

Chapter 5 and Chapter 6 deal with the application of the grey box models on data from the Lundtofte pilot scale plant and the Aalborg West WWTP, respectively. The models of the two chapters also represent a step-wise development of the grey box models. The use of extensive time series shows that the identification of Monod-kinetic expressions is feasible. Furthermore, most of the parameter estimates obtained from the models are interpretable and relate to the theory of the processes given in Chapter 2 and 3, and comparison of these parameter estimates with suggested values from the literature show a reasonable correspondence. The parameter estimates are found to give a clear indication of the state of the plant at any time. These two chapters are self-containing and may to some extent be read independently of the rest of the thesis.

The prospects of using the grey box models for prediction based control are dealt with in Chapter 7. The methods include off-line simulations of control strategies and on-line model-based predictive control of the BIO-DENITRO and BIO-DENIPHO processes. The considered controlling actions are the oxygen concentration setpoint and phase lengths of the aerobic and anoxic periods. Several strategies for control of the oxygen concentration setpoint and the aerobic/anoxic phase lengths, and a cost function for evaluating the strategies incorporating cost of operation and nutrient discharge, are proposed. In a simulation study the effect of improved plant operation is investigated.

Numerical methods are indispensable for the application of the grey box models on real data, due to the complexity of the models and the sizes of the applied data sets. Methods for stabilizing the Kalman filter recursions and optimization techniques are presented in Appendix A. The presentation of the applied methods is self-contained, and this appendix has only little relevance for the understanding of the previous chapters.

Chapter 2

The biological processes

The theory of the activated sludge processes has been developed steadily in the last decades. One major step towards combining the theory of the different processes and unifying the terminology used to describe the processes, was made by the introduction of the IAWPRC model no. 1 (Henze et al. (1987)). In this chapter the significant biological processes essential to a biological nutrient removal system, are presented. The presentation of the processes given here is very simplified, but it is sufficient for most practical applications.

In the first section of this chapter the basic activities of the microorganisms in the activated sludge are discussed, followed by a description of the aerobic organic carbon removal process, the nitrification process, the denitrification process, and the biological phosphorus removal process. In the last section some of the environmental factors influencing the processes are mentioned. For a more detailed description of the processes, see Eckenfelder & Grau (1992) and Randall et al. (1992).

2.1 Microorganisms and their activities

The biological processes in a WWTP are carried out by many different types of bacteria. The most important microorganisms in the activated sludge process are bacteria, while fungi, algae, and protozoa are of secondary importance. Thus, for the biological processes considered in the following the term bacteria is used in a more general sense to represent all the microorganisms in the activated sludge.

The different types of organisms which can be found in the activated sludge on a specific WWTP, are also found in the raw wastewater led to the plant and/or the immediate surroundings of the plant (e.g. air and soil). The predominant genera of bacteria in the activated sludge is mainly determined by the composition of the raw wastewater, the design of the plant, and to some extent the operation of the specific plant.

Bacteria need energy permanently in order to grow and to support essential life activities. Growing cells utilize exogenous substrate (located outside the cell membrane) and exogenous nutrients for growth and energy

$$\text{Substrate} + \text{Nutrients} + \text{Oxygen} \longrightarrow \text{Biomass} + \text{Energy}$$

The major part of bacteria in the activated sludge (called heterotrophic bacteria) use organic carbon in the form of small organic molecules as substrate, and some bacteria (called autotrophic bacteria) which are essential to biological nutrient removal, use inorganic carbon as substrate. When the bacteria decay the organic carbon of the bacteria is partly reused. The lifecycle of biomass is illustrated in Figure 2.1, which is a very simplified illustration of the biochemical processes in the activated sludge. Some of the biomass originates from the raw wastewater as indicated by the dotted arrow.

Substrates and nutrients are absorbed within the biomass faster than they are utilized, but the bacteria cannot accumulate large amounts of such products. Instead the substrates and nutrients are chemically modified

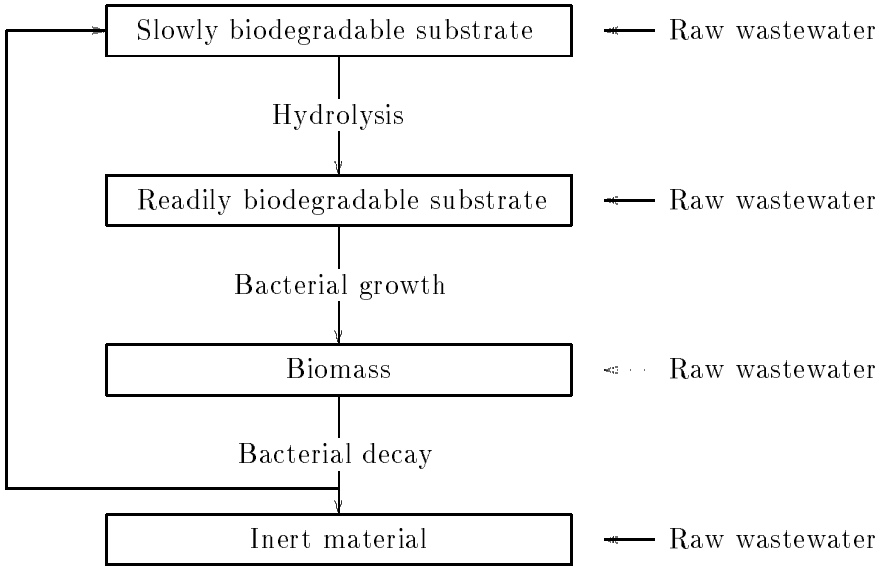

Figure 2.1. *Biomass lifecycle. The regeneration and production of biomass in the activated sludge.*

into a few types of large molecules (typically polysaccharides, lipids, and polyphosphates), which can be stored for a long period of time without significant energetic expenses.

2.1.1 Hydrolysis

Hydrolysis is an enzymatic accelerated process transforming larger organic molecules (including both soluble and particulate organic materials) into smaller, readily bio-degradable molecules. The hydrolysis process rate is slow compared to the rate of growth of biomass and it will be the rate limiting factor for the growth of biomass, if the substrate in the raw wastewater primarily consists of larger organic molecules.

Because hydrolysis is a generic term for a great number of different biochemical processes, the rate of the total process is often given by a first order kinetic expression

$$\frac{dS_h}{dt} = k_h \cdot S_h \tag{2.1}$$

where S_h is the slowly bio-degradable organic substrate concentration and k_h is the time constant of the process. When a more detailed rate expression for the hydrolysis process is desired, Monod kinetic expressions (see below) for the rate limiting concentrations can be used (see Henze et al. (1987)).

2.1.2 Growth of bacteria

Readily bio-degradable substrate is considered to be the only substrate which can be used for growth of biomass. The readily bio-degradable material consists of small organic molecules like acetic acid, methyl alcohol, ethyl alcohol, propionic acid, glucose, etc. The growth rate of biomass and the influence of limiting nutrient or substrate concentrations can be modelled using Monod-kinetics, e.g. the influence of a single limiting nutrient concentration can be described as follows:

$$\frac{dX_B}{dt} = \mu_{max} \frac{S_n}{S_n + K_S} \cdot X_B \tag{2.2}$$

where

S_n	=	the concentration of the rate limiting nutrient or substrate
X_B	=	the concentration of active biomass
μ_{max}	=	the maximum specific growth rate of biomass
K_S	=	the appropriate half-saturation constant

The Monod-fraction in (2.2) show that the Monod-kinetic approximates a zero-order kinetic (i.e. constant expression on right-hand side of (2.2) for $S_n \gg K_S$ and a first-order kinetic in S_n (i.e. first-order differential

equation) for $S_n \ll K_S$. For a more detailed description of the different kinetic expressions, see Monod (1949). Multiple limitations on the growth rate can be modelled by multiplying the right-hand side of (2.2) with the appropriate number of Monod-fractions of the limiting substrate, oxygen, or nutrient concentrations.

The growth of biomass is related to a proportional consumption of nutrients and substrates, and the proportion of biomass produced, ΔX_B, to nutrient or substrate removed, $-\Delta S$ is called the observed yield coefficient Y_{obs}, i.e.

$$Y_{obs} = -\frac{\Delta X_B}{\Delta S} \tag{2.3}$$

Thus, for the limiting nutrient concentration S_n in (2.2), the rate of nutrient consumption is given as follows:

$$\frac{dS_n}{dt} = -\frac{\mu_{max}}{Y_{obs}} \cdot \frac{S_n}{S_n + K_S} \cdot X_B \tag{2.4}$$

If several nutrients and substrates are used for growth of bacteria, the consumption of the given nutrient or substrate is found by dividing the growth rate of bacteria with the individual observed yield coefficients of the given nutrient or substrate.

2.1.3 Decay of bacteria

Biomass is lost by decay, which incorporates a large number of mechanisms including endogenous metabolism, death, predation, and lysis. Bacterial decay is the transformation of active biomass into slowly bio-degradable substrate as illustrated in Figure 2.1. Part of the bacterial decay is considered inert, because the hydrolysis process is too slow relative to the sludge retention time of a typical WWTP. The decay of biomass is described as a first order kinetic process

$$\frac{dX_B}{dt} = -b \cdot X_B \tag{2.5}$$

where b is the decay rate ($b > 0$). The decay rate is assumed to be independent of environmental factors, e.g. temperature, oxygen concentration, nutrients, and substrates.

2.2 Aerobic removal of organic carbon

The organic matter in the raw wastewater is often divided into a number of categories as shown in Figure 2.1. The most widely used subdivision is based on bio-degradability. While the slowly or readily bio-degradable substrate is utilized for biochemical processes and therefore changes its form, inert material leaves the biological nutrient removal system in the same form as it enters. Inert material is of little interest for the operation of the plant unless it is toxic. The readily bio-degradable substrate is used for growth of biomass and supply of energy, and the slowly bio-degradable substrate is hydrolyzed to readily bio-degradable substrate.

In practice, the aerobic heterotrophic yield of biomass with no limitations to growth of bacteria is in the range 0.5-0.6 g COD biomass/g COD substrate, which makes the bacteria very fast growing. The formation of a typical biomass compound ($C_5H_7NO_2$) from a typical substrate ($C_{18}H_{19}O_9N$) with a typical yield coefficient is given by the following reaction:

$$\begin{aligned} C_{18}H_{19}O_9N + 0.74\,NH_4^+ + 8.80\,O_2 \longrightarrow \\ 1.74\,C_5H_7NO_2 + 9.30\,CO_2 + 4.52\,H_2O + H^+ \end{aligned} \tag{2.6}$$

The end-products on the right-hand side of the biochemical reaction are obviously harmless to the environment. It should also be noted that additional to the removal of organic matter, ammonia is removed by growth of heterotrophic bacteria.

The removal of readily bio-degradable substrate under aerobic conditions with no other limitations to the growth rate than the readily substrate concentration, is given by the following Monod-kinetic expression:

$$\frac{dS_S}{dt} = -\frac{\mu_{max,H}}{Y_{obs,S}} \cdot \frac{S_S}{S_S + K_S} \cdot \frac{S_{O_2}}{S_{O_2} + K_{O_2}} \cdot X_{B,H} \tag{2.7}$$

where

S_S	=	the concentration of readily bio-degradable substrate
S_{O_2}	=	the concentration of dissolved oxygen
$X_{B,H}$	=	the concentration of active heterotrophic bacteria
$\mu_{max,H}$	=	the maximum specific growth rate of heterotrophic bacteria
$Y_{obs,S}$	=	the observed biomass yield coefficient of substrate
$K_S\,, K_{O_2}$	=	the appropriate half-saturation constants

In case nutrients impose limitations to the growth rate of heterotrophic bacteria during aerobic conditions, the appropriate Monod-fractions would need to be multiplied on the right-hand side of (2.7).

2.3 The nitrification process

Nitrification is a two-step micro-biological process transforming ammonia into nitrite and subsequently into nitrate. The process is well-known from the biosphere, where it has a major influence on oxygen conditions in soil, streams, and lakes. Soluble ammonia serves as the energy source and nutrient for growth of biomass of a special group of autotrophic bacteria, called nitrifiers. The intermediate formation and removal of nitrite is not considered here.

If ammonia is only used as a source of energy, the first step of oxidizing ammonia into nitrite is:

$$NH_4^+ + 1.5\,O_2 \longrightarrow NO_2^- + H_2O + 2H^+ \tag{2.8}$$

and the second step of oxidizing nitrite into nitrate is:

$$NO_2^- + 0.5\,0_2 \longrightarrow NO_3^- \tag{2.9}$$

A typical representative for the first step is the bacteria of the genus Nitrosomonas and for the second step the bacteria of the genus Nitrobacter.

Because the processes (2.8) and (2.9) only give a small energy yield, the nitrifying bacteria are characterized by a low biomass yield. This is an essential problem for the nitrification process in biological nutrient removal systems. The observed yield coefficients for Nitrosomonas and Nitrobacter are typically significantly smaller compared to those of the heterotrophic bacteria, which makes the nitrifying bacteria a rather slow growing population. Using these yield coefficients for autotrophic growth of biomass, the following reaction for the total nitrification process is obtained:

$$\begin{aligned} &NH_4^+ + 1.86\,O_2 + 1.98\,HCO_3^- \longrightarrow \\ &0.020\,C_5H_7NO_2 + 0.98\,NO_3^- + 1.88\,H_2CO_3 + 1.04\,H_2O \end{aligned} \tag{2.10}$$

where HCO_3^- is the form of soluble carbon-dioxide for pH-values in the range from 5 to 9. From the reaction above (2.10) it is seen that a large amount of alkalinity is destroyed for every NH_4^+ being oxidized. However, the wastewater of many areas contains large alkalinity buffers, but some wastewater treatment facilities require the addition of lime or soda ash to maintain desirable pH-levels for nitrification.

For practical reasons in a WWTP, the nitrification process is considered as a one-step process, which incorporates kinetic parameters for the total process. In (2.10) the three components on the left-hand side may all be rate limiting, but in practice only the ammonia and oxygen concentration

impose limitations to the growth of nitrifiers. Thus, for the removal of ammonia by nitrification, the following expression can be obtained

$$\frac{dS_{NH_4^+}}{dt} = -\frac{\mu_{max,A}}{Y_{obs,NH_4^+}} \cdot \frac{S_{NH_4^+}}{S_{NH_4^+} + K_{NH_4^+}} \cdot \frac{S_{O_2}}{S_{O_2} + K_{O_2}} \cdot X_{B,A} \tag{2.11}$$

where

$S_{NH_4^+}$	=	the concentration of NH_4^+
S_{O_2}	=	the concentration of dissolved oxygen
$X_{B,A}$	=	the concentration of active autotrophic biomass
$\mu_{max,A}$	=	the maximum specific growth rate of autotrophic bacteria
Y_{obs,NH_4^+}	=	the observed biomass yield coefficient of ammonia
$K_{NH_4^+}, K_{O_2}$	=	the appropriate half-saturation constants

For the simultaneous formation of nitrate a similar kinetic expression is found:

$$\frac{dS_{NO_3^-}}{dt} = \frac{\mu_{max,A}}{Y_{obs,NO_3^-}} \cdot \frac{S_{NH_4^+}}{S_{NH_4^+} + K_{NH_4^+}} \cdot \frac{S_{O_2}}{S_{O_2} + K_{O_2}} \cdot X_{B,A} \tag{2.12}$$

The observed yield coefficient for the formation of nitrate Y_{obs,NO_3^-} will be larger than Y_{obs,NH_4^+}, which is clearly seen from (2.10) where less nitrate is produced than ammonia removed.

Operating a WWTP requires special attention to the nitrification process, because the slow rate of growth makes the nitrifiers more vulnerable to inhibitions, changes in the operation of the plant, and the composition of the raw wastewater.

2.4 The denitrification process

Denitrification is a micro-biological heterotrophic process transforming nitrate into nitrogen gas, using nitrate instead of oxygen as the oxidation agent. The conditions during which this process occurs, are called anoxic, because oxygen is not present and some heterotrophic bacteria are able to use nitrate for oxidation. Denitrification is also well-known from the biosphere, where it is common in soil and stationary waters beneath the surface.

Most of the heterotrophic bacteria are optional to the use of oxidation agent, but the energy yield of using nitrate is less than using oxygen. Thus, if oxygen is present, the bacteria prefer to use oxygen. In practice, denitrification only takes place at low oxygen concentrations. The overall mechanism can be described by a typical microbial reaction of a saccharide with nitrate:

$$5\,C_6H_{12}O_6 + 24\,NO_3^- \longrightarrow 12\,N_2 + 24\,HCO_3^- + 6\,CO_2 + 18\,H_2O \quad (2.13)$$

The lower energy yield for the heterotrophic bacteria during the anoxic conditions is also reflected in a somewhat smaller biomass yield coefficient. Denitrifying bacteria using ammonia and the typical form of organic substrate ($C_{18}H_{19}O_9N$) in wastewater for bacterial growth with an observed yield coefficient of 0.47 g biomass/g substrate gives the following reaction:

$$0.61\,C_{18}H_{19}O_9N + 4.54\,NO_3^- + 0.39\,NH_4^+ + 4.15\,H^+ \longrightarrow C_5H_7NO_2 + 2.27\,N_2 + 6.70\,CO_2 + 5.12\,H_2O \quad (2.14)$$

Fortunately, some of the alkalinity lost by nitrification is gained by denitrification. Combining the typical reactions for the nitrification (2.10) and denitrification (2.14) processes, a total of 1.07 eq. alkalinity/mole NO_3^--N removed is lost. Also, from (2.14) it is seen, that 82% of the nitrogen resulting from the reaction is in the form of nitrogen gas.

On the left-hand side of (2.14), three concentrations appear to be rate-limiting for the denitrification process, i.e. the readily organic substrate, nitrate, and ammonia concentration. The required amount of ammonia for cell growth is however very little, and the heterotrophic bacteria are capable of using nitrate for cell growth in lack of ammonia, such that the ammonia concentration in fact does not impose a limitation to the rate of the process. Thus, for the removal of nitrate by denitrification, the following kinetic expression can be obtained:

$$\frac{dS_{NO_3^-}}{dt} = -\frac{\mu_{max}}{Y_{obs,NO_3^-}} \cdot \frac{S_S}{S_S + K_S} \cdot \frac{S_{NO_3^-}}{S_{NO_3^-} + K_{NO_3^-}} \cdot X_{B,H} \quad (2.15)$$

where

$S_{NO_3^-}$	=	the concentration of NO_3^-
S_S	=	the concentration of readily bio-degradable substrate
$X_{B,H}$	=	the concentration of active heterotrophic biomass
$\mu_{max,H}$	=	the maximum specific growth rate of heterotrophic bacteria
Y_{obs,NO_3^-}	=	the observed biomass yield coefficient of nitrate
$K_{NO_3^-}, K_S$	=	the appropriate half-saturation constants

The inhibitory effect of the presence of oxygen on the nitrate removal rate can be modelled by multiplying (2.15) with $\frac{K'_{O_2}}{K'_{O_2}+S_{O_2}}$, where S_{O_2} is the dissolved oxygen concentration, and K'_{O_2} is the inhibition constant for oxygen (K'_{O_2} and K_{O_2} in (2.12) are two distinct constants). For the WWTP types considered in the present context the change from aerobic to anoxic conditions is normally quite clear to detect as the oxygen approaches zero rather rapidly after the aeration of the wastewater has stopped.

A very important parameter for the denitrification process is the organic carbon/nitrogen-fraction (C/N-ratio) of the raw wastewater, which also plays a significant role for the design and operation of the WWTP. The denitrification depends to a large extent on the readily bio-degradable substrate concentration in the raw wastewater, because the hydrolysis of organic substrate is slow during anoxic conditions. In practice, the C/N-ratio of the raw wastewater should at least be 8-9 g COD/g N for the most typical WWTP's, in order to assure a relative high denitrification rate.

2.5 The biological phosphorus removal process

In the first section of this chapter, the accumulation of phosphates in the bacterial cell, used as an energy storage in the form of intra-cellular polyphosphates, was shortly mentioned. Polyphosphates are an energy source, which is built up during aerobic and anoxic conditions, and during anaerobic conditions the polyphosphates are stripped and energy gained in order to store organic substrate.

Some of the heterotrophic bacteria are able to store phosphates, but the bacteria of the genus Acinetobacter are the most important for this process. The bacteria of the genus Acinetobacter can only store polyphosphates during aerobic conditions, but they effectively compete with the facultative species in the biological nutrient removal system. A minor part of the phosphate accumulating bacteria are also capable of performing denitrification. Thus, the formation rate of polyphosphates is significantly higher during aerobic conditions compared to anoxic conditions in the activated sludge.

During anaerobic conditions the phosphate accumulating bacteria use their energy storage by stripping phosphates to accumulate readily bio-degradable substrate, which is used for cell growth during aerobic/anoxic conditions. This ability gives the phosphate accumulating bacteria an advantage to

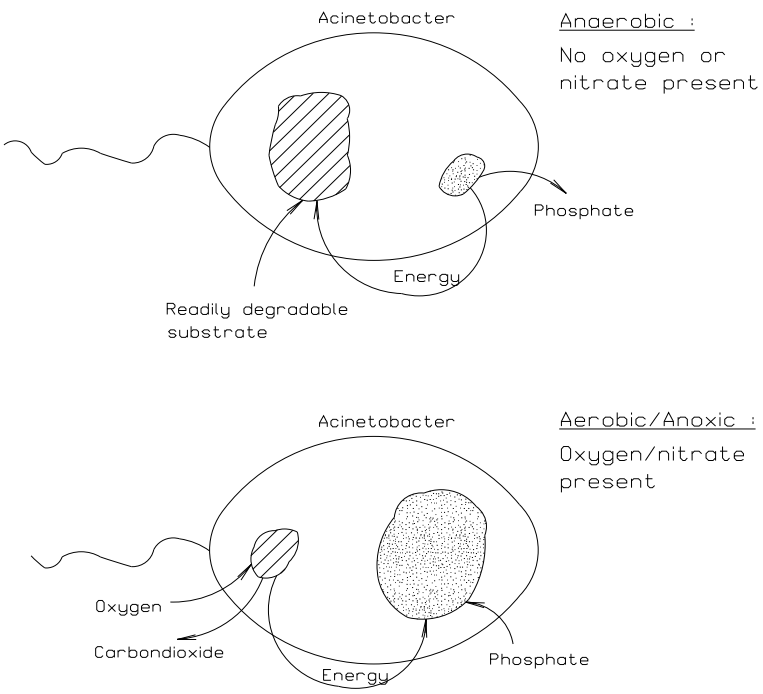

Figure 2.2. *Illustration of the biological phosphorus removal process.*

other heterotrophic bacteria during anaerobic periods, which can be used for selecting the phosphate accumulating bacteria by continuous cycling of the activated sludge through aerobic/anoxic and anaerobic conditions. The process of phosphate uptake/release and the simultaneous readily bio-degradable consumption/uptake is depicted in Figure 2.2.

The heterotrophic phosphate accumulating bacteria grow at the same rate as other heterotrophic bacteria, i.e. a biomass yield of 0.5-0.6 g COD biomass/g COD substrate. The bacteria can store polyphosphates to a maximum of approximately 50% of the total cell weight, i.e. phosphorus

alone makes up 15-20% of the biomass of the Acinetobacter and other phosphate accumulating bacteria. In practice, 5-8% of the biomass of Acinetobacter is made up of phosphorus, and the phosphorus is thus removed biologically by removing excess sludge.

The formation of polyphosphates during aerobic conditions assuming the accumulated readily bio-degradable substrate to be in the form of acetic acid and Y_{obs}=0.4 g COD biomass/g COD substrate, is given by the following reaction:

$$C_2H_4O_2 + 0.16\,NH_4^+ + 1.2\,O_2 + 0.2\,PO_4^{3-} \longrightarrow 0.16\,C_5H_7NO_2 + 1.2\,CO_2 + 0.2(HPO_3)_n + 0.44\,OH^- + 1.44\,H_2O \quad (2.16)$$

and during anoxic conditions:

$$C_2H_4O_2 + 0.16\,NH_4^+ + 0.2\,PO_4^{3-} + 0.96\,NO_3^- \longrightarrow 0.16\,C_5H_7NO_2 + 1.2\,CO_2 + 0.2(HPO_3)_n + 1.4\,OH^- + 0.48\,N_2 + 0.96\,H_2O \quad (2.17)$$

where $(HPO_3)_n$ is the phosphate stored intra-cellular as polyphosphate and PO_4^{3-} denotes the phosphate in the wastewater, which for moderate pH-values is in the form of HPO_4^{2-} and $H_2PO_4^-$. The readily bio-degradable substrate uptake and simultaneous phosphate release during anaerobic conditions is described as follows:

$$2\,C_2H_4O_2 + (HPO_3)_n + H_2O \longrightarrow (C_2H_4O_2)_2 + PO_4^{3-} + 3\,H^+ \quad (2.18)$$

where $(C_2H_4O_2)_2$ is the intra-cellular substrate formed of acetic acid.

The alkalinity is only influenced a little by the phosphate uptake during aerobic and anoxic periods. Both processes, (2.16) and (2.17), produce alkalinity (0.04 and 1.0 eq. alkalinity/mole acetic acid used), but combined

with the slow rate of phosphate uptake during anoxic conditions, the alkalinity almost remains unchanged by the intra-cellular accumulation of phosphates. The phosphate release process (2.18), however, removes some alkalinity.

The uptake of phosphates during aerobic conditions assuming that the phosphate concentration is the only limiting nutrient concentration, and the readily bio-degradable substrate (both endogenous and exogenous) and oxygen concentration are not rate-limiting, can be described by the following Monod-expression:

$$\frac{dS_{PO_4^{3-}}}{dt} = -\frac{\mu_{max,P}}{Y_{obs,PO_4^{3-}}} \cdot \frac{S_{PO_4^{3-}}}{S_{PO_4^{3-}} + K_{PO_4^{3-}}} \cdot X_{B,P} \quad (2.19)$$

where

$S_{PO_4^{3-}}$	=	the concentration of PO_4^{3-}
$X_{B,P}$	=	the concentration of active phosphate accumulating biomass
$\mu_{max,P}$	=	the maximum specific growth rate of phosphate accumulating bacteria
$Y_{obs,PO_4^{3-}}$	=	the observed biomass yield coefficient of phosphate
$K_{PO_4^{3-}}$	=	the appropriate half-saturation constant

Occasionally, the readily bio-degradable substrate or the oxygen concentration turns out to be rate limiting as well, which requires multiplication of the right-hand side of (2.19) by the appropriate Monod-fraction. During anoxic conditions, a similar expression to (2.19) holds with $\mu_{max,P}$ being significantly lower in this case. The reason is, that all phosphorus accumulating bacteria can take up phosphate under aerobic conditions whereas only part of the phosphorus accumulating bacteria take up phosphate under anoxic conditions.

The release of phosphate during anaerobic conditions is typically limited only by the concentration of readily bio-degradable substrate (mainly in the form of acetic acid, HAc).

$$\frac{dS_{PO_4^{3-}}}{dt} = k_{max,PO_4^{3-}} \cdot \frac{S_{HAc}}{S_{HAc} + K_{HAc}} \cdot X_{B,P} \qquad (2.20)$$

where

$S_{PO_4^{3-}}$	=	the concentration of PO_4^{3-}
S_{HAc}	=	the concentration of acetic acid
$X_{B,P}$	=	the concentration of active phosphate accumulating biomass
$k_{max,PO_4^{3-}}$	=	the maximum specific release of phosphate
K_{HAc}	=	the appropriate half-saturation constant

The release of phosphate automatically stops, when all the intra-cellular polyphosphate is used. The amount of polyphosphate in the biomass, itself, however does not affect the release rate of phosphate.

Exposing the activated sludge to anaerobic periods in the operation of a WWTP favors the Acinetobacter and other phosphate accumulating bacteria, which results in a larger amount of phosphate accumulating bacteria of the total biomass and a larger removal of phosphorus. Thus, for a biological nutrient removal system, the period lengths of aerobic, anoxic, and anaerobic conditions should be determined according to the composition of the raw wastewater and biomass, and the given regulatory discharge requirements.

2.6 Environmental influence on the biological processes

For the processes described above a number of environmental factors influence the rates of the processes. These factors include temperature, effect of pH-value, toxic and inhibiting materials, and rate-limiting concentrations of nutrients and substrates. Some of the rate-limiting concentrations of the processes are already incorporated in the rate-expressions given previously,

while other seldom impose limitations to the growth of bacteria. In order to model the influences of environmental factors, μ_{max} in the expressions above, is defined as being a function of these factors, which have not been incorporated in the rate expressions above. The maximum specific growth rate of biomass is besides the bio-degradability of the substrate and the specific biomass composition given by factors such as:

$$\mu_{max} = f(T, pH, S_x, S_y, \ldots) \qquad (2.21)$$

where

T	=	the temperature in the activated sludge
pH	=	the pH-value
S_x, S_y	=	the concentrations of rate-limiting materials

The maximum specific growth rate μ_{max} is reported to grow exponentially from 0-32°C with approximately 10% for every degree Celsius. In the range 32-40°C μ_{max} is approximately constant, while it decreases very rapidly for temperatures above 40°C. Thus, the rates of the processes may differ by more than a factor of 2 from winter to summer temperatures. The bacteria are also sensitive to rapid changes in the temperature of the raw wastewater, which often occur during rainy weather and the melting of snow.

The biological processes are also sensitive to the pH-value in the raw wastewater, and the pH-value should at least be within the range of 5-10. Heterotrophic bacteria attain the highest maximum specific growth rate for pH-values ranging from 7-9, while autotrophic bacteria prefer a little more alkali wastewater, typically a pH-value within 8-9. Recent work of Antoniou et al (1990) suggests a cross-correlation effect of the pH-value and temperature on μ_{max}, indicating a greater pH effect at lower temperatures.

Many organic compounds and inorganic metal compounds have a toxic effect on the biological processes, even though these processes are rather robust in the mixed bacterial cultures of the activated sludge. Quantification of toxicity in wastewater treatment systems is difficult due to the number of factors that may affect the rates of the processes. Knowledge of

toxicity of different compounds is often found from laboratory batch tests on a single specific bacterial culture. However, toxicity on larger WWTP's are mainly caused by industrial outlet of toxic materials, and the compound causing the toxicity may be identified by a closer examination of the industries in the catchment area.

Some compounds which are not toxic to the biomass, inhibits the biological processes, causing the rates of the processes to decrease. The inhibition of a given matter can be modelled by multiplying the rate expression with the following fraction:

$$\frac{K_{S,I}}{K_{S,I} + S_{S,I}} \tag{2.22}$$

where

$S_{S,I}$ = the concentration of the inhibiting material
$K_{S,I}$ = the appropriate half-inhibition constant

The inhibition of a specific bacterial culture, which makes the specific bacterial growth rate slow, combined with the removal of excess sludge, may result in loss of the given bacterial culture.

2.7 Conclusion

In the previous sections the biological processes of a biological nutrient removal system and rates of the processes have been presented. In order for the processes to actually occur, some basic nutrients and substrates are crucial. These materials are normally present in the wastewater and produced by hydrolysis. The rates of the biological processes heavily depend on the concentration of these basic substances, but other factors (oxygen concentration, temperature, pH-value, toxic materials, inhibitory materials, etc.) have a significant influence on the rates. The different bacterial genera found in the activated sludge is determined by the composition of

the wastewater and the operation of the plant, by means of which also the amount of specific bacterial genera to some extend can be controlled. Assuring optimal conditions for the biological processes is an important task for the operation of a biological nutrient removal system.

Chapter 3

Wastewater and treatment plants

Two important factors for the performance of the biological processes described in the previous chapter are: the composition of the raw wastewater and the design/operation of the WWTP. In fact, the design/operation of a plant is largely determined by the composition of the raw wastewater, which can vary a lot in both volume and composition of materials. Thus, it is crucial when designing a WWTP or setting up operation strategies for the plant to know the variation of wastewater loads. In the first section, measures to characterize the wastewater loads of a typical municipal WWTP plant are given, followed by description of biological nutrient removal plants and particularly the BIO-DENITRO/BIO-DENIPHO-processes, which will be modelled later. The last section deals with the theory of the reaction vessels or tanks used in an activated sludge process.

3.1 Characterization of wastewater

The raw or untreated wastewater of a typical municipal WWTP originates from households, industries, institutions, infiltration from the ground water, and generally also rainwater of the catchment area. In spite of the mixing of the produced wastewater in the sewer, the WWTP is faced with strongly time-varying loads, both in volume and composition of materials such as organic substrate and nutrients.

In the following subsections three main characteristics of the raw wastewater are dealt with:

- Flow to the plant
- Organic materials
- Nutrients

but other characteristics needs to be shortly mentioned.

The temperature in the raw wastewater affects the overall temperature in the activated sludge, which has a large influence on the rates of the processes described in the previous section. Actually, due to the energy gained from the biological processes the temperature of the activated sludge is slightly higher than the temperature of the raw wastewater. In Denmark the temperature of the activated sludge normally ranges from 7-10 degrees C° in winter to 17-20 degrees C° in summer, but rainy weather and melting of snow may decrease the temperature of the activated sludge significantly.

The alkalinity of the raw wastewater influences the pH-value in the activated sludge, because alkalinity in total is removed by the biological processes. Henze et al. (1990) states that the biological processes will not be affected by the loss in alkalinity, if the alkalinity of the raw municipal wastewater is above 5 eq. alkalinity/m^3 wastewater. The alkalinity

is mainly geographically determined and as such, it does not vary significantly over longer periods of time. Though, rainy weather and melting of snow may temporarily change the alkalinity of the raw wastewater.

Inorganic materials are found in various concentrations in the raw wastewater. Especially anions like sulphate (SO_4^{2-}), and chloride (Cl^-) are found together with cations like potassium (K^+), calcium (Ca^{2+}), sodium (Na^+), and magnesium (Mg^{2+}). Results reported by Pattarkine (1991) have shown that the presence of both magnesium and potassium is essential to the biological phosphorus removal process. Fortunately, the requirements are considerably less than the quantities of these two cations found in most wastewaters. Also, many heavy metals are found in the raw wastewater of which the most typical are lead, cadmium, chromium, nickel, and copper. Sometimes, these heavy metals are found in concentrations which may have an inhibiting effect on the biological processes.

3.1.1 Flow to the plant

The influent flow rate to the WWTP shows a large variation due to human behaviour and weather conditions such as rain, snow, and temperature. While weather conditions can be quite unpredictable, human behaviour follows a regular pattern which consist of a diurnal, weekly, and yearly variation. Figure 3.1 shows the diurnal variation of the measured flow rate to Aalborg West WWTP on a typical weekday without precipitation. The curve serves as a smoothed and delayed illustration of human activities due to highly varying retention times in the different sub-nets of the sewer. Figure 3.2 shows the daily total inlet flow to the Aalborg West WWTP over a 26 days period, where days with precipitation are marked with a square. There seems to be a significant difference in the flow to the plant between weekdays and weekends.

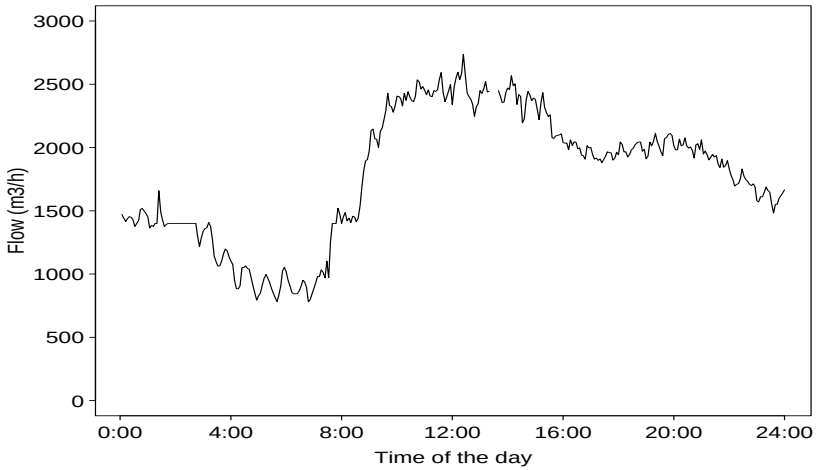

Figure 3.1. *Flow variations on November, 9th 1992 (Monday) at the Aalborg West WWTP. Samples taken every fourth minute.*

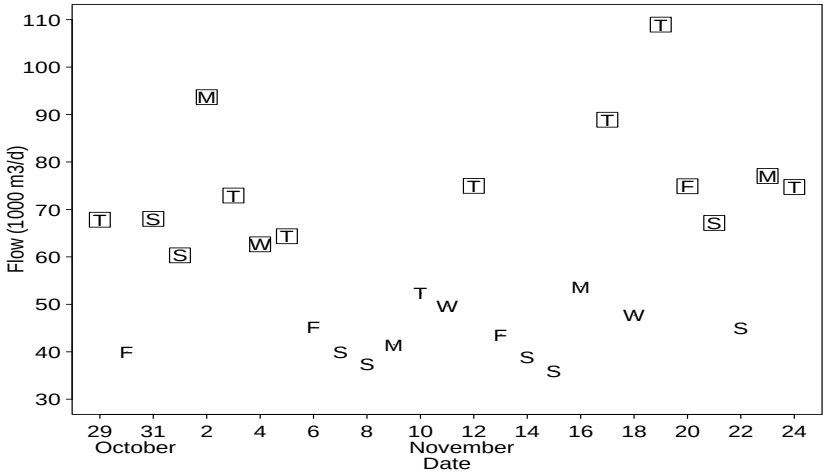

Figure 3.2. *Daily flow to the Aalborg West WWTP over a 27 day period. The type-of-days is indicated by letters and days with precipitation are marked with squares.*

3.1.2 Organic materials

Wastewater normally contains thousands of different organic compounds of different sizes, which makes organic materials the significantly largest component group as to both quantity and diversity. The organic compounds are grouped into readily-, slowly-, and non-bio-degradable substrate with respect to the degradation time. The general rule is: the larger the organic compound is, the slower is the degradation process.

Three measures of organic matter concentration and composition have gained acceptance and are widely used: Biochemical Oxygen Demand (BOD), Chemical Oxygen Demand (COD), and Total Organic Carbon (TOC). The measures are not to be explicitly compared, because each measure gives an individual characteristic of the wastewater composition, but COD is the preferred measure.

The basic idea of the BOD-analysis is, that oxygen demand is caused by microorganisms when degrading organic matter. BOD is found as the total oxygen consumption of a sample after 5 days and nights at a temperature of 20°C. The disadvantage of this measure is, that it takes 5 days before the results are obtained, and it is difficult to make reproducible. The COD-analysis is performed by adding potassiumdichromate ($K_2Cr_2O_7$) to oxidize the organic carbon. Some inorganic compounds are also oxidizes, but for most wastewaters this is of less importance. The analysis is rather fast (1-2 hours), and it can be automated. TOC is equal to the production of carbon-dioxide after heating the sample to high temperatures. However, as COD it tells little about the actual oxygen consumption and the fraction of organic carbon, that can be removed from the wastewater. Table 3.1 summarizes typical values of the three measures for three different types of wastewater. More details on the different organic carbon measures can be found in Carstensen (1992) or Henze et al. (1990).

Biological nutrient removal cannot be accomplished without sufficient biodegradable substrate. Ekama & Marais (1984) state that 8.6 mg COD is needed to reduce 1 mg of NO_3^--N to nitrogen gas and approximately 50-59

Measure	Unit	Heavily loaded wastewater	Moderately loaded wastewater	Lightly loaded wastewater
BOD	g O_2/m^3	350	250	150
COD	g O_2/m^3	740	530	320
TOC	g C/m^3	250	180	110

Table 3.1. *Measures of organic matter in typical Danish wastewater. Data from Henze et al. (1990).*

mg COD is needed to remove 1 mg PO_4^{3-}-P from the wastewater. The biological phosphorus removal is as described in the previous chapter strongly affected by the specific organic compound available for assimilation. The bio-degradable substrate for biological nutrient removal mainly comes from the raw wastewater, but a minor part originates from the fermentation of sludge.

3.1.3 Nutrients

Nitrogen in the raw wastewater consists primarily of ammonia and organic nitrogen, however, a small fraction of nitrite and nitrate may also be found. The fraction of nitrogen including ammonia and organic nitrogen is often referred to as Kjeldahl nitrogen. Typically, the organic nitrogen to COD ratio of the raw wastewater is rather constant in the range 0.08-0.15 g N/g COD, and the organic nitrogen in the non-bio-degradable substrate is also considered inert. Table 3.2 summarizes typical values for nitrogen in the raw wastewater.

Phosphorus is found in raw wastewater as inorganic phosphate (PO_4^{3-}), inorganic polyphosphates (long chains of phosphates), and organic phosphorus. Likewise, Table 3.2 summarizes typical values for phosphorus in the raw wastewater.

Measure	Unit	Heavily loaded wastewater	Moderately loaded wastewater	Lightly loaded wastewater
Total nitrogen	g N/m^3	80	50	30
Ammonia	g N/m^3	50	30	18
Organic nitrogen	g N/m^3	30	20	12
Total phosphorus	g P/m^3	23	16	10
Phosphate	g P/m^3	14	10	6
Polyphosphate	g P/m^3	5	3	2
Organic phosphorus	g P/m^3	4	3	2

Table 3.2. *Measures of nutrients in typical Danish wastewater. Data from Henze et al. (1990).*

3.2 Biological nutrient removal systems

A WWTP with biological nutrient removal is made up of two parts: the mechanical treatment and the biological treatment. In most cases the mechanical treatment consists of a grid and a primary sedimentation basin, where larger particles and grease are removed before the wastewater enters the biological part, where it is mixed with returned sludge.

The basic idea of an activated sludge WWTP is to keep the activated sludge suspended in the wastewater through mixing and/or aeration in the reaction tanks. After processing the wastewater, the activated sludge is allowed to settle in the secondary sedimentation basin (also called clarifier), where the activated sludge is recycled in order to maintain a high concentration of activated sludge in the reaction tanks. From top of the secondary sedimentation basin processed wastewater is led to the effluent.

An activated sludge system must include one or more un-aerated zones in order to accomplish biological nutrient removal. Furthermore, the activated sludge must recycle through all zones (anaerobic, anoxic, aerobic) for the selection of the desired types of bacteria, i.e. the WWTP must be a single

sludge system. Biological phosphorus removal can be maximized by placing the anaerobic zone first so that the phosphorus-removing bacteria have the first opportunity to utilize the organic substrate, thus giving them a competitive edge over those bacteria that cannot utilize or store substrate under anaerobic conditions. Likewise, nitrogen removal can be maximized by placing the anoxic zone first, but nitrogen removal is less sensitive to the types of organic compounds available, so the anaerobic zone is usually placed before the anoxic zone.

The first process configurations for biological nutrient removal appeared in the 1960s. Today, the number of process configurations is very large, and it must be recognized that there is not merely one type of plant which will always prove optimal. Some of the major contributions to the development of biological nutrient removal are due to Ludzack & Ettinger (1962), Levin & Shapiro (1965), Barnard (1973), and Barnard (1975). In this investigation the modelling of the BIO-DENITRO/BIO-DENIPHO process configuration is concerned. This will be examined in the next section.

3.3 The BIO-DENITRO and BIO-DENIPHO process

The BIO-DENITRO configuration uses multiple oxidation ditches in an alternating operation mode, which enables a ditch to be isolated for a specific treatment objective. The alternating operation mode provides phased treatment in each ditch. The operation cycle of a BIO-DENITRO plant with indication of flow patterns and phases is sketched in Figure 3.3. To illustrate the duration of the different phases, a time schedule for a typical operation cycle is also shown. The phases of nitrification and denitrification are indicated on the Figure by N and DN.

Influent wastewater can be divided to multiple ditches where operating conditions are alternated, i.e. aerobic/anoxic conditions. Operational phases in a ditch are short relative to hydraulic retention time (3.3) and the amount

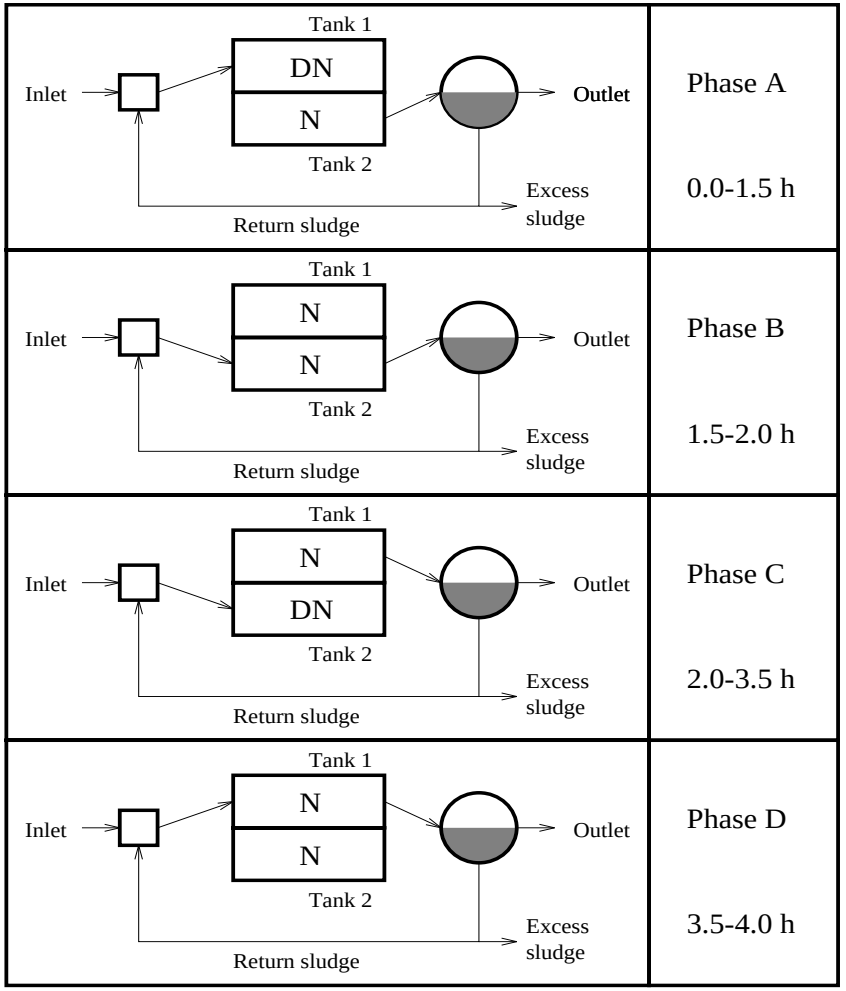

Figure 3.3. *The BIO-DENITRO process operation with typical phase lengths. The nitrification and denitrification processes are alternated between the two tanks.*

of wastewater entering a ditch during a specific operating phase is small compared to the ditch volume. Therefore, the reactor mode approaches that of a batch process. The ditches are connected through a spill-way to enable the clarifier of large hydraulic loads induced by the switching of phases. Automatically controlled weirs regulate flow to and from ditches to implement the alternating treatment mode, and rotor aerators and (optional) propellers satisfy all aeration and mixing requirements. Thus, phase lengths and operating conditions can be varied to achieve a specific treatment objective.

The BIO-DENITRO process for biological nitrogen removal has been extended to include biological phosphorus removal by introducing an anaerobic contact tank into the system. In this tank, the raw wastewater and the returned sludge from the secondary sedimentation basin are mixed before entering the BIO-DENITRO system. By this process, the wastewater first passes the anaerobic pretreatment tank where only a mixing takes place, and where neither nitrate nor oxygen is present. This new process is known as the BIO-DENIPHO process.

A process flow scheme for the BIO-DENIPHO process is shown in Figure 3.4 with a total operation cycle of four hours. Only the first two hours of the operation cycle are shown, while the last two hours of the cycle are performed with the flow direction and the denitrification/nitrification phases interchanged between the two tanks.

For a more detailed description of the BIO-DENITRO and BIO-DENIPHO processes, and experiences of implementing these processes, see Bundgaard (1988). In Einfeldt (1992) a case study of implementing the BIO-DENIPHO process on the Aalborg West WWTP is given.

3.4 Dynamics of the reaction vessel

In the previous section the operation mode of the BIO-DENITRO and BIO-DENIPHO processes were described, and in the previous chapter the

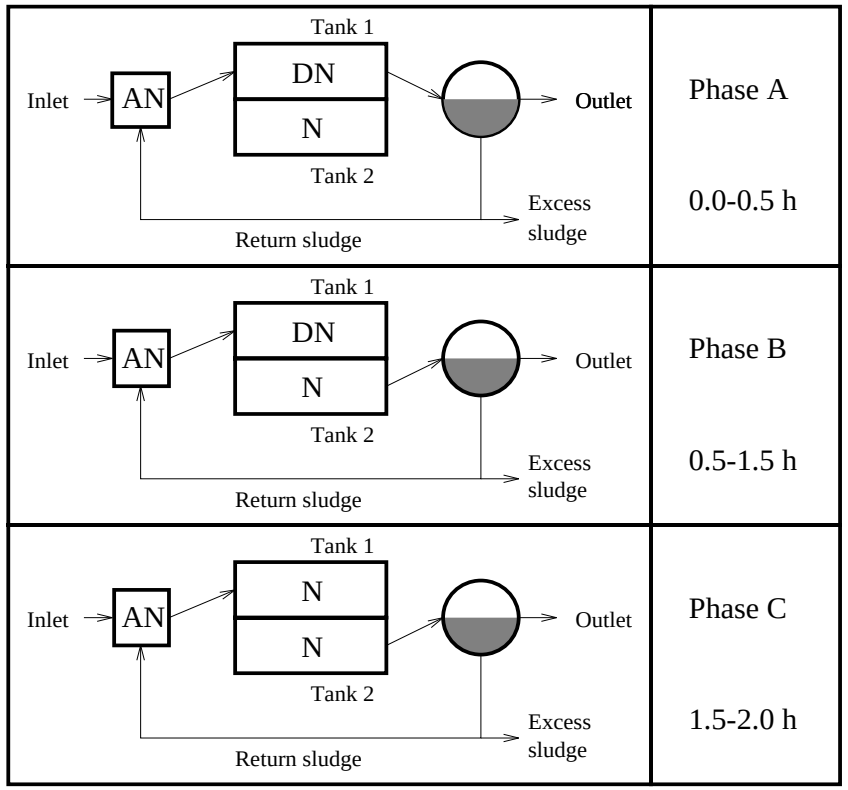

Figure 3.4. *The BIO-DENIPHO process operation with typical phase lengths. The nitrification and denitrification processes are alternated in the two aeration tanks, while phosphorus accumulating bacteria are selected by introducing the anaerobic pretreatment tank.*

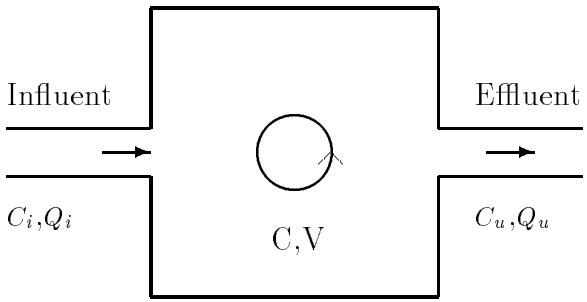

Figure 3.5. *Illustration of an ideally mixed tank with the notation used in this section.*

dynamics of the biological processes were explained. In order to model the dynamics of the plant, the dynamics of the reaction tanks also needs to be examined. In Figure 3.5 a reaction vessel is illustrated with an index notation which will be used throughout this section.

The following identities are valid for the reaction tank:

$$Q_{i,t} = Q_{u,t} + \frac{dV_t}{dt} \tag{3.1}$$

$$Q_{i,t}C_{i,t} = Q_{u,t}C_{u,t} + \frac{dV_tC_t}{dt} \tag{3.2}$$

where Q is the flow, C is the concentration of a given matter, and V is the volume of the tank. However, the volume of the tank is assumed to be constant in the following, i.e. $V_t = V$ and as a result $Q_{i,t} = Q_{u,t} = Q_t$.

The most commonly used parameter to characterize a reaction vessel is the hydraulic retention time.

$$T_h = \frac{V}{Q} \tag{3.3}$$

If the flow, Q, is time-varying the average flow $\overline{Q}$ to the tank is used in (3.3). Thus, the hydraulic retention time expresses the average retention time of a particle in the reaction vessel. However, particles differing in their degree of suspension may have very different retention times.

The reaction tanks used in a WWTP are equipped with aerator and/or propellers in order to keep the activated sludge suspended. The mixing of the tanks approximates that of ideal mixing, i.e. the concentration of a given matter being measured is unrelated to the position of the sample being taken in the tank. The concentration of the given matter is thus constant with respect to the position in the tank, and the outlet concentration of the tank is equal to the overall concentration of the tank ($C_{u,t} = C_t$). Applying this result to (3.2) and using (3.3) gives the following differential equation:

$$\frac{dC_t}{dt} = \frac{C_{i,t} - C_t}{T_h} \tag{3.4}$$

The inlet concentration, $C_{i,t}$, to the aeration ditches in the BIO-DENITRO and BIO-DENIPHO processes can be characterized by a step-function with a step equal to the average inlet concentration of the phase with influent load to the reaction tanks. The influence of a step-function load in an ideally mixed tank is illustrated in Figure 3.6. The solution to (3.4) with a step-function load is as follows:

$$C_t = \overline{C}_i - (\overline{C}_i - C_0) \cdot e^{-\frac{t}{T_h}} \tag{3.5}$$

where $\overline{C}_i$ is the average inlet load concentration and C_0 is the concentration in the ideally mixed tank of the given matter at the starting time of the influent load as indicated in Figure 3.6.

The basic assumption of ideal mixing is generally valid for the reaction vessels of the BIO-DENITRO and BIO-DENIPHO processes, but non-ideal mixing can be modelled by connecting several ideally mixed tanks with identical volume holdings in series. As shown in Harremoës et al. (1989), a

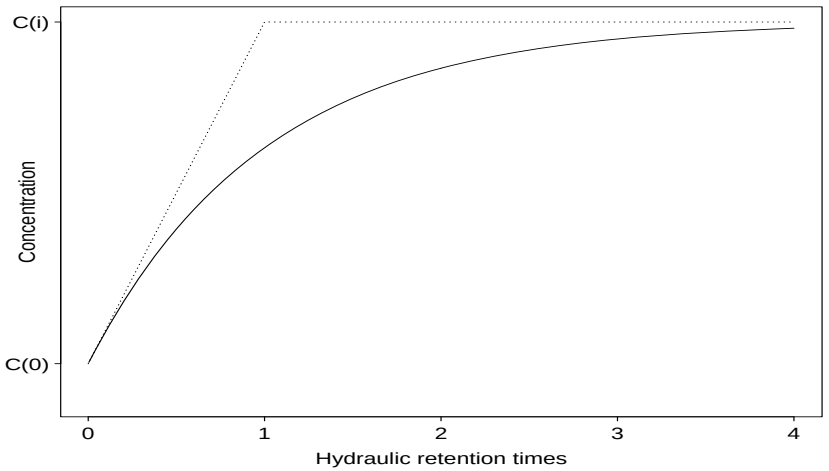

Figure 3.6. *Response of a step-function load in an ideally mixed tank.*

large number of identical ideally mixed tanks in series approximates a pipe without any mixing. Thus, non-ideal mixing can be modelled by connecting the appropriate number of identical ideally mixed tanks in series. In Chapter 6, this issue will be further investigated.

3.5 Summary

In the previous sections the important characteristics of the raw wastewater have been presented, and especially the variations of these characteristics, which have a major impact on the operation of a WWTP, have been discussed. The main characteristics of the raw wastewater are: flow, organic materials (quantity and composition), and nutrients. The design and operation of a plant is largely determined by these three characteristics.

The basic principle of biological wastewater treatment is, that the plant must be a single sludge system, which must include at least one un-aerated zone. Biological phosphorus removal requires that the activated sludge

is exposed to anaerobic conditions, while denitrification and nitrification occur in the anoxic and aerobic zones of the WWTP, respectively. BIO-DENITRO and BIO-DENIPHO are two alternating process configurations, which are able to perform biological nutrient removal. These processes will be modelled for the two considered cases in Chapter 5 and Chapter 6, respectively. The reaction tanks of these two processes are considered as being ideally mixed, and the various consequences of these tanks have been described in the last section of this chapter.

Chapter 4

Structural modelling of time series

In the two previous chapters the theory of the wastewater processes, biological and hydraulic processes, was explained, and models describing the dynamics of these processes in continuous time were examined. The parameters of these models have the disadvantage of not being able to be estimated on the basis of available measurements on a WWTP. In particular, it should be stressed that measurements of the concentration of active biomass ($X_{B,A}$, $X_{B,H}$, or $X_{B,P}$) do not exist. Hence, they are calibrated with some preset parameters in order to reflect the dynamics of the measurements. In this chapter the use of structural models is proposed, which can be identified on the basis of the available data but at the same time incorporates the most important knowledge of the wastewater processes. The first section deals with the modelling methodology of time series analysis, and the second section describes the tools used for structural modelling. The third section gives a theoretical and a practical explanation on the identifiability of parameters. The structural models of the wastewater processes are formulated in the fourth section. In the last four sections the

technicalities of getting the structural models into a form, where they can be estimated via the Kalman filter, are explained. A number of tests and criteria used to select the best fitting model are also described. However, the central part of this chapter is the model formulation set out in the fourth section. A lot of inspiration for this chapter is due to Harvey (1989).

4.1 Modelling methodology

A physical phenomenon can be modelled using either deterministic or stochastic models. Deterministic models are obtained explicitly from mathematical functions and physical constants. Such mechanistic models of processes give rise to deterministic description of data since, for the system of equations comprising the model, the output can be calculated exactly given values of the input and initial conditions. Study of phenomena usually begins with the assumption that the physical world is fundamentally deterministic, but in order to give a mechanistic description of the processes, the inclusion of a great number of parameters is often required. Unfortunately, it is often found that a large class of phenomena is not deterministic or the underlying theory of the processes is so complex, that a mechanistic description cannot be achieved.

Modelling these phenomena gives rise to a stochastic modelling approach. That is, rather than founding the model on a theoretical conception of the system with subsequent validation by comparison with actual data, the data itself guides the model development with the result being a model minimizing the difference between actual data and model predictions. The model structure obtained using these procedures does not necessarily correspond to a known mechanism, but underlying mechanisms found in data may be included. In the present context, the stochastic models are characterized by fewer parameters for the description of data compared to the deterministic models.

In Box & Jenkins (1976) a stochastic process is defined as "statistical phenomena that evolves in time according to probabilistic laws". An example

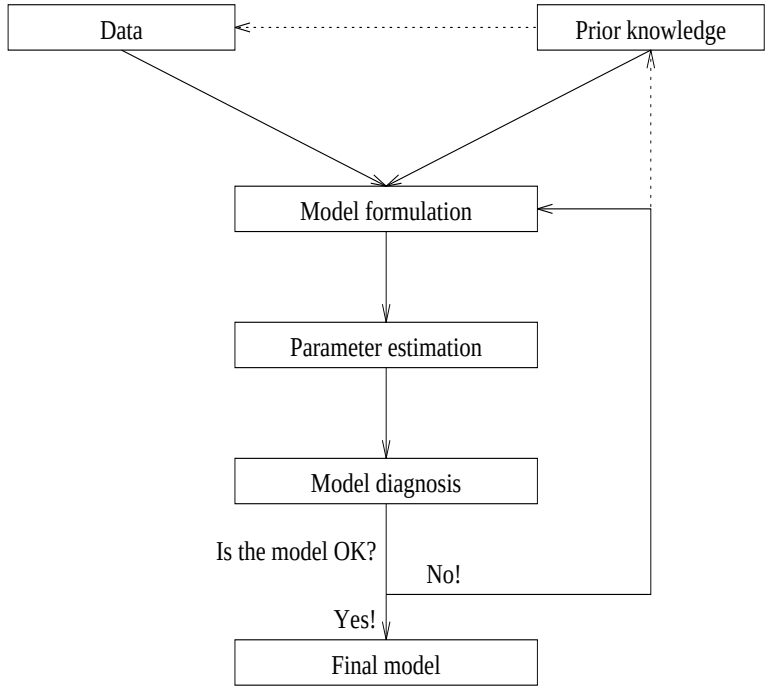

Figure 4.1. *Illustration of the iterative model identification process.*

of such a process is the raw influent flow to the WWTP over time which is shown in Figure 3.1 for the Aalborg West WWTP. The daily flow pattern can be modelled deterministicly using trigonometric functions or a set of dummy variables, but the daily average flow to the plant shown in Figure 3.2, also shows large variations such that a deterministic function to describe the flow only would apply for "an average day". Data are usually found to be dependent on past values of the same or different variables, and modelling of this time dependency is of interest in this chapter. The methods of describing data using stochastic time-varying models based on the statistical properties are generally known as time series analysis.

The building of stochastic structural models is an iterative process, where model diagnostics by statistical methods leads to the formulation of new models. This is illustrated in Figure 4.1. Data and the known underlying mechanisms of the process being modelled are used to formulate a class of models with the estimation of the parameters being feasible. The formulated models are assessed using a set of statistical tools typically based on the models performance of reproducing the measured data. Based on the model diagnostics new classes of models are proposed to remedy the model deficiencies. Model testing occasionally leads to the inclusion of additional prior knowledge which may lead to the procurement of new data.

The following criteria for a good model have been proposed in Harvey (1981a).

(a) *Parsimony* A parsimonious model is one which contains a relatively small number of parameters and, other things being equal, a simpler model is to be preferred to a complicated one.

(b) *Data coherence* Diagnostic checks are performed to see if the model is consistent with the data. The essential point is that the model should provide a good fit to the data, and the residuals, as well as being relatively small, should be approximately random.

(c) *Consistency with prior knowledge* The estimated model should be consistent with any prior information on the size or magnitude of the various parameters.

(d) *Data admissibility* A model should be unable to predict values which violate definitional constraints. For example many variables cannot be negative.

(e) *Structural stability* As well as providing a good fit within the sample, a model should also give a good fit outside the sample.

(f) *Encompassing* A model is said to encompass a rival formulation if it can explain the results given by the rival formulation. If this is the case, the rival model contains no information which could be used to improve the preferred model. In order to be encompassing a model does not need to be more general than its rivals. Indeed the notion of parsimonious encompassing is essential to avoid vacuous formulations.

The structural stability criterion does not always apply to stochastic models which are often restricted by the span of data used for estimation, i.e. the stochastic models may not be well-suited for describing effects which are not found in the data used for identifying the structure of the model.

4.1.1 Time series operators

In this subsection the time series operators used to formulate stochastic models in the following are defined. The notation follows that of Box & Jenkins (1976) and Madsen (1989).

Let y_t, $t = 1, \ldots, N$ denote the time series of a given variable. The back-shift operator or lag operator B plays a fundamental role in the mathematics of time series analysis. It is defined by the transformation

$$By_t = y_{t-1} \tag{4.1}$$

Applying B to y_{t-1} yields $By_{t-1} = y_{t-2}$, and so, in general,

$$B^\tau y_t = y_{t-\tau} \tag{4.2}$$

The order of the lag operator, τ, only takes integer values, and $B^0 y_t = y_t$ in order to complete the definition.

A polynomial in the back-shift operator takes the form

$$\Phi(B) = 1 + \phi + \ldots + \phi^q \tag{4.3}$$

where $\phi, \ldots, \phi$ are parameters or constants. The roots of such a polynomial are defined as the q values of B which satisfy the polynomial equation

$$\Phi(B) = 0 \tag{4.4}$$

The first-difference operator is defined as

$$\Delta = 1 - B \tag{4.5}$$

Thus, $\Delta y_t = y_t - y_{t-1}$. The root of $\Delta = 0$ is equal to unity. Similar to (4.5) the seasonal difference operator is defined

$$\Delta_S = 1 - B^S \tag{4.6}$$

where S is the length of the season, i.e. the number of observations in a periodic cycle.

4.2 Stochastic components

A stochastic model is based on certain probabilistic assumptions, which attempt to capture the essential characteristics of the data generation process. For this purpose the stochastic model can be structured in a way similar to the underlying mechanisms of the process being modelled. Structural time series models are built up by formulating stochastic components which, when combined, give forecasts of the expected form. The stochastic components are autoregressive models, trend, cyclic effects, type-of-day effects and explanatory variables, each of which are dealt with in the following subsections. Combining the different types of models of the different components yields an infinite number of models. Thus, formulating a structural time series model requires a somewhat goal-directed iterative search in the infinite class of structural time series models.

The structural components are often assumed to have an additive effect on y_t. A typical time series model consisting of a trend and a cyclic effect would thus be decomposed in the following form:

Observed series=trend+cyclic+irregular

where the "irregular" component reflects non-systematic movements in the series. Sometimes, a multiplicative form:

Observed series=trend×cyclic×irregular

may prove more appropriate. However, a multiplicative model may be handled within the additive framework by a logarithmic transformation of data.

4.2.1 Autoregressive models

A stochastic process in which the current value, y_t, depends on the previous value, y_{t-1}, and a white noise disturbance term, ε_t, is known as an autoregressive process. It may be written

$$y_t = -\phi y_{t-1} + \varepsilon_t \tag{4.7}$$

where ε_t is an identical independent distributed (i.i.d.) sequence with mean zero and variance σ^2, and ϕ is a parameter. Although the time series is first observed at time $t = 1$, the process is regarded as having started at some time in the remote past. If $\phi = 1$ the process (4.7) is known as a random walk.

If $|\phi| < 1$, the process hovers around a constant mean of zero, and is said to be stationary. Likewise, when $|\phi| \geq 1$, the influence of the noise

disturbance does not diminish over time, and the process is said to be instationary. The process defined in (4.7) is a first-order autoregressive model or AR(1)-model.

It is straight forward to extend the model so that y_t depends on several lagged values. Thus, the AR(p)-model is defined as

$$y_t = \sum_{i=1}^{p} -\phi_i y_{t-i} + \varepsilon_t \tag{4.8}$$

Using the polynomial notation introduced in (4.3), the AR(p)-model (4.8) takes the form

$$(1 + \phi_1 B + \ldots + \phi_p B^p) y_t = \varepsilon_t \tag{4.9}$$

Model identification using autoregressive models requires determination of the order p of the AR-model, and subsequently estimation of the appropriate parameters of the order p.

In order for the process to be stationary, the p roots of $\Phi(B)$ satisfying (4.4) must all have a modulus greater than one. For certain values of the parameters, $\phi_1, \ldots, \phi_p$, the roots of the polynomial are complex, which reflects the fact that the process exhibits some kind of oscillatory behaviour.

The autoregressive model (4.9) is often extended to include a moving average (MA) of the error terms ε_t,

$$(1 + \phi_1 B + \ldots + \phi_p B^p) y_t = (1 + \theta_1 B + \ldots + \theta_q B^q) \varepsilon_t \tag{4.10}$$

but the use of MA-terms have not been employed in the present context due to unstability of the estimation procedure.

Multivariate autoregressive models are formulated similar to (4.8) with y_t being a vector of length k and ϕ_i a matrix at dimension $k \times k$. In fact, the one-dimensional AR(p)-process in (4.8) can be formulated as a p-dimensional AR(1)-process and a k-dimensional AR(p)-process can be formulated as a $k \times p$-dimensional AR(1)-process (for details, see Harvey (1981b) or Appendix C).

4.2.2 Trend

The trend has often been used to characterize the long term change in mean which can be extrapolated into the future. Granger (1966) defines "trend in mean" as comprising all frequency components whose wavelength exceeds the length of the observed series. In the classical time series analysis time series were made stationary by detrending or differencing. However, a trend can be modelled as a structural component which may describe both short-term and long-term movements in the time series, for instance by introducing appropriate smoothing constants.

The simplest structural component used to model a trend, μ_t, is the deterministic linear trend

$$\mu_t = \alpha + \beta t \tag{4.11}$$

This deterministic trend may be converted into a stochastic trend by letting α and β be given by stochastic autoregressive models as described in the previous subsection (e.g. random walks). A more satisfactory model is obtained by working directly with the current level, μ_t, rather than the intercept. Since μ_t may be obtained recursively from

$$\mu_t = \mu_{t-1} + \beta \tag{4.12}$$

with $\mu_0 = \alpha$. Stochastic terms may be introduced by letting β be a stochastic process or by adding noise.

$$\mu_t = \mu_{t-1} + \beta_{t-1} \tag{4.13}$$

The scale parameter of the trend, β_t, can be modelled by combining all the structural components presented in this section. The model (4.13) can be used to describe both local and global trends in the mean by formulating the appropriate model for β_t.

4.2.3 Cyclic effects

Some time series exhibit variation at a fixed period due to some physical cause or human behaviour. These cycles may be due to diurnal variations, weekly variations, monthly variations, yearly variations, or another periodic cycle reflected in the data induced by an external physical phenomenon. In addition some time series exhibit oscillations which do not have a fixed period but which are predictable to some extend (e.g. the prey/predator population of animals or sunspot activity).

When formulating a model for periodic cyclic phenomena it is required that the cyclic effects sum to zero if the model contains another parameter for the mean. If a time series exhibits cyclic behaviour with a period of S samples the cyclic effect can be modelled using S dummy variables, which always sum to zero, i.e.

$$\sum_{i=0}^{S-1} \gamma_{t-i} = 0 \tag{4.14}$$

By introducing a disturbance term with zero mean expectation into the right-hand side of this equation, the seasonal effects can be allowed to change stochastically over time. Formally, the model is:

$$\gamma_t = \sum_{i=1}^{S-1} \gamma_{t-i} + \varepsilon_t \tag{4.15}$$

Unfortunately, for large values of S, the formulation of a structural model with a cyclic effect as given in (4.15) requires a large number of parameters which might conflict with the concept of parsimony given in Section 4.1.

Alternatively, let ρ_t be a cyclical function of time with a period of S measured in samples. Such a cycle can be expressed as a mixture of sine and cosine waves. The simplest trigonometric function used to describe the periodic cycle is:

$$\rho_t = \alpha \cos 2\pi t/S + \beta \sin 2\pi t/S \tag{4.16}$$

where $(\alpha^2+\beta^2)^{\frac{1}{2}}$ is the amplitude of the wave and $\arctan(\beta/\alpha)$ is the phase. The trigonometric function can be extended to include multiple higher-order frequencies or overtones to describe cyclic phenomena deviating from a pure "single-tone" model as (4.16).

$$\rho_t = \sum_{i=1}^{S/2} (\alpha_i \cos \frac{2\pi it}{S} + \beta_i \sin \frac{2\pi it}{S}) \tag{4.17}$$

When S is even, the sine term disappears for $i = S/2$ and so the number of trigonometric parameters, the α_i's and β_i's, is always $S-1$, which is the same as the number of coefficients in the dummy variable formulation. However, the number of parameters in (4.17) can be reduced by bringing only a limited number of the higher order frequencies into the model formulation. The sufficient number of overtones for describing the cyclic behaviour can be determined by use of statistical tools presented in Section

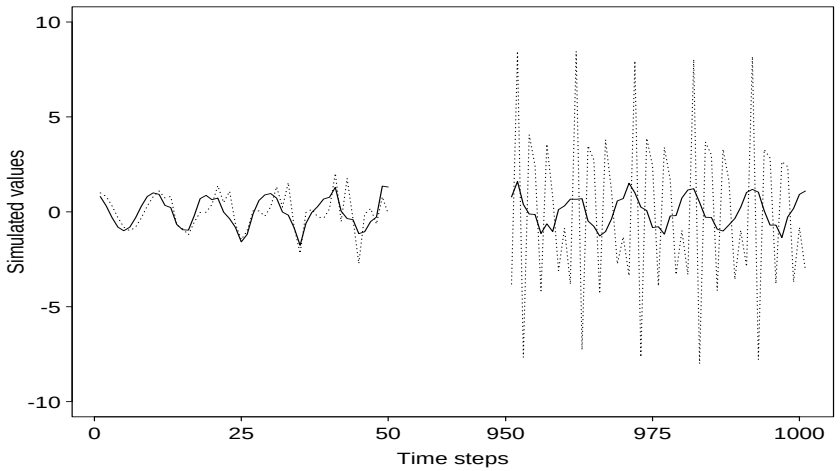

Figure 4.2. *Simulations of cyclic effects using the Fourier-expansion (solid line) and the model of dummy variables (dotted line).*

4.8. In order to make (4.16) and (4.17) stochastic, a noise term, ε_t, is added on the right-hand side.

One major advantage of formulating the periodic variation by use of trigonometric functions instead of dummy variables comes when the observations are irregularly sampled, i.e. the time between observations is not constant. Though,the two types of models have different adaptivity to cyclic effects. While (4.17) consists of deterministic functions and therefore the cyclic effect does not change its form, (4.15) can easily adapt to changes in the periodic phenomenon. This is illustrated in Figure 4.2, where the two models have been simulated using the same random innovation sequence. The model of dummy variables clearly have changed its form from a pure cosine wave to a very different but still periodic signal.

Periodic variations can also be modelled using the autoregressive models described in Section 4.2.1 which are known as seasonal AR-models. Thus, a seasonal AR(1)-model takes the form

$$y_t = -\phi_S y_{t-S} + \varepsilon_t \tag{4.18}$$

where ε_t is an i.i.d. sequence with mean zero and variance σ^2, and ϕ_S is a parameter. Likewise, the seasonal AR(P)-model takes the form

$$y_t = \sum_{i=1}^{P} -\phi_{iS} y_{t-i\cdot S} + \varepsilon_t \tag{4.19}$$

and when using the polynomial notation

$$(1 + \phi_S B^S + \ldots + \phi_{PS} B^{PS}) y_t = \varepsilon_t \tag{4.20}$$

In order for this process to be stationary the P roots of B^S satisfying $\Phi_S(B^S) = 0$ must all have a modulus greater than one. By combining the AR(p)-model with the seasonal AR(P)-model in a multiplicative fashion, the well-known multiplicative autoregressive seasonal model or AR(p)$\times$AR(P)$_S$-model arises (see Box & Jenkins (1976)).

4.2.4 Type-of-day effects

Time series related to human behaviour often show different variations on different types of days. The important task is to find the number of different types of day in a week, and categorize the days of the week. For example, all weekdays are alike, but Saturdays and Sundays are different. In this case, there are three categories of days to be modelled. This situation can, however, be further simplified by assuming that Saturdays and Sundays are alike, which reduces the types of days to weekdays and weekends. Holidays show the same pattern as Sundays due to close-down of industries, etc. and are categorized as such.

Let $\omega_{weekday,t}$ and $\omega_{weekend,t}$ denote the type-of-day effects for the two separate classes of days with the restriction that only one of them affects the observation at any particular point in time. Using type-of-day effects in the formulation of a model it is required that the effects sum to zero over a week if the model contains another parameter for the mean, due to the identifiability of the model. Thus, in this case

$$k_{weekday} \cdot \omega_{weekday,t} + k_{weekend} \cdot \omega_{weekend,t} = 0 \tag{4.21}$$

where $k_{weekday} = 5$ (number of weekdays) and $k_{weekend} = 2$ (number of weekend days). Another approach is to characterize the mean by two parameters, $\mu_{weekday}$ and $\mu_{weekend}$. The type-of-day effects, $\omega_{weekday,t}$ and $\omega_{weekend,t}$ can be formulated as stochastic models (e.g. random walks) with the restriction (4.21) in mind. For further details about type-of-day effects, see Harvey (1989).

4.2.5 Explanatory variables

So far the variable y_t has been modelled in terms of past values of itself and its position with respect to time. Suppose now that the information set is expanded to include l observable variables, and that these variables are able to explain some of the movements in y_t. The additional variables are considered exogenous if there is no feedback between them and the dependent variable, y_t. If the explanatory variables, $\boldsymbol{u}_t$, are exogenous and the relationship between $\boldsymbol{u}_t$ and y_t is linear, the model may be written as:

$$y_t = \boldsymbol{\delta}^T \boldsymbol{u}_t + \varepsilon_t \tag{4.22}$$

The vector $\boldsymbol{\delta}$ of length l contains the parameters associated with the explanatory variables. More generally, the explanatory variables may also be

used in describing the trend, cycles or type-of-day effects, and the relationship between y_t and $\boldsymbol{u}_t$ need not be linear. Lagged values of the explanatory variables may also enter the $\boldsymbol{u}_t$-vector despite the index.

4.3 Identifiability

The question of identifiability is a fundamental one in stochastic modelling. Loosely speaking, the problem is whether the identification procedure will yield unique values of the parameters of the model structure given the data. In order to give the standard definition of identifiability of the statistical literature it is important to distinguish between a model and a structure. A model specifies a distribution for y_t while a structure specifies the parameters determining that distribution. Given this background, the following concepts may be defined:

(a) If two models based on different structures have the same joint density function they are said to be observationally equivalent.

(b) A structure is identifiable if there exists no other observationally equivalent structure.

(c) A model is identifiable if its structure is identifiable.

The concepts above are also known as theoretical identifiability. In order to illustrate the concept of identifiability, consider the Monod-kinetic expression in (2.4), which includes two variables (S_n and X_B) and three parameters (μ_{max}, Y_{obs}, and K_S). A simultaneous identification of μ_{max} and Y_{obs} is not feasible for obvious reasons and at least one of these parameters needs to be fixed or regarded as constant. With the observed yield coefficient, Y_{obs}, set to a constant value, the model (2.4) is actually theoretically identifiable if X_B can be measured.

Identifiability has an immediate bearing on estimation. If two structures are observationally equivalent (i.e. have the same joint density function),

the probability of generating a particular set of observations is the same for both structures. Thus, there is no way of differentiating between them on the basis of data. Furthermore, it will often be the case that attempts to estimate models which are not identifiable will run into practical difficulties.

This leads to another question of identifiability: the practical identifiability. This issue involves aspects on whether the data set is informative enough (persistently excited) to distinguish between different models (i.e. could the dataset result from two different distributions with the same probability). If so, will different sets of values of the parameters give equal models? Holmberg & Ranta (1982) have shown that the parameters of a Monod-type model similar to (2.11) with $\mu_{max,A}$ and Y_{obs,NH_4^+} modelled as one parameter is not always practically identifiable even though it is theoretically identifiable. The simulated data set, however, only included a limited number of observations. The practical identifiability of the parameters is also referred to as the identification of parameters in the following.

4.4 Grey box modelling of wastewater processes

The basis for the grey box modelling approach is the prior available information about the processes to be modelled. This knowledge can be expressed in a multitude of ways, e.g. as parameter values or model structure. It is important to include the prior knowledge in the modelling in order to improve the precision and interpretability of the parameters that are to be estimated. The concept of grey box modelling is illustrated in Figure 4.3, where the grey box models cover the broad area between the "white" deterministic models and the black box models. The grey box modelling is approached from both sides of the scale, but the models in the present context are obtained starting from the black box side and gradually incorporating more physical knowledge of the system. In Carstensen et al. (1992) grey box models of the wastewater processes were found to perform significantly better than the traditional ARMAX-model (see Ljung (1987)).

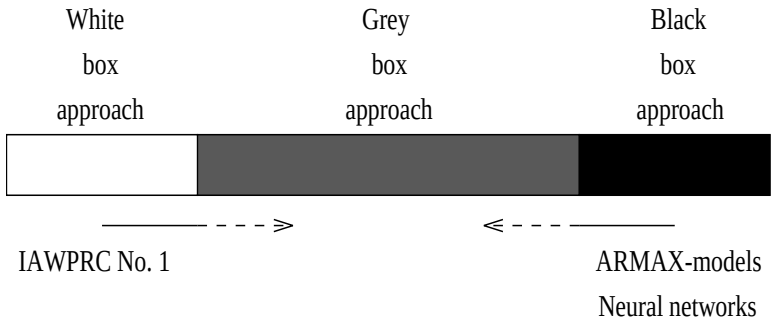

Figure 4.3. *The spectrum of models - from deterministic models over grey box models to black box models.*

The tools used for the grey box modelling are the structural components described in Section 4.2, which are combined in order to bring the physical knowledge into the models.

In this section grey box modelling of the wastewater processes described in the two previous chapters is concerned. Modelling these processes is done by combining the theory of the processes with significant effects found in data. By this approach the important terms of the differential equations given in Chapter 2 and 3 are extracted and lacks of these deterministic terms to describe data are compensated for by adding noise to the equations, i.e. by formulating stochastic models.

In this thesis modelling of the processes for the ammonia, nitrate, and phosphate concentrations is concerned. Other processes including oxygen concentrations and suspended solids (SS) concentrations are assumed to be perfectly controllable through control of aerators and return sludge pumping and used as explanatory variables. The influent flow, however, is not controllable, but if measurements are available the influent flow may serve as explanatory variable, too. Furthermore, control signals for the weirs and gates of the WWTP are used as explanatory variables.

Let y_t denote the measured concentration of the dependent variable, i.e. the concentration of ammonia, nitrate, or phosphate. The measured concentration is naturally encumbered with some uncertainty due to the measuring system. In the following the notation $t = 1, \ldots, N$ has been left out, but it is implicitly assumed unless otherwise stated. Thus, with the assumption of an additive noise structure

$$y_t = m_t + \nu_t \tag{4.23}$$

where m_t is the true concentration and ν_t is an i.i.d. sequence of measurement errors with mean zero and variance σ_ν^2. If explanatory variables, $\boldsymbol{u}_t$, are able to explain some of the movements in y_t in an additive way, the equation get this form:

$$y_t = m_t + \boldsymbol{\kappa}^T \boldsymbol{u}_t + \nu_t \tag{4.24}$$

where $\boldsymbol{\kappa}$ contains the parameters associated with the elements of $\boldsymbol{u}_t$. The equations (4.23) and (4.24) are referred to as observational equations. Figure 4.4 shows a time series of measurements of ammonia, nitrate, and phosphate concentrations in the aeration tank from the Aalborg West WWTP. The alternating operation mode of the BIO-DENIPHO process is clearly recognized from the curves.

The upward and downward slopes of the curves may be considered as local trends with a steepness determined by the biological and hydraulic processes taking place in the tank. In fact, the wastewater processes directly affect the change in concentration of ammonia, nitrate, or phosphate and thereby indirectly the absolute concentration. This can be formulated in the following way:

$$m_t = m_{t-1} + \mu_t + \eta_t \tag{4.25}$$

or

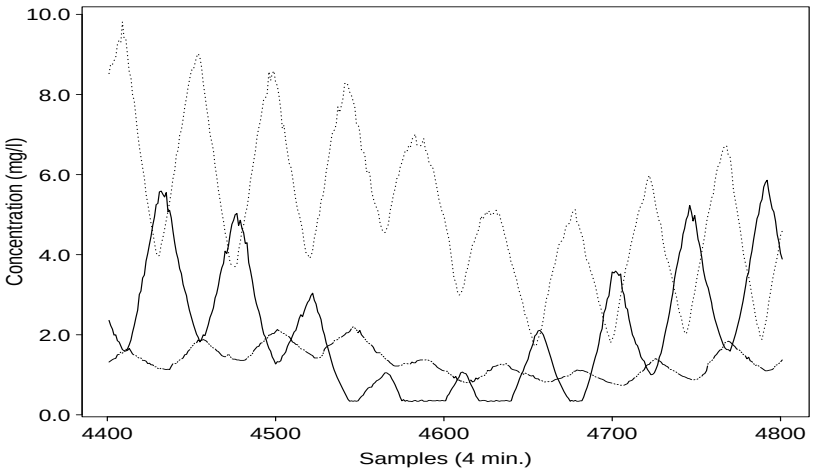

Figure 4.4. *Online measurements of ammonia (solid curve), nitrate (dotted curve), and phosphate (dashed curve) concentrations from Aalborg West WWTP. The operation of the plant follows the BIO-DENIPHO scheme.*

$$\Delta m_t = \mu_t + \eta_t \tag{4.26}$$

where μ_t is the mean process rate determined by the biological and hydraulic processes active at time t, and η_t is an additive noise structure which can be modelled as an autoregressive model of order p

$$\eta_t = \sum_{i=1}^{p} -\phi_i \eta_{t-i} + e_t \tag{4.27}$$

where e_t has zero mean and variance σ_e^2. The model (4.27) describes the time-wise correlation in η_t, which is the error arising from explaining the change in the true concentration Δm_t by the mean process rate μ_t. Incorporating prior knowledge of the biological and hydraulic processes into the modelling of μ_t is dealt with in the following subsection.

Combining (4.26) and (4.27) yields the following equation:

$$(1 + \phi_1 B + \ldots + \phi_p B^p)(\Delta m_t - \mu_t) = e_t \tag{4.28}$$

when using the polynomial notation of the autoregressive model. If explanatory variables, $\boldsymbol{u}_t$, are used to explain some of the movements in Δm_t in an additive way, the equation looks like this:

$$(1 + \phi_1 B + \ldots + \phi_p B^p)(\Delta m_t - \mu_t) = \boldsymbol{\delta}^T \boldsymbol{u}_t + e_t \tag{4.29}$$

where $\boldsymbol{\delta}$ contains the parameters associated with the elements of $\boldsymbol{u}_t$. The equations above (4.28) and (4.29) are referred to as the process equations.

Using Δm_t in the process equation is very reasonable for a grey box modelling approach. The reason for this is, that the theory of the biological and hydraulic processes use differential equations to describe the variation of these processes. Hence, if sampling is carried out relatively fast compared to the rates of these processes, then

$$\Delta m_t \approx \frac{dm}{dt} \cdot T_S \tag{4.30}$$

is a reasonable approximation with T_S being the time between samples. Therefore, Δm_t approximates the left-hand side of the theoretical differential equations described in Chapter 2 and 3 and μ_t may contain expressions approximating the right-hand side of these differential equations. This will become more obvious in the following subsection.

4.4.1 Modelling the mean process rate

The amount of biological processes taking place in the aeration tank of a WWTP is tremendous, and only a very limited number of these processes

can actually be identified from statistical analysis of data. For the data considered in this thesis, the following processes have been identified:

Hydraulic processes:

- Influent load to aeration tanks ($r_{load,t}$)
- Nutrient transport of the aeration tanks ($r_{transport,t}$)

Biological processes:

- Hydrolysis and growth of biomass ($r_{hydrolysis,t}$)
- Nitrification ($r_{nit,t}$)
- Denitrification ($r_{denit,t}$)
- Biological phosphate uptake in biomass ($r_{P-uptake,t}$)
- Stripping of phosphate ($r_{P-strip}$)

The rates of these processes, denoted by $r_{<process>}$, are assumed to have an additive effect and no interaction effect on μ_t. The three time series of ammonia, nitrate, and phosphate concentrations are not influenced by all of the processes. The ammonia concentration is influenced by the influent load of ammonia, transport of ammonia between the alternating tanks and clarifier, hydrolysis of ammonia, and nitrification of ammonia. Hence, for the time series of ammonia concentrations

$$\mu_{NH_4^+,t} = r_{load,NH_4^+,t} + r_{transport,NH_4^+,t} + r_{hydrolysis,NH_4^+,t} + r_{nit,NH_4^+,t}, \tag{4.31}$$

For the time series of nitrate concentrations, where the nitrate concentration of the influent is assumed to be negligible

$$\mu_{NO_3^-,t} = r_{transport,NO_3^-,t} + r_{nit,NO_3^-,t} + r_{denit,t} \tag{4.32}$$

and for the time series of phosphate concentrations without chemical precipitation

$$\mu_{PO_4^{3-},t} = r_{load,PO_4^{3-},t} + r_{transport,PO_4^{3-},t} + r_{hydrolysis,PO_4^{3-},t} + r_{P-uptake,t} + r_{P-strip,t} \quad (4.33)$$

The processes influencing μ_t above are active ($r_{<process>,t} \neq 0$) when certain conditions are present in the aeration tanks and inactive ($r_{<process>,t} = 0$) if these conditions are not present. For the processes above affecting more than one time series of concentrations, the influence on the different time series is indicated by indexing the rate with the formula of the concentration being affected. Sometimes, when more than one time series can be used as index, this is marked with a period (.).

Influent load

The raw wastewater entering the biological part of a WWTP mainly consists of organic materials, ammonia, and phosphate. It is mixed with returned sludge, which is assumed to have a vanishing concentration of soluble nutrients, i.e. ammonia, nitrate, and phosphate. The raw wastewater mixed with returned sludge is led into the aeration ditches of the BIO-DENITRO and BIO-DENIPHO processes mainly during the anoxic phase of the specific tank.

Due to the alternating operation mode each of the tanks is only influenced by influent flow half the time of a total operation cycle. Thus, the theory of a step-function load given in (3.5) apply. Despite a highly time-varying flow to the plant the concentration in the tank will increase approximately at a constant rate as illustrated in Figure 3.6, because the influent flow phases are kept for a short time relative to the average hydraulic retention time of the aeration ditch. This is also verified by inspecting the measurements of ammonia and phosphate concentrations in Figure 4.4. Naturally, the load rate is dependent of the flow rate which normally does not change

significantly during the inlet phase of an operation cycle, but certainly shows significant variations over a 24 hours period, see Figure 3.1. Thus,

$$r_{load,NH_4^+,t} = \begin{cases} k_{load,NH_4^+} \cdot Q_{t-1} & \text{inlet gate open} \\ 0 & \text{inlet gate closed} \end{cases} \quad (4.34)$$

where Q_{t-1} is the influent flow rate to the tank and k_{load,NH_4^+} is a parameter. The reason for using lagged values of Q_t in (4.34) will be explained in the following. However, k_{load,NH_4^+} will be allowed to vary from one operation cycle to another, as will be described in the following. A similar expression to (4.34) holds for the load process of phosphate with the parameter $k_{load,PO_4^{3-}}$.

Differentiating the step-load response function (3.5) with respect to time and using the fact that C_0 is in general very small relative to the average inlet concentration $\overline{C}_i$ for both ammonia and phosphate, the following approximations appears from using (3.3) and (4.30) on (4.34)

$$k_{load,NH_4^+} \approx \frac{\overline{C}_{i,NH_4^+}}{V} \cdot T_S \quad (4.35)$$

and the similar process rate equation for phosphate concentrations

$$k_{load,PO_4^{3-}} \approx \frac{\overline{C}_{i,PO_4^{3-}}}{V} \cdot T_S \quad (4.36)$$

where T_S is the time between samples.

Thus, estimating k_{load,NH_4^+} and $k_{load,PO_4^{3-}}$ from the inclining curves of ammonia and phosphate concentrations and knowing the volume V of the tank, an estimate of the average influent concentration of ammonia and phosphate to the aeration ditch is found. For the BIO-DENITRO process these estimates are equivalent with the concentration of ammonia and phosphate where the mixing of raw wastewater and returned sludge takes

place, and estimates of the ammonia and phosphate (no chemical precipitation is assumed) concentrations in the raw wastewater may be obtained if flow rates of the raw wastewater and returned sludge are available. For the BIO-DENIPHO process these estimates are equivalent with the ammonia and phosphate concentration of the anaerobic pretreatment tank, and, similar to the BIO-DENITRO process, the ammonia concentration in the raw wastewater can be estimated by knowing the flow rates of the raw wastewater and returned sludge. Such an estimate of the phosphate concentration can, however, not be obtained, due to the lack of information on the stripping of phosphate in the anaerobic tank.

Municipal wastewater mainly originates from households, and it is often found that the load of organic materials, ammonia, and phosphate are correlated (this can also be verified by comparing Table 3.1 and Table 3.2). Thus, k_{load,NH_4^+} and $k_{load,PO_4^{3-}}$ can be used as an indicator of the level of organic materials in the raw wastewater for the BIO-DENITRO process. Naturally, only k_{load,NH_4^+} can be used as indicator for the BIO-DENIPHO process.

Nutrient transport of the aeration tanks

In order to give interpretable estimates of the processes to be modelled the mass balance of nutrients needs to be taken into account. However, it is difficult to give an exact theoretical model for the hydraulic effects between the two alternating tanks in the BIO-DENITRO and BIO-DENIPHO processes because of the continuous switching of flow pattern in the WWTP, see Figure 3.3 and 3.4. The two alternating tanks are operated at different levels of wastewater in the tanks in such a way, that in general the tank with influent flow has the highest level of wastewater while the tank with effluent flow has the lowest level of wastewater. When switching influent and effluent flow between the tanks it takes a while before the flow between the two tanks changes. The hydraulic effects of the two tanks are determined by the flow and the control of inlet and outlet weirs.

Assuming that the flow pattern has reached a steady state for the main phases of the BIO-DENITRO process (phase A and phase C on Figure 3.3) and the BIO-DENIPHO process (phase B (and phase C) on Figure 3.4), the differential equation for the transport of materials (3.4) apply. Combining this with the approximation (4.30) yields for the transport of ammonia in the tank with effluent flow:

$$r_{transport,NH_4^+,t} = \begin{cases} k_{transport,NH_4^+}(S^I_{NH_4^+,t-1} - S_{NH_4^+,t-1}) \cdot Q_{t-1} & \text{outlet gate open} \\ 0 & \text{outlet gate closed} \end{cases} \tag{4.37}$$

where $S^I_{NH_4^+,t}$ is the ammonia concentration in the tank with influent flow, $S_{NH_4^+,t}$ is the ammonia concentration in the tank with effluent flow, Q_t is the influent flow rate, and $k_{transport,NH_4^+}$ is a parameter. Similar expressions hold for the transport of phosphate in the tank with effluent flow.

The transport of ammonia and phosphate in the tank with influent flow was modelled as a load process for the transport of ammonia and phosphate by which the influent concentration of ammonia and phosphate could be estimated. The nitrate concentration in the influent flow was assumed to be vanishing and as such not estimated as a load process. There is, however, still a transport of nitrate from the tank which can be modelled similar to (4.37) by setting $S^I_{NO_3^-,t} = 0$. Thus, the transport of nitrate is given by

$$r_{transport,NO_3^-,t} = \begin{cases} k_{transport,NO_3^-}(S^I_{NO_3^-,t-1} - S_{NO_3^-,t-1}) \cdot Q_{t-1} & \text{inlet gate closed and outlet gate open} \\ -k_{transport,NO_3^-} \cdot S_{NO_3^-,t-1} \cdot Q_{t-1} & \text{inlet gate open} \\ 0 & \text{otherwise} \end{cases} \tag{4.38}$$

where $k_{transport,NO_3^-}$ is the transportation parameter for nitrate. The transport of nutrients between the two alternating tanks in phase B and

phase D (Figure 3.3) of the BIO-DENITRO process and phase A (Figure 3.4) of the BIO-DENIPHO process is neglected.

If measurements of ammonia concentrations are only obtained from one of the aeration ditches (the tank with effluent flow in (4.37)), an estimator of $S^I_{NH_4^+,t}$ is the ammonia concentration in the monitored tank half an operation cycle ago, due to the alternating operation model (see Figure 4.4). This estimator can also be applied for nitrate and phosphate concentrations.

Comparing the transportation rates above with (3.4) and using (4.30) it might be argued, that $k_{transport,\cdot} \approx \frac{T_S}{V}$, where V is the volume of the aeration tank. However, due to the lack of information on the hydraulic effects when switching the flow pattern and the relative smaller significance of the process compared to some of the biological processes, $k_{transport,\cdot}$ is estimated instead of being fixed to $\frac{T_S}{V}$. Estimating $k_{transport,\cdot}$ serves for testing the model formulation of the nutrient transport process.

Hydrolysis and growth of biomass

Hydrolysis is a joint designation for many biochemical processes transforming larger organic molecules from the raw wastewater or dead biomass into smaller digestible organic compounds, ammonia, and phosphate as described in Section 2.1.1. The rate of the hydrolysis is best identified when most of the other processes listed above are in-activated in some periods of the time series and the load has been stable for a while. The rate, however, also includes the rate of the simultaneous uptake of ammonia and phosphate used for bacterial growth not associated with any of the other biological processes. Because the two processes, hydrolysis and bacterial growth, are simultaneous, the two process rates cannot be separately identified. Hence, the rates of the two processes together are considered as one process rate - a net hydrolysis rate.

The processes of hydrolysis and growth of biomass are always present in the reaction tanks, but the rates of the processes vary a lot depending on what substrate is available. Both processes will affect the ammonia

and phosphate concentrations by producing and removing ammonia and phosphate, respectively. Normally, the rate of the hydrolysis process is larger than the simultaneous rate of ammonia and phosphate uptake for growth of biomass.

In the deterministic theory of the processes establishing the system of differential equations to describe the processes would require a great number of parameters and assumptions of the load of hydrolysable compounds. In a statistical sense this would lead to fatal over-parameterization. For the time series used in this thesis only one parameter may be used for the identification of the net hydrolysis rate, $r_{hydrolysis,NH_4^+,t}$ for the time series of ammonia concentrations and $r_{hydrolysis,PO_4^{3-}}$ for the time series of phosphate concentrations.

Thus, $r_{hydrolysis,\cdot,t}$ may be modelled as being constant throughout the time series or proportional to another component, e.g. the load rate of ammonia

$$r_{hydrolysis,NH_4^+,t} = k_{hydrolysis,NH_4^+} \cdot k_{load,NH_4^+} \cdot Q_{t-1} \tag{4.39}$$

and

$$r_{hydrolysis,PO_4^{3-},t} = k_{hydrolysis,PO_4^{3-}} \cdot k_{load,NH_4^+} \cdot Q_{t-1} \tag{4.40}$$

The load rate of phosphate may also be used for the BIO-DENITRO process, if there is no chemical precipitation.

The nitrification process

During the aerobic phase of the operation cycle of the BIO-DENITRO and BIO-DENIPHO processes ammonia is removed and nitrate is produced by the nitrification process. The theory of the process was given in Section 2.3. However, no methods for measuring the concentration of autotrophic biomass exist and therefore the suspended solids concentration, $X_{SS,t}$, is used as a correlated measure.

Following the discussion in Section 4.3, it is clear that the maximum specific growth rate of autotrophic bacteria, $\mu_{max,A}$, and the observed biomass yield coefficients, Y_{obs,NH_4^+} and Y_{obs,NO_3^-}, in (2.11) and (2.12) are not theoretically identifiable. Thus, from the declining curves of ammonia concentrations, as depicted in Figure 4.4, the following rate expression can be identified:

$$r_{nit,NH_4^+,t} = \begin{cases} -k_{nit,max,NH_4^+} \cdot \frac{S_{NH_4^+,t-1}}{S_{NH_4^+,t-1}+K_{NH_4^+}} \cdot \frac{S_{O_2,t-1}}{S_{O_2,t-1}+K_{O_2}} \cdot X_{SS,t-1} & \text{aerobic conditions} \\ 0 & \text{anoxic/anaerobic conditions} \end{cases} \tag{4.41}$$

and from the inclining curves of nitrate concentrations, also depicted in Figure 4.4, the following expression can be identified:

$$r_{nit,NO_3^-,t} = \begin{cases} k_{nit,max,NO_3^-} \cdot \frac{S_{NH_4^+,t-1}}{S_{NH_4^+,t-1}+K_{NH_4^+}} \cdot \frac{S_{O_2,t-1}}{S_{O_2,t-1}+K_{O_2}} \cdot X_{SS,t-1} & \text{aerobic conditions} \\ 0 & \text{anoxic/anaerobic conditions} \end{cases} \tag{4.42}$$

The reason for using lagged values on the right-hand side of (4.41), (4.42), and also in the previous rate expressions for the influent load process and the transport of nutrients is twofold. Firstly, the change in concentration due to the nitrification process from $t-1$ to t is determined by the state of the process at $t-1$ (i.e. using the state of the process at time t in (4.41) and (4.42) would result in a non-causal process). Secondly, making the rate expression conditional on past values facilitates the estimation of the parameters as will be explained later.

Using lagged values in the Monod-kinetic expression gives biased estimates of the half-saturation constants. Estimating $K_{NH_4^+}$ and K_{O_2} in (4.41) and (4.42) will likely give too high estimates of the half-saturation constants

in (2.11) and (2.12), because the process rate is only adjusted at the sample points in time for (4.41) and (4.42), while it is continuously adjusted in (2.11) and (2.12). In order to compensate for this lack of continuous adjustment of the process rate in discrete time a higher value of $K_{NH_4^+}$ and K_{O_2} in (4.41) and (4.42) will yield the same dynamics as in continuous time. If the time between samples, T_S, is small relative to the rate of the process, the bias of the estimated half-saturation constants will also be small, and if the time between samples approaches zero, the estimates of $K_{NH_4^+}$ and K_{O_2} will approach the values of (2.11) and (2.12) and become unbiased.

Comparing (4.41) and (2.11) and using the approximation (4.30) the following result is obtained:

$$k_{nit,max,NH_4^+} \approx \frac{\mu_{max,A}}{Y_{obs,NH_4^+}} \cdot \frac{\overline{X}_{B,A,t}}{\overline{X}_{SS,t}} \cdot T_S \tag{4.43}$$

and similarly when comparing (4.42) and (2.12):

$$k_{nit,max,NO_3^-} \approx \frac{\mu_{max,A}}{Y_{obs,NO_3^-}} \cdot \frac{\overline{X}_{B,A,t}}{\overline{X}_{SS,t}} \cdot T_S \tag{4.44}$$

Assuming that $X_{B,A,t}$ and $X_{SS,t}$ show similar dynamics and knowing the values of $\mu_{max,A}$, Y_{obs,NH_4^+}, and Y_{obs,NO_3^-}, two estimates of the average proportion over time of autotrophic biomass in the suspended sludge (suspended solids in the reaction tanks practically consists of suspended sludge) can be obtained. Unfortunately, in the literature many different values of especially $\mu_{max,A}$, but also Y_{obs,NH_4^+} and Y_{obs,NO_3^-} have been proposed (see Eckenfelder & Grau (1992) and Henze et al. (1990)). Thus, it is not possible to get an estimate of the average proportion of autotrophic biomass in the suspended sludge, since it will depend on constants with virtually unknown values. However, the approximations above can be utilized to assess the activity of the autotrophic biomass by letting k_{nit,max,NH_4^+} and k_{nit,max,NO_3^-} be time-varying, as will be explained in the following.

The denitrification process

During the anoxic phase of the operation cycle of the BIO-DENITRO and BIO-DENIPHO processes nitrate is transformed into nitrogen gas by the denitrification process. The theory of this process was given in Section 2.4. Similarly to the modelling of the nitrification process, the suspended solids concentration, $X_{SS,t}$, is used as a correlated measure of the concentration of heterotrophic biomass.

Likewise, no measuring equipment for on-line monitoring of the readily bio-degradable substrate concentration, S_S, is available at present, although much effort is put into the development of such a device. However, using the often found correlation between the ammonia concentration and the readily bio-degradable substrate concentration in the raw wastewater, the estimated load rate of ammonia may prove adequate of describing the readily bio-degradable substrate dependency of the denitrification process. This is based on the rather crude assumption that an approximately constant load rate of readily bio-degradable substrate will maintain an approximately constant S_S concentration in the reaction tank, i.e. the consumption of readily bio-degradable substrate is proportional to the load. Alternatively, the rate of the denitrification process is Monod-dependent of the influent load rate, $r_{load,NH_4^+,t}$ when the inlet gate is open, i.e. $k_{load,NH_4^+} \cdot Q_{t-1}$. Thus, from the declining curves of nitrate concentrations, as depicted in Figure 4.4 and because $\mu_{max,H}$ and Y_{obs,NO_3^-} in (2.15) cannot be theoretically identified, the following rate expression can be identified:

$$r_{denit,t} = \begin{cases} -k_{denit,max} \frac{S_{NO_3^-,t-1}}{S_{NO_3^-,t-1}+K_{NO_3^-}} \frac{k_{load,NH_4^+} Q_{t-1}}{k_{load,NH_4^+} Q_{t-1}+K_{load,NH_4^+}} X_{SS,t-1} & \text{anoxic conditions} \\ 0 & \text{aerobic/anaerobic conditions} \end{cases} \tag{4.45}$$

The reason for using lagged values on the right-hand side of (4.45) is similar to that of the nitrification process and was previously discussed.

Comparing (4.45) and (2.15) and using the approximation (4.30) under the assumption of using $r_{load,NH_4^+,t}$ as a correlated measure to S_S the following result is obtained:

$$k_{denit,max} \approx \frac{\mu_{max,H}}{Y_{obs,NO_3^-}} \cdot \frac{\overline{X}_{B,H,t}}{\overline{X}_{SS,t}} \cdot T_S \tag{4.46}$$

It should be noticed that the approximation is based on two assumptions of which one of them is rather crude. Thus, caution must be observed before making conclusions based on this approximation. Like before, the approximation (4.46) cannot be used for obtaining a valuable estimate of the average proportion of heterotrophic biomass, but it can be utilized to assess the activity of the heterotrophic biomass by letting $k_{denit,max}$ be time-varying. This is explained later.

Biological phosphate uptake in biomass

During the aerobic phase of the operation cycle of the BIO-DENIPHO process phosphate is intra-cellular stored as poly-phosphates in the biomass. The theory of the process was given in Section 2.5. Similar to the two previously described processes the suspended solids concentration, $X_{SS,t}$, is used as a correlated measure of the concentration of phosphate accumulating biomass, $X_{B,P,t}$.

Assuming that neither the oxygen concentration nor the readily bio-degradable substrate concentration are rate limiting and knowing that $\mu_{max,P}$ and $Y_{obs,PO_4^{3-}}$ are not theoretically identifiable, the following rate expression can be identified:

$$r_{P-uptake,t} = \begin{cases} -k_{P-uptake,max} \cdot \frac{S_{PO_4^{3-},t-1}}{S_{PO_4^{3-},t-1}+K_{PO_4^{3-}}} \cdot X_{SS,t-1} & \text{aerobic conditions} \\ -k'_{P-uptake,max} \cdot \frac{S_{PO_4^{3-},t-1}}{S_{PO_4^{3-},t-1}+K_{PO_4^{3-}}} \cdot X_{SS,t-1} & \text{anoxic conditions} \\ 0 & \text{anaerobic conditions} \end{cases} \quad (4.47)$$

where $k'_{P-uptake,max}$ is found to be significantly lower than $k_{P-uptake,max}$ in Kerrn-Jespersen & Henze (1993). The reason for using lagged values on the right-hand side of (4.47) is similar to that of the nitrification process and was previously discussed.

When comparing (4.47) and (2.19) by use of the discrete time sampling approximation (4.30), the following approximation appears:

$$k_{P-uptake,max} \approx \frac{\mu_{max,P}}{Y_{obs,PO_4^{3-}}} \cdot \frac{\overline{X}_{B,P,t}}{\overline{X}_{SS,t}} \cdot T_S \quad (4.48)$$

which provides information on the activity of the phosphate accumulating biomass in the activated sludge.

Stripping of phosphate

Anaerobic periods occasionally occur in the aeration tanks at the end of the anoxic period, when all nitrate is removed by the denitrification process and the aerators has not been turned on. In this situation the phosphorus accumulating bacteria will strip phosphate in order to uptake readily bio-degradable substrate as described in Section 2.5. The amount of phosphate stripped is given by (2.20), but lack of information on the concentration of readily bio-degradable substrate which can be accumulated directly in the phosphorus accumulating biomass and the rareness of the phosphate

stripping occurrences only makes the identification of a constant phosphate stripping rate, $k_{P-strip}$, possible:

$$r_{P-strip,t} = \begin{cases} k_{P-strip} & \text{anaerobic conditions} \\ 0 & \text{aerobic/anoxic conditions} \end{cases} \quad (4.49)$$

Furthermore, the anaerobic conditions occur in the tank with influent flow, and thereby influent load of ammonia and phosphate. Thus, the rate of the phosphate stripping process has to be identified on top of an influent load rate, $r_{load,PO_4^{3-},t}$.

4.4.2 Transient modelling

The switching of phases in the BIO-DENITRO and BIO-DENIPHO processes often introduce transient phenomena in the time series. This is due to hydraulic effects which have not been modelled in the previous section (transient dynamics from the switching of flow-patterns) and non-ideal mixing of the aeration tanks, and the uncertainty induced by the switching from aerobic to anoxic conditions and reverse.

Let the explanatory variable vector $\boldsymbol{u}_t$ be given by

$$\boldsymbol{u}_t = [I_t, O_t]^T \quad (4.50)$$

where

$$I_t = \begin{cases} 1 & \text{at time when the inlet gate is opened} \\ -1 & \text{at time when the inlet gate is closed} \\ 0 & \text{otherwise} \end{cases} \quad (4.51)$$

and

$$O_t = \begin{cases} 1 & \text{at time when the aerators are turned on} \\ -1 & \text{at time when the aerators are turned off} \\ 0 & \text{otherwise} \end{cases} \tag{4.52}$$

The vector $\boldsymbol{u}_t$ may be extended to include also lagged values of I_t and O_t. Functions of the same form as I_t and O_t are called interventions, a term which was introduced by Glass (1972) and that became popular through the work of Box & Tiao (1975).

The explanatory variable vector may affect both the observation equation through the parameter vector $\boldsymbol{\kappa}$ in (4.24) and the process equation through the parameter vector $\boldsymbol{\delta}$ in (4.29) in order to describe the transient phenomena. However, the transient is very different for the two methods. The influence of an intervention at time t in the observation equation only affects y_t at time t, while the influence of an intervention at time t in the process equation affects $\Delta m_t, \Delta m_{t+1}, \ldots$, with exponentially decreasing weights due to the autoregressive polynomial on the left-hand side of (4.29).

4.4.3 Operation cycle time domain

The alternating operation mode of the BIO-DENITRO and BIO-DENIPHO processes introduces natural break-points in the time series of ammonia, nitrate, and phosphate concentrations, which can be used in subsequently modelling of the wastewater processes described in Section 4.4.1. This is considered as a new time domain, where a given operation cycle (normally covering 2-4 hours of samples) is equal to one time-step. The time-points of the operation cycle domain are denoted by f, $f = 1, \ldots, N_f$, where N_f is the number of operation cycles in the time series. The start of the operation cycle for the given aeration tank is defined as the time where the influent flow starts. For the BIO-DENITRO process in Figure 3.3 the operation cycle starts at Phase D and ends at Phase C for Tank 1, and the operation cycle starts at Phase B and ends at Phase A for Tank 2. The operation cycle starts at Phase A in Tank 1 for the BIO-DENIPHO process depicted in Figure 3.4.

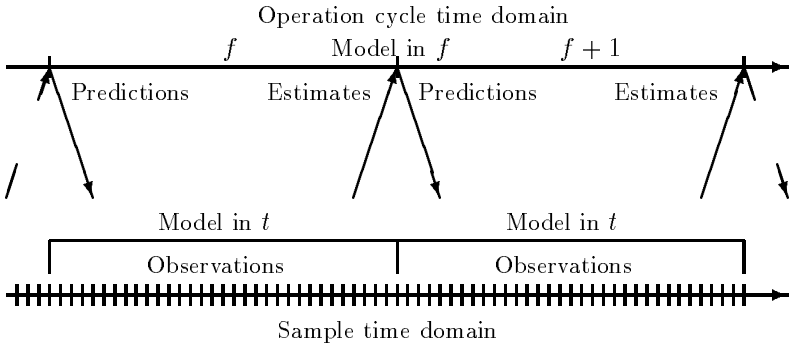

Figure 4.5. *The exchange of information between the sample time domain and the operation cycle time domain. Time of the exchange is determined by the operation scheme.*

Some of the parameters used to model the hydraulic and biological processes previously were assumed to be constant within an operation cycle in the sample time domain, though it was pointed out that these parameters were allowed to change from one operation cycle to another. The following three parameters from three different processes are modelled in the operation cycle domain,

- Influent load rate of nutrients
- Maximum nitrification rate
- Maximum denitrification rate

but the grey box models may be extended to include models in the operation cycle domain for some of the other parameters described in Section 4.4.1.

The interaction of the models in the sample time domain and the operation cycle time domain is illustrated in Figure 4.5. Once the operation cycle f is finished all the data from this single operation cycle is used to produce

estimates of the time-varying parameters listed above based on the models of the sample time domain. These estimates are considered as observations in the models of the operation cycle time domain, which bring new information to the process such that new predictions of the parameters are obtained. The predictions are then fed back as parameter values to the models in the sample time domain. This exchange of information between the models of the two time domains is resumed at the end of operation cycle $f+1$.

Influent load rate of nutrients

Looking at Figure 4.4 it is noted that the upward slopes of ammonia and phosphate concentrations are approximately constant within one operation cycle and vary between operation cycles. This is due to both a changing flow rate and changing influent concentrations of ammonia and phosphate. Information concerning the flow rate is obtained from on-line measurements of the very same and the influence on the slope was modelled in (4.34), while the influent concentration of ammonia and phosphate are estimated from the individual slopes of each operation cycle using (4.35). Thus, models for the variation of $k_{load,NH_4^+,f}$ (obtained from (4.34)) and $k_{load,PO_4^{3-},f}$ can be set up in the operation cycle time domain. Because the composition of the wastewater is mainly determined by human behaviour, a diurnal variation and a weekly variation is to be expected when disregarding rainy weather periods.

These cyclic variations can be modelled using a multiplicative seasonal AR(p)×AR(P)-model for the diurnal variation

$$\Phi_{load}(B)\Phi_{load,S}(B^S)(k_{load,\cdot,f}-\mu_{load,\cdot,f})=e_{load,\cdot,f} \tag{4.53}$$

where $e_{load,\cdot,f}$ has zero mean and variance $\sigma^2_{e,load,\cdot}$, and $\mu_{load,\cdot,f}$ describes the weekly variation as a type-of-day effect

$$\mu_{load,\cdot,f}=\begin{cases}\mu_{weekday,\cdot} & \text{if operation cycle } f \text{ is on a weekday}\\ \mu_{weekend,\cdot} & \text{if operation cycle } f \text{ is on a weekend}\end{cases} \tag{4.54}$$

where $\mu_{weekday,\cdot}$ is the mean load level on weekdays and $\mu_{weekend,\cdot}$ is the mean load level on weekends.

Alternatively, the daily variation can be modelled using a Fourier-expansion (4.17) of order s which gives the following model for the load process in the operation cycle time domain:

$$\Phi_{load}(B)(k_{load,\cdot,f}-\mu_{load,\cdot,t})=e_{load,\cdot,f} \tag{4.55}$$

where

$$\mu_{load,\cdot,t}=\begin{cases}\mu_{weekday,\cdot}\cdot\rho_t & \text{if the samples of the operation cycle are on a weekday}\\ \mu_{weekend,\cdot}\cdot\rho_t & \text{if the samples of the operation cycle are on a weekend}\end{cases} \tag{4.56}$$

and

$$\rho_t=\sum_{i=0}^{s}(\alpha_i\cos\frac{2\pi it}{T}+\beta_i\sin\frac{2\pi it}{T}) \tag{4.57}$$

where T is the number of samples in a day and $\alpha_0=1$.

The two alternative models for the mean load (4.53) and (4.55) are also known as the process equations for the load process in the operation cycle time domain. The autoregressive polynomial $\Phi_{load}(B)$ models the variation of $k_{load,\cdot,f}$ from one operation cycle to another. This is not incorporated in $\mu_{load,\cdot,f}$ or $\mu_{load,\cdot,t}$.

Estimates of $k_{load,\cdot,f}$ can be obtained using data from only one operation cycle for all f, $f = 1, \ldots, N_f$ (i.e. every single operation cycle). These estimates will, however, be encumbered with some uncertainty

$$\widehat{k}_{load,\cdot,f} = k_{load,\cdot,f} + \xi_{load,\cdot,f} \tag{4.58}$$

where $\xi_{load,\cdot,f}$ has zero mean and variance $\sigma^2_{\xi,load,\cdot}$. This equation is referred to as the observation equation for the load rate process in the operation cycle time domain. The model for the influent load in the operation cycle time domain apply for both ammonia and phosphate concentrations as indicated in the equations by the period. Using the approximations (4.35) and (4.36), the results from estimating the load process in the operation cycle time domain may be interpreted as influent ammonia and phosphate concentrations.

Maximum nitrification rate

In Section 4.3 it was mentioned that Holmberg & Ranta (1982) had observed that a practical identification of the parameters in a Monod-type expression (e.g. k_{nit,max,NH_4^+}, $K_{NH_4^+}$, and K_{O_2} in (4.41)), based on observations from a single declining curve, is not practically feasible. However, if several declining curves of ammonia concentrations are available a practical identification of the three parameters is actually feasible. In fact, if large time series are available (covering more than 50 operation cycles) estimates of $k_{nit,max,NH_4^+,f}$ for the separate operation cycles may be obtained (indicated by the index f), when $K_{NH_4^+}$ and K_{O_2} are estimated based on all observations. Thus, $K_{NH_4^+}$ and K_{O_2} are regarded as constant parameters which are estimated on all available observations, and these estimates are used to give estimates of $k_{nit,max,NH_4^+,f}$, $f = 1, \ldots, N_f$, based on data from one operation cycle using (4.41). The estimates are naturally encumbered with some uncertainty

$$\widehat{k}_{nit,max,NH_4^+} = k_{nit,max,NH_4^+} + \xi_{nit,NH_4^+,f} \tag{4.59}$$

where $\xi_{nit,NH_4^+,f}$ has zero mean and variance $\sigma^2_{\xi,nit,NH_4^+}$. A similar result holds for the nitrification process based on observations of nitrate concentrations. The equation (4.59) and the similar equation found for the time series of nitrate concentrations are referred to as the observation equations for the maximum nitrification rate process in the operation cycle time domain.

The half-saturation constants $K_{NH_4^+}$ and K_{O_2} may be regarded as constant for a limited number of operation cycles, but for larger time series algorithms for recursive estimation of these parameters should be applied (see Kulhavy (1990)). Knowles et al. (1965) have reported $K_{NH_4^+}$ as being a function of temperature, but effects of calibration offset errors on the ammonia and oxygen sensors could also be handled by a recursive estimation procedure.

Applying the approximations (4.43) and (4.44) to the estimates of the maximum nitrification rate, $k_{nit,max,NH_4^+,f}$ and $k_{nit,max,NO_3^-,f}$, the dynamics of the activity of the autotrophic biomass is assessed. It is assumed that $k_{nit,max,NH_4^+,f}$ and $k_{nit,max,NO_3^-,f}$ in general show similar variations, because the variations of the two parameters is caused by the very same process. Hence, the same type of model is used to describe the variations in both parameters for the considered cases in Chapter 5 and 6. An autoregressive model is found adequate for the nitrification process

$$\Phi_{nit}(B)(k_{nit,max,\cdot,f} - \mu_{nit,max,\cdot,f}) = e_{nit,\cdot,f} \tag{4.60}$$

where $e_{nit,\cdot,f}$ has zero mean and variance $\sigma^2_{e,nit,\cdot}$. This equation applies for both time series of ammonia and nitrate concentrations which is indicated by indexing with a period.

Information on the influence of explanatory variables (e.g. temperature (T), alkalinity (pH), ammonia load, composition of raw wastewater) on the maximum nitrification rate may be incorporated by letting $\mu_{nit,max,\cdot,f}$ be a function of the available observations for modelling of $k_{nit,max,\cdot,f}$.

$$\mu_{nit,max,,f} = f(T, pH, k_{load,NH_4^+,f-1}, \ldots) \tag{4.61}$$

Maximum denitrification rate

Following the discussion above $K_{NO_3^-}$ and K_{load,NH_4^+} in (4.45) are estimated using all the available observations of the time series of nitrate, while estimates of $k_{denit,max,f}$ are obtained for all the separate operation cycles based on the estimates of $K_{NO_3^-}$ and K_{load,NH_4^+}. The estimates of the maximum denitrification rate at operation cycle f is also encumbered with some uncertainty

$$\widehat{k}_{denit,max,f} = k_{denit,max,f} + \xi_{denit,f} \tag{4.62}$$

where $\xi_{denit,f}$ has zero mean and variance $\sigma^2_{\xi,denit}$. The equation (4.62) is referred to as the observation equation for the maximum denitrification rate process in the operation cycle time domain. A recursive estimation of the half-saturation parameters $K_{NO_3^-}$ and K_{load} should be applied for larger time series. Such algorithms are found in Kulhavy (1990).

The dynamics of the activity of the heterotrophic biomass is assessed when the approximation (4.46) is applied to the estimates of $k_{denit,max,f}$. The variations of the maximum denitrification rate may be modelled using an autoregressive model

$$\Phi_{denit}(B)(k_{denit,max,f} - \mu_{denit,max,f}) = e_{denit,f} \tag{4.63}$$

where $e_{denit,f}$ has zero mean and variance $\sigma^2_{e,denit}$, and the influence of explanatory variables (e.g. temperature (T), alkalinity (pH), ammonia load, composition of raw wastewater) is incorporated in the model by letting $\mu_{denit,max,f}$ be a function of the available observations.

$$\mu_{denit,max,f} = f(T, pH, k_{load,NH_4^+,f-1}, \ldots) \tag{4.64}$$

In Appendix B the grey box models presented in this section for the time series of ammonia, nitrate, and phosphate concentrations are summarized for the purpose of getting an overview of all the models.

4.5 The state space model

Behavior of dynamic systems can be conveniently described in the framework of the state space notation. The state space form is a powerful tool which opens the way to handling a wide range of time series models and other models. Once a model has been put into a state space form, the Kalman filter may be applied and this in turn leads to algorithms for prediction, filtering, and smoothing. In Aoki (1987) the conversion of traditional time series models into state space models and visa-versa is shown. The grey box models presented in the previous section can also be formulated in the framework of state space modelling. Kitagawa & Gersch (1984) have shown that time series which are decomposed into several components, also can be formulated as state space models.

The state space form arises by introducing the state vector $\boldsymbol{x}_t$ of dimension n, which contains all the available information from previous samples of the system being modelled. The measurement at time t is related to the state vector via the observation equation

$$y_t = \boldsymbol{c}\boldsymbol{x}_t + \boldsymbol{\kappa}^T\boldsymbol{u}_t + \nu_t \tag{4.65}$$

where $\boldsymbol{c}$ is a vector of length n, and the dynamic of the system is given by the process equation or transition equation

$$\boldsymbol{x}_t = \boldsymbol{A}\boldsymbol{x}_{t-1} + \boldsymbol{D}\boldsymbol{u}_t + \boldsymbol{b}e_t \tag{4.66}$$

where $\boldsymbol{A}$ is a matrix of dimension $n \times n$, $\boldsymbol{b}$ is a vector of length n, and $\boldsymbol{D}$ is a matrix of dimension $n \times l$, where l is the number of elements in the explanatory variable $\boldsymbol{u}_t$.

The relationship between the grey box models of the previous section and the state space form above, ((4.65) and (4.66)), may be implicitly recognized. However, the vectors and matrices of the state space form showing the direct relationship are given in Appendix C. The state space form of the grey box models in Section 4.4 is not linear with respect to the parameters, and the mean process rate μ_t is stochastic in that it depend on observations available at time $t-1$. With the information at time $t-1$ available, μ_t may be regarded as being fixed. If the noise disturbances are normally distributed, the state space form is a conditionally normally distributed model (the state vector is normally distributed). The state space form is employed for the use of a Kalman filter.

4.6 The Kalman filter

The Kalman filter is a recursive procedure for computing the optimal estimator of the state vector at time t, based on the information available at time t. This information consists of the observations up to and including y_t. Thus, the Kalman filter provides on-line estimation of the state vector, $\boldsymbol{x}_t$, which is continually updated as new observations become available.

The derivation of the Kalman filter (see e.g. Kalman (1960) or Anderson & Moore (1979)) rests on the assumption that the disturbances and initial state vector are normally distributed. A standard result on the multivariate normal distribution is then used to show how it is possible to calculate recursively the distribution of $\boldsymbol{x}_t$, conditional on the information set at time t. For the presentation of the Kalman filter the following notation is applied

$$\widehat{\boldsymbol{x}}_{t|t} = E[\boldsymbol{x}_t|\boldsymbol{Y}_t] \tag{4.67}$$

$$\widehat{\boldsymbol{P}}_{t|t} = V[\boldsymbol{x}_t|\boldsymbol{Y}_t] \tag{4.68}$$

$$\widehat{y}_{t+1|t} = E[y_{t+1}|\boldsymbol{Y}_t] \tag{4.69}$$

$$\widehat{R}_{t+1|t} = V[y_{t+1}|\boldsymbol{Y}_t] \tag{4.70}$$

where $\boldsymbol{Y}_t$ represents all observations made at time t and previously (i.e. $y_t, y_{t-1}, \ldots, \boldsymbol{u}_t, \boldsymbol{u}_{t-1}, \ldots$) and the distribution of the initial state vector, $\boldsymbol{x}_0$.

Given $\widehat{\boldsymbol{x}}_{t-1|t-1}$ and $\widehat{\boldsymbol{P}}_{t-1|t-1}$, the optimal predictor of $\boldsymbol{x}_t$ based on information available at $t-1$ is given by (see (4.66))

$$\widehat{\boldsymbol{x}}_{t|t-1} = \boldsymbol{A}\widehat{\boldsymbol{x}}_{t-1|t-1} + \boldsymbol{D}\boldsymbol{u}_t \tag{4.71}$$

and the optimal predictor of y_t is found using (4.65)

$$\widehat{y}_{t|t-1} = \boldsymbol{c}\widehat{\boldsymbol{x}}_{t|t-1} + \boldsymbol{\kappa}^T\boldsymbol{u}_t \tag{4.72}$$

while the optimal estimator of the covariance matrix of $\boldsymbol{x}_t$ is

$$\widehat{\boldsymbol{P}}_{t|t-1} = \boldsymbol{A}\widehat{\boldsymbol{P}}_{t-1|t-1}\boldsymbol{A}^T + \boldsymbol{b}\sigma_e^2\boldsymbol{b}^T \tag{4.73}$$

and the variance of y_t is

$$\widehat{R}_{t|t-1} = \boldsymbol{c}\widehat{\boldsymbol{P}}_{t|t-1}\boldsymbol{c}^T + \sigma_\nu^2 \tag{4.74}$$

These four equations are known as the prediction equations, and the four predictions are the mean and variance of the prior distribution of $\boldsymbol{x}_t$ and y_t.

Once the new observation, y_t, becomes available, the estimates of $\boldsymbol{x}_t$ and $\boldsymbol{P}_t$ can be updated using

$$\widehat{\boldsymbol{x}}_{t|t} = \widehat{\boldsymbol{x}}_{t|t-1} + \boldsymbol{K}_t(y_t - \widehat{y}_{t|t-1}) \tag{4.75}$$

$$\widehat{\boldsymbol{P}}_{t|t} = \widehat{\boldsymbol{P}}_{t|t-1} - \boldsymbol{K}_t \widehat{R}_{t|t-1} \boldsymbol{K}_t^T \tag{4.76}$$

where the Kalman gain is given by

$$\boldsymbol{K}_t = \widehat{\boldsymbol{P}}_{t|t-1} \boldsymbol{c}^T \widehat{R}_{t|t-1}^{-1} \tag{4.77}$$

These three equations are known as the updating equations, and (4.75) and (4.76) are the mean and variance of the posterior distribution of $\boldsymbol{x}_t$.

Missing observations due to e.g. failure in the measurement system is handled conveniently by the Kalman filter algorithm. If the observation at time t is a missing value new information is not obtained and thus, $\boldsymbol{x}_t$ and $\boldsymbol{P}_t$ are not updated, i.e.

$$\widehat{\boldsymbol{x}}_{t|t} = \widehat{\boldsymbol{x}}_{t|t-1} \tag{4.78}$$

$$\widehat{\boldsymbol{P}}_{t|t} = \widehat{\boldsymbol{P}}_{t|t-1} \tag{4.79}$$

The recursions of the Kalman filter are obtained by again using the updated estimates for $\boldsymbol{x}_t$ and $\boldsymbol{P}_t$ to make predictions for $t+1$ in (4.71-4.74). The starting values for the Kalman filter may be specified in terms of $\widehat{\boldsymbol{x}}_{0|0}$ and $\widehat{\boldsymbol{P}}_{0|0}$. Given these initial conditions, the Kalman filter delivers the optimal estimator of the state vector as each new observation becomes available.

The Kalman filter recursions are in a steady state if the covariance matrix of $\boldsymbol{x}_t$ is time-invariant, that is

$$\widehat{\boldsymbol{P}}_{t|t-1} = \overline{\boldsymbol{P}} \tag{4.80}$$

and as a result the variance of y_t (4.74) is also time-invariant

$$\overline{R} = \boldsymbol{c}\overline{\boldsymbol{P}}\boldsymbol{c}^T + \sigma_\nu^2 \tag{4.81}$$

when σ_ν^2 is regarded as a constant parameter.

4.7 Maximum likelihood estimation

The state space form and the Kalman filter recursions provide the predictions used in estimating the parameters of a grey box model using maximum likelihood techniques. The joint density function of the observations, $\boldsymbol{Y}_N = y_1, \ldots, y_N$, is assumed to depend on a set of n unknown parameters in the vector $\boldsymbol{\Psi} = (\psi_1, \ldots, \psi_n)^T$. It will be denoted $L(\boldsymbol{Y}_N; \boldsymbol{\Psi})$. Given the observations, $L(\boldsymbol{Y}_N; \boldsymbol{\Psi})$ may be interpreted as a likelihood function, which may be evaluated for different sets of $\boldsymbol{\Psi}$. The maximum likelihood estimator is found as the value $\boldsymbol{\Psi}$ which maximizes $L(\boldsymbol{Y}_N; \boldsymbol{\Psi})$.

If the disturbances and the initial state vector $\boldsymbol{x}_0$ all are normally distributed, then the distribution of y_t conditional on $\boldsymbol{Y}_{t-1}$ will also be normal. Thus, the probability density function for y_t conditional on $\boldsymbol{Y}_{t-1}$ is given by

$$p(y_t|\boldsymbol{Y}_{t-1}) = \frac{1}{\sqrt{2\pi \widehat{R}_{t|t-1}}} \exp\left(-\frac{v_t^2}{2\widehat{R}_{t|t-1}}\right) \tag{4.82}$$

where

$$v_t = y_t - \widehat{y}_{t|t-1} \tag{4.83}$$

is the prediction error. The prediction $\widehat{y}_{t|t-1}$ and the variance $\widehat{R}_{t|t-1}$ are provided by the Kalman filter.

The joint density function conditional on the initial state is therefore given by

$$L(\boldsymbol{Y}_N;\boldsymbol{\Psi}|\boldsymbol{x}_0) = \prod_{t=1}^{N} p(y_t|\boldsymbol{Y}_{t-1})$$
$$= \prod_{t=1}^{N} \frac{1}{\sqrt{2\pi\widehat{R}_{t|t-1}}} \exp(-\frac{v_t^2}{2\widehat{R}_{t|t-1}}) \qquad (4.84)$$

Maximizing the likelihood with respect to the parameters most frequently takes place after forming a logarithmic transformation

$$\log L(\boldsymbol{Y}_N;\boldsymbol{\Psi}|\boldsymbol{x}_0) = -\frac{N}{2}\log 2\pi - \frac{1}{2}\sum_{t=1}^{N}\log \widehat{R}_{t|t-1} - \frac{1}{2}\sum_{t=1}^{N}\frac{v_t^2}{\widehat{R}_{t|t-1}} \qquad (4.85)$$

This is also known as the prediction error decomposition form of the likelihood. It should be stressed, that some of the standard deviations of the estimates obtained from estimating the models in Chapter 5 and 6 are too small due to the optimization routine (see Appendix A).

If prior information is available on the elements of $\boldsymbol{x}_0$, then the Kalman filter yields the exact likelihood function of the observations, $\boldsymbol{Y}_N$. Unfortunately, prior information on the distribution of $\boldsymbol{x}_0$ of the exact value of $\boldsymbol{x}_0$ is rarely available. Hence, the initial values of $\boldsymbol{x}_0$ and $\boldsymbol{P}_0$ may be incorporated into the likelihood function (4.84) and thereby estimated, or if the number of observations, N, is sufficiently large such that the specification of initial values has a minor influence, appropriate values of $\boldsymbol{x}_0$ and $\boldsymbol{P}_0$ may be chosen.

4.8 Testing and model selection

Methods for testing hypotheses and parameter significance can be derived systematically using the maximum likelihood approach. The maximum likelihood function itself provides a possible criterion for discriminating between different types of grey box models. However, it is advisable to make some allowance for the number of parameters in the model. Several of the procedures for differentiating between models presented in this section are at the same time used to determine the applicability of the given types of models.

The basic test procedure is the likelihood ratio test. Consider the problem of testing a hypothesis H_0: $\boldsymbol{\Psi}\in M_0$ against H_1: $\boldsymbol{\Psi}\in M_1\backslash M_0$, where $M_0 \subset M_1$, i.e. does the reduced parameter set M_0 of M_1 give an equally good description of the data? If the maximized likelihood function under H_0, $L(\boldsymbol{Y}_N;\widehat{\boldsymbol{\Psi}}_0)$, is much smaller than the unrestricted maximum likelihood function, $L(\boldsymbol{Y}_N;\widehat{\boldsymbol{\Psi}}_1)$, there is evidence against the null hypothesis. This result is formalized in the Neyman-Pearson lemma which shows that a test based on the likelihood-ratio

$$\lambda = \frac{L(\boldsymbol{Y}_N;\widehat{\boldsymbol{\Psi}}_0)}{L(\boldsymbol{Y}_N;\widehat{\boldsymbol{\Psi}}_1)} \qquad (4.86)$$

is the most powerful for testing H_0 against H_1.

Sometimes it is possible to transform the likelihood ratio into a statistic having an exact known distribution under H_0. When this cannot be done, the following asymptotic result may be applied. This is based on the result that the statistic

$$LR = -2\log\lambda \qquad (4.87)$$

is asymptotically χ^2-distributed under H_0 for large sample sizes, with degrees of freedom equal to the number of restrictions or reduction of parameters. The proof for this result regarding the distribution of LR which is based on a Taylor-expansion of (4.85), is found in Rao (1965) or Goodwin & Payne (1977).

If variances of the parameter estimates, $\widehat{\sigma}^2_{\psi_i}$, $i = 1, \ldots, n$, are obtained from the estimation procedure, the hypothesis H_0: $\psi_i = \psi_{i0}$ against H_1: $\psi_i \neq \psi_{i0}$ may be tested using the statistic

$$T = \frac{\psi_i - \psi_{i0}}{\sqrt{\widehat{\sigma}^2_{\psi_i}}} \tag{4.88}$$

which is t-distributed with $N - n$ degrees of freedom. However, this is not a very strong test of the H_0-hypothesis, but for the grey box models presented here it has been used as a guidance in the model development.

When comparing two different models, which cannot be made identical by restrictions on the parameters of one of the models, the likelihood ratio test (4.87) does not apply. In this case the prediction error variance may be used as a basic measure of goodness-of-fit. For large sample sizes this is practically the same as comparing the maximized likelihood functions. However, in order to avoid developing over-parameterized models a penalty for the number of parameters should be used in conjunction with the maximum likelihood function. Many different statistics have been proposed to assess the goodness-of-fit of a given model, most of which are derivatives of the two general criteria, Akaike information criterion (AIC) (Akaike (1974)) and Bayes information criterion (BIC) (Schwarz (1978)). AIC is reluctant to bring in more parameters than BIC into the model for large sample sizes due a smaller penalty for the number of parameters.

Letting $L(\boldsymbol{Y}_N; \widehat{\boldsymbol{\Psi}}|\boldsymbol{x}_0)$ denote the likelihood function evaluated at the maximum likelihood estimates $\widehat{\boldsymbol{\Psi}}$ and n the number of parameters, then

$$AIC = -2 \log L(\boldsymbol{Y}_N; \widehat{\boldsymbol{\Psi}}|\boldsymbol{x}_0) + 2n \tag{4.89}$$

and

$$BIC = -2 \log L(\boldsymbol{Y}_N; \widehat{\boldsymbol{\Psi}}|\boldsymbol{x}_0) + n \log N \tag{4.90}$$

where the optimal number of parameters is given by the minimum of AIC or BIC.

Ljung (1987) has proposed a general identification and estimation method using AIC based on a given model structure. However, as Jenkins (1982) showed, abandoning judgement altogether in model selection can lead to the potential of selecting even more inappropriate models. Lütkepohl (1985) shows that AIC will yield biased estimates of the model order of an autoregressive process.

In a well-specified model, the residuals should be approximately random. This can be checked by various graphical procedures and various test. For the analysis of the residuals of the grey box models presented in this thesis the correlogram and the cumulated periodogram have been applied to the normalized residuals

$$\epsilon_t = \frac{v_t}{\sqrt{\widehat{R}_{t|t-1}}} \tag{4.91}$$

The correlogram is a plot of the sample autocorrelation function of the residuals, $r(\tau)$, for different lag values, τ, which describes the time-wise correlation of the residuals (see Madsen (1989) and Harvey (1981b)).

$$r(\tau) = \frac{\frac{1}{N}\sum_{t=\tau+1}^{N}(\epsilon_t - \overline{\epsilon})(\epsilon_{t-\tau} - \overline{\epsilon})}{\frac{1}{N}\sum_{t=1}^{N}(\epsilon_t - \overline{\epsilon})(\epsilon_t - \overline{\epsilon})} \tag{4.92}$$

For large sample sizes the values of $r(\tau)$, $\tau = 1, \ldots$, are approximately normally and independently distributed with a mean of zero and variance $1/N$ under the assumption that ϵ_t is white noise.

The periodogram is calculated at the frequencies $f_i = i/N$, $i = 0, 1, \ldots, [n/2]$, for the stochastic process ϵ_t by

$$\widehat{I}(f_i) = \frac{1}{N}[\sum_{t=1}^{N} \epsilon_t \exp(-i2\pi f_i t)]^2 \tag{4.93}$$

i.e. $\widehat{I}(f_i)$ describes the part of the variation of ϵ_t at the frequency f_i. The normalized cumulated periodogram is then found as

$$\widehat{C}(f_j) = \frac{\sum_{i=1}^{j} \widehat{I}(f_i)}{\sum_{i=1}^{N/2} \widehat{I}(f_i)} \tag{4.94}$$

which is a non-decreasing function defined at the frequencies $f_i = i/N$, $i = 1, \ldots, [N/2]$. A formal test for departures of randomness is obtained by constructing two parallel lines to the 45° line, $s = j/[N/2]$, defined by

$$s = \pm s_0 + \frac{j}{[N/2]} \tag{4.95}$$

where s_0 is a significance value which depends on n and may be read off directly from a table given in Durbin (1969). The cumulated periodogram should lie in-between the two significance lines.

The diagnostics of the correlogram and periodogram may suggest further extensions to the grey box models as illustrated in Figure 4.1. Furthermore, the information obtained from the two graphical procedures also serves as a test of the assumption of randomness of the residuals upon which the models are built.

4.9 Conclusion

In this chapter statistical tools for the formulation, estimation, and validation of time series models are proposed. Incorporating prior knowledge of the system being modelled into the models is emphasized. This is

obtained by incorporating deterministic terms, and lacks of these terms to describe the variations of the wastewater processes using traditional stochastic terms. However, time series modelling is an iterative procedure which occasionally leads to the inclusion of additional physical knowledge and additional explanatory variables.

The models proposed in this chapter are built up of five components: autoregressive models, trends, cyclic effects, type-of-day effects, and the use of explanatory variables. Combining these components into operational models such that the parameters of these models are physically interpretable, is called grey box modelling. However, caution for the identifiability of the parameters should be observed, e.g. a theoretically identifiable model may not be practically identifiable due to the data available.

The grey box models in this chapter are modelled in two time domains, the sample time domain and the operation cycle time domain. While the observations in the sample time domain consist of measurements, the observations in the operation cycle time domain consist of parameter estimates of the models in the sample time domain based on the measurements of one operation cycle. In the time domain the following significant processes are modelled

- Influent load
- Nutrient transport
- Hydrolysis and growth of biomass
- Nitrification
- Denitrification
- Biological phosphate uptake in biomass
- Stripping of phosphate

and the following three parameters obtained from the sample time domain are modelled in the operation cycle time domain

- Influent load rate of nutrients
- Maximum nitrification rate
- Maximum denitrification rate

Most of the parameters used in the grey box modelling of the wastewater processes relate to the theory of the processes in Chapter 2 and 3, but some of these parameters may not yield unbiased estimates due to assumptions made in the discrete time series modelling. Transient phenomena occurring due to the alternating operation mode of the BIO-DENITRO and BIO-DENIPHO processes are also handled by the grey box models.

Finally, the grey box models apply to a state space form, which makes the models treatable by the Kalman filter. The Kalman filter leads to algorithms of prediction, reconstruction, and maximum likelihood estimation of unknown parameters through the prediction error decomposition. In order to differentiate between different types of grey box models estimated by the maximum likelihood method, tests and criteria for selecting the best fitting model are proposed. Furthermore, analysis of the residuals also serves as a goodness-of-fit criterion, by means of which extensions to the analyzed model may be obtained and the assumptions of randomness of the error terms are tested.

Chapter 5

Case - The Lundtofte pilot scale plant

The grey box models described in Chapter 4 were mainly developed on data from one of the aeration tanks at the Lundtofte pilot scale plant. This is primarily due to a reliable measurement system for monitoring of nutrient salt concentrations and the short time between samples from one of the aeration tanks, facilitating the identification of the hydraulic and biological processes. Furthermore, some of the results from estimating the grey box models are validated through additional measurements at the well-monitored plant. However, these additional measurements have not been used in the modelling phase, since they will rarely be available on a full-scale plant. A short introduction of the plant is given in the first section of this chapter. The measurement system of the plant introduces some correlated measurement noise, which is modelled in the second section. The third and fourth section deal with the modelling of the hydraulic and biological processes in the sample time domain of two different data sets. Different models are proposed from the data sets in order to illustrate the evolution of the grey box models in this context. The last section covers the grey

box modelling in the operation cycle time domain of the second data set. Some of the results of this chapter are also documented in Carstensen et al. (1993). It should be emphasized that the models presented in this chapter are derived by statistical methods from the class of grey box models in Chapter 4 giving the best fit of data.

5.1 Introduction

The Lundtofte Pilot Plant is a pilot scale facility belonging to the Department of Environmental Engineering at the Technical University of Denmark. The pilot plant is fed with clarified wastewater from the neighboring Lundtofte WWTP of Lyngby municipality. The raw wastewater input has been pre-clarified at the municipal facility in order to remove large particles, sand, and oils.

The biological wastewater treatment process is carried out in four vessels as sketched in Figure 5.1 and the operation of the plant follows the BIO-DENIPHO process (see Figure 3.4). The throughput of the plant is held constant on the order of 90 liters per hour, which is mixed with returned sludge also at a constant flow rate of 90 liters per hour. In this way the plant is ideal for identifying the dynamics of the biological processes without disturbances from hydraulic loads. The approximate holding volumes of the pretreatment column (PRE), the two aeration tanks (T1 and T2) and the sedimentation tank (SED) are 200, 800, 800, and 1100 liters respectively, i.e. the hydraulic retention time (3.3) is approximately 1, 4, 4, and 6 hours, respectively.

The pretreatment column is maintained anaerobic for selection of phosphorus accumulating bacteria. The primary process taking place in this tank is the stripping of phosphate. The two aeration tanks T1 and T2 are operated in an alternating manner scheduled prior to the operation. Here the nitrification and denitrification processes take place alternatively under aerobic and anoxic conditions, respectively, and phosphate is accumulated in the biomass in both aerobic and anoxic periods. Oxygen is

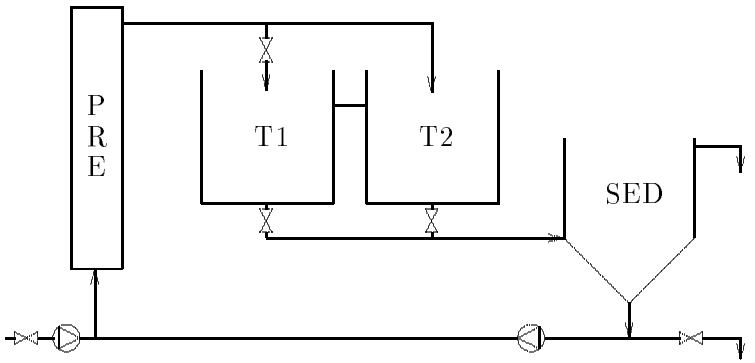

Figure 5.1. *Schematic diagram of pilot scale wastewater treatment plant with symbols of the tanks used in the following.*

supplied to the two tanks through diffusers controlled by a PLC according to a provided setpoint with hysteresis values. In that way an approximately constant oxygen concentration within the range 1-2 mg O_2/l is maintained throughout the aerobic phase. The feed to the two tanks is controlled by one valve and each tank has a separate valve controlling the outlet of the tank, as indicated on Figure 5.1. These valves are either open or closed, i.e. controlled by an on/off signal similar to the oxygen diffuser. The operation scheduling of the valves can be derived from Figure 3.4. The pretreatment tank and the aeration tanks are all equipped with stirrers for keeping the activated sludge suspended.

In the sedimentation vessel, the heavier sludge falls out of suspension, and from top of the vessel the processed effluent is removed from the system. The sludge is returned via the sludge return pump and mixed with the fluid entering the pretreatment column. The sludge concentration is held approximately constant throughout intermittent removal of excess sludge from the system at the point where it exits the sedimentation vessel. Significant loss of activated sludge does not occur, because the plant is not

exposed to large hydraulic loads during rainy weather. In fact, the throughput of the plant is constant.

Samples are taken from four different locations in the plant: in the inlet, in the outlet of the anaerobic pretreatment column, in the aeration tank T2, and in the outlet of the plant. Samples from the four locations and from a standard solution (used for calibration) are pumped through a multi-port valve to the Flow Injection Analysis (FIA) systems. Three FIA systems connected in series monitor the concentration of ammonia, nitrate and phosphate at the four positions at the plant as well as the standard solution. Procedures have been included in the controlling software system to eliminate the effect of isolated gas bubbles and to initiate a vacuum cycle if there should be signs of a significant amount of gas in the system. An overview of the sample selection system and FIA analyzers is provided in Figure 5.2. More detailed descriptions of the pilot scale wastewater treatment plant and the on-line measurement system are given in Pedersen et al. (1990) and Isaacs et al. (1992).

In this chapter two data sets are considered. For these data sets the sample system was set up for a cycle of 8 measurements, with every second sample taken from aeration tank T2 and the remaining four samples taken from the inlet of the plant, the outlet of the pretreatment column, the outlet of the plant, and the standard solution. The sample cycle is controlled by the multi-port valve shifting position every 90 seconds approximately. This gives a total cycle length of 12 minutes and a sample from aeration tank T2 every 3 minutes. The sample cycle is illustrated in Figure 5.3.

The two data sets consist of measurements of ammonia, nitrate, and phosphate concentrations from the measurement cycle, and the control signals for the inlet and outlet valves of the aeration tanks. Furthermore, measurements of the oxygen concentration in T2 and the corresponding control signal for the diffuser in T2 are available. Due to the setpoint control of the diffuser the measurements of the oxygen concentration are considered as a constant signal of the setpoint value covered with noise during the aerobic phase of operation cycle. Hence, the effect of different oxygen concentrations on the biological processes have not been investigated, but the

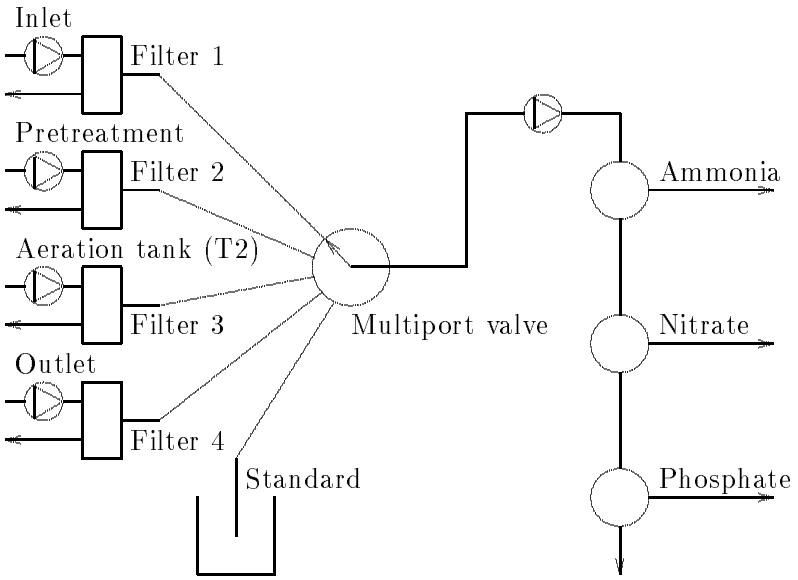

Figure 5.2. *Overview of the sample selection system and the three FIA analyzers connected in series.*

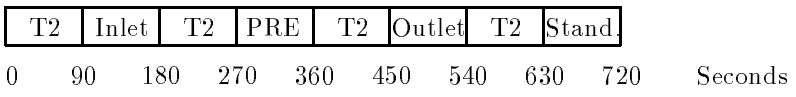

Figure 5.3. *Scheduling of the sample cycle.* T2 *is the aeration tank* T2, PRE *is outlet of pretreatment column, and* Stand. *is the standard solution.*

measurements of the oxygen concentration and nitrate concentration have been used to divide the time series into aerobic, anoxic, and anaerobic periods.

Aerobic conditions	if $S_{O_2,t-1} > 0.5$ mg O_2/l
Anoxic conditions	if $S_{O_2,t-1} < 0.5$ mg O_2/l and $S_{NO_3^-,t-1} > 0.5$ mg NO_3^--N/l
Anaerobic conditions	if $S_{O_2,t-1} < 0.5$ mg O_2/l and $S_{NO_3^-,t-1} < 0.5$ mg NO_3^--N/l

The measurements from the inlet of the plant, the outlet of the pretreatment column, and the outlet of the plant have not been used in the grey box modelling, because this information would rarely be available on a full scale plant, and the objective is to model the wastewater processes based on measurements available on a full scale plant. The first data set consists of 468 observations covering nearly one day (October, 26th 1991, Saturday), and it has only been used for modelling in the sample time domain due to the short period of sampling. This data set was used in the first developing stage of the grey box models given in Section 4.4, and the models of this data set have been left unaltered to show the process of grey box modelling. However, the models of this data set also contain some interesting features. The second data set consists of 7765 samples covering more than a 16 days period (from March, 19th to April, 4th 1992, starting on a Thursday and ending on a Saturday) with highly varying loads of materials. This data set has been used for modelling in both the sample time domain and the operation cycle domain.

5.2 Modelling the measurement system

The basic assumption when estimating a grey box model by use of the Kalman filter and the maximum likelihood approach in Section 4.7 is, that the noise terms are Normal and Independently Distributed (NID). If residual analysis (see Section 4.8) shows correlation amongst the residuals, it is often interpreted as a deficiency of the process equation (4.28) or (4.29).

However, at the pilot plant the measurement error, ν_t, in the observation equation (4.23) or (4.24) (or see (5.9) later) is not NID due to changing of the sample points in the measurement cycle of the measurement system described in the previous section and the short time between samples of the measurement cycle. Hence, a model for the measurement error must be formulated.

It is found, that the samples from the aeration tank T2 are highly correlated with the intermediate measurements from the inlet of the pilot plant, the pretreatment column, the outlet of the pilot plant, and the standard solution of the measurement cycle. The dependency of the sample points of the intermediate measurements is modelled as a constant term for each of the four samples from T2 in the measurement cycle, s_i, $i = 1, 2, 3, 4$, where i indicates where the previous sample in the measurement cycle was taken. The effects of the intermediate measurements must sum to zero.

$$\sum_{i=1}^{4} s_i = 0 \tag{5.1}$$

Furthermore, due to the dynamics of the ammonia, nitrate, and phosphate concentrations in the inlet of the plant, the pretreatment column, and the outlet of the plant from one measurement cycle to another, ν_t will also show some cyclic variations in addition to the constant term, s_i. Because the information from the intermediate measurements of the measurement cycle is not used in the modelling stage as described previously, a more empirical model (refer to (4.20) is used to describe the variations in the measurement error.

$$\Phi_4(B^4)\Phi(B)\nu_t = \eta_{i,t} \tag{5.2}$$

where $\eta_{i,t}$ is NID with $E[\eta_{i,t}] = s_i$ and $V[\eta_{i,t}] = \sigma^2_{\eta,i}$, and i indicates the position of the previous sample in the measurement cycle. The index, i, may be found as $i = \text{mod}_4(t) + 1$, where $\text{mod}_4(t)$ is the modulus function of division by 4. Thus, the error term is normally distributed with four different

means and variances reflecting the relationship to the intermediate measurements in the measurement cycle, and $\Phi_4(B^4)$ describes the deviation from these four means caused by the variations of the ammonia, nitrate, and phosphate concentrations in the inlet to the plant, the pretreatment column, and the outlet of the plant. The correlation in the measurement error between subsequent samples from T2 is modelled through $\Phi(B)$. This term describes correlation due to the fast sampling, clogging of tubes, and deposits covering the probes of the FIA-analyzers.

Data set No.1

This data set covers a short period of time with a relative stable load to the plant. The time series of the measurements of ammonia, nitrate, and phosphate concentrations are shown in Figure 5.4. The measurement error, ν_t, of the ammonia concentration FIA-analyzer is adequately modelled as follows:

$$(1-\phi B)\nu_t = \eta_{i,t} \tag{5.3}$$

where $\eta_{i,t}$ is given by four distributions with different means, s_i, and variances, $\sigma^2_{\eta,i}$. The measurement error of the nitrate concentration FIA-analyzer is adequately modelled as follows:

$$(1-\phi B)\nu_t = \eta_t \tag{5.4}$$

where η_t has zero mean and variance σ^2_η, while the measurement error of the phosphate concentration FIA-analyzer is modelled as follows:

$$\nu_t = \eta_{i,t} \tag{5.5}$$

where $\eta_{i,t}$ is given by four distributions with different means, s_i, and the same variance σ^2_η. The estimates from modelling the measurement error ν_t

Parameter	Ammonia	Nitrate	Phosphate
ϕ	0.159	0.185	-
s_1	-0.053	-	-0.049
s_2	0.151	-	0.031
s_3	-0.023	-	0.043
s_4	-0.075	-	-0.026
$\sigma^2_{\eta,1}$	0.00328	0.00549	0.00575
$\sigma^2_{\eta,2}$	0.00462	0.00549	0.00575
$\sigma^2_{\eta,3}$	0.00251	0.00549	0.00575
$\sigma^2_{\eta,4}$	0.00433	0.00549	0.00575

Table 5.1. *Parameter estimates from modelling the measurement system on data set No.1.*

given the observation equation (5.9) and the process equation (5.10) (see later) on data set No.1 are shown in Table 5.1. The error terms, $\eta_{i,t}$, are NID in the equations above.

The model of the measurement error on the measurements of ammonia concentrations is clearly the most extensive, followed by the models of the measurement error on the measurements of phosphate and nitrate concentrations. This is due to the fact that the measurements of ammonia concentrations in T2 are more affected by the intermediate measurements of the measurement cycle, because the ammonia concentration in the inlet of the plant and pretreatment tank are high relative to the ammonia concentration in T2. Similarly, the measurements of phosphate concentrations are affected by the intermediate measurements from the inlet of the plant and pretreatment column, but the influence on ν_t is smaller due to the relative smaller phosphate concentrations of the inlet as shown in Table 3.2. This is reflected in significantly smaller s_i-estimates in Table 5.1 and a smaller model in general. The nitrate concentrations in the sample points of the intermediate measurements are very small relative to the nitrate concentrations of T2, and as a result the model for the measurement error becomes very simple.

In the data set no information is available on the actual sampling sequence of the measurement cycle, or where the measurements previous to the samples of T2 were taken. Thus, it is difficult to draw any conclusions on the estimates, but relating s_2 to the inlet sampling point and s_3 to the pretreatment column sampling point might be a good guess. However, it should be stressed that the estimates are associated with uncertainty, i.e. the standard deviation of the estimates ranges from 5-20% of the estimate.

Data set No.2

The second data set from the pilot scale plant, which covers a long period of time, contained several gaps in the time series due to calibration of the FIA-analyzers, cleaning of the probes, and shutdown of the data acquisition system. These gaps caused interruption breaks in the sampling sequence of the measurement cycle, and unfortunately, no information is available on the previous sample positions in the measurement cycle. As a result the grey box models were at first estimated on every single part of the time series without any gaps, and the estimates of s_i from the different parts of the time series were combined to detect the most likely resumption of the sampling sequence after an interrupt. However, there is no guarantee that the sampling sequence of the different parts of the time series have been joined correctly, due to the uncertainty associated with the estimates of s_i.

Only time series of ammonia and nitrate concentrations are modelled for this data set as described in the following. Models for the measurement noise on the ammonia and nitrate FIA-analyzers are of the type (5.2) with the extension, that the variances, $\sigma^2_{\eta,i}$, are made time-varying (heteroscedastic) using an ARCH-structure (AutoRegressive model with Conditional Heteroscedasticity). For details on ARCH-models, see Tong (1990).

$$\sigma^2_{\eta,i,t} = \sigma^2_{\eta,i} + \theta_\eta \eta^2_{i,t-4} \tag{5.6}$$

where θ_η is a parameter. In practice, when estimating (5.6) $\eta_{i,t-4}$ is substituted by the prediction error, v_{t-4} and the initial value of $\eta_{i,t-4}$ is chosen

arbitrarily. Long time series like data set No.2 rarely have a constant variance on the measurement error, due to varying accuracy in the measuring equipment. The ARCH-structure is a convenient way of describing this phenomenon, because the variance of $\eta_{i,t}$ is a slow varying process partly reflected in the squared residuals.

The following models are obtained using (5.2) for the measurement error of the ammonia concentration FIA-analyzer

$$(1 - \phi_4 B^4)\nu_t = \eta_{i,t} \tag{5.7}$$

and for the measurement error of the nitrate concentration FIA-analyzer

$$\nu_t = \eta_{i,t} \tag{5.8}$$

where $\eta_{i,t}$ is NID with mean s_i and a variance given by (5.6). The estimates from modelling the measurement error ν_t on data set No.2 are shown in Table 5.2. The standard deviation of the estimates ranges from 2-10% of the estimated values, which is somewhat smaller than the standard deviations obtained from the previous data set due to the large number of observations.

Following the discussion from modelling the measurement error of data set No.1, the estimates of s_i based on measurements of ammonia concentrations are more significant than those obtained from the measurements of nitrate concentrations. The ϕ_4-parameter for the measurement error of the nitrate concentration FIA-analyzer is found to be insignificant for the same reason. Modelling (5.6) for this dataset, the number of $\sigma^2_{\eta,i}$-parameters can be reduced by sequentially testing $\sigma^2_{\eta,i} = \sigma^2_{\eta,j}$ for different values of i and j using the likelihood ratio approach (4.86). Thereby, the number of $\sigma^2_{\eta,i}$-parameters could be reduced by two for both time series. In Table 5.2 this testing has resulted in equal values for some of the $\sigma^2_{\eta,i}$-parameters.

Analysis of the residuals weighted by the variance of the prediction errors from the estimation of the models of Section 6.4 and 6.5 shows a correlation in lag 4 of the correlogram, which is significantly different from zero.

Parameter	Ammonia	Nitrate
ϕ_4	0.158	-
s_1	0.087	0.008
s_2	-0.032	0.011
s_3	-0.039	-0.008
s_4	-0.015	-0.012
θ_η	0.094	0.115
$\sigma^2_{\eta,1}$	0.00130	0.00067
$\sigma^2_{\eta,2}$	0.00039	0.00067
$\sigma^2_{\eta,3}$	0.00130	0.00067
$\sigma^2_{\eta,4}$	0.00039	0.00312

Table 5.2. *Parameter estimates from modelling the measurement system on data set No.2.*

This indicates that the model of the measurement system does not give a sufficient description of the noise introduced by the measurement cycle. Thus, a more detailed model is required to assure that the error terms are NID. In fact, this correlation also has a major influence on the convergence of the maximum likelihood estimation, in particular, for the modelling of the ammonia concentrations. The use of an ARCH-structure to model the variation of the variance of $\eta_{i,t}$ showed to be crucial for the convergence. Attempts to estimate reduced models for the measurement system have shown not to converge.

5.3 Modelling in the sample time domain - data set No.1

In the introduction of this chapter it was mentioned that this data set was used in the early stage of the development of the grey box models presented in Section 4.4. Therefore, some of the models in this section may differ from the more general grey box models of the pilot plant presented in the

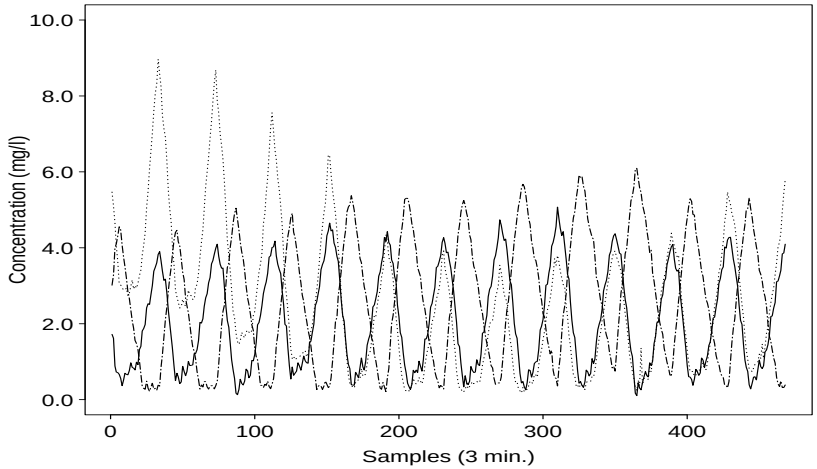

Figure 5.4. *Online measurements of ammonia (solid curve), nitrate (dashed curve), and phosphate (dotted curve) concentrations from the Lundtofte pilot scale plant (data set No.1). The operation of the plant follows the BIO-DENIPHO scheme (see Figure 3.4).*

next section, but they illustrate the evolution of grey box modelling of the hydraulic and biochemical processes. Grey box models for the time series of phosphate concentrations are only estimated on this data set, because the measurements of phosphate concentrations in data set No.2 were unreliable. Furthermore, the nutrient transport process of the aeration tanks is not incorporated in these preliminary models and thus not described below. The measurements of ammonia, nitrate, and phosphate concentrations are shown in Figure 5.4.

The observation equations for the three time series of ammonia, nitrate, and phosphate concentrations have the same form

$$y_t = m_t + \nu_t \tag{5.9}$$

where models for ν_t were given in the previous section and m_t is the true concentration of ammonia, nitrate, or phosphate. The process equation for the three time series are identified as simple autoregressive models of the type

$$(1-\phi B)(\Delta m_t - \mu_t) = \boldsymbol{\delta}^T \boldsymbol{u}_t + e_t \tag{5.10}$$

where μ_t is given in (4.31-4.33) and ϕ is tested to be identical zero for the modelling of ammonia and nitrate concentrations, and $\widehat{\phi} = 0.35$ (with a standard deviation of ± 0.01) for the modelling of phosphate concentrations. The explanatory variables on the right-hand side of (5.10) are used to describe transient phenomena, as described in Section 4.4.2. However, the modelling of transient phenomena will be not be discussed any further in this chapter, but it has been incorporated into the models. The significance of the ϕ-parameters may also be verified by inspecting Figure 5.4, where the dynamics of the operation cycles are similar for the measurements of both ammonia and nitrate concentrations. The measurements of the phosphate concentrations show larger variations. Actually, the time series of ammonia and nitrate concentrations in this data set do appear to have a very systematic variation.

5.3.1 Influent load

Assuming the nitrate concentration in the influent to the aeration tanks to be vanishing, the influent load process is only estimated for the time series of ammonia and phosphate. For this data set a rate expression similar to (4.34) is found adequate for these two load processes. However, it should be stressed, that the flow rate to the pilot plant is held constant and models for the operation cycle time domain have not been estimated. Thus, in order to describe the the diurnal variations of the load rate, a profile, ρ_t, is applied

$$r_{load,.,t} = \begin{cases} k_{load,.} \cdot \rho_t \cdot Q & \text{inlet valve open} \\ 0 & \text{inlet valve close} \end{cases} \tag{5.11}$$

where the period in $r_{load,.,t}$ and $k_{load,.}$ indicates that the model is valid for both ammonia and phosphate concentrations. The diurnal profile, ρ_t, is described by a second order Fourier expansion (4.17).

$$\rho_t = 1 + \alpha_1 \cos\frac{2\pi t}{S} + \beta_1 \sin\frac{2\pi t}{S} + \alpha_2 \cos\frac{4\pi t}{S} + \beta_2 \sin\frac{4\pi t}{S} \tag{5.12}$$

where $S = 480$ is the number of observations in a day. Using the approximation in (4.35) it is found that

$$k_{load,NH_4^+}\frac{V}{T_S} \approx \overline{C}_{i,NH_4^+} \tag{5.13}$$

i.e. the average influent concentration of ammonia may be found from the estimate of k_{load,NH_4^+}. Multiplying k_{load,NH_4^+} by ρ_t describes the diurnal variation of the influent concentrations of ammonia. In Figure 5.5 the estimated influent concentrations of ammonia is compared to the measured concentrations of ammonia in the pretreatment column, which are not used in the modelling. The diurnal profile clearly has some deficiencies in describing the fast dynamics of the measurements from the pretreatment column, but the general trend of the measured concentrations is contained in ρ_t. The estimated influent concentrations are significantly lower than the measured values. The reason for this will be explained in the subsequent section.

The approximation (4.36) does not implicitly apply to the estimate of $k_{load,PO_4^{3-}}$, because the simultaneous phosphate uptake during anoxic conditions cannot be identified. Thus, $k_{load,PO_4^{3-}}$ is the rate of the combined influent phosphate load process and biological phosphate uptake in biomass process during anoxic conditions, which is considered as a net influent phosphate load process. In Figure 5.6 the equivalent influent phosphate concentrations of the net influent load process is compared to the measured

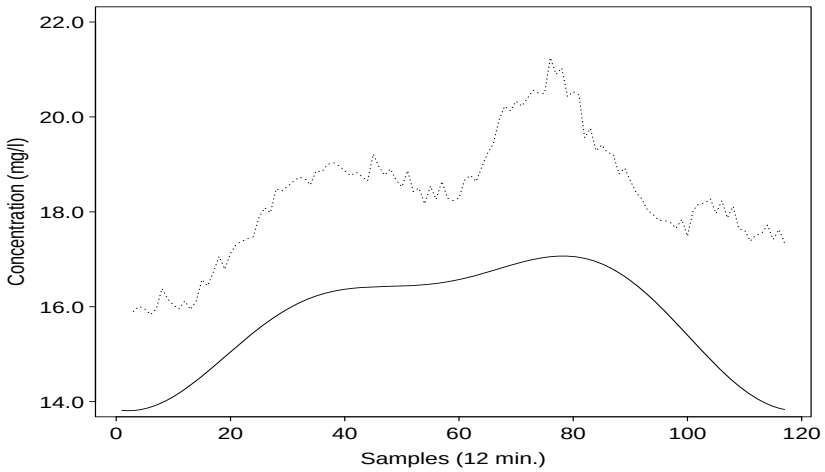

Figure 5.5. *Estimated (solid curve) and measured (dotted curve) influent concentration of ammonia to aeration tank T2.*

phosphate concentrations of the outlet of the pretreatment column. The cyclic phenomena in the measured phosphate concentrations of the outlet is due to a small amount of nitrate being recycled from the sedimentation vessel.

The profile of the estimated net influent phosphate load does contain the general slow dynamics of the measured phosphate concentration in the outlet of the pretreatment column without the cyclic effects from the alternating operation, but the net influent phosphate load rate is approximately half the magnitude of the true influent phosphate load, as indicated on Figure 5.6. Thus, the phosphate uptake during anoxic conditions is approximately of the same magnitude as the net influent phosphate load rate, i.e. approximately 3.1 mg PO_4^{3-}-P/l/h is accumulated in the biomass during anoxic conditions. With a maintained constant suspended solids concentration in the aeration tanks of 4-5 g SS/l, the phosphate uptake during anoxic conditions is in the range 0.6-0.8 mg PO_4^{3-}-P/h/g SS. Kerrn-Jespersen & Henze (1993) have found from batch tests with activated sludge, that the

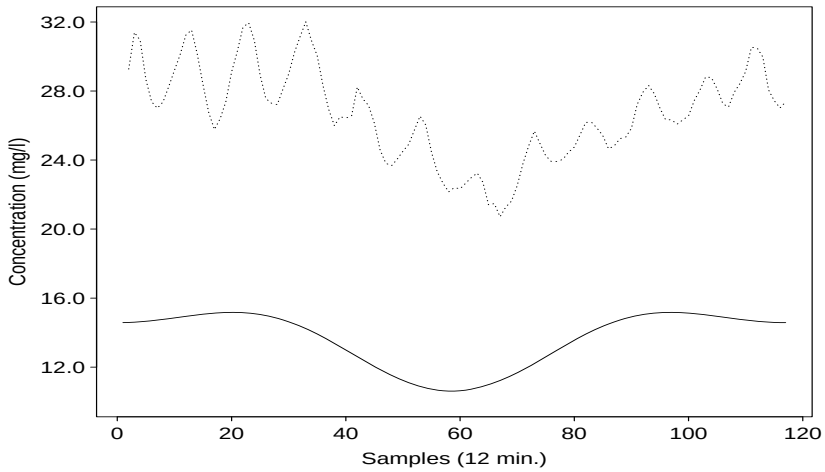

Figure 5.6. *Estimated (solid curve) and measured (dotted curve) influent concentration of phosphate to aeration tank T2.*

phosphate uptake rate during anoxic conditions is in the range 0.4-1.0 mg PO_4^{3-}-P/h/g SS at a temperature of 14°C.

The diurnal profile of the influent ammonia load process resembles that of the flow rate to the Aalborg West WWTP in Figure 3.1, but the diurnal profile of the net influent phosphate load process is very different. This could be due to an unusual high load of readily bio-degradable substrate at night-time in the anaerobic pretreatment column causing the phosphate accumulating bacteria to strip an excessive amount of phosphate. When estimating the profile, ρ_t, insignificant parameters have been removed in (5.12). The estimates of the process are shown in Table 5.3.

Parameter	Ammonia	Phosphate
$\overline{C}_i$	15.8 (±0.2)	13.6 (±0.3)
α_1	-0.086	0.145
β_1	-0.026	-
α_2	-0.036	-0.077
β_2	-	-0.012

Table 5.3. *Parameter estimates from modelling the influent load process on data set No.1.*

5.3.2 Hydrolysis and growth of biomass

The hydrolysis and growth of biomass process is the least significant process estimated on this data set, and it can only be identified by a single parameter. However, the variation of the process is assumed to be correlated to the ammonia load process. The hydrolysis and growth of biomass process is mainly identified from the time series of ammonia and phosphate concentrations, when there is no influent load to T2 and oxygen is not present. In Figure 5.4 the hydrolysis and growth of biomass process is graphically recognized from the slightly increasing curves of ammonia and phosphate concentrations at the bottom of the graph, i.e. the time between the switch off of the diffuser and the opening of the inlet valve.

In order to describe this process, the rate was identified as follows

$$r_{hydrolysis_{i,.},t} = k_{hydrolysis_{i,.}} \cdot \rho_t \tag{5.14}$$

where $k_{hydrolysis_{i,.}}$ is the parameter being estimated and the ammonia load profile ρ_t is given by (5.12). The hydrolysis and growth of biomass process is assumed to have the same diurnal profile as the load process of ammonia, simply because a separate profile for the process cannot be identified. It is found, that on average 1.09 mg NH_4^+-N/l (±0.03) and 0.24 mg PO_4^{3-}-P/l (±0.04) is produced from this process during the sampling period of data

set No.1. On the assumption that the returned sludge is not hydrolyzed this corresponds to an influent concentration of 9.7 mg organic N/l (±0.3) and 2.1 mg organic P/l (±0.3), which can be hydrolyzed. Comparing this to the typical measures of organic nitrogen and organic phosphorus in the raw wastewater of Table 3.2, only half of the organic nitrogen and 2/3 of the organic phosphorus of the raw wastewater appears to be hydrolyzed. However, as mentioned in Section 4.4.1, the estimated process rate is a net hydrolysis rate including the simultaneous production of ammonia and phosphate by hydrolysis and removal of ammonia and phosphate by growth of biomass. Thus, the influent concentrations of organic nitrogen and phosphorus which can be hydrolyzed are larger than the estimated values above.

5.3.3 The nitrification process

In these preliminary models two different submodels for the nitrification process are proposed: one based on the time series of ammonia concentrations and the other based on the time series of nitrate concentrations. As described in the introduction of this chapter, the diffusers are controlled such that the oxygen concentration is practically constant in the aerobic period. For this data set measurements of the oxygen concentrations are available, but an expression like (4.41) cannot be satisfactorily identified because of noise on the oxygen measurements and the fact that an almost constant oxygen level makes the practical identification of K_{O_2} impossible. Thus, in order to identify a Monod-kinetic expression for the oxygen dependency of the nitrification process, the data set should contain periods with different oxygen setpoints. Instead, the oxygen measurements are used to distinguish aerobic periods from anoxic and anaerobic periods, when the measurements of the oxygen concentration exceeds 0.5 mg O_2/l. Furthermore, measurements of the suspended solids concentration are not available at the pilot plant, but it is maintained constant through removal of excess sludge and because the plant is not exposed to hydraulic loads of rainwater.

For this data set the nitrification process is identified as follows for the measurements of ammonia concentrations

$$r_{nit,NH_4^+,t} = \begin{cases} -k_{nit,max,NH_4^+} \cdot \frac{S_{NH_4^+,t-1}}{S_{NH_4^+,t-1}+K_{NH_4^+}} & \text{aerobic conditions} \\ 0 & \text{anoxic/anaerobic conditions} \end{cases} \tag{5.15}$$

where $\widehat{k}_{nit,max,NH_4^+} = 7.4$ mg NH_4^+-N/l/h (± 0.1) and $\widehat{K}_{NH_4^+} = 0.12$ mg NH_4^+-N/l (± 0.01). The mean of the posterior distribution for m_t is used as the optimal estimator of the true ammonia concentration in T2, i.e. $S_{NH_4^+,t-1}$ is replaced by the Kalman update $\widehat{m}_{t-1|t-1}$ in (5.15). The estimate of $K_{NH_4^+}$ is low compared to the values given in the literature (Henze et al. (1990) suggest $K_{NH_4^+}$ to be in the range 0.3-0.7 mg NH_4^+-N/l). This could be due to an offset calibration error in the ammonia FIA-analyzer. However, the estimate is based on measurements of ammonia concentrations of which almost all have values above 0.5 mg NH_4^+-N/l (only two observations below the estimated half-saturation constant), due to an operation strategy experiment. For this data set the diffuser are switched off, when the concentration of ammonia lies below 1.0 mg NH_4^+-N/l. Thus, the estimate is naturally uncertain, but it is found to be significantly different from zero (which would give a zero order kinetic process).

A totally different and more empirical model is proposed for the same process based on measurements of nitrate concentrations.

$$r_{nit,NO_3^-,t} = \begin{cases} -k_{nit,max,NO_3^-} - \gamma(t-t_0)\rho_t & \text{aerobic conditions} \\ 0 & \text{anoxic/anaerobic conditions} \end{cases} \tag{5.16}$$

where t_0 denotes the time for the start of the aerobic phase, and ρ_t is a diurnal profile similar to (5.12), but estimated for the time series of nitrate concentrations. An obvious disadvantage of modelling the nitrification process by (5.16) is the fact that long periods of aeration would eventually result in removal of nitrate! For the phase lengths of the aerobic periods in this data set, the nitrification rate would decrease from 9.2 mg NO_3^--N/l/h (± 0.07) in the beginning of the aerobic phase to approximately 3.0 mg NO_3^--N/l/h at the end of the aerobic phase. The model does not reflect the true characteristics of the nitrification process, but it serves the purpose of showing the evolution from "dark grey" box models to the grey box models, which are shown in the subsequent section.

5.3.4 The denitrification process

It has previously been mentioned that periods of time in the operation cycle occur when there is neither oxygen present nor influent load. For the time series of ammonia and phosphate concentrations these periods were characterized by the hydrolysis and growth of biomass process as shown in Figure 5.4, while the denitrification process is the most significant process in these periods of the nitrate concentration time series. However, the concentration of readily bio-degradable substrate is much lower in these periods without influent load compared to the anoxic periods with influent load, and as a result the rate of the denitrification process differs significantly. A reduced model of (4.45) is identified for the given data set.

$$r_{denit,t} = \begin{cases} -k^1_{denit,max} \cdot \frac{S_{NO_3^-,t-1}}{S_{NO_3^-,t-1}+K_{NO_3^-}} \cdot \rho_t & \text{anoxic conditions and no influent load} \\ -k^2_{denit,max} \cdot \frac{S_{NO_3^-,t-1}}{S_{NO_3^-,t-1}+K_{NO_3^-}} \cdot \rho_t & \text{anoxic conditions and influent load} \\ 0 & \text{aerobic/anaerobic conditions} \end{cases} \tag{5.17}$$

The maximum denitrification rate in anoxic periods with no influent load, $k^1_{denit,max}$, and in anoxic periods with influent load, $k^2_{denit,max}$, are estimated to 6.1 mg NO_3^--N/l/h (± 0.09) and 7.0 mg NO_3^--N/l/h (± 0.12), respectively, while the half-saturation constant, $K_{NO_3^-}$, is estimated to 0.71

mg NO_3^--N/l (± 0.03). The mean of the posterior distribution for m_t is used as the optimal estimator of the true nitrate concentration in T2, i.e. $S_{NO_3^-,t-1}$ is replaced by the Kalman update $\widehat{m}_{t-1|t-1}$ in (5.17). A diurnal profile, ρ_t, of the form (5.12) is used in the denitrification expression in order to describe some of the dependency of the readily bio-degradable substrate concentration. Estimates from the diurnal profile also suggest a peak load of readily bio-degradable substrate at night-time.

The relative high denitrification rate in anoxic periods without influent load could be a result of the experimental operational strategy of switching off the aeration when the ammonia concentration drops below 1.0 mg NH_4^+-N/l. However, further investigations are required to confirm an overall improved denitrification.

5.3.5 Biological phosphate uptake in biomass

The biological phosphate uptake is identified using a model similar to (4.47) with the exception that the phosphate uptake during anoxic conditions cannot be identified, and therefore it was included in the net influent phosphate load process described previously. Furthermore, measurements of the suspended solids concentration are not available, but the suspended solids concentration is maintained approximately constant. Thus, the following model of type (4.47) can be identified:

$$r_{P-uptake,t} = \begin{cases} -k_{P-uptake,max} \cdot \frac{S_{PO_4^{3-},t-1}}{S_{PO_4^{3-},t-1}+K_{PO_4^{3-}}} \cdot \rho_t & \text{aerobic conditions} \\ 0 & \text{anoxic/anaerobic conditions} \end{cases} \tag{5.18}$$

where $\widehat{k}_{P-uptake} = 10.1$ mg PO_4^{3-}-P/l/h (± 0.12) and $\widehat{K}_{PO_4^{3-}} = 2.11$ mg PO_4^{3-}-P/l (± 0.07), and the diurnal profile is identical to the profile estimated for the influent load of phosphate. The mean of the posterior distribution of m_t is used as the optimal estimator of the true phosphate concentration in T2, i.e. $S_{PO_4^{3-},t-1}$ is replaced by the Kalman update $\widehat{m}_{t-1|t-1}$ in (5.18).

The estimated uptake rate during aerobic conditions is significantly larger than the presumed phosphate uptake rate during anoxic conditions, which was loosely estimated in Section 6.3.1. However, it is a biased estimate due to the estimate of $K_{PO_4^{3-}}$, which is very high for a Monod-kinetic expression. Furthermore, it should be stressed that (5.18) does not take the storage of intra-cellular substrate into account, which may be rate-limiting for the process. In fact, comparing the estimate of $K_{PO_4^{3-}}$ with the estimates of the half-saturation constants for the nitrification and denitrification processes, the Monod-expression in (5.18) cannot be considered as being a simple term for the diffusion of phosphate. Combining this with the fact that the model for the rate of biological phosphate uptake in biomass is improved using a diurnal variation, it must be concluded that a physical model of the process has to include additional rate-limiting terms (e.g. a Monod-kinetic expression for the dependency of simple organic compounds used by the phosphorus accumulating bacteria). However, these terms cannot be identified in a grey box model. Hence, (5.18) gives a satisfactory description of data, but the physical interpretability of the parameters give less satisfaction.

5.3.6 Stripping of phosphate

In the time series of phosphate concentrations there are six occurrences of phosphate stripping. This process only occur when the nitrate concentration is below 0.5 mg NO_3^--N/l in the anoxic phase of the operation cycle, i.e. anaerobic conditions are present in the aeration tank T2. The stripping of phosphate is identified on top of the influent load process of phosphate, which is seen as a crack on the inclining curves of phosphate concentrations in Figure 5.4. The following expression is identified for the process:

$$r_{P-strip,t} = \begin{cases} k_{P-strip} \cdot \rho_t^* & \text{anaerobic conditions} \\ 0 & \text{aerobic/anoxic conditions} \end{cases} \tag{5.19}$$

where ρ_t^* indicates that the stripping process shows a diurnal variation which is different from the diurnal profile of the influent phosphate load. Actually, the two profiles are similar in form, but the profile in (5.19) has a phase displacement of 8 hours relative to the profile of the phosphate influent load, i.e. the maximum phosphate stripping rate occurs 8 hours after the maximum influent phosphate concentration has been identified. It has been estimated that during the stripping of phosphate an average of 2.3 mg PO_4^{3-}-P/l/h (± 0.12) is released.

5.4 Modelling in the sample time domain - data set No.2

This second data set from the pilot scale plant was used for developing grey box models in both the sample time domain and operation cycle time domain. In this section the models of the sample time domain are concerned.

The models presented in this section are more comparable to the grey box models described in Section 4.4, than the models of the previous section. However, some allowances for the lack of information on the suspended solids concentration and lack of different oxygen setpoint in the operation of the plant, are made. Furthermore, models based on observations of phosphate concentrations are not estimated, because the measurements are unreliable in large periods of the time series. The time series of ammonia and nitrate concentrations correspond to those shown in Figure 5.4, but showing far more variation in the slopes of the curves. For this data set the aeration was solely controlled by prior scheduled phase-lengths of the aerobic phases, regardless of the present ammonia concentrations in the aeration tanks as opposed to the previous data set.

The observation equations for the time series of ammonia and nitrate are identical and given by (4.23),

$$y_t = m_t + \nu_t \tag{5.20}$$

where ν_t was modelled separately for the time series in Section 6.2 and m_t is the true concentration of ammonia or nitrate. The process equation for the two time series is both described by

$$(1-\phi B)(\Delta m_t - \mu_t) = \boldsymbol{\delta}^T \boldsymbol{u}_t + e_t \tag{5.21}$$

where e_t is NID, and $\widehat{\phi} = 0.60$ (± 0.01) for the model of the ammonia concentrations and $\widehat{\phi} = 0.57$ (± 0.01) for the model of the nitrate concentrations. These estimates of ϕ are larger than the estimates obtained from the previous data set indicating that the variations of the concentration gradient, Δm_t, are more stochastic, i.e. there are larger variations in the slopes of the ammonia and nitrate measurements. The explanatory variables on the right-hand side of (5.21) are used to describe transient phenomena, as described in Section 4.4.2, which will not be discussed any further. In order to manage variations in the model performance of (5.21), the variance of e_t is modelled as an ARCH-structure (see Tong (1990)).

$$\sigma_{e,t}^2 = \sigma_e^2 + \theta e_{t-1}^2 \tag{5.22}$$

where θ is a parameter. In practice, when estimating an expression like (5.22), e_{t-1} is substituted by the prediction error, v_{t-1}, and the initial value of e_{t-1} is chosen arbitrarily. However, during the switching of flowpatterns an expression like (5.22) is found inappropriate, and as a result a separate parameter for the variance of e_t during the switching of flowpatterns is estimated.

5.4.1 Influent load

The ammonia load to the pilot plant is modelled according to (4.34) with k_{load,NH_4^+} being a time-varying parameter of the operation cycle time domain (see the subsequent section), i.e.

$$r_{load,NH_4^+,t} = \begin{cases} k_{load,NH_4^+,f} \cdot Q & \text{inlet valve open} \\ 0 & \text{inlet valve closed} \end{cases} \tag{5.23}$$

where Q is the constant flow into the aeration tanks (180 l/h). Thus, the load rate is constant during a given operation cycle, and estimating the load rate based on observations from one operation cycle, f, by use of e.g. a least squares algorithms, an estimate of $k_{load,NH_4^+,f}$ is obtained. This estimate is used for updating the model of the influent load rate of ammonia in the operation cycle time domain. The average influent load rate, $\overline{k}_{load,NH_4^+} \cdot Q$, is estimated to 2.0 mg NH_4^+-N/l/h, which is equivalent to an average influent ammonia concentration of 8.9 mg NH_4^+/l.

5.4.2 Nutrient transport of the aeration tanks

The nutrient transport process affects both the ammonia and nitrate concentration, and it is important to incorporate this process into the grey box models in order to yield better estimates of other processes and making the mass balance of nutrients agree. Unfortunately, an identification of this process for the time series of ammonia and the parameter of (4.37) is not possible, because the processes of influent ammonia load, nitrification, and hydrolysis and growth of biomass are more significant, and at least one of these three processes is always active. The process could be modelled without any estimation of the related parameter $k_{transport,NH_4^+}$ by using the actual volume holding, V, and describing the process as a purely deterministic process. This is, however, inconsistent with the concept of statistical identification of the process for two reasons. Firstly, the hydraulic effects when switching flow patterns have not been sufficiently described and secondly, the assumption of ideal mixing of the aeration tanks may prove wrong. Due to the insignificance of the process, omission of the process rate in the μ_t-expression (4.31) will have little influence on the other processes affecting the ammonia concentration.

For the time series of nitrate concentrations the nutrient transport process is identified. From the curves of the nitrate measurements the process is mainly identified during aerobic periods, when the nitrification becomes slow due to low concentrations of ammonia, i.e. the nitrate concentration eventually decreases because more nitrate is transported from the tank than produced by the nitrification process. Furthermore, the nitrate concentration is on average twice as high as the ammonia concentration in T2, thereby making the transport process of nitrate twice as significant as the transport process of ammonia.

The transport of nitrate into and from T2 is modelled as follows:

$$r_{transport,NO_3^-,t} = \begin{cases} k_{transport,NO_3^-}(S^I_{NO_3^-,t-1} - S_{NO_3^-,t-1}) \cdot Q & \\ \qquad\qquad \text{outlet valve open} & \\ -k_{transport,NO_3^-} \cdot S_{NO_3^-,t-1} \cdot Q & \\ \qquad\qquad \text{inlet valve open} & \end{cases} \tag{5.24}$$

where $S^I_{NO_3^-,t-1}$ is replaced by the nitrate measurement in T2 half an operation cycle ago, and $S_{NO_3^-,t-1}$ is replaced by the optimal estimator of the true nitrate concentration in T2, $\widehat{m}_{t-1|t-1}$, which is the mean of the posterior distribution for m_t. It is found, that $\widehat{k}_{transport,NO_3^-} = 0.0014\ \text{l}^{-1}$ $(\pm 0.8 \cdot 10^{-4})$, which under the assumption of ideal mixing in the aeration tanks and little hydraulic effect from switching flow patterns corresponds to a volume holding of 713 l $(^{+45}_{-41})$ and a hydraulic retention time of 4.0 h. These estimates are close to the actual physical parameter values ($T_h = 4.4$ h and $V = 800$ l), but the fact that $\widehat{k}_{transport,NO_3^-}$ is larger than the actual physical parameter value slightly indicates that the aeration tank T2 may not be ideally mixed, i.e. there are different nitrate concentrations in different parts of the tank. However, this hypothesis is based on an estimate from one of the less significant processes, and further investigation is required if it should be concluded whether the aeration tanks at the pilot scale plant are ideally mixed. It is, however, of minor importance for the total process.

5.4.3 Hydrolysis and growth of biomass

The hydrolysis and growth of biomass process is graphically identified at the bottom curves of the ammonia measurements, but it is assumed to be active at a constant rate throughout one operation cycle. The rate of the process is best described as being proportional to the inlet load rate (5.23), $r_{load,NH_4^+,t}$, with the inlet valve open, i.e.

$$r_{hydrolysis,NH_4^+,t} = k_{hydrolysis,NH_4^+} \cdot k_{load,NH_4^+,f} \cdot Q \tag{5.25}$$

This is based on the fact that ammonia and organic loads are correlated. It is found, that in average 0.78 mg NH_4^+-N/l/h ($\pm$0.02) on weekdays and 0.57 mg NH_4^+-N/l/h ($\pm$0.02) on weekends is produced from this process during the sampling period of data set No.2. The variations of the hydrolysis and growth of biomass process rate are enforced by the model for the variations of $k_{load,NH_4^+,f}$, which are graphically illustrated in Figure 5.7. The hydrolysis and growth of biomass process rate is lower for this data set compared to the results given in Section 6.3.2. This is due to the fact that data set No.1 covers an over-average loaded day with high loads of hydrolysable compounds, while data set No.2 covers a longer period with a mix of high- and low-loaded days. Thus, the rate of hydrolysis and growth of biomass estimated for data set No.2 is more representative of the overall process rate.

5.4.4 The nitrification process

Following the discussion in Section 6.3.3 a practical identification of K_{O_2} in (4.41) and (4.42) is not feasible, but the oxygen measurements are used to distinguish aerobic periods from anoxic and anaerobic periods when the measurements of the oxygen concentration exceeds 0.5 mg O_2/l. Measurements of the suspended solids concentration are not available, but it is maintained constant through removal of excess sludge and because the pilot plant is not exposed to hydraulic loads of rainwater. Thus, reduced

Parameter	Unit	Ammonia	Nitrate
$\overline{k}_{nit,max,\cdot}$	mg N/l/h	10.5	9.8
$\widehat{K}_{NH_4^+}$	mg NH_4^+-N/l	0.44 ($\pm$0.02)	0.35 ($\pm$0.01)

Table 5.4. *Parameter estimates from modelling the nitrification process on data set No.2.*

models of the grey box models for the nitrification process in (4.41) and (4.42) are identified for the ammonia concentrations

$$r_{nit,NH_4^+,t} = \begin{cases} -k_{nit,max,NH_4^+,f} \cdot \frac{S_{NH_4^+,t-1}}{S_{NH_4^+,t-1}+K_{NH_4^+}} & \text{aerobic conditions} \\ 0 & \text{anoxic/anaerobic conditions} \end{cases} \tag{5.26}$$

and for the nitrate concentrations

$$r_{nit,NO_3^-,t} = \begin{cases} k_{nit,max,NO_3^-,f} \cdot \frac{S_{NH_4^+,t-1}}{S_{NH_4^+,t-1}+K_{NH_4^+}} & \text{aerobic conditions} \\ 0 & \text{anoxic/anaerobic conditions} \end{cases} \tag{5.27}$$

where models for the variation of $k_{nit,max,NH_4^+,f}$ and $k_{nit,max,NO_3^-,f}$ in the operation cycle time domain are given in the subsequent section. The mean of the posterior distribution for m_t is used as the optimal estimator of the true ammonia concentration in T2, i.e. $S_{NH_4^+,t-1}$ is replaced by the Kalman update $\widehat{m}_{t-1|t-1}$ in (5.26) and (5.27). The results of estimating the nitrification process on data set No.2 in the sample time domain are given in Table 5.4.

The estimates of the average maximum nitrification rate given in Table 5.4 are larger than the estimate found in Section 6.3.3, due to higher estimates of the half-saturation constant $K_{NH_4^+}$. However, the estimates found in

Table 5.4 are more reliable, because data set No.2 covers a longer period of time with a great number of ammonia measurements above and below the estimated half-saturation constants. A likelihood ratio test has proven that $\widehat{K}_{NH_4^+} = 0.40$ mg NH_4^+-N/l is a sufficient estimate for both time series, and as a result the standard deviations of the estimates in Table 5.4 are likely too small. Given the estimates of $K_{NH_4^+}$ based on all observations from the two time series, estimates of $k_{nit,max,NH_4^+,f}$ and $k_{nit,max,NO_3^-,f}$ are obtained using the observations from one operation cycle, f, and the estimators (5.26) and (5.27). These estimates are used for updating the models of the maximum nitrification rate in the operation cycle time domain.

The estimates of the half-saturation constant and the estimates related to the model of the maximum nitrification rate, $k_{nit,max,NH_4^+,f}$ which is given in Section 6.5.2, are naturally more internally correlated compared to the other estimates, but the correlation is found to be statistically insignificant. Thus, it can be concluded that a practical identification of Monod-kinetic expressions is feasible, if an extensive data set is available.

5.4.5 The denitrification process

Examination of data has shown that the dependency of readily biodegradable substrate used for the denitrification process can be described by a Monod-kinetic expression of the influent ammonia load rate. Assuming that the non-monitored suspended solids concentration is maintained constant the following expression can be identified (see also (4.45):

$$r_{denit,t} = \begin{cases} -k^1_{denit,max,f} \cdot \frac{S_{NO_3^-,t-1}}{S_{NO_3^-,t-1}+K_{NO_3^-}} \cdot \frac{k_{load,NH_4^+,f-1} \cdot Q}{k_{load,NH_4^+,f-1} \cdot Q + K_{load}} \\ \qquad \text{anoxic conditions and no influent load} \\ -k^2_{denit,max,f} \cdot \frac{S_{NO_3^-,t-1}}{S_{NO_3^-,t-1}+K_{NO_3^-}} \cdot \frac{k_{load,NH_4^+,f-1} \cdot Q}{k_{load,NH_4^+,f-1} \cdot Q + K_{load}} \\ \qquad \text{anoxic conditions and influent load} \\ 0 \qquad \text{aerobic/anaerobic conditions} \end{cases} \tag{5.28}$$

where the two maximum denitrification parameters are assumed to have the following relationship

$$k^1_{denit,max,f} = k^2_{denit,max,f} - \gamma \tag{5.29}$$

where $\gamma > 0$ is a constant parameter. Assuming the two maximum denitrification parameters to be proportional did not give a better description of data. Thus, $k^1_{denit,max,f}$ and $k^2_{denit,max,f}$ show identical variations in the operation cycle time domain but shifted by the value of γ. The reason for modelling $k^1_{denit,max,f}$ as a function of $k^2_{denit,max,f}$ is, that $k^1_{denit,max,f}$ cannot be modelled as a self-contained process in the operation cycle time domain. The mean of the posterior distribution for m_t is used as the optimal estimator of the true nitrate concentration in T2, i.e. $S_{NO_3^-,t-1}$ is replaced by the Kalman update $\widehat{m}_{t-1|t-1}$ in (5.28). The estimated load parameter of the previous operation cycle, $\widehat{k}_{load,NH_4^+,f-1}$, is used in the second Monod-kinetic term in (5.28).

The average maximum denitrification rate in periods with no influent load, $\overline{k}^1_{denit,max,f}$, and in periods with influent load, $\overline{k}^2_{denit,max,f}$, are estimated to 3.29 mg NO_3^--N/l/h and 4.35 mg NO_3^--N/l/h, respectively, while the half-saturation constant $\widehat{K}_{NO_3^-} = 0.40$ mg NO_3^--N/l (± 0.01). Estimating the correlated Monod-expression for the dependency of readily bio-degradable substrate in (5.28), it is found that $\widehat{K}_{load} = 0.43$ mg NH_4^+-N/l/h (± 0.05), i.e. with a load of 0.43 mg NH_4^+-N/l/h to the aeration tanks the denitrification rate is only half the maximum attainable, $k^2_{denit,max,f}$, under

the assumption that $S_{NO_3^-,t} \gg K_{NO_3^-}$. Assuming that all the readily biodegradable substrate for denitrification comes from the raw wastewater and the COD to ammonia ratio in the wastewater entering the aeration tank is 18 mg COD/mg NH_4^+-N (using Table 3.1 and Table 3.2 for moderately loaded wastewater), this estimate corresponds to $\widehat{K}_S = 15.0$ mg COD/l (± 1.74). Henze et al. (1990) suggest that K_S is in the range 10-20 mg COD/l when using raw wastewater as the carbon source.

The estimates above are more reliable than those obtained in the previous section, because data set No.2 covers a longer period of time with a larger variation in loads, and because the model estimated on this data set includes a term which is capable of describing some of the dependency of readily bio-degradable substrate. Given the estimates of $K_{NO_3^-}$ and K_{load} based on all observations from the time series, estimates of $k^2_{denit,max,f}$ are obtained using the observations from one operation cycle, f, and (5.28) as estimator. These estimates are used for updating the models of the maximum denitrification rate in the operation cycle time domain.

5.5 Modelling in the operation cycle time domain - data set No.2

The alternating operation mode of the Lundtofte pilot scale plant introduces break-points into the time series, such that some of the parameters given in the previous section may be modelled in the operation cycle time domain. The interaction of the two time domains and exchange of information is illustrated in Figure 4.5.

In the last section estimators based on data from one operation cycle, f, of $k_{load,NH_4^+,f}$, $k_{nit,max,NH_4^+,f}$, $k_{nit,max,NO_3^-,f}$, and $k^2_{denit,max,f}$ were formulated. The data set contains 152 operation cycles of approximately 50 samples covering more than 16 days. Thus, 152 observations in the operation cycle time domain are available for modelling the influent load rate

of ammonia, the maximum nitrification rate, and the maximum denitrification rate. It might be argued that these parameters vary within a total operation cycle, but these variations are relatively small and treated as stochastic fluctuations, which is modelled using the AR-term in (5.21).

Each of the estimates of $k_{load,NH_4^+,f}$, $k_{nit,max,NH_4^+,f}$, $k_{nit,max,NO_3^-,f}$, and $k^2_{denit,max,f}$ is encumbered with some uncertainty as described in Section 4.4.3 from the observation equations of the four processes (indicated by $\xi_{<process>,f}$) and the process equation of the four processes (indicated by $e_{<process>,f}$). Thus, each of the four models in the operation cycle time domain are put into state space forms, which is handled by the Kalman filter. However, the variances of the $\xi_{<process>,f}$-terms are found to be insignificant relative to the variances of the $e_{<process>,f}$-terms, i.e. $\sigma^2_{\xi,<process>} = 0$ for all the four mentioned processes. This is mainly due to a poor performance of the models in the operation cycle time domain given by the process equations.

5.5.1 Influent load rate of ammonia

The modelling of $k_{load,NH_4^+,f}$ corresponds to describing the variations of the influent concentration of ammonia to T2 when applying the approximation (4.35). Hence, a multiplicative seasonal AR-model of the type (4.53) is found adequate

$$(1-\phi_{load}B)(1+\phi_{load,S}B^S)(k_{load,NH_4^+,f}-\mu_{load,NH_4^+,f}) = e_{load,NH_4^+,f} \tag{5.30}$$

where $e_{load,NH_4^+,f}$ is NID with zero mean and variance $\sigma^2_{e,load,NH_4^+}$, and

$$\mu_{load,NH_4^+,f} = \begin{cases} \mu_{weekday,NH_4^+} & \text{if operation cycle } f \text{ is on a weekday} \\ \mu_{weekend,NH_4^+} & \text{if operation cycle } f \text{ is on a weekend} \end{cases} \tag{5.31}$$

and S denotes the number of operation cycles in a day. However, S is not a fixed parameter, because the number of operation cycles in a day may vary. Thus, when estimating this process it is crucial to keep track of the number of operation cycles in the last 24 hours such that $B^S k_{load,NH_4^+,f}$ always denotes the k_{load,NH_4^+}-value 24 hours back in time.

The estimated parameters of (5.31) correspond to average influent ammonia concentrations (i.e. the ammonia concentration in the outlet of the anaerobic pretreatment column) of 10.3 mg NH_4^+-N/l (± 0.36) on weekdays and 7.5 NH_4^+-N/l (± 0.46) on weekends. Assuming a vanishing ammonia concentration in the returned sludge, estimates of the ammonia concentration in the raw wastewater are found by multiplying the estimated influent ammonia concentrations by two. Surprisingly, the AR-parameter for the diurnal variation, $\phi_{load,S}$, in (5.30) turned out to be insignificant, while $\widehat{\phi}_{load} = 0.77$ (± 0.03).

The estimated influent concentrations of ammonia from each operation cycle and the one-step predictions of (5.30) with $\phi_{load,S} = 0$ are shown in Figure 5.7. The measured ammonia concentration from the outlet of the pretreatment column covering the same period of time are shown in Figure 5.8. These measurements have not been used for modelling the ammonia concentration in T2. The dynamics of the estimated (Figure 5.7) and the measured ammonia concentration (Figure 5.8) in the outlet of the pretreatment column are very similar. This estimation method nearly reveals all existing dynamic in the measured values, however the scaling of the curves is slightly different. This is due to a combination of two reasons.

Firstly, the approximation (4.35) yields a lower biased estimate of $\overline{C}_{i,NH_4^+}$, because the exponential curve in Figure 3.6 is linearized and the concentration in T2 at time of opening the inlet valve, C_0, is neglected. Linearizing the exponential curve result in an error of the magnitude 0-2% of the estimate with the given hydraulic retention time and lengths of the phases with influent load. Neglecting C_0 is in the range 0.0-0.5 mg NH_4^+-N/l for the majority of operation cycles, except for a few peak loads, where the ammonia concentration is in the range 0.5-1.5 mg NH_4^+-N/l when the inlet valve to T2 is opened.

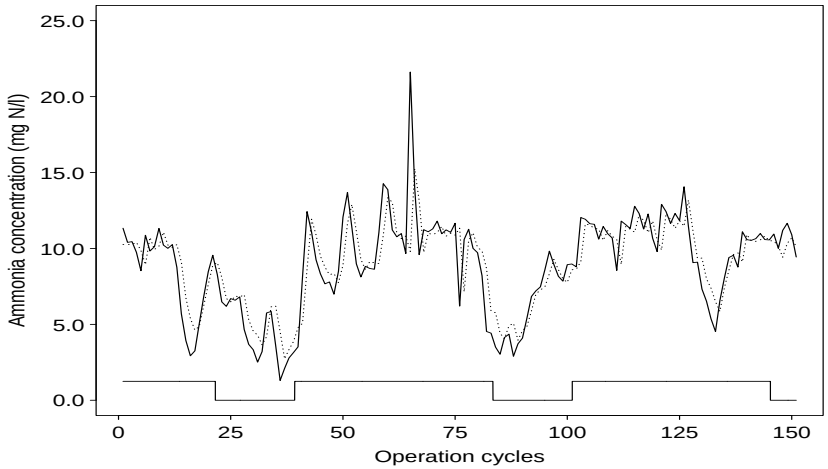

Figure 5.7. *Estimated (solid curve) and one-step predictions (dotted curve) of influent ammonia concentrations to T2. The lower solid curve indicates weekdays and weekends.*

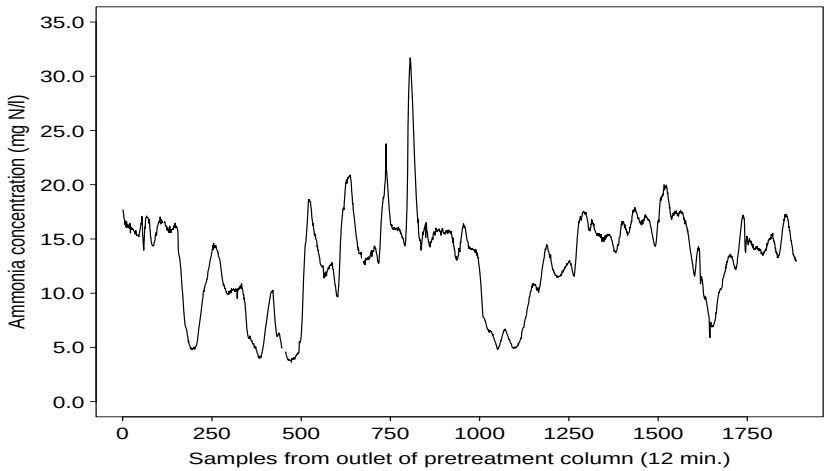

Figure 5.8. *Measured ammonia concentration from outlet of pretreatment column. One operation cycle approximately covers 12 samples from the outlet of the pretreatment column (few observations are missing).*

Secondly, in the models of the sampling time domain it is assumed that approximately 25% of the increase in ammonia concentration during the anoxic phase with influent load is produced by the hydrolysis and growth of biomass. However, the assumption of a constant positive net hydrolysis rate could very well be wrong. There are strong reasons to believe that the net hydrolysis process rate is actually zero or below zero in the anoxic periods with influent load, i.e. the ammonia uptake of the biomass is equal to or above the production of ammonia by hydrolysis. If the additional amount of ammonia required due to the higher denitrification in anoxic periods with influent load is taken into account, the estimates of the ammonia concentration in the outlet of the pretreatment column would be approximately 4% higher. Furthermore, the storage of ammonia in the biomass may be significantly larger in periods with influent load.

The curves in Figure 5.7 reveals an important phenomenon for the modelling of the influent load rate - rainy weather. Rainfall events give a high flow rate to the Lundtofte municipality plant, while the flow rate to the pilot scale plant remains constant. On the other hand, rainfall events result in a low ammonia concentration of the raw wastewater, which is loaded to the pilot plant. Unfortunately, information on the flow rate to the Lundtofte municipality plant for the analyzed period has not been obtainable for the given period in a reasonable form, but the rainy weather periods are clearly recognized on Figure 5.7 where the estimated inlet concentration drops below 7 mg NH_4^+-N/l. However, these rainfall events cannot be predicted due to lack of information on the flow rate to the municipality plant. The rainy weather periods of the time series also interrupt the diurnal pattern of influent ammonia concentrations, resulting in the parameter for the diurnal variation, $\phi_{load,S}$, being insignificant. Thus, if flow rates to the Lundtofte municipality plant were to be incorporated into (5.30), the model of the influent ammonia load rate would be improved and $\phi_{load,S}$ would most likely become significant. This would also improve the variance of the error terms in the process equation, $\sigma^2_{e,load,NH_4^+}$, significantly. For the present model, the standard deviation of $e_{load,NH_4^+,f}$ is found to correspond to 1.5 mg NH_4^+-N/l for the estimated influent concentration of ammonia.

Parameter	Unit	Ammonia	Nitrate
ϕ_{nit}	-	0.73 ($\pm$0.07)	0.78 ($\pm$0.04)
$\widehat{\mu}_{nit,max,\cdot}$	mg N/l/h	10.6 ($\pm$0.19)	9.7 ($\pm$0.09)
$\widehat{K}_{NH_4^+}$	mg NH_4^+-N/l	0.44 ($\pm$0.02)	0.35 ($\pm$0.01)
$\widehat{\sigma}_{e,nit,\cdot}$	mg N/l/h	0.71	0.82

Table 5.5. *Parameter estimates from modelling the maximum nitrification process rate on data set No.2.*

5.5.2 Maximum nitrification rate

In the sample time domain, estimators of $k_{nit,max,NH_4^+,f}$ and $k_{nit,max,NO_3^-,f}$ based on data from one operation cycle were derived by using (5.26) and (5.27) with the half-saturation constant $K_{NH_4^+}$ estimated on all available observation in the data set. Due to lack of information on explanatory variables which could describe some of the variations of $k_{nit,max,NH_4^+,f}$ and $k_{nit,max,NO_3^-,f}$ (e.g. temperature, C/N-ratio, composition of wastewater), a first order autoregressive model is proposed.

$$(1-\phi_{nit}B)(k_{nit,max,\cdot,f}-\mu_{nit,max,\cdot}) = e_{nit,max,\cdot,f} \qquad (5.32)$$

where $\mu_{nit,max,\cdot}$ is the mean maximum nitrification rate estimated separately for the time series of ammonia and nitrate concentrations, and $e_{nit,max,\cdot,f}$ is NID with zero mean and variance $\sigma^2_{e,nit,\cdot}$. In case information on explanatory variables influencing $k_{nit,max,\cdot,f}$ becomes available, $\mu_{nit,max,\cdot}$ may be modelled as a function of those (4.61). The estimates of this process are given in Table 5.5. A likelihood ratio test has shown, that the mean of the estimates from the two time series, $\overline{\mu}_{nit,max} = 10.12$ mg N/l/h and $\overline{K}_{NH_4^+} = 0.40$ mg NH_4^+-N/l, are reasonable estimates for both.

The estimated maximum nitrification rates, $\widehat{k}_{nit,max,\cdot,f}$, for each operation cycle on observations of ammonia and nitrate concentrations are shown in Figure 5.9 and Figure 5.10 as solid curves, respectively. Estimates of

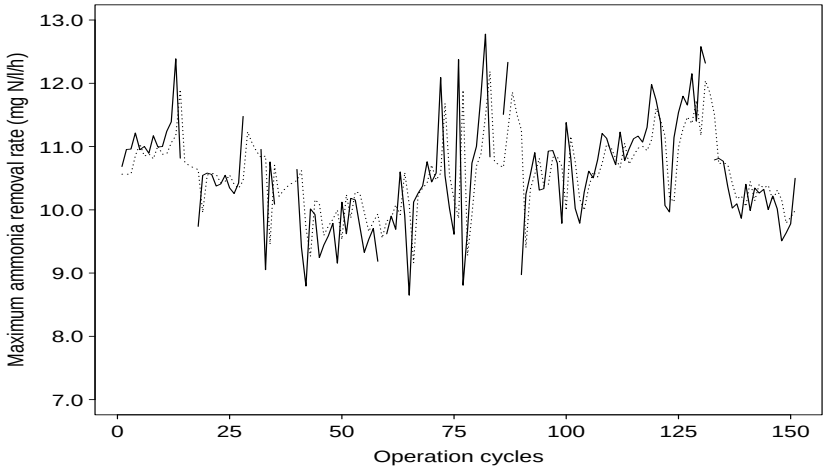

Figure 5.9. *Estimated (solid curve) and one-step predictions (dotted curve) of the maximum nitrification rate based on observations of ammonia concentrations.*

$k_{nit,max,\cdot,\cdot,f}$ based on less than four observations in the sample time domain have been rejected, since the estimators (5.26) and (5.27) would not yield reliable estimates on three or less observations. These estimates are treated as missing values in the operation cycle time series indicated by the gaps in the solid curves. The estimates related to the two series correspond reasonably with each other except for a possible slight drift in the scaling of one of the two FIA-analyzers.

As indicated on Figure 4.5, the one-step predictions of (5.32) are used as parameter values in the sample time domain for the subsequent operation cycle. The one-step predictions are given as dotted curves on Figure 5.9 and Figure 5.10. Thus the dotted should to some extend reflect the dynamic of the solid curves. However, the simple structure of (5.32) and the estimated values of ϕ_{nit} compared to the dynamics of the estimated maximum nitrification rates on the figures indicate that (5.32) is not appropriate for long-term predictions of $k_{nit,max,\cdot,\cdot,f}$, because the model in fact does not contain any physical knowledge. This is easily incorporated into

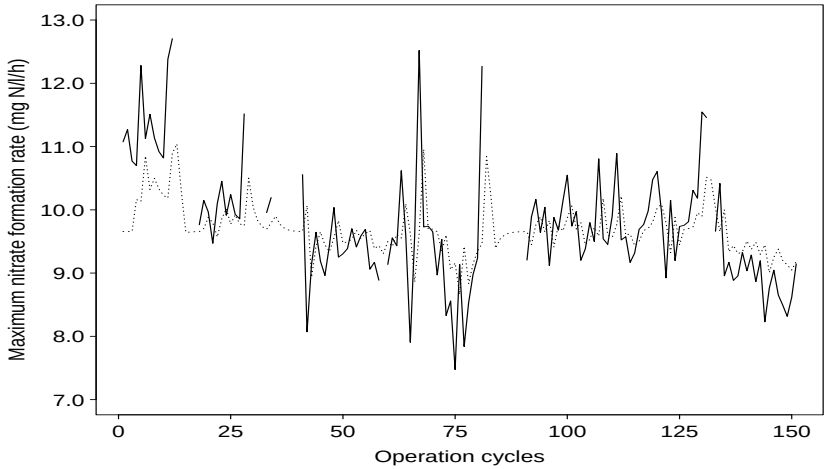

Figure 5.10. *Estimated (solid curve) and one-step predictions (dotted curve) of the maximum nitrification rate based on observations of nitrate concentrations.*

the model, if information on explanatory variables influencing $k_{nit,max,\cdot,\cdot,f}$ is available as described previously. In this case, the estimates of ϕ_{nit} and the variances of the prediction error, $\sigma^2_{e,nit,\cdot}$ will become smaller.

Assuming that the suspended solids concentration and the oxygen concentration in the aerobic periods are maintained constant, the activity of autotrophic biomass is assessed applying the approximations (4.43) and (4.44). Inspecting the figures, it is seen, that the activity of the autotrophic biomass may change by 20-30% within a few days. This effect cannot be accounted for solely by the removal of excess sludge and the change in the fraction of nitrifiers. Also, it appears that some of the rainfall events identified from Figure 5.7 causes the maximum nitrification rate to drop subsequently, and high/low loads of ammonia causes the maximum nitrification rate to increase/decrease, respectively. The rainy weather periods might lower the overall temperature in the activated sludge causing the

Parameter	Unit	Nitrate
ϕ_{denit}	-	0.46 ($\pm$0.05)
$\widehat{\mu}_{denit,max}$	mg NO_3^--N/l/h	4.7 ($\pm$0.13)
$\widehat{K}_{NO_3^-}$	mg NO_3^--N/l	0.40 ($\pm$0.01)
$\widehat{K}_{load}$	mg NH_4^+-N/l/h	0.43 ($\pm$0.05)
$\widehat{\sigma}_{e,denit}$	mg NO_3^--N/l/h	0.51

Table 5.6. *Parameter estimates from modelling the maximum denitrification process rate on data set No.2.*

activity of the bacteria to decrease, while the influence of the influent ammonia load on the maximum nitrification rate is investigated in Chapter 6.

5.5.3 Maximum denitrification rate

In the sample time domain an estimator of $k_{denit,max,f}$ based on data from one operation cycle was obtained by using (5.28) with the half-saturation constants $K_{NO_3^-}$ and K_{load} estimated on the entire time series of nitrate concentrations. A first order autoregressive model for describing the variations of $k_{denit,max,f}$ is proposed.

$$(1-\phi_{denit}B)(k_{denit,max,f}-\mu_{denit,max}) = e_{denit,max,f} \qquad (5.33)$$

where $\mu_{denit,max}$ is the mean maximum denitrification rate and $e_{denit,max,f}$ is NID with zero mean and variance $\sigma^2_{e,denit}$. Due to lack of information on external variables capable of explaining some of the variations in $k_{denit,max,f}$, the mean maximum denitrification rate, $\mu_{denit,max}$, is modelled as a constant parameter. The estimates of this process are given in Table 5.6.

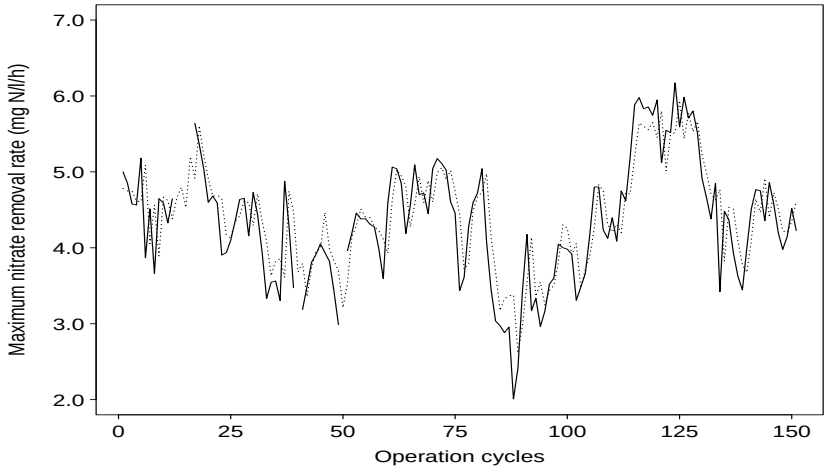

Figure 5.11. *Estimated (solid curve) and one-step predictions (dotted curve) of the maximum denitrification rate.*

The estimated maximum denitrification rates, $\widehat{k}_{denit,max,f}$, for each operation cycle are shown in Figure 5.11 with the one-step predictions of (5.33). Estimates of $k_{denit,max,f}$ based on less than four observations have been rejected, since the estimator (5.28) would not yield reliable estimates on fewer than four observations. These estimates are treated as missing values in the operation cycle time domain, which is indicated by the gaps of the solid curve in Figure 5.11.

Incorporating explanatory variables in (5.33) will most likely improve the model and thereby reduce the variance of the prediction error, $\sigma^2_{e,denit}$. The trends of the curve (the slow dynamic) could be described by some explanatory variables.

Assuming that the suspended solids concentration is maintained constant, the activity of the heterotrophic biomass is assessed applying the approximation (4.46). Similar to the variations of the maximum nitrification rate, the maximum denitrification rate appears to be influenced by the rainfall events and the load of ammonia. However, due to the assumption of using

$k_{load,NH_4^+,f} \cdot Q$ as a correlated measure of the readily bio-degradable substrate concentration in the aeration tank, some of the fluctuations in Figure 5.11 are very likely caused by a change in the raw wastewater composition. Comparing the trends of the maximum nitrification rate in Figure 5.9 and 5.10 with the trend of the maximum denitrification rate in Figure 5.11, it appears that $k_{nit,max,,,f}$ and $k_{denit,max,f}$ to some extend have similar variations. These similar variations may very well be due to external influence of e.g. the temperature or C/N-ratio.

5.6 Conclusion

In this chapter the grey box models described in Chapter 4 have been applied to two different data sets from the Lundtofte pilot scale plant. The first data set covers a single day and was primarily used in the developing stage of the grey box models. The time series of ammonia, nitrate, and phosphate concentrations in this data set are only modelled in the sample time domain. The second data set covers more than a 16 days period, and grey box models in both the sample time domain and operation cycle time domain are estimated. However, due to unreliable measurements, the phosphate concentrations has not been modelled for the second data set.

The measurement cycle at the pilot plant introduces a correlated noise structure, which has to be modelled in order to make the error terms of the grey box models normal and independent distributed such that the model may be estimated by use of the prediction error decomposition and the Kalman filter, as described in Chapter 4. Some of the variances of the error terms in the grey box models are time-varying and modelled using autoregressive models with conditional heteroscedasticity. Furthermore, it is found that the convergence of the maximum likelihood estimation routine is sensitive to correlation of the error terms. Thus, inadequacy of describing this correlation may result in difficulties of obtaining the maximum likelihood estimates.

Parameter	Unit	Estimates data set No.1	Estimates data set No.2	Literature
$\overline{C}_{i,NH_4^+}$	mg N/l	15.8	9.6	-
$\overline{k}_{nit,max,NH_4^+}$	mg N/l/h	7.4	10.6	-
$\overline{k}_{nit,max,NO_3^-}$	mg N/l/h	9.2	9.7	-
$\widehat{K}_{NH_4^+}$	mg N/l	0.12	0.44	0.3-0.7
	mg N/l	-	0.35	0.3-0.7
$\overline{k}_{denit,max}$	mg N/l/h	7.0	4.8	-
$\widehat{K}_{NO_3^-}$	mg N/l	0.71	0.40	0.2-0.5
$\overline{k}_{P-uptake,max}$	mg P/l/h	10.1	-	-
$\widehat{K}_{PO_4^{3-}}$	mg P/l	2.11	-	0.1-0.5

Table 5.7. *Selected parameter estimates from grey box modelling of data from the Lundtofte pilot scale plant. The suggested values from the literature are found in Henze et al. (1990).*

A practical identification of Monod-kinetic expressions is feasible, if an extensive data set is available. Selected estimates of the grey box models for the two data sets are summarized in Table 5.7 with suggested values from the literature of the kinetic parameters. The estimates obtained from data set No.2 are more representative, because this data set covers a longer period of time with highly varying loads of materials. The estimated half-saturation constants of data set No.2 are all within the range given by Henze et al. (1990), while the estimated half-saturation constants of data set No.1 differ significantly, mainly due to model deficiencies and the characteristics of the available data used for modelling. However, it should be stressed that offset errors in the calibration of the FIA-analyzers will displace the half-saturation constants.

Biased estimates of the influent concentrations of ammonia and phosphate to the aeration tanks are obtained from estimating the influent load processes of ammonia and phosphate. However, the estimates are biased yielding lower estimates of the measured values from the outlet of the

pretreatment column. The estimated rate expression for the net influent phosphate load consists of the rates of two distinct simultaneous processes, which cannot be separately identified. These are the influent phosphate load and the phosphate uptake during anoxic conditions. An estimate of the phosphate uptake rate during anoxic conditions may be obtained by combining the estimated net influent phosphate load with the measured phosphate concentrations of the outlet of the pretreatment column. The estimates of the ammonia load process is used as a correlated measure of the readily bio-degradable substrate load for modelling the denitrification process.

The activity of the autotrophic and heterotrophic biomass is assessed from estimates of the nitrification and denitrification process in the operation cycle time domain. However, the models used to describe the variations of this activity suffer from lack of information on the temperature, C/N-ratio, wastewater composition, and other explanatory variables having a major influence on the biomass activity. The grey box models may be improved if better data are available, and some of the assumptions implied in this chapter may be tested as well. Due to the constant throughput of the pilot plant, the influence of different hydraulic loads has not been investigated. This effect will be examined in the following chapter. Finally, it should be stressed that the interpretation of the estimates of the grey box models should be done cautiously, always keeping the standard error of the estimates in mind.

Chapter 6

Case - The Aalborg West wastewater treatment plant

This chapter deals with the estimation of grey box models on data from the Aalborg West WWTP, which is a well-monitored plant. The data from the plant was made available in the last stage of this research project, and the models of this chapter represent a further refinement of the models estimated on data set No.2 in Chapter 5. Compared to the models of the pilot scale plant the models of this chapter have two interesting aspects in addition. Firstly, the flow rate to the plant is time-varying, and secondly, the Aalborg West WWTP is a full-scale plant which in particular has an impact on the hydraulic processes, due to the large volume holding of the aeration tanks. In addition, the measurement system at the Aalborg West WWTP does not introduce the same strong correlation in the measurement noise sequence, which makes it easier to model. The first section of this chapter gives an introduction of the plant and the measurements available, while the second and third section describes the estimated grey box

models in the sample time domain and the operation cycle time domain, respectively. Some of the results of this chapter are also documented in Carstensen et al. (1994). It should be emphasized that the models presented in this chapter are derived by statistical methods from the class of grey box models in Chapter 4 giving the best fit of data.

6.1 Introduction

The Aalborg West WWTP serves the Danish city of Aalborg with approximately 150,000 inhabitants. Figure 6.1 shows an aerial photograph of the plant, which was inaugurated in 1989. It is designed for 265,000 PE (Person Equivalent) with the purpose of treating the wastewater from the western and central part of the city which formerly was discharged untreated to the recipient, a sound with brackish water. In the catchment area of the plant a brewery, abattoirs, dairies, and fish processing industries produce some high strength wastewater comprising at least two thirds of the organic load to the plant. The design loads of the plant are given in Table 6.1, and Einfeldt (1992) describes the implementation of biological nutrient removal on the plant. The effluent standards for the plant are 15 mg BOD/l, 6 mg total N/l (six months of summer), 8 mg total N/l (six months of winter), and 1.5 mg total P/l. The plant has an excellent performance, and compliance with the effluent standard have been obtained from start of operation.

The wastewater handling facility of the plant consists of an inlet pumping station, 4 primary clarifiers, an intermediate pumping station, 3 anaerobic pretreatment tanks (each subdivided into 3 separate anaerobic tanks in series), 6 oxidation ditches, and 15 secondary clarifiers, which is schematically shown in Figure 6.2. The WWTP is operated according to the BIO-DENIPHO process. However, a major part of the phosphate in the wastewater is chemically precipitated by adding ferrosulphate.

The six oxidation ditches are operated in three parallel lines of two alternating aeration tanks. Two of the oxidation ditches (denoted LT5 and

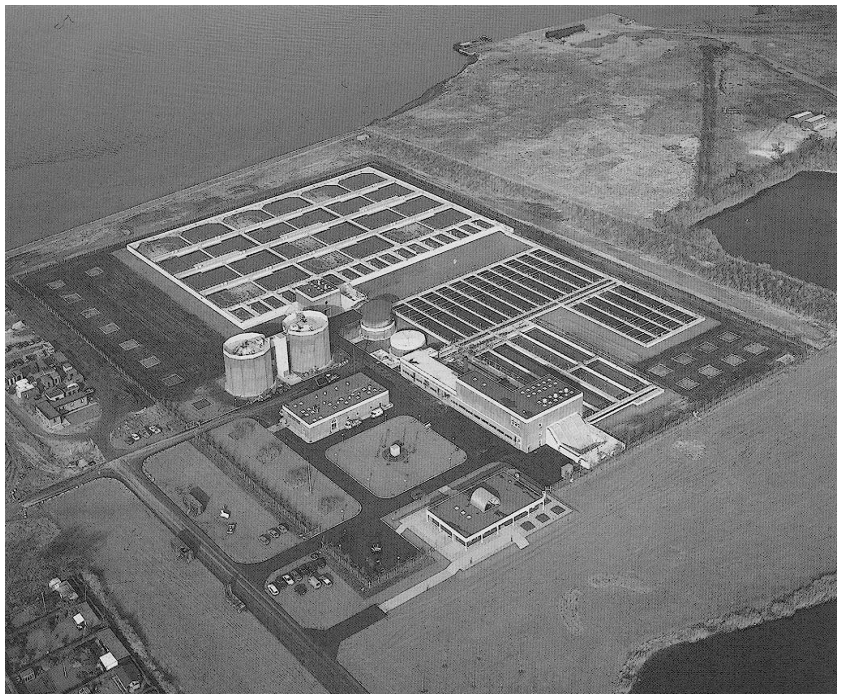

Figure 6.1. *Aerial view of the Aalborg West WWTP. The aeration tanks are located in the far end of the plant.*

LT6) have been equipped with sensors for monitoring of ammonia and nitrate concentrations (both tanks), phosphate concentrations (only LT6), oxygen concentrations (two sensors in each tank), and suspended solids concentrations (only LT6). The sampling points for some of the on-line measurements are sketched in Figure 6.2, where the aeration tanks are numbered from LT1 to LT6 starting from the bottom of the figure. The flow rate to the biological part of the plant is also monitored. Furthermore, settings of the inlet and outlet weirs of the aeration tanks and the oxygen supply rate (OSR) are registered. The oxygen supply rate is found from the number of aeration rotors, that has been switched on in the given aeration tank for the last five minutes. Table 6.2 summarizes the monitored

Flow	**Average**		**Maximum**	
dry weather	54,900	m^3/day	60,000	m^3/day
			3,600	m^3/h
rainy weather, to plant			15,000	m^3/h
to biology			5,800	m^3/h
Pollution				
BOD	15,800	kg/day	19,800	kg/day
SS	15,500	kg/day	17,000	kg/day
Total-N	2,350	kg/day	2,600	kg/day
Total-P	650	kg/day	720	kg/day

Table 6.1. *Design loads for the Aalborg West WWTP. Data from Einfeldt (1992).*

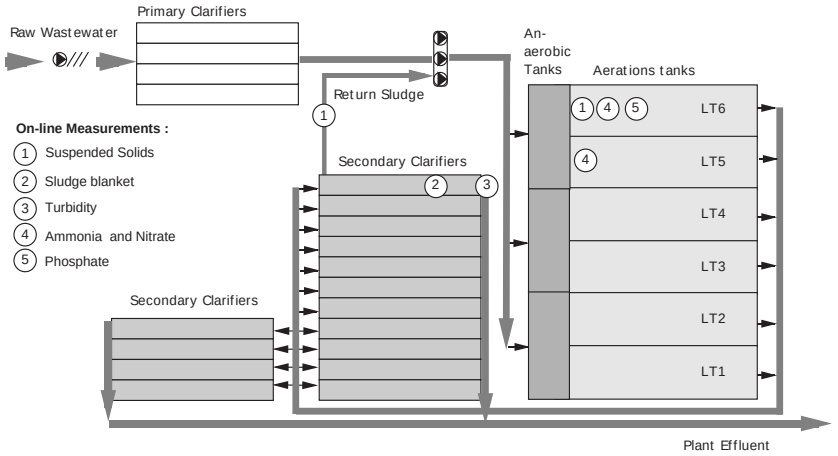

Figure 6.2. *Schematic diagram of the wastewater treatment facility at the Aalborg West WWTP.*

	Variable	Unit
Weir (inlet LT5)	$W_{i,LT5,t}$	0/1 (closed/open)
Weir (inlet LT6)	$W_{i,LT6,t}$	0/1 (closed/open)
Weir (outlet LT5)	$W_{o,LT5,t}$	0/1 (closed/open)
Weir (outlet LT6)	$W_{o,LT6,t}$	0/1 (closed/open)
Oxygen Supply Rate LT5	$OSR_{LT5,t}$	g O_2/h/m^3
Oxygen Supply Rate LT6	$OSR_{LT6,t}$	g O_2/h/m^3
Oxygen concentration LT5, sensor 1	$S_{O_2,LT5,1,t}$	mg O_2/l
Oxygen concentration LT5, sensor 2	$S_{O_2,LT5,2,t}$	mg O_2/l
Oxygen concentration LT6, sensor 1	$S_{O_2,LT6,1,t}$	mg O_2/l
Oxygen concentration LT6, sensor 2	$S_{O_2,LT6,2,t}$	mg O_2/l
Ammonia concentration LT5	$S_{NH4,LT5,t}$	mg NH4-N/l
Ammonia concentration LT6	$S_{NH4,LT6,t}$	mg NH4-N/l
Nitrate concentration LT5	$S_{NO3,LT5,t}$	mg NO3-N/l
Nitrate concentration LT6	$S_{NO3,LT6,t}$	mg NO3-N/l
Phosphate concentration LT6	$S_{PO4,LT6,t}$	mg PO4-N/l
SS concentration LT6	$X_{SS,LT6,t}$	g/l
Flow biological part of plant	$Q_{bio,t}$	m^3/h

Table 6.2. *Summary of available measurements and registered controlling signals.*

variables, which have been used for modelling in this chapter with the exception, that grey box models of the phosphate concentrations have not been estimated on data from the Aalborg West WWTP, because the time series of phosphate concentrations do not reflect much biological activity due to chemical precipitation. The measurements of ammonia and nitrate are the dependent variables to be modelled using past information from all the variables listed in Table 6.2.

The plant has been equipped with a SCADA system (Supervision, Control, And Data Acquisition) called STAR (Superior Tuning And Reporting-system, see Nielsen & Lynggaard-Jensen (1993)), where the measurements of Table 6.2 are used as input for control of setpoints in the SCADA system.

The controlling system is based on a set of rules combined with criteria functions from empirical and mathematical expressions. The sensors used for monitoring of nutrient salt concentrations have been chosen according to an investigation in Thomsen & Nielsen (1992), such that sufficient stability and low maintenance cost of the sensors are ensured.

From October, 29th to November, 24th 1992 a data set of 9507 observations without large interrupts in the sampling was obtained. The time between samples is four minutes, and a few outliers and measurements taken during calibration of the sensors has been removed from the data set and replaced with missing values, which are accordingly handled by the Kalman filter. The time of an average operation cycle is approximately 3 hours, but it may vary within the range from 1.5 to 4.5 hours, due to the operation strategies in the STAR-system. The total number of operation cycles in the data set is 227. Hence, there are sufficient observations for modelling in the operation cycle time domain.

Some of the explanatory variables in Table 6.2 have large fluctuations due to measurement noise. Thus, in order to make use of these variables in the grey box models, a filtering is required (e.g. a low-pass filtering). A weighted moving average filter with the filter weights given below is found adequate for these variables.

$$\begin{aligned}
\overline{S}_{O_2,LT5,t} &= (3S_{O_2,LT5,1,t} + 3S_{O_2,LT5,2,t} + 2S_{O_2,LT5,1,t-1} \\
&\quad + 2S_{O_2,LT5,2,t-1} + S_{O_2,LT5,1,t-2} + S_{O_2,LT5,2,t-2})/12 \quad (6.1)\\
\overline{S}_{O_2,LT6,t} &= (3S_{O_2,LT6,1,t} + 3S_{O_2,LT6,2,t} + 2S_{O_2,LT6,1,t-1} \\
&\quad + 2S_{O_2,LT6,2,t-1} + S_{O_2,LT6,1,t-2} + S_{O_2,LT6,2,t-2})/12 \quad (6.2)\\
\overline{OSR}_{LT5,t} &= (OSR_{LT5,t} + OSR_{LT5,t-1} + OSR_{LT5,t-2})/3 \quad (6.3)\\
\overline{OSR}_{LT6,t} &= (OSR_{LT6,t} + OSR_{LT6,t-1} + OSR_{LT6,t-2})/3 \quad (6.4)\\
\overline{X}_{SS,t} &= (X_{SS,LT6,t} + X_{SS,LT6,t-1} + X_{SS,LT6,t-2})/3 \quad (6.5)\\
\overline{Q}_{bio,t} &= (Q_{bio,t} + Q_{bio,t-1} + Q_{bio,t-2})/3 \quad (6.6)
\end{aligned}$$

Alternatively, the filter weights could be designed from a frequency analysis of the esplanatory variables, but applying such filters in the grey box models have very little effect on the description of data. The suspended solids concentration in LT6 is also assumed to be representative for the suspended solids concentration in LT5. In order to determine which biological processes are active at a given time, the measurements of the oxygen concentrations are used to divide the time series into aerobic and anoxic periods using a hysteresis setting. Examination of data has shown that a reasonable hysteresis setting is to change from aerobic to anoxic conditions when the oxygen concentration drops below 0.5 mg O_2/l and to change from anoxic to aerobic conditions when the oxygen concentration exceeds 1.0 mg O_2/l. Employing the low-pass filtered oxygen concentration with the hysteresis setting, distinct periods of aerobic and anoxic conditions are determined (i.e. only one anoxic and one aerobic period in one operation cycle). Anaerobic periods rarely occur in the aeration tanks, and for the modelling of ammonia and nitrate concentrations anaerobic conditions have little interest.

6.2 Modelling in the sample time domain

For modelling the time series of ammonia and nitrate concentrations at the Aalborg West WWTP, four hydraulic and biochemical processes may be identified.

- Influent ammonia load.
- Transport of nutrients
- The nitrification process
- The denitrification process

The hydrolysis and growth of biomass process cannot be identified for the given data set, because the anoxic periods of the time series without influent load to the aeration tanks (i.e. the periods where the hydrolysis and

growth of biomass normally is the most significant process for the ammonia concentration) are few and short. Secondly, attempts to estimate the rate of hydrolysis and growth of biomass process in these periods failed, due to statistical insignificance.

The rate expressions for the significant processes above are more extensive compared to the rate expressions for the processes at the Lundtofte pilot scale plant given in Chapter 5. This is due to the monitoring of the suspended solids concentration and the use of different oxygen set-points during the aerobic phases. With this information available, grey box models almost identical to those presented in Section 4.4 are formulated. Furthermore, the monitoring of ammonia and nitrate concentrations in both LT5 and LT6 give rise to double estimates of the same processes. Hence, the validity of the grey box models is investigated by comparing the estimates from the two tanks.

One major difference between the models of the previous chapter and the models of this chapter is the variable flow rate to the biological part of Aalborg West WWTP. The diurnal flow rate of a typical dry weather day is depicted in Figure 3.1 (see page 30), while the total daily flow for the 27 days period is depicted in Figure 3.2. The highly varying flow rate to the plant give rise to strong variations in the dynamics of the wastewater processes, especially during peak hydraulic loads caused by rainy weather. However, information obtained from measurements of the flow rate to the plant is used to detect the occurrences of rainfall events and the consequently low influent ammonia concentration. Recalling the discussion in Section 6.5.1, the lack of information on rainfall events at the pilot scale plant is an evident deficiency of the model for the influent load rate of ammonia in the operation cycle time domain (5.30).

The observation equation for the time series of ammonia and nitrate are, as usual, given by

$$y_t = m_t + \nu_t \tag{6.7}$$

where m_t is the true concentration of ammonia or nitrate and ν_t is Normal and Independent Distributed (NID) with zero mean and variance given by an ARCH-structure (Tong (1990)), i.e.

$$\sigma^2_{\nu,t} = \sigma^2_{\nu,0} + \theta_\nu \nu^2_{t-1} \tag{6.8}$$

where ν_{t-1} in (6.8) is replaced by the prediction error, v_{t-1}, for practical applications, and θ_ν is a parameter.

The process equation for each of the four time series of ammonia and nitrate concentrations is found to be adequately modelled using

$$(1 - \phi B)(\Delta m_t - \mu_t) = \boldsymbol{\delta}^T \boldsymbol{u}_t + e_t \tag{6.9}$$

where e_t is NID with zero mean and a variance which is found to be conditional on the previous concentration level, i.e.

$$\sigma^2_{e,t} = \sigma^2_{e,0} + \theta_e m^2_{t-1} \tag{6.10}$$

where $\sigma^2_{e,0}$ and θ_e are parameters. Hence, the process equation (6.9) is better at modelling low level concentrations than high level concentrations. Two explanations for this phenomenon are given. Firstly, the steps of the concentration gradient, Δm_t, are larger for high level concentrations resulting in larger error terms, e_t. Secondly, switching from aerobic to anoxic conditions and reverse introduces some noise into the processes, which is partly modelled as transient phenomena. The switching from aerobic to anoxic conditions and reverse cannot be clearly defined by simply choosing an oxygen concentration threshold dividing aerobic and anoxic periods. Therefore, the ammonia and nitrate concentrations on top of the time series curves are more unpredictable. The mean of the posterior distribution, $\widehat{m}_{t-1|t-1}$, is used as the optimal estimator of m_{t-1} in (6.10). The AR-parameter estimates, $\widehat{\phi}$, are in the range 0.71-0.81 ($\pm$0.01), which is somewhat larger than those estimated on data set No.2 from the pilot plant.

This implies that the mean process rate, μ_t, does not give as persistent an estimate of the concentration gradient for the models of this chapter.

6.2.1 Influent ammonia load in dry weather

The ammonia load to Aalborg West WWTP is modelled according to (4.34) during dry weather periods with k_{load,NH_4^+} being a time-varying parameter of the operation cycle time domain (see following section), i.e.

$$r_{load,NH_4^+,t} = \begin{cases} k_{load,NH_4^+,f} \cdot \overline{Q}'_{bio,t-1} & \text{inlet weir open} \\ 0 & \text{inlet weir closed} \end{cases} \tag{6.11}$$

where $\overline{Q}'_{bio,t-1}$ is the filtered flow rate of wastewater and returned sludge entering the BIO-DENIPHO line consisting of LT5 and LT6. The flow rate to the biological part of the plant, $Q_{bio,t}$, is equally mixed with returned sludge and then divided into three parallel lines of alternating aeration tanks. Thus,

$$\overline{Q}'_{bio,t-1} = \frac{2\overline{Q}_{bio,t-1}}{3} \tag{6.12}$$

The rate of the returned sludge may vary slightly below the influent flow rate, but this does not affect the applicability of the model. Using the data from one operation cycle an estimate of $k_{load,NH_4^+,f}$ is obtained from (6.11) which can be used for updating the models of the influent ammonia load rate in the operation cycle time domain. An estimate of the influent ammonia concentration to the aeration tanks is obtained from the approximation (4.35), but the estimator will be biased as discussed in Section 6.5.1. The ammonia load rate, $k_{load,NH_4^+,f} \cdot \overline{Q}'_{bio,t-1}$, is also used as a correlated measure for the load of readily bio-degradable substrate, which is employed for modelling of the denitrification process.

6.2.2 Influent ammonia load with rainy weather periods

A rainfall event in the catchment area is typically characterized by a large volume of low loaded wastewater entering the WWTP, due to the mixing of wastewater produced by households and industries, and rainwater. However, when modelling a rainfall event some allowances for the large buffer of wastewater in the sewerage should be made. In Figure 6.3 an idealized picture of a typical rainfall event is sketched. This illustration is used to derive a simplified model for the ammonia load rate in rainy weather periods.

When rain starts falling in the catchment area, the flow of rainwater and produced wastewater into the sewerage increases momentarily. The ammonia concentration of the mixed rainwater and produced wastewater consequently drops to a lower concentration, which in this simplified model is assumed to be constant. When the rainfall event subsequently stops only wastewater from households and industries is flushed into the sewer. Consequently, the flow rate and ammonia concentration of the wastewater return to the dry weather levels. At the WWTP the flow rate increases shortly after the rain has started falling. However, due to a large buffer of highly loaded wastewater in the sewerage, the influent ammonia concentration of the raw wastewater to the plant slowly decreases towards the low ammonia concentration of produced wastewater mixed with rainwater running into the sewer. Similarly, when the rain stops falling the flow rate to the plant decreases rather fast after a short period of time, while the influent ammonia concentration to the plant slowly increases towards the ammonia concentration level of produced wastewater, due to the large buffer of low loaded wastewater in the sewerage.

The rainy weather periods are detected from the measurements of the flow rate to the biological part of the plant, despite the fact that during rainfalls a significant part of the raw wastewater is bypassed, i.e. all the raw wastewater is mechanically processed and a fraction of this wastewater is led to the effluent of the plant without biological treatment. The start of a

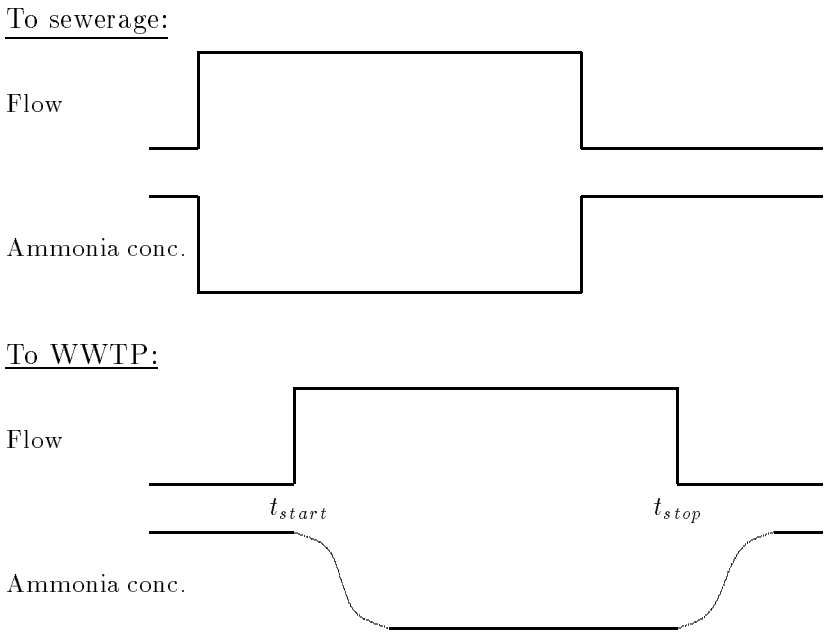

Figure 6.3. *Illustration of the dynamics in the sewerage during a rainy weather period. The two points in time, t_{start} and t_{stop}, show the length of the rainy weather period determined by the measured flow rate to the plant.*

rainfall event is defined as $\overline{Q}_{bio,t}$ exceeding 4000 m^3/h, and it is considered to be finished when $\overline{Q}_{bio,t}$ has been below 3500 m^3/h for two hours. The starting and stopping time of a rainfall event are denoted t_{start} and t_{stop} as indicated on Figure 6.3, and the length of the rainy weather period is given by $t_{stop} - t_{start}$.

The large buffer volume of the sewerage, primary clarifiers, and anaerobic pretreatment tanks that the wastewater has to pass before entering the aeration tanks, can neither be considered as one big ideally mixed tank nor as one large pipe without mixing. In particular, partially mixing occur in

the sewerage due to varying hydraulic retention times of the different subsewerages and the geographical movement of the precipitation. In order to describe the partial mixing of produced wastewater with rainwater in the large buffer volume of the sewerage, primary clarifiers, and anaerobic pretreatment tanks, a simple model of N ideally mixed tanks with identical volume holdings in series is found adequate.

The response of a step-function load on N identical ideally mixed tanks in series is obtained by successively applying (3.4) with the response of the n'th tank being the input to the $n+1$'th tank ($n < N$). The response is most conveniently found by applying the Laplace transformation.

$$C_t = C_i(1 - e^{-\frac{t}{T_h}} - \frac{t}{T_h}e^{-\frac{t}{T_h}} - \ldots - \frac{t^{N-1}}{(N-1)!T_h^{N-1}}e^{-\frac{t}{T_h}}) \tag{6.13}$$

where C_i is the influent concentration to the first tank and T_h is the hydraulic retention time of the individual ideally mixed tanks. The concentration in all N tanks at the starting time of the step-function is assumed to be constant and C_t is the deviation from this steady state level.

Thus, in order to incorporate the effects of rainy weather on the influent ammonia load rate, (6.11) needs to be modified.

$$r_{load,NH_4^+,t} = \begin{cases} k'_{load,NH_4^+,f,t} \cdot \overline{Q}'_{bio,t-1} & \text{inlet weir open} \\ 0 & \text{inlet weir close} \end{cases} \tag{6.14}$$

where

$$k'_{load,NH_4^+,f,t} = k_{load,NH_4^+,f} + (k_{load,NH_4^+,f} - k_{rain}) \cdot \varrho_N(t - t_{stop}) + (k_{rain} - k_{load,NH_4^+,f}) \cdot \varrho_N(t - t_{start}) \tag{6.15}$$

and

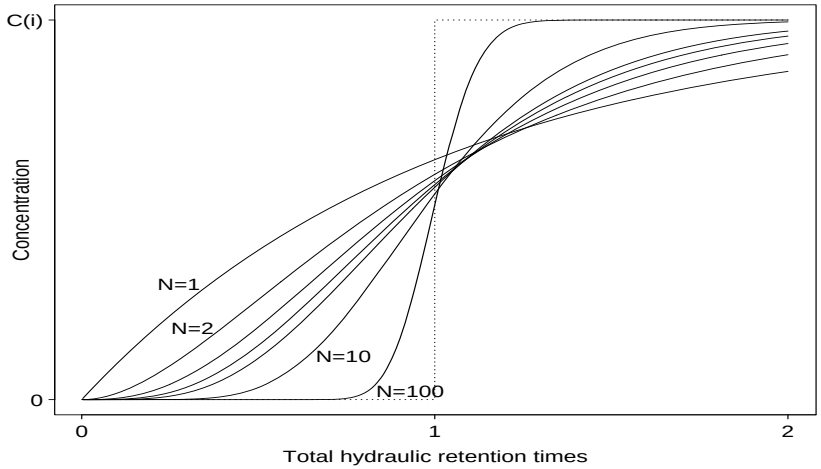

Figure 6.4. *Response of a step-function load on N ($N = 1, 2, 3, 4, 5, 10, 100$) identical ideally mixed tanks in series. The response approximates a pipe with no mixing for $N \to \infty$ as indicated by the dotted line.*

$$\varrho_N(t) = \begin{cases} 1 - e^{-\frac{t}{T_h}} - \frac{t}{T_h} e^{-\frac{t}{T_h}} - \ldots - \frac{t^{N-1}}{(N-1)! T_h^{N-1}} e^{-\frac{t}{T_h}} & t \geq 0 \\ 0 & t < 0 \end{cases} \quad (6.16)$$

Figure 6.4 shows $\varrho_N(t)$ for different values of N and a constant total hydraulic retention time, $T_{h,total} = N \cdot T_h$. For $t \gg t_{start}$ and $t \gg t_{stop}$ (i.e. no rain for a while) the load process (6.14) approximates the dry weather influent load rate given in (6.11). Hence, (6.14) is a more general rate expression for the influent ammonia load which handles both dry and rainy weather periods, while (6.11) is used to produce estimates of $k_{load,NH_4^+,f}$ for updating the model of the influent ammonia load rate in the operation cycle time domain. Consequently, using the approximation (4.35), $k'_{load,NH_4^+,f,t}$ describes the variations of the influent ammonia concentration to the aeration tanks and $k_{load,NH_4^+,f}$ describes the variation of the ammonia concentration in the wastewater produced by households and industries. Estimating

Parameter	Unit	LT5	LT6
$\overline{C}_i$	mg NH_4^+-N/l	6.8	8.0
$\widehat{C}_{rain}$	mg NH_4^+-N/l	2.9 ($\pm$0.1)	2.7 ($\pm$0.1)
$\widehat{T}_{h,rain,total}$	h	2.3 ($\pm$0.1)	2.3 ($\pm$0.1)

Table 6.3. *Parameter estimates from modelling the influent ammonia load process in rainy and dry weather.*

k_{rain} yields an estimate of the average influent ammonia concentration to the aeration tanks, when it has been raining for a long while. However, it should be stressed that the estimates of $k_{load,NH_4^+,f}$ are not used for updating the models of the operation cycle time domain during rainy weather periods and the first operation cycle after the rainy period. The purpose of dividing the wastewater into the two categories, rainwater and wastewater from households and industries, is to obtain a simple and better model for the influent ammonia load process of households and industries.

Modelling the sewerage, the primary clarifiers, and the anaerobic pretreatment tanks as $N = 2$ ideally mixed tanks in series with a hydraulic retention time of approximately 1.2 hours gave the best fitting of the two time series of ammonia concentrations considered in this chapter. However, using $N = 3$ ideally mixed tanks in series with an hydraulic retention time of approximately 0.8 hour, a fit nearly as good as using $N = 2$ is obtained. The estimates from employing $N = 2$ is given in Table 6.3, where $\widehat{C}_{rain}$ is the asymptotic influent ammonia concentration to LT5 and LT6 during a rainfall event. $\overline{C}_i$ is the average of the estimated influent ammonia concentrations, based on the estimates of $k_{load,Nh_4^+,f}$ for all operation cycles. The estimates of the influent ammonia concentration in Table 6.3 are smaller for LT5 than LT6. This will be explained later.

6.2.3 Nutrient transport of the aeration tanks

Incorporating the mass balance of nutrients is important but not crucial for obtaining interpretable estimates of the remaining wastewater processes. Fortunately, both aeration tanks at Aalborg West WWTP are equipped with on-line sensors of ammonia and nitrate concentrations. Thus, for the transport of ammonia

$$r_{transport,NH_4^+,t} = \begin{cases} k_{transport,NH_4^+}(S^I_{NH_4^+,t-1} - S_{NH_4^+,t-1}) \cdot Q_{t-1} & \\ & \text{outlet weir open} \\ 0 & \text{otherwise} \end{cases} \tag{6.17}$$

and for the transport of nitrate

$$r_{transport,NO_3^-,t} = \begin{cases} k_{transport,NO_3^-}(S^I_{NO_3^-,t-1} - S_{NO_3^-,t-1}) \cdot Q_{t-1} & \\ & \text{inlet weir closed and outlet weir open} \\ -k_{transport,NO_3^-} \cdot S_{NO_3^-,t-1} \cdot Q_{t-1} & \text{inlet weir open} \\ 0 & \text{otherwise} \end{cases} \tag{6.18}$$

where $S^I_{NH_4^+,t-1}$ and $S^I_{NO_3^-,t-1}$ are the ammonia and nitrate concentrations of the alternating tank. $S^I_{NH_4^+,t-1}$ and $S^I_{NO_3^-,t-1}$ are replaced by the measurements of the ammonia and nitrate concentrations in the alternating tank, while $S_{NH_4^+,t-1}$ and $S_{NO_3^-,t-1}$ are replaced by the optimal estimates of the true ammonia and nitrate concentration, $\widehat{m}_{t-1|t-1}$. The estimated parameters of the model are given in Table 6.4.

The estimates of $k^{-1}_{transport,\cdot}$ are larger than the actual physical holding volumes of the aeration tanks (6500 m^3). This is mainly due to lack of information on the hydraulic effects when switching flow patterns, i.e. the wastewater levels in the two alternating tanks are different, and switching the influent and effluent flow between the two tanks will gradually result

$k_{transport,\cdot}$	Unit	LT5	LT6
Ammonia	10^{-4}m^{-3}	1.07 ($\pm$0.04)	1.49 ($\pm$0.05)
Nitrate	10^{-4}m^{-3}	1.49 ($\pm$0.04)	1.18 ($\pm$0.06)
$k^{-1}_{transport,\cdot}$	Unit	LT5	LT6
Ammonia	m^3	9350 ($^{+310}_{-260}$)	6700 ($^{+240}_{-200}$)
Nitrate	m^3	6700 ($^{+210}_{-180}$)	8500 ($^{+510}_{-440}$)

Table 6.4. *Parameter estimates from modelling the nutrient transport of the aeration tanks.*

in a change of flow between the two tanks. This will make the estimates of $k_{transport,\cdot}$ smaller.

6.2.4 The nitrification process

The monitoring of ammonia and nitrate concentrations in both LT5 and LT6, permits the identification of the nitrification process from four different time series. Thus, if the estimates from the four time series show consistency, this will validate the general model structure. In the considered period of time the plant has been operated with different oxygen setpoints, where the employment of two oxygen sensors in each tank combined with the filtering (6.1) and (6.2) has made the identification of a Monod-kinetic term for the dependency of the oxygen concentration possible. Furthermore, due to the monitoring of the suspended solids concentration, expressions like (4.41) and (4.42) are identified. However, during high loads at the Aalborg West WWTP the rotors must have been turned on for a while before the oxygen concentration reaches its setpoint. This period of time is considered anoxic because of the low oxygen concentration, but ammonia is in fact nitrified due to an excessive amount of oxygen being aerated into the aeration tanks. Fortunately, the oxygen supply rate is registered and it is assumed that nitrification rate is proportional to $\overline{OSR}_{t-1}$ in this period.

Thus, for the time series of ammonia concentrations

$$r_{nit,NH_4^+,t} = \begin{cases} -k_{nit,max,NH_4^+} \cdot \frac{S_{NH_4^+,t-1}}{S_{NH_4^+,t-1}+K_{NH_4^+}} \cdot \frac{S_{O_2,t-1}}{S_{O_2,t-1}+K_{O_2}} \cdot X_{SS,t-1} & \\ \qquad\qquad \text{aerobic conditions} & \\ -k_{OSR,NH_4^+} \cdot OSR_{t-1} \qquad \text{anoxic/anaerobic conditions} & \end{cases} \tag{6.19}$$

and for the time series of nitrate concentrations

$$r_{nit,NO_3^-,t} = \begin{cases} k_{nit,max,NO_3^-} \cdot \frac{S_{NH_4^+,t-1}}{S_{NH_4^+,t-1}+K_{NH_4^+}} \cdot \frac{S_{O_2,t-1}}{S_{O_2,t-1}+K_{O_2}} \cdot X_{SS,t-1} & \\ \qquad\qquad \text{aerobic conditions} & \\ k_{OSR,NO_3^-} \cdot OSR_{t-1} \qquad \text{anoxic/anaerobic conditions} & \end{cases} \tag{6.20}$$

where $S_{O_2,t-1}$, $X_{SS,t-1}$, and OSR_{t-1} are replaced with the filtered values given in (6.1-6.5) for the practical identification. The mean of the posterior distribution for m_{t-1} is used as the optimal estimator of the true ammonia concentration in the aeration tanks, i.e. $S_{NH_4^+,t-1}$ is replaced by the Kalman update $\widehat{m}_{t-1|t-1}$ in (6.19) and (6.20). The results of estimating the nitrification process on data from Aalborg West WWTP are given in Table 6.5.

Fortunately, there is a consistency between the estimates of the nitrification process obtained from the four time series in Table 6.5, validating the general grey box model structure for the nitrification process. Though, the estimates from the time series of ammonia concentrations in LT5 differ slightly. The reason for this is explained in the subsequent section. Henze et al. (1990) suggest that $K_{NH_4^+}$ should lie in the range 0.3-0.7 mg NH_4^+-N/l and K_{O_2} should lie in the range 0.5-1.0 mg O_2/l. Thus, all the estimated half-saturation parameters values are in the suggested range, except for $\widehat{K}_{NH_4^+}$ estimated on measurements of the ammonia concentration in LT5. However, due to the discrete time formulation of the Monod-kinetic expressions the grey box models will yield biased and larger estimates of the half-saturation constants in continuous time as discussed in Section 4.4.1.

	Parameter	Unit	LT5	LT6
Ammonia	$\overline{k}_{nit,max,NH_4^+}$	mg N/h/g SS	1.02	1.28
	$\widehat{K}_{NH_4^+}$	mg N/l	0.76 (±0.02)	0.56 (±0.03)
	$\widehat{K}_{O_2}$	mg O_2/l	0.71 (±0.01)	0.77 (±0.01)
	$\widehat{k}_{OSR,NH_4^+}$	mg N/g O_2	16.4 (±0.5)	27.4 (±0.7)
Nitrate	$\overline{k}_{nit,max,NO_3^-}$	mg N/h/g SS	1.50	1.47
	$\widehat{K}_{NH_4^+}$	mg N/l	0.60 (±0.04)	0.49 (±0.05)
	$\widehat{K}_{O_2}$	mg O_2/l	0.67 (±0.02)	0.85 (±0.03)
	$\widehat{k}_{OSR,NO_3^-}$	mg N/g O_2	58.5 (±1.3)	57.5 (±1.6)

Table 6.5. *Parameter estimates from modelling the nitrification process on data from Aalborg West WWTP.*

The estimates of $k_{nit,max,NO_3^-,f}$ are less biased estimates of the maximum nitrification rate than $k_{nit,max,NH_4^+,f}$, because the hydrolysis and growth of biomass process is not incorporated in the grey box models of the Aalborg West WWTP. Hence, $k_{nit,max,NH_4^+,f}$ is an estimator of the net maximum nitrification rate, which includes the simultaneous removal of ammonia by nitrification and growth of biomass, and production of ammonia by hydrolysis. This is also reflected in the lower estimates of $\overline{k}_{nit,max,NH_4^+,f}$ and k_{OSR,NH_4^+} in Table 6.5. In fact, in the anoxic periods with the rotors turned on, twice as much nitrate is produced as ammonia removed. The effect of aerating during anoxic conditions on the denitrification rate is neglected, but it is a topic for future research. Comparing the stoichiometric coefficient of (2.10) with the estimates of $k_{OSR,\cdot}$, it is seen that 10-25% of the oxygen supplied by the rotors in the anoxic period is used for nitrification, while the rest of the oxygen supplied is used for heterotrophic respiration and, in particular, raising the overall oxygen concentration in the aeration tank to the setpoint value. Given the values of $\widehat{K}_{NH_4^+}$ and $\widehat{K}_{O_2}$ estimated on the entire data set, estimates of $k_{nit,max,\cdot,f}$ are obtained from the data of operation cycle f.

6.2.5 The denitrification process

Assuming that the load rate of ammonia is highly correlated with the average concentration of readily bio-degradable substrate in the aeration tanks during the anoxic phase with influent load, the following expression is identified:

$$r_{denit,t} = \begin{cases} 0 & \text{anoxic conditions and no influent load} \\ -k_{denit,max,f} \frac{S_{NO_3^-,t-1}}{S_{NO_3^-,t-1}+K_{NO_3^-}} \cdot \frac{k_{load,NH_4^+,f-1} \cdot Q_{t-1}}{k_{load,NH_4^+,f-1} \cdot Q_{t-1}+K_{load}} X_{SS,t-1} & \text{anoxic conditions and influent load} \\ 0 & \text{aerobic/anaerobic conditions} \end{cases} \quad (6.21)$$

where Q_{t-1} and $X_{SS,t-1}$ are replaced with the filtered values given in (6.12) and (6.5) for the practical identification of (6.21). The mean of the posterior distribution for m_{t-1} is used as the optimal estimator of the true nitrate concentration in the aeration tank, i.e. $S_{NO_3^-,t-1}$ is replaced by the Kalman update $\widehat{m}_{t-1|t-1}$ in (6.21). The estimated ammonia load parameter of the previous operation cycle in both dry and rainy weather, $\widehat{k}'_{load,NH_4^+,f-1}$ given by (6.15), is used in the second Monod-kinetic term in (6.21). It should be stressed that the rate of the denitrification process during anoxic conditions without influent load is found to be insignificant, mainly due to lack of readily bio-degradable substrate in LT5 and LT6 after the aerobic phase. This result corresponds to the similarly very low and insignificant hydrolysis and growth of biomass process rate. The results of estimating the denitrification process on data from Aalborg West WWTP are given in Table 6.6.

Similar to the estimates of the nitrification process, the estimates in Table 6.6 are consistent for the two time series. Though, the estimates of $K_{NO_3^-}$ are somewhat higher than the suggested values of the literature (Henze et al. (1990) suggest $K_{NO_3^-}$ lies in the range 0.2-0.5 mg NO_3^--N/l). This may be due to deficiencies in: 1) the assumption of high correlation

Parameter	Unit	LT5	LT6
$\overline{k}_{denit,max}$	mg N/h/g SS	1.20	1.18
$\widehat{K}_{NO_3^-}$	mg N/l	0.99 ($\pm$0.06)	1.08 ($\pm$0.13)
$\widehat{K}_{load}$	mg N/l/h	1.55 ($\pm$0.05)	1.73 ($\pm$0.16)

Table 6.6. *Parameter estimates from modelling the denitrification process on data from Aalborg West WWTP.*

between the ammonia load rate and the load of readily bio-degradable material, and 2) the assumption of a constant influent load rate of organic materials resulting in a constant concentration of readily bio-degradable substrate. However, in the absence of sensors for monitoring the readily bio-degradable substrate on-line, the denitrification process is more adequately described in (6.21) than leaving the second Monod-kinetic term out. Using the design loads in Table 6.1 for the Aalborg West WWTP and applying three assumptions, the estimates of K_{load} are interpreted in terms of BOD. First assumption is, that the influent concentrations of ammonia and BOD are left unaltered by passage of the pretreatment tanks. Secondly, it is assumed that 60% of the total nitrogen to the plant is in the form of ammonia using Table 3.2 for moderately loaded wastewater. Thirdly, BOD in returned sludge is not used for denitrification. Based on these assumptions the estimates of K_{load} corresponds to $\widehat{K}_S = 8.8$ mg BOD/l ($\pm$0.3) for LT5 and $\widehat{K}_S = 8.4$ mg BOD/l ($\pm$0.3) for LT6. Finally, using the COD/BOD-ratio for moderately loaded wastewater in Table 3.1, the estimates of K_S are found to lie in the range 10-20 mg COD/l, as suggested by Henze et al. (1990).

Given the estimates of $K_{NO_3^-}$ and K_{load} based on the entire time series of measurements of nitrate concentrations, estimates of $k_{denit,max,f}$ are obtained from the observations of operation cycle f. These estimates are used for updating the model of the maximum denitrification rate in the operation cycle time domain.

6.3 Modelling in the operation cycle time domain

Some of the essential parameters for modelling wastewater processes in the sample time domain are known to be time-varying and estimators of these parameters based on observations from a single operation cycle were derived in the previous section. Thus, for updating the models of the operation cycle time domain, 227 estimates of the influent ammonia load rate, the maximum nitrification rate, and the maximum denitrification rate are available.

6.3.1 Influent load rate of ammonia

In Section 6.2.1, an estimator of $k_{load,NH_4^+,f}$ was derived and making use of the approximation (4.35), $\widehat{k}_{load,NH_4^+,f}$ corresponds to an estimate of the influent ammonia concentration to the aeration tanks. The estimates of the influent ammonia concentration in LT5 and LT6 are shown in Figure 6.5 and Figure 6.6 as solid curves. Estimated influent ammonia load rates based on less than four observations are considered as missing values, as indicated by the gaps for the solid curves.

The two curves for LT5 and LT6 should correspond well with each other since both are determined by the same process, the ammonia concentration of the raw wastewater. Due to the time-wise displacement of the periods with influent load to LT5 and LT6 and changing ammonia concentrations in the raw wastewater, the dynamics of the two curves may differ slightly. However, the two curves only appear to agree for the last half of the operation cycles. This is caused by a drift in the ammonia sensor in LT5, which was re-calibrated on November, 9th. At the time of calibration, which correspond to the 112th operation cycle (f=112), the sensor was measuring more than 25% below the actual value. Thus, gradually scaling the estimated influent concentration of ammonia in Figure 6.5 from

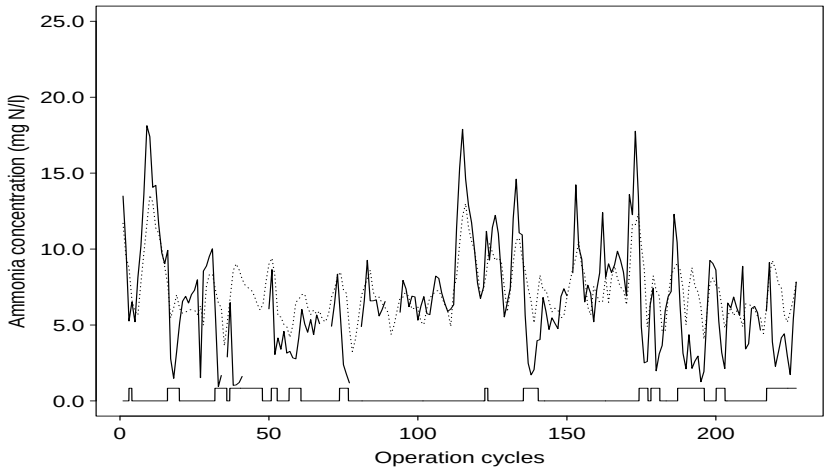

Figure 6.5. *Estimated (solid curve) and one-step predictions (dotted curve) of influent ammonia concentrations to LT5. The lower solid curve indicates the rainy weather periods.*

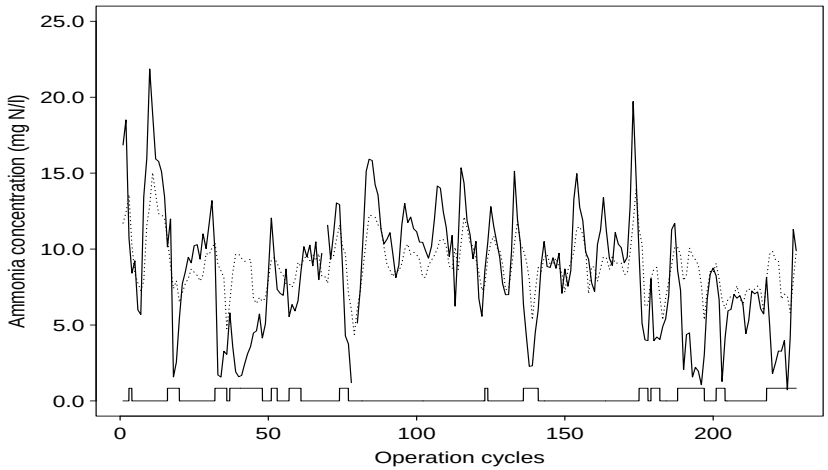

Figure 6.6. *Estimated (solid curve) and one-step predictions (dotted curve) of influent ammonia concentrations to LT6. The lower solid curve indicates the rainy weather periods.*

$f = 0$ to 112 yields a dynamic similar to that of Figure 6.6. The miscalibration of the ammonia sensor in LT5 also explains the low estimates of the average influent ammonia concentration in Table 6.3 and the average maximum nitrification rate in Table 6.5, when estimated on data from LT5. The ammonia concentration of the raw wastewater is approximately twice the estimated influent ammonia concentration, because the raw wastewater is equally mixed with returned sludge with a vanishing ammonia concentration. Though, in the discussion of Section 6.5.1 it was found that the estimator $k_{load,NH_4^+,f}$ yields lower biased estimates of the actual influent ammonia load rate. Hence, the ammonia concentration of the raw wastewater is presumably more than twice the estimated curves of Figure 6.5 and 6.6.

The influent load rate of ammonia to the WWTP arising from households and industries show typical diurnal and weekly patterns due to human behaviour. Thus, formulating a model for $k_{load,NH_4^+,f}$ these basic human activities are sought captured.

$$(1 - \phi_{load} B)(k_{load,NH_4^+,f} - \mu_{load,NH_4^+,t}) = e_{load,NH_4^+,f} \tag{6.22}$$

where $e_{load,NH_4^+,f}$ is NID with zero mean and variance $\sigma^2_{e,load,NH_4^+}$, and $\mu_{load,NH_4^+,f}$ describes the diurnal variation using a second-order Fourier expansion and type-of-day effects

$$\mu_{load,NH_4^+,t} = \begin{cases} \mu_{weekday,NH_4^+} \cdot \rho_t & \text{if operation cycle } f \text{ is on a weekday} \\ \mu_{weekend,NH_4^+} \cdot \rho_t & \text{if operation cycle } f \text{ is on a weekend} \end{cases} \tag{6.23}$$

and

$$\rho_t = 1 + \alpha_1 \cos\frac{2\pi t}{S} + \beta_1 \sin\frac{2\pi t}{S} + \alpha_2 \cos\frac{4\pi t}{S} + \beta_2 \sin\frac{4\pi t}{S} \tag{6.24}$$

where $S = 360$ is the number of samples in a day. The diurnal profile, ρ_t, is assumed to be identical on weekdays and weekends. The AR(1)-process in (6.22) describes the correlated deviations from the average mean load of ammonia, $\mu_{load,NH_4^+,t}$, from one operation cycle to another, i.e. if the ammonia load of the last operation cycle was lower than the mean load of ammonia at the given time (6.23), it is likely that the ammonia load of the present operation cycle will also be lower. The one-step predictions of (6.22) are shown as dotted curves in Figure 6.5 and Figure 6.6 for LT5 and LT6, respectively.

In the rainy periods which are indicated by the lower curves on Figure 6.5 and 6.6, the model (6.22) is not updated with the estimated ammonia load rates, because (6.22) describes the ammonia load of households and industries. Therefore, during the rainfall events the one-step predictions of $k_{load,NH_4^+,f}$ will approach $\mu_{load,NH_4^+,t}$, while the actual ammonia load rate is modelled by (6.14) in the sample time domain. Besides the rainy weather periods, the one-step predictions of (6.22) corresponds to the estimated influent ammonia load rate except for short term peak loads, which are difficult to predict as they cannot be described as simple diurnal variations and they have not been found correlated with other measurements at the WWTP.

The estimates of $k_{load,NH_4^+,f}$ obtained from the data of one operation cycle are encumbered with some uncertainty

$$\widehat{k}_{load,NH_4^+,f} = k_{load,NH_4^+,f} + \xi_{load,NH_4^+,f} \tag{6.25}$$

where $\xi_{load,Nh_4^+,f}$ is NID with zero mean and variance $\sigma^2_{\xi,load,NH_4^+}$.

The process equation (6.22) and observation equation (6.25) for the influent ammonia load rate process has a state space representation which can be handled by applying the Kalman filter. Hence, the variances of the error terms can be estimated by the maximum likelihood approach, if appropriate weights for the prediction errors in the sample time domain relative to the prediction errors in the operation cycle time domain are supplied in the

calculation of the likelihood function. Alternatively, if the variance of the prediction error in the operation cycle time domain is assumed to be time-invariant (4.80), estimates of $\sigma^2_{e,load,NH_4^+}$ and $\sigma^2_{\xi,load,NH_4^+}$ are obtained by estimating the constant Kalman gain K_{load,NH_4^+} and the variance of the prediction error R_{load,NH_4^+}. This will be shown in the following. Due to the simple form of (6.22), all the variables for the Kalman filter are scalar.

From the sequence of prediction errors of the influent ammonia load process, $v_{load,f}$, $f = 1, \ldots, 227$, an estimate of the variance of the predictions errors is obtained, $\widehat{R}_{load,NH_4^+}$. Thus, with the estimated Kalman gain and (4.77) where $\boldsymbol{c}$=1 is scalar

$$\widehat{P}_{load,NH_4^+} = \widehat{K}_{load,NH_4^+} \cdot \widehat{R}_{load,NH_4^+} \tag{6.26}$$

The estimates of the variances of the error terms in (6.22) and (6.25) are found applying the prediction equation of $\widehat{P}_{load,NH_4^+}$ to (4.73) and $\widehat{R}_{load,NH_4^+}$ to (4.74)

$$\widehat{\sigma}^2_{e,load,NH_4^+} = \widehat{P}_{load,NH_4^+}(1 - \widehat{\phi}^2_{load}) \tag{6.27}$$

and

$$\widehat{\sigma}^2_{\xi,load,NH_4^+} = \widehat{R}_{load,NH_4^+} - \widehat{P}_{load,NH_4^+} \tag{6.28}$$

The estimates of the influent ammonia load process are given in Table 6.7, where the standard deviations of the error terms and the average mean influent ammonia loads are listed using the equivalent influent ammonia concentrations.

The estimates of ϕ_{load} in Table 6.7 are somewhat smaller than the estimates obtained from data set No.2 at the pilot plant, due to the incorporation of a rainy weather ammonia load model. The estimates of the mean influent ammonia concentration and the standard deviations of the error terms in

Parameter	Unit	LT5	LT6
$\widehat{\mu}_{weekday,NH_4^+}$	mg N/l	8.0 ($\pm$0.1)	9.4 ($\pm$0.1)
$\widehat{\mu}_{weekday,NH_4^+}$	mg N/l	6.2 ($\pm$0.5)	8.1 ($\pm$0.5)
$\widehat{\phi}_{load}$	-	0.68 ($\pm$0.01)	0.50 ($\pm$0.02)
$\widehat{\sigma}_{e,load}$	mg N/l	1.8	2.7
$\widehat{\sigma}_{\xi,load}$	mg N/l	1.6	1.1

Table 6.7. *Parameter estimates from modelling the influent ammonia load rate process in the operation cycle time domain.*

the LT5 column are too low due to the bad calibration of the ammonia sensor in LT5, as mentioned previously. The standard deviations of the error terms are, in general, rather high showing that the model (6.22) will predict the influent ammonia concentration within an interval of $\pm$5.0 mg NH_4^+-N/l with a probability of 95%. This is mainly due to bad model performance of predicting peak influent ammonia concentration. The in Table 6.7 estimates could be improved by applying a robust estimation procedure, where the peak loads have a relative small weight in the calculation of the likelihood function and the estimation of the variance of the prediction error, R_{load,NH_4^+}. However, a large number of the peak loads are caused by dewatering of excess sludge as a part of the plant operation. Thus, it is preferable to incorporate knowledge on the times of the excess sludge dewatering into the model, if such information can be obtained. Disregarding the peak loads in Figure 6.5 and 6.6 the standard deviations of $e_{load,NH_4^+,f}$ graphically appears to be much lower.

6.3.2 Maximum nitrification rate

From the slopes of ammonia and nitrate curves during the aerobic phase of the operation cycle, estimates of $k_{nit,max,,,f}$ are obtained given the values of $K_{NH_4^+}$ and K_{O_2} estimated on all available observations. These estimates are naturally encumbered with some uncertainty

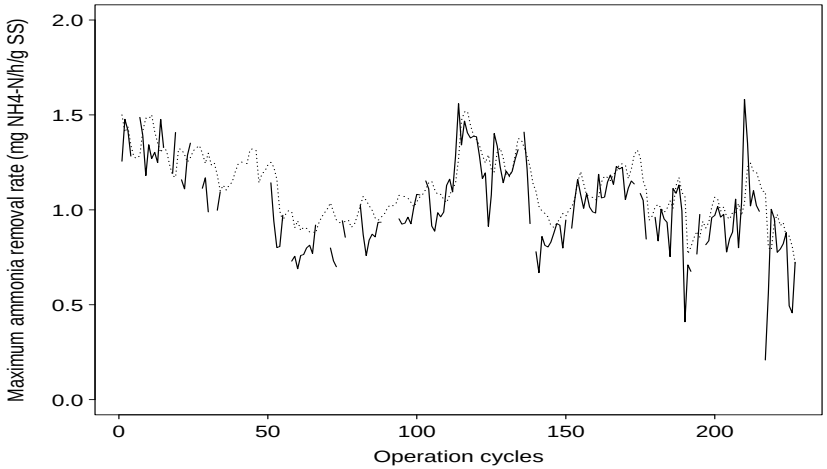

Figure 6.7. *Estimated (solid curve) and one-step predictions (dotted curve) of maximum nitrification rates based on ammonia concentrations from aeration tank LT5.*

$$\widehat{k}_{nit,max,\cdot,f} = k_{nit,max,\cdot,f} + \xi_{nit,max,\cdot,f} \tag{6.29}$$

where $\xi_{nit,max,\cdot,f}$ is NID with zero mean and variance $\sigma^2_{\xi,nit,\cdot}$, and the indexed period indicates that (6.29) is valid for the modelling of $k_{nit,max,NH_4^+,f}$ and $k_{nit,max,NO_3^-,f}$ on data from both aeration tanks. Thus, four sets of estimates from this process are obtained. The estimated maximum nitrification rates from the four considered time series, $\widehat{k}_{nit,max,\cdot,f}$, for each operation cycle are shown in Figure 6.7-6.10 by the solid curves. Estimates of $k_{nit,max,\cdot,f}$ based on less than four observations in the sample time domain are rejected due to unreliable estimates.

The variations of the maximum nitrification rate are modelled using a first-order AR-process

$$(1 - \phi_{nit}B)(k_{nit,max,\cdot,f} - \mu_{nit,max,\cdot,f}) = e_{nit,max,\cdot,f} \tag{6.30}$$

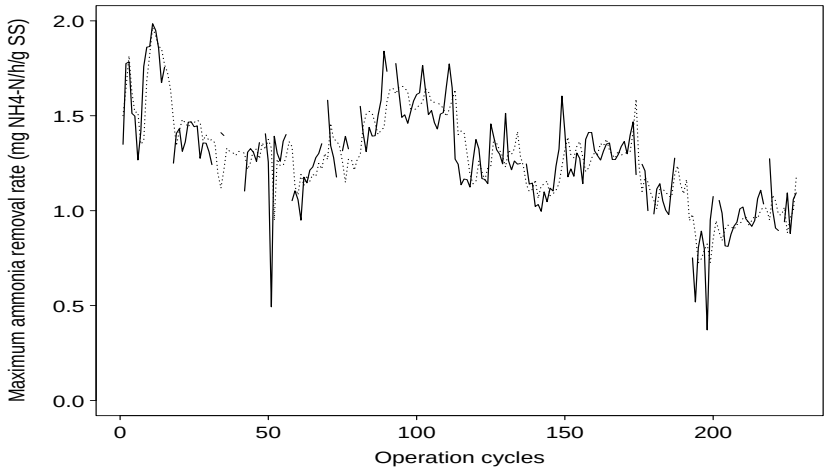

Figure 6.8. *Estimated (solid curve) and one-step predictions (dotted curve) of maximum nitrification rates based on ammonia concentrations from aeration tank LT6.*

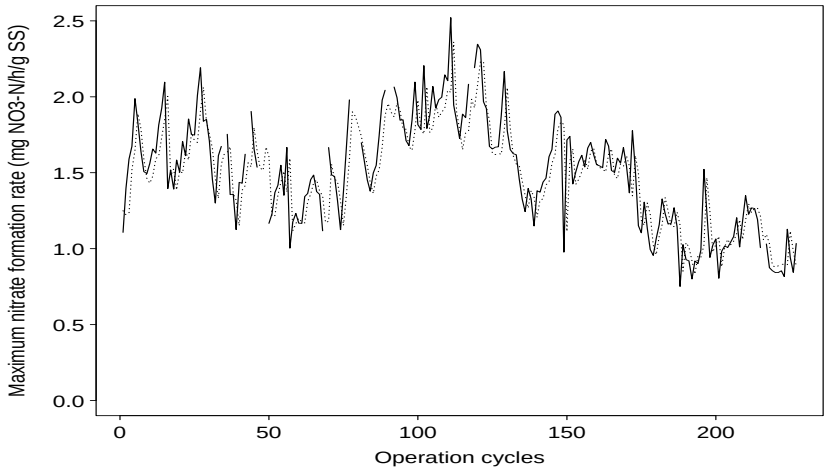

Figure 6.9. *Estimated (solid curve) and one-step predictions (dotted curve) of maximum nitrification rates based on nitrate concentrations from aeration tank LT5.*

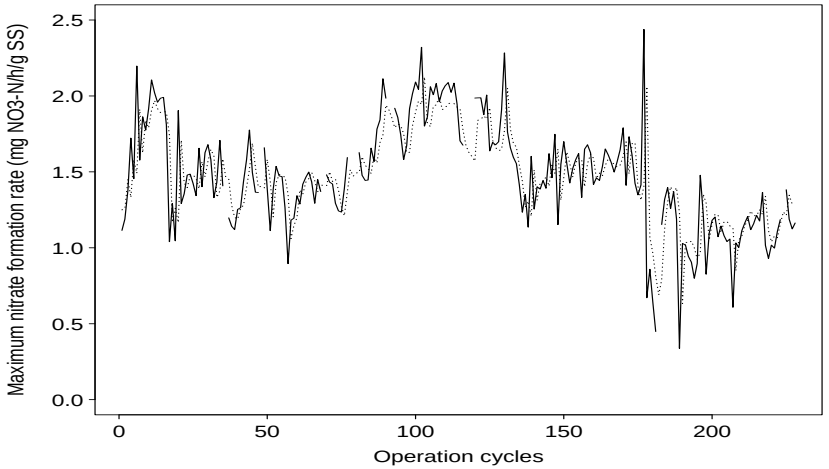

Figure 6.10. *Estimated (solid curve) and one-step predictions (dotted curve) of maximum nitrification rates based on nitrate concentrations from aeration tank LT6.*

where $e_{nit,max,,f}$ is NID with zero mean and variance $\sigma^2_{e,nit,,}$, and $\mu_{nit,max,,f}$ is the mean maximum nitrification rate for operation cycle f. Correlation between the estimates of $k_{nit,max,,f}$ and past values of the ammonia load rate has been found, and this correlation is formulated as a linear relationship

$$\mu_{nit,max,,f} = \mu^0_{nit,max,,} + \gamma \cdot k_{load,NH_4^+,f-1} \cdot Q'_{bio,f-1} \qquad (6.31)$$

where $Q'_{bio,f-1}$ is the average flow rate to LT5 and LT6 for the operation cycle $f-1$ and, $\mu^0_{nit,max,,}$ and γ are parameters. In practice, when estimating (6.31) $k_{load,NH_4^+,f}$ is replaced by the Kalman update of (6.22) in dry weather periods and $\widehat{k}'_{load,NH_4^+,f}$ given in (6.15) in rainy weather periods. The parameter estimates of (6.29-6.31) are found in Table 6.8. The variances of the error terms in (6.29) and (6.30) are found applying similar equations of (6.26), (6.27), and (6.28). The linear relationship proposed

	Parameter	Unit	LT5	LT6
Ammonia	$\widehat{\mu}^0_{nit,max,NH_4^+}$	mg N/h/g SS	1.30 ($\pm$0.01)	1.38 ($\pm$0.06)
	$\widehat{\gamma}$	-	0.28 ($\pm$0.02)	0.29 ($\pm$0.02)
	$\widehat{\phi}_{nit}$	-	0.93 ($\pm$0.02)	1.00 ($\pm$0.02)
	$\widehat{\sigma}_{e,nit,NH_4^+}$	mg N/h/g SS	0.06	0.06
	$\widehat{\sigma}_{\xi,nit,NH_4^+}$	mg N/h/g SS	0.12	0.12
Nitrate	$\widehat{\mu}^0_{nit,max,NO_3^-}$	mg N/h/g SS	1.35 ($\pm$0.04)	1.37 ($\pm$0.14)
	$\widehat{\gamma}$	-	0.20 ($\pm$0.03)	0.15 ($\pm$0.03)
	$\widehat{\phi}_{nit}$	-	0.91 ($\pm$0.04)	0.86 ($\pm$0.05)
	$\widehat{\sigma}_{e,nit,NO_3^-}$	mg N/h/g SS	0.18	0.20
	$\widehat{\sigma}_{\xi,nit,NO_3^-}$	mg N/h/g SS	0.08	0.12

Table 6.8. *Parameter estimates from modelling the maximum nitrification process in the operation cycle time domain.*

in (6.31) is rather empirical and further investigations lies ahead in order to determine a more appropriate relationship, if it exists. The one-step predictions of (6.30) are shown in Figure 6.7-6.10 as dotted curves.

In general, the trends of the estimated maximum nitrification rate in the four figures correspond well, except for the first 112 estimates in Figure 6.7, which are influenced by the mis-calibration ammonia sensor in LT5. Similarly, the estimates in Table 6.8 show a consistency which is interpreted as an approval of the model structure for the nitrification process in the sample time domain. The nitrification rates estimated on nitrate concentration are less biased than the rates estimated on ammonia concentrations, because ammonia is produced by hydrolysis simultaneously with the nitrification process and, the hydrolysis and growth of biomass process cannot be identified from the given data set. This is reflected in larger estimates of $k_{nit,max,NO_3^-,f}$ in Figure 6.9 and Figure 6.10. The high ϕ_{nit}-estimates indicate some slow variations in the maximum nitrification rate, which are not contained in (6.31). In fact, the AR(1)-process in (6.30) is instationary for the ammonia concentrations of LT6. As a result, $\mu_{nit,max,,f}$ is not an

unbiased estimator of $k_{nit,max,NH_4^+,f}$ which is also clearly seen by comparing the values of $\overline{k}_{nit,max,NH_4^+,f}$ in Table 6.5 with the estimates related to $\mu_{nit,max,,,f}$ in Table 6.8. Due to the high ϕ_{nit}-values based on ammonia concentrations, the estimates related to $\mu_{nit,max,NH_4^+,f}$ are merely estimates of the maximum nitrification rate in the beginning of the time series, and the slow variations of $k_{nit,max,NH_4^+,f}$ are contained in the AR(1)-process (6.30), which for the modelling of the maximum nitrification rates based on ammonia concentrations in LT6 actually is a random walk (refer to (4.7)). The γ-parameter in (6.31) only describes a short term dependency of the previous influent ammonia load rate, since the influent ammonia load rate does not contain much of the trend of the maximum nitrification rate. In Figure 6.7-6.10, this may be recognized as a diurnal variation.

The uncertainty of the estimates based on nitrate concentrations in Table 6.5 and in Table 6.8 is larger than the uncertainty of the of the estimates based on ammonia concentrations. This is due to a built-in filtering of the ammonia concentration sensors, such that the uncertainty of the ammonia measurements in general is smaller. However, the filtering also removes some of the dynamics of the ammonia concentration in the tank, thereby making the estimates based on measurements of ammonia concentrations more biased. The built-in filtering will likely yield somewhat higher estimates of the half-saturation constants, $K_{NH_4^+}$ and K_{O_2}. Furthermore, the larger uncertainty on nitrate measurements results in larger variances of the error terms for the maximum nitrification rate in the operation cycle time domain in Table 6.8.

Using the approximations (4.43) and (4.44) the activity of the autotrophic biomass may be assessed. The variations of Figure 6.7-6.10 are larger than the removal of excess sludge can account for. Some of the rainfall events causes a subsequent drop in the autotrophic biomass activity, while some do not appear to have any effect. This might indicate a significant effect of the temperature in the activated sludge, which is lowered by a large amount of cold rainwater. Thus, in order to describe some of the slow variations in the autotrophic biomass activity, explanatory variables such as temperature and wastewater composition must be incorporated into (6.31). Figure

6.11 show measurements of temperature (marked by triangles) and sludge volume index (marked by squares) from the considered period. The measurements are performed on a daily basis (Monday through Friday) for the temperature with occasionally observations of the sludge volume index. The observations have been synchronized with the operation cycle time, such that the measurements are plotted at the operation cycle number of the sample performance. Unfortunately, these explanatory variables are monitored too inconsistently to be used in the grey box models, but there appears to be a correlation between the slow variations of the estimated maximum nitrification rate and both the measured temperature (positive correlation) and sludge volume index (negative correlation). Formulating the correlation between the maximum nitrification rate and the sludge volume index as a functional relation in (6.31) would result in misleading conclusions, because the variation in both variables is most likely caused by another common factor, e.g. the wastewater composition. Hence, online monitoring of temperature and wastewater composition will improve the performance of the model for the maximum nitrification rate (6.30) and the parameter estimates of the operation cycle time domain.

6.3.3 Maximum denitrification rate

Given the estimators of $k_{denit,max,f}$ derived in Section 7.2.4 based on the values of $K_{NO_3^-}$ and K_{load} in Table 6.6, 227 observations of the maximum denitrification rate in LT5 and LT6 may be used for modelling in the operation cycle time domain. The estimates of $k_{denit,max,f}$ are encumbered with some uncertainty

$$\widehat{k}_{denit,max,f} = k_{denit,max,f} + \xi_{denit,max,f} \tag{6.32}$$

where $\xi_{denit,max,f}$ is NID with zero mean and variance $\sigma^2_{\xi,denit}$. The estimated maximum denitrification rates in LT5 and LT6, $\widehat{k}_{denit,max,f}$, are shown in Figure 6.12 and Figure 6.13, respectively. Estimates of $k_{denit,max,f}$

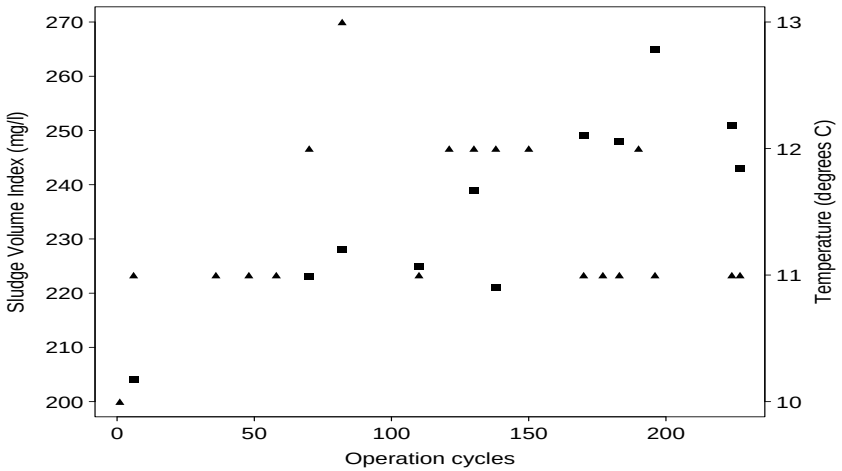

Figure 6.11. *Measurements of temperature (triangles) and sludge volume index (squares) during the considered period. The sample time points of the measurements are depicted in the operation cycle time domain.*

based on less than four observations are discarded due to unreliable estimates.

The variations of the maximum denitrification rate is modelled as an AR(1)-process

$$(1 - \phi_{denit}B)(k_{denit,max,f} - \mu_{denit,max}) = e_{denit,max,f} \tag{6.33}$$

where $e_{denit,max,f}$ is NID with zero mean and variance $\sigma^2_{e,denit}$, and $\mu_{denit,max}$ is the mean maximum denitrification rate. Attempts to model $\mu_{denit,max}$ as a function of the influent ammonia load rate have not been made for two reasons. Firstly, the estimated maximum denitrification rates in Figure 6.12 and 6.13 do not reflect the same strong correlation to the influent ammonia load rate as the maximum nitrification rate does. This is typically illustrated by a weaker diurnal variation in the figures. Also, the incentive

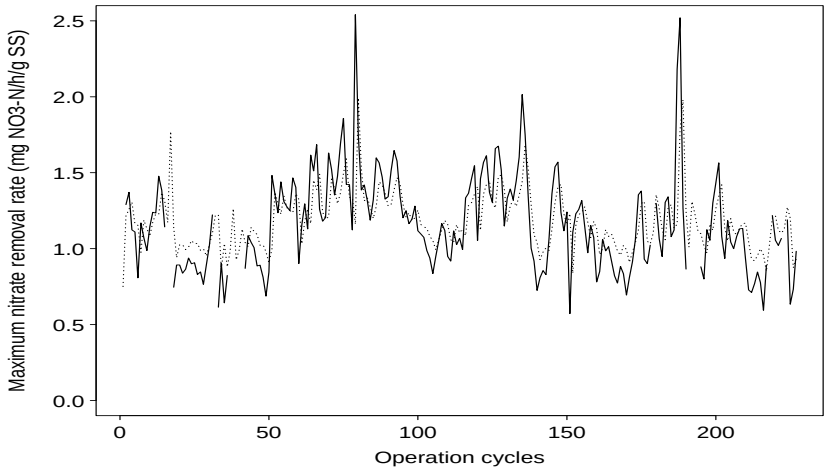

Figure 6.12. *Estimated (solid curve) and one-step predictions (dotted curve) of maximum denitrification rates based on nitrate concentrations from aeration tank LT5.*

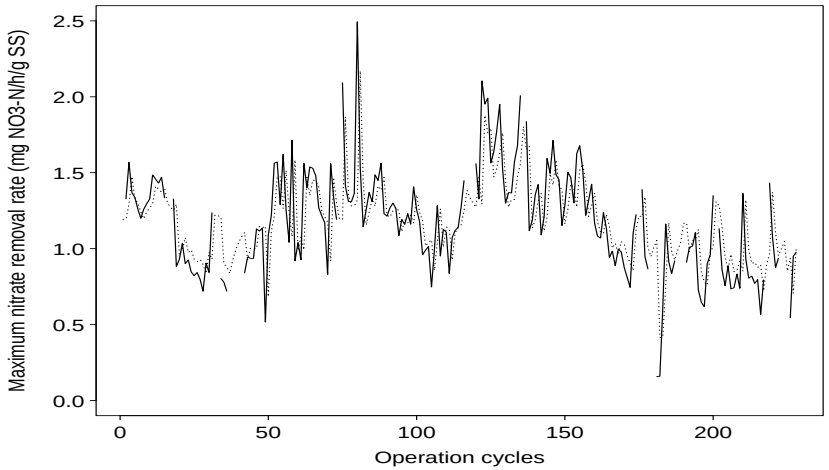

Figure 6.13. *Estimated (solid curve) and one-step predictions (dotted curve) of maximum denitrification rates based on nitrate concentrations from aeration tank LT6.*

Parameter	Unit	LT5	LT6
$\widehat{\mu}_{denit,max}$	mg N/h/g SS	1.22 ($\pm$0.03)	1.19 ($\pm$0.09
$\widehat{\phi}_{denit}$	-	0.59 ($\pm$0.04)	0.75 ($\pm$0.06)
$\widehat{\sigma}_{e,denit}$	mg N/h/g SS	0.26	0.28
$\widehat{\sigma}_{\xi,denit}$	mg N/h/g SS	0.00	0.00

Table 6.9. *Parameter estimates from modelling the maximum denitrification process in the operation cycle time domain.*

for modelling the maximum denitrification rate as a function of the influent ammonia load rate is much smaller, because the heterotrophic biomass does not heavily depend on the availability of nitrate. Secondly, there is a large risk that K_{load} and the parameters used for modelling such a relationship will be strongly correlated and thus, these parameters are likely to be biased and lose their interpretability. The one-step predictions of (6.33) are shown in Figure 6.12 and 6.13 as dotted curves, and the parameter estimates of (6.32) and (6.33) are shown in Table 6.9. The variances of the error terms in (6.32) and (6.33) are found applying similar equations of (6.26), (6.27), and (6.28).

The trends of the estimated maximum denitrification rates in Figure 6.12 and Figure 6.13 correspond reasonably. The estimates of ϕ_{denit} show that the slow variations of the maximum denitrification rate are not as significant as those obtained for the maximum nitrification rate. However, some of the variations in the maximum denitrification rate are similar to the variations of the maximum nitrification rate, thus indicating some kind of common external influence on the overall biomass performance (e.g. temperature and wastewater composition). A major part of the fast fluctuations is likely due to changes in the readily bio-degradable substrate concentration of the raw wastewater relative to the influent ammonia load rate. For example, the peak maximum denitrification rate at operation cycle $f = 80$ in Figure 6.12 and Figure 6.13 is presumably due to a high load of readily bio-degradable substrate relative to the ammonia load. If these short-term fluctuations are disregarded the estimated maximum denitrification rates

are more stable (in the range 1.0-1.5 mg NO_3^--N/h/g SS) than the estimated maximum nitrification rates (in the range 1.0-2.0 mg N/h/g SS).

Finally, the estimated half-saturation constants are large compared to the suggested values in the literature as discussed in Section 7.2.5, but the general experience with estimating grey box models is that inadequate or misspecified models of Monod-kinetics often result in larger biased estimates of the half-saturation constants. Thus, the high estimates of $K_{NO_3^-}$ and K_{load} could be due to inadequacy of modelling the dependency of readily bio-degradable substrate.

6.4 Conclusion

The Aalborg West WWTP is a well-monitored plant, where measurements of ammonia and nitrate concentrations are obtained from two alternating aeration tanks. Furthermore, measurements of flow rates, oxygen supply rates, oxygen concentrations, and suspended solids concentrations in the aeration tanks are available. Measurements of phosphate concentrations in one of the aeration tanks are also monitored but not modelled, because a major part of the phosphate is chemically precipitated. In this chapter a data set covering a 27 days period has been used for estimating the grey box models presented in Chapter 4 in the sample time and operation cycle time domain.

The considered data set contains several rainy weather periods, typically characterized by a high flow rate to the plant and low loads of materials. However, some allowances should be made for the large buffer capacity of the sewerage. For modelling purposes, it is convenient to divide the raw wastewater volume into wastewater arising from households and industries, and rainwater. The influent ammonia load to the plant is modelled according to human behaviour (i.e. diurnal and weekly patterns), while the ammonia load during a rainfall event is modelled using a simplified model of two identical ideally mixed tanks in series with a total hydraulic retention time of approximately 2.3 hours. This estimate corresponds to the

hydraulic retention times of the sewerage, primary clarifiers, and anaerobic pretreatment tanks during rainy weather.

A practical identification of Monod-kinetic expressions is feasible, because the data set is extensive. Selected parameter estimates of the grey box models estimated on data from Aalborg West WWTP are shown in Table 6.10 with suggested values from the literature of the kinetic parameters. The estimates in Table 6.10 show consistency, which validates the general grey box model structure. All of the estimated half-saturation constants of the nitrification process are within the range given by Henze et al. (1990), except for $K_{NH_4^+}$ estimated on ammonia concentrations in the aeration tank labelled LT5. However, the ammonia sensor in LT5 was mis-calibrated for the first half of this time series, which is clearly recognized from the estimated dynamics of the influent ammonia concentrations. Unfortunately, the estimated half-saturation constants for the denitrification process are too large compared to the values of the literature. This is mainly due to some inadequacy of modelling the dependency of readily bio-degradable substrate by the correlated influent ammonia load rate. Though, it should be stressed that the estimates of the half-saturation constants in general are biased yielding slightly too high values.

The activity of the autotrophic and heterotrophic biomass is assessed from the estimates of the maximum nitrification rate and the maximum denitrification rate in the operation cycle time domain. A short term correlation between the activity of the autotrophic biomass and the influent ammonia load rate is found and modelled using a simple linear relationship. The correlation is typically recognized as a diurnal variation in the autotrophic biomass activity. The trends of the maximum nitrification rates and maximum denitrification rates show similar variations in the operation cycle time domain indicating some kind of common external influence on the overall biomass performance. Incorporating on-line measurements of temperature and wastewater composition will most likely improve the performance of the grey box models.

Parameter	Unit	LT5	LT6	Literature
$\widehat{C}_{i,weekday,NH_4^+}$	mg N/l	8.0	9.4	
$\widehat{C}_{i,weekend,NH_4^+}$	mg N/l	6.2	8.1	
$\overline{k}_{nit,max,NH_4^+}$	mg N/l/g SS	1.02	1.28	
$\overline{k}_{nit,max,NO_3^-}$	mg N/l/g SS	1.50	1.47	
$\widehat{K}_{NH_4^+}(NH_4^+)$	mg N/l	0.76	0.56	0.3-0.7
$\widehat{K}_{NH_4^+}(NO_3^-)$	mg N/l	0.60	0.49	0.3-0.7
$\widehat{K}_{O_2}(NH_4^+)$	mg O_2/l	0.71	0.77	0.5-1.0
$\widehat{K}_{O_2}(NO_3^-)$	mg O_2/l	0.67	0.85	0.5-1.0
$\overline{k}_{denit,max}$	mg N/l/g SS	1.20	1.18	
$\widehat{K}_{NO_3^-}$	mg N/l	0.99	1.08	0.2-0.5

Table 6.10. *Selected parameter estimates from grey box modelling of data from Aalborg West WWTP. The suggested values from the literature are found in Henze et al. (1990).*

Chapter 7

Prediction based control

The main objective of the developing of the grey box models in the previous chapter is the employment of these models for control of WWTP's. The first section of this chapter deals with the information needed for the development of prediction based control systems, and some of the potential actuators for controlling the BIO-DENITRO and BIO-DENIPHO processes are listed. In the classical control theory, the main concern is controlling a system according to a given reference value (for an overview of classical control theory applied to activated sludge processes, see Andrews (1992)). However, this theory does not apply to the control of the alternating processes since the control of such a type of plant cannot be associated with the minimization of the deviations from a given reference value. Thus, strategies for control of alternating processes have to be developed, and the grey box models serve as a predictive tool for simulating these strategies and calculating on-line estimates of the state of the plant. This is described in the second and third section, where the examples of using the grey box models in off-line simulations and on-line model-based predictive control are given. In the fourth section an alternating process is simulated with data from Aalborg West WWTP and the strategies presented in the two previous sections are evaluated. The essence of this chapter is the potential

application of the grey box models for control of the BIO-DENITRO and BIO-DENIPHO processes.

7.1 System variables analysis

The operation of a WWTP is in general based on a number of available measurements and actuators, which are called the system variables. The available measurements and actuators are very specific to a given plant, i.e. the system variables depend on the process design of the plant and the installed measurements. In particular, the control system design is largely determined by the process design of the plant as appropriate sensors may be installed to provide the control system with the required information. Thus, the control of the process operation of a WWTP cannot be generalized since there are strong interactions between the process design, the available measurements, and the control system design. In fact, with the multitude of process designs and available measurements, a vast number of control system design exist. Though, in the present context the process operation control of the BIO-DENITRO and BIO-DENIPHO type of plants are solely considered. The interaction of the control system, available measurements, and the process operation is illustrated in Figure 7.1.

The following measurements are assumed to be available on the BIO-DENITRO or BIO-DENIPHO plant:

- Flow rate to the plant.
- Oxygen concentration in the aeration tanks.
- Ammonia concentration in the aeration tanks.
- Nitrate concentration in the aeration tanks.
- Phosphate concentration in the aeration tanks.
- Suspended solids concentration in the aeration tanks.

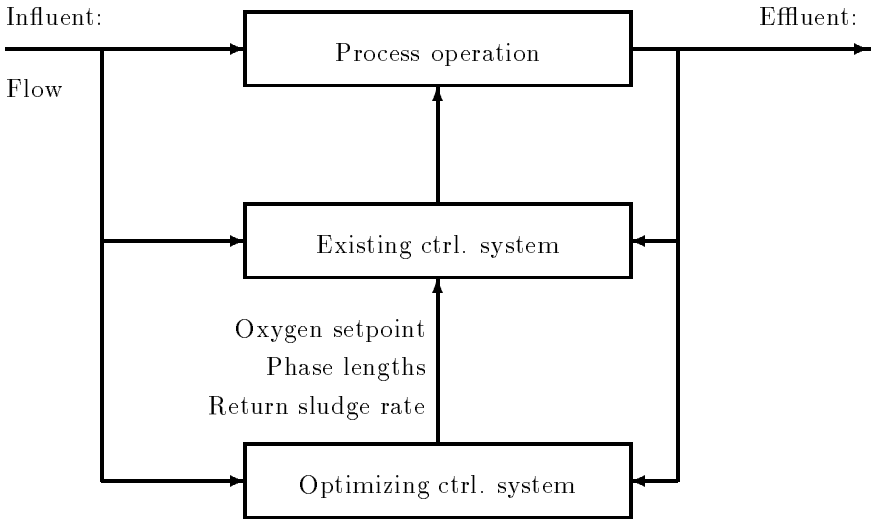

Figure 7.1. *Illustration of the interaction of the measured variables and potential controlling actions of the BIO-DENITRO and BIO-DENIPHO processes.*

The influent flow rate to the BIO-DENITRO or BIO-DENIPHO system is assumed to be the only measure of load, as illustrated in Figure 7.1, although the influent concentrations of nutrients and organic materials have a major effect on the process operation performance. However, a major advantage of implementing the grey box models on-line in a control system is, that estimates of these concentrations are obtained from the models, if the load of ammonia, phosphate, and organic materials is assumed to be correlated, and the influent nitrate concentration is assumed to be vanishing.

Lack of information from the measurements above naturally reduces the design of the control system and the effectiveness of the process operation control. In fact, the majority of WWTP's in Denmark are equipped with a very limited number of the measurements listed above. However, savings

from an expected improved process operation should always be compared with the initial expenditures of installing such equipment and the maintenance costs, if the installing of on-line measurements is to be decided. Some measurements which have not been used in the system analysis of Chapter 4 are temperature, redox, wastewater composition and pH-value. Information from these measurements may be incorporated into the grey box models of the previous chapter, if instruments for measuring these variables are installed. Experiences with installing and maintenance of ammonia, nitrate, phosphate, and suspended solids sensors are found in Thomsen & Nielsen (1992).

Controlling the process operation of a BIO-DENITRO or BIO-DENIPHO plant based on the grey box models of the previous chapter requires access to the following control actions:

- Oxygen concentration setpoints in aerobic periods.
- Phase lengths of aerobic/anoxic periods.
- Return sludge rate.

In fact, these three actuators are controlled by adjusting aerators, inlet and outlet gates of the aeration tanks, and intensity of the return sludge pump, but they are, however, to some extent assumed to be perfectly controllable (in most plants these three parameters are controlled by a PLC).

The load of nutrients and organic materials to the plant usually varies according to a diurnal and weekly pattern, which requires an appropriate adjustment of the oxygen setpoint and aerobic/anoxic phase lengths. Peak loads of nutrients and organic materials may call for the adjustment of the return sludge rate (in this case the clarifier design must also be considered).

In the following two sections two different types of control systems are considered. *Off-line simulations of control strategies* are based on computer simulations of strategies which can be implemented on a plant without an on-line updating of the grey box models, i.e. the control system is based

on simple strategies which in most cases can be installed on a PLC. Thus, the control system does not have access to any of the stochastic features of the grey box models, i.e. the estimated state variables (e.g. ammonia load, actual nitrification rate, actual denitrification rate). The simulations are performed on a computer which is not connected to the PLC, using the grey box models and a random number generator. *On-line model-based predictive control* is assumed to be implemented on a computer with access to the system variables. The control strategies may incorporate values of stochastic features (e.g. estimated ammonia load, nitrification rates, and denitrification rates) from the grey box models as well as available measurements. The grey box models are updated on-line as new measurements become available and updated values for the operating points of the control strategies are found. This is exemplified in the last section of this chapter. In fact, the simple control strategies may also be implemented in an on-line model-based predictive control system, but the on-line updating of the grey box models makes the implementation of more advanced control strategies possible.

7.2 Off-line simulations of control strategies

At present, many WWTP's are not equipped with a supervising system for control or even sensors for monitoring of nutrient concentrations. However, the grey box models are applicable for control of these plants by off-line simulations of simple control strategies which can be implemented. In this case, the grey box models only serve as a simulation tool to choose one optimal strategy among several.

Computer simulation has both advantages and disadvantages to a physical simulation of a control strategy. Considerable knowledge of the wastewater processes can be gained from the model simulations, but model performance and sensitivity of specific parameters could also be observed. Time can be compressed on the computer with simulations being conducted in seconds or minutes. This is especially important for the biological processes used in

wastewater treatment where rates are relatively slow and physical experimentation may require weeks or even months. Computer simulations are done easier, cheaper, and faster than physical experimentation, and in the case of wastewater treatment it is also more hygienic. The disadvantages are, that the computer simulations are no better than the model and data they are based on, and if the model is not a reasonable representation of the WWTP, computer simulations result in the generation of large quantities of worthless results. In particular, the simulation of control strategies bringing the system into a state which has not been used for estimating the model, may lead to fatal conclusion regarding the control of the system. As a general rule, computer simulations should at first be used for validating the model structure, and secondly to choose the optimal control strategy to be used in a physical experiment.

Assuming that the oxygen concentration and the suspended solids concentration in the aeration tanks are perfectly controlled according to their setpoints, the grey box models of Section 4.4 represent a simulation tool for off-line testing of control strategies. The required input flow rate to the grey box models can be simulated using a sinusoidal signal, or a time series of historic flow rates may be applied. The grey box models have the advantage to other models, that the process parameters used for simulation are estimated on actual data from the given plant. However, there are some limitations to the use of the grey box models in simulations. The models may not be appropriate of simulating load situations which are not reflected in the data set used for estimation. Thus, the parameter estimation of the grey box models should be based on data with highly time-varying loads. The control strategies proposed below are simple strategies, which can be implemented on a PLC without an on-line use of the grey box models. More advanced strategies are proposed in the next section.

For the control of the oxygen concentration setpoint the following off-line control strategies are proposed:

(1) A constant oxygen concentration setpoint.

(2) A sinusoidal oxygen concentration setpoint which is a linear function of the estimated diurnal variation of the influent ammonia load rate (4.57).

and for the control of aerobic and anoxic phase lengths:

(a) Constant phase lengths.

(b) Switching off the aeration once the ammonia concentration in the aerobic period lies below a certain value, e.g. 1.0 mg NH_4^+-N/l.

(c) The strategy (b) combined with switching of phases once the nitrate concentration lies below a certain value, e.g. 4.0 mg NO_3^--N/l.

The strategies listed above are only examples of a vast number of strategies that can be simulated off-line. Strategies for control of the return sludge rate are not proposed, because the simulation of such strategies using the grey box models would not take the influence on the clarifiers into account. Raising the return sludge rate results in higher suspended solids concentrations in the aeration tanks yielding higher removal rates of nutrients, but it also increases the likelihood of activated sludge loss to the effluent.

The different control strategies are evaluated by a cost function, which may incorporate the cost of aeration, switching of phases, return sludge pumping, and the discharge of ammonia, nitrate, and phosphate to the effluent assuming that the concentration of dissolved nutrient salts is unchanged by passage of the clarifier. While the costs of the operations on the plant can be calculated in terms of money, the discharge of nutrients does not have an immediate cost related to it, unless regulatory limits of discharge are exceeded. A cost function of the type illustrated in Figure 7.2 may prove appropriate, where $\Delta\alpha$ is the additional cost of discharging an additional 1 mg/l below the discharge limit, $\Delta\beta$ is the additional cost of discharging an additional 1 mg/l above the discharge limit, and β_0 is the cost of exceeding the regulatory limit. The values of $\Delta\alpha$, $\Delta\beta$, and β_0 may be chosen according to the expected effects of nutrient discharge on the effluent, and in lack of such knowledge appropriate values are chosen.

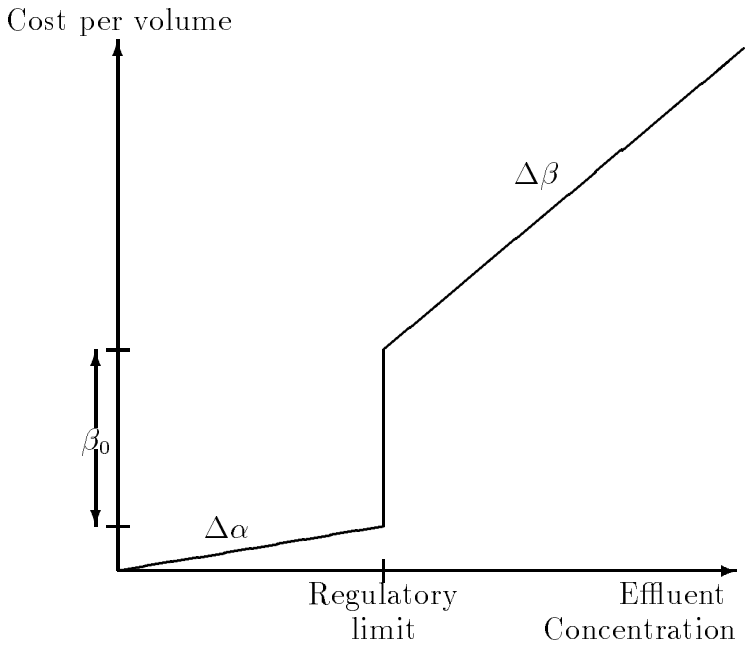

Figure 7.2. *Suggested cost function for the discharge of nutrients. $\Delta\alpha$ and $\Delta\beta$ are the additional costs per volume of discharging an additional 1 mg/l below and above the regulatory discharge limit.*

Off-line simulations of the grey box models may also be applied to WWTP's without on-line sensors permanently installed, if data can be sampled from the plant in a representative period using a mobile measuring equipment. These data are used to estimate the grey box models for the given plant, and off-line simulations of strategies which are possible, based on the permanently available information at the plant, are performed. This optimization of the existing control system applies to smaller plants, where the costs of installing on-line sensors may exceed the benefits of improved operation.

The grey box models also represent a tool which can be used for assessing the effect of operational strategies regarding the biomass activity (both autotrophic and heterotrophic). If an extensive data set is monitored during the physical experiment of improving the overall biomass activity, the parameter estimates of the maximum nitrification rate and maximum denitrification rate are statistics by means of which an improvement can be recognized, assuming that external variables influencing the biomass activity (e.g. temperature, wastewater composition, pH-value) are constant or somehow compensated for. For instance, the effect of adding ferrosulphate and other iron salts for chemical precipitation on the biomass activity may be assessed.

7.3 On-line model-based predictive control

Assuming that the WWTP is equipped with a SCADA-system (Supervision, Control, And Data Acquisition) such that a data-interchange between the on-line measurements, an on-line model, and the actuators is possible. In this case, the grey box models of Section 4.4 provide an optimal on-line estimation (filtering) of the monitored nutrient concentrations using the Kalman filter, and on-line predictions of nutrient concentrations are obtained which can be used for prediction based control. Employing on-line predictions in the operation control is advantageous, because the on-line measurements of nitrate, phosphate, and especially ammonia concentrations are associated with time delays due to the filtering of the sample and the composition analysis. At present, the time delays in the commercial monitoring systems of nutrient salt concentrations are of the magnitude 5-15 minutes, while the time delay of the monitoring systems for oxygen and suspended solids concentrations are considerably less. This means that the operation control strategies can be effectuated more precisely when predictions are applied, thereby resulting in an improved operation performance. Furthermore, on-line updating gives access to the stochastic features of the grey box models (e.g. estimated ammonia loads, nitrification rates, denitrification rates), which can be used for developing control strategies.

The implementation of a control strategy in an on-line model-based predictive control system differs significantly from the implementation of an off-line simulated control strategy in the way the controlling actions are effectuated. While the methods of the previous section are associated with the assessment of the measured values (e.g. switching off the aeration when the measured ammonia concentration lies below 1.0 mg NH_4^+-N/l), the controlling actions of a model-based predictive control system are associated with the assessment of the predictions and estimates using their distributions (e.g. switching off the aeration when the 15-minutes ahead prediction of the ammonia concentration lies below 0.5 mg NH_4^+-N/l with a probability of 90%). In the following the control strategies, which are presented, are based on predictions at time of operation, i.e. the time delays of the sensors are incorporated in the predictions.

The information obtained from the grey box models can be used to develop more advanced controlling strategies in addition to those proposed in the previous section. For the control of the oxygen concentration setpoint the following additional on-line strategy is proposed:

(3) An adjustment of the oxygen concentration setpoint proportional to the predicted nitrification rate ($\widehat{r}_{nit,NH_4^+,t}$ or $\widehat{r}_{nit,NO_3^-,t}$) at time of operation.

and for the control of the aerobic and anoxic periods:

(d) Switching from the aerobic to the anoxic phase when $\widehat{r}_{nit,.,t} < \alpha$, where α is an appropriately chosen constant and $r_{nit,.,t}$ is the predicted nitrification rate at time of operation. This strategy corresponds in principle to strategy (b) with the major difference being, that this strategy uses a stochastic feature from the grey box models in the evaluation of the plant operation.

(e) Switching from the aerobic to the anoxic phase when $\widehat{r}_{nit,.,t} < \beta \widehat{r}_{denit,t}$, where $\widehat{r}_{nit,.,t}$ is the predicted nitrification rate at time of operation and $\widehat{r}_{denit,t}$ is the predicted denitrification rate obtained from the present operating conditions if the switching is performed. Similarly, switching from the anoxic phase to the aerobic phase when $\widehat{r}_{denit,t} < \alpha \widehat{r}_{nit,.,t}$, where $\widehat{r}_{denit,t}$ is the predicted denitrification rate at time of operation and $\widehat{r}_{nit,.,t}$ is the predicted nitrification rate obtained from the present operating conditions if the switching is performed. Thus, the potential removals of ammonia and nitrate are compared at every time step using α and β, which are appropriately chosen constants. Figure 7.3 shows the feasibility area of this strategy, where the present operating conditions of the plant are maintained as long as the operation point ($\widehat{r}_{nit,.,t}$, $\widehat{r}_{denit,t}$) is within the boundaries of the operation area.

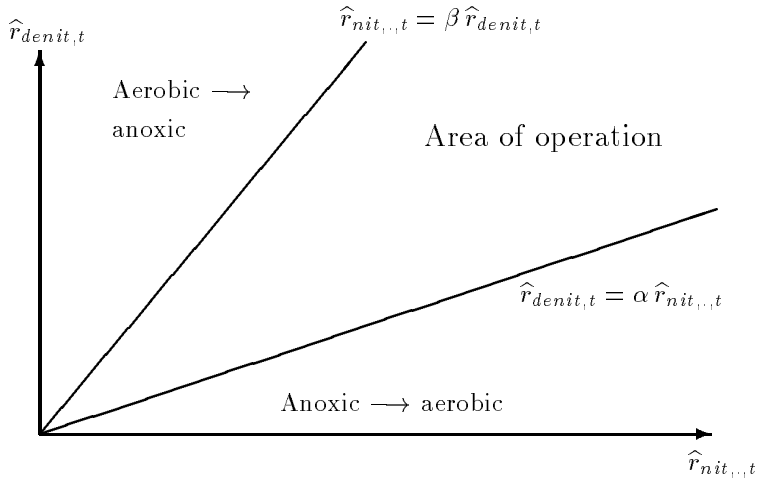

Figure 7.3. *Illustration of the feasibility area of operation strategy (e). At each time-step the operation point* ($\widehat{r}_{nit,t}, \widehat{r}_{denit,t}$) *is plotted, and if it is outside the operation area, the phases are switched. The operation of the plant will move from lower boundary to upper boundary and reverse in an alternating manner.*

The listing above only represents examples of the innumerable possible on-line model-based control strategies. The strategies for phase control of the BIO-DENITRO and BIO-DENIPHO processes presented above only include the main phases of these processes (the lengths of the aerobic and anoxic periods in the operation cycle, i.e. Phase A and C in Figure 3.3 and Phase B in Figure 3.4). Including the control of influent and effluent flow from the alternating tanks in the strategies yields many new alternatives. Selection of the most appropriate on-line model-based predictive control strategy is primarily performed by off-line simulations of the wastewater processes and the plant operation evaluated by a cost function as described in the previous section. Secondly, a physical implementation of the control strategy may be performed to validate the effect of the given strategy.

Furthermore, implementing the grey box models on-line in the SCADA-system, occurrences of inhibition and toxicity may be detected by continuously assessing the estimated maximum nitrification rate and maximum denitrification rate. In this case, the grey box models serve the function of surveillance. In addition, automatic strategies or alarming the personnel are employed in order to minimize the effect of inhibition and toxicity. Procedures for detection of failures in the measuring equipment for nutrient salt concentrations are also easily applied due to the grey box models. For example, if the last three measurements of the ammonia concentration lies outside the 95% confidence limits of the predicted values, the ammonia sensor is most likely mis-functioning. However, scaling and offset calibration errors are more difficult to detect unless two sets of the same measure or estimate can be compared. For example, if both alternating aeration tanks are equipped with ammonia sensors, the results of estimating the grey box models on both time series should correspond reasonably with allowances to the uncertainty of the estimates.

7.4 A simulation study

In order to investigate the strategies proposed in the two previous sections, the grey box models of Section 4.4 are used for simulating a full-scale plant with variable loads and nitrogen removal rates. A biological nutrient removal system consisting of two alternating tanks (each having a volume of 6.500 m^3) is simulated using parameter values, which are estimated on a large data set from the Aalborg West WWTP (see Chapter 6). Throughout the simulation, a constant suspended solids concentration of 3.5 g SS/l is maintained in the aeration tanks. A total of 10 days (starting with a Monday) without any excessive disturbances from rainfall events is simulated.

The load of wastewater entering the biological nutrient removal system is simulated using a diurnal profile in the form of a Fourier expansion (4.17). This profile has been estimated on historic data from Aalborg West WWTP. The average influent flow to the aeration tanks (i.e. the raw wastewater mixed with returned activated sludge) is 1000 m^3/h on weekdays and 800 m^3/h on weekends. The load of ammonia to the plant is simulated using (4.34) and (4.55-4.57) with the parameter estimates from the last column of Table 6.7. In a similar way, the nitrification, denitrification, and nutrient transport processes are simulated by use of the appropriate equations of Section 4.4 with the parameter estimates found in Tables 6.5, 6.6, 6.8, and 6.9. All the simulations in this section are excited by the same noise sequence for generating the innovations of the grey box models.

7.4.1 The cost function

The control strategies proposed previously (strategies (1)-(3) for control of the oxygen setpoint concentration and strategies (a)-(e) for control of the aerobic and anoxic phase lengths) are evaluated against each other using the cost function for the discharge of nutrients sketched in Figure 7.2 and a cost function of aerating the activated sludge. Furthermore, in order to

compare the control strategies to the typical time scheduling of the BIO-DENIPHO process at Aalborg West WWTP, this plant operation is also simulated and evaluated by the same cost function.

In the present example the cost of discharging ammonia and nitrate to the recipient when effluent concentrations are below regulatory limits, is, respectively

$$\begin{aligned} \Delta\alpha_{NH_4^+} &= 30.0 \quad \text{DKK/kg } NH_4^+\text{-N} \\ \Delta\alpha_{NO_3^-} &= 20.0 \quad \text{DKK/kg } NO_3^-\text{-N} \end{aligned}$$

The cost of discharging ammonia and nitrate to the recipient when effluent concentrations are above regulatory limits, is, respectively

$$\begin{aligned} \Delta\beta_{NH_4^+} &= 90.0 \quad \text{DKK/kg } NH_4^+\text{-N} \\ \Delta\beta_{NO_3^-} &= 60.0 \quad \text{DKK/kg } NO_3^-\text{-N} \end{aligned}$$

and the cost of exceeding the regulatory limits at any time is

$$\begin{aligned} \beta_{0,NH_4^+} &= 20.0 \quad \text{DKK/1000 m}^3 \\ \beta_{0,NO_3^-} &= 10.0 \quad \text{DKK/1000 m}^3 \end{aligned}$$

The regulatory discharge limits for the ammonia and total nitrogen concentrations are 1.5 mg NH_4^+-N/l and 8.0 mg N/l in the majority of receiving waters in Denmark, today. However, since the organic nitrogen concentration in the effluent is not known, it is assumed that approximately 12.5% of the total nitrogen in the effluent is organicly bound. Hence, if the combined inorganic nitrogen concentration in the effluent exceeds 7.0 mg/l, an additional cost on the nitrate concentration can be added to the cost function. Furthermore, it is assumed that effluent concentrations of ammonia and nitrate from the aeration tanks remain unchanged by passage of the clarifier into the recipient, i.e. there are no significant nitrogen removal processes taking place in the clarifier. Thus, a cost function of discharging ammonia may be formulated

$$Cost_{NH_4^+,t} = \begin{cases} \Delta\alpha_{NH_4^+} \cdot S^E_{NH_4^+,t} \cdot Q_t \\ \qquad \text{if } S^E_{NH_4^+,t} \leq \alpha_{limit,NH_4^+} \\ \Delta\alpha_{NH_4^+} \cdot \alpha_{limit,Nh_4^+} \cdot Q_t + \beta_{0,NH_4^+} \cdot Q_t \\ \quad + \Delta\beta_{NH_4^+} \cdot (S^E_{NH_4^+,t} - \alpha_{limit,NH_4^+}) \cdot Q_t \\ \qquad \text{if } S^E_{NH_4^+,t} > \alpha_{limit,NH_4^+} \end{cases} \tag{7.1}$$

where $\alpha_{limit,NH_4^+} = 1.5$ mg NH_4^+/l, and similarly for the discharge of nitrate

$$Cost_{NO_3^-,t} = \begin{cases} \Delta\alpha_{NO_3^-} \cdot S^E_{NO_3^-,t} \cdot Q_t \\ \qquad \text{if } S^E_{NH_4^+,t} + S^E_{NO_3^-,t} \leq \alpha_{limit,N_{inorganic}} \\ \Delta\alpha_{NO_3^-} \cdot \alpha_{limit,N_{inorganic}} \cdot Q_t + \beta_{0,NO_3^-} \cdot Q_t \\ \quad + \Delta\beta_{NO_3^-} \cdot (S^E_{NH_4^+,t} + S^E_{NO_3^-,t} - \alpha_{limit,N_{inorganic}}) \cdot Q_t \\ \qquad \text{if } S^E_{NH_4^+,t} + S^E_{NO_3^-,t} > \alpha_{limit,N_{inorganic}} \end{cases} \tag{7.2}$$

where $\alpha_{limit,N_{inorganic}} = 7.0$ mg N/l. The superscript E in (7.1) and (7.2) indicates that the effluent concentration of ammonia and nitrate to the recipient are equal to the ammonia and nitrate concentrations in the alternating tank with effluent flow.

The cost parameters for discharge of nitrogen are adequately chosen with respect to the estimated cost of removing ammonia and nitrate in a WWTP and expected causal effect on the ecological system of the recipient. However, the choice of these cost parameters for the discharge of nutrients to the recipient should be addressed to the local authorities and the politicians, i.e. the people with the power to decide if advanced on-line control should be implemented on the municipal plants.

The cost of aerating may be easily derived if a model for the oxygen setpoint concentration as a function of rotor RPM and plant load is given. However, such a relationship has not been identified in the present context, but it has been estimated at the Aalborg West WWTP, that the cost of aerating 1 kg NH_4^+-N is approximately 8 DKK. It is assumed that the cost of aerating is not simply related to the removal of ammonia, but that this cost is related to maintaining the activated sludge aerated. Thus, the following cost function of aerating may be appropriate

$$Cost_{O_2,t} = 8 \text{ DKK/kg N} \cdot k_{load,NH_4^+,f} \cdot Q_t \cdot V \cdot \frac{O_{2,saturation}}{O_{2,saturation} - O_{2,setpoint}} \tag{7.3}$$

where $O_{2,saturation} = 10$ mg O_2/l is the saturation constant for oxygen and $k_{load,NH_4^+,f} \cdot Q_t \cdot V$ is the actual mass load of ammonia to the plant at time t. The last term in (7.3) describes the efficiency of the aerating equipment as a function of the oxygen setpoint concentration, $O_{2,setpoint}$. Hence, the cost of aerating is assumed to be proportional to the ammonia load of the given operation cycle and a term for aerating according to the oxygen setpoint concentration of the control strategy. The cost function above (7.3) is likely to overestimate the actual cost of aerating, since the cost of keeping the activated sludge aerated is lower than the cost of both removing ammonia and keeping the activated sludge aerated. However, in the present simulation study (7.3) is only used for exemplifying the concept of prediction based control.

In the present simulations example the total cost of operation is related to nitrogen discharge and aeration, which is found as follows:

$$Cost_{total} = \sum_{t=1}^{3600} Cost_{NH_4^+,t} + Cost_{NO_3^-,t} + Cost_{O_2,t} \tag{7.4}$$

The time-step in the simulation is set to 4 minutes which gives a total of 3600 observations.

The parameters values used in the cost functions above and the behavior of the cost functions may be disputed. However, the key issue of the present simulation study is not addressed to the derivation of exact savings by implementing on-line model-based predictive control, but it is addressed to an internal evaluation of the proposed control strategies and the demonstration of the advantages using estimated grey box models for evaluating and improving control strategies. Thus, if the cost functions and related parameters could be determined more exactly (e.g. in the form of a political decision), better estimates on the savings of implementing advanced control strategies can be found. Finally, other costs related to the plant operation such as excess sludge disposals, the number of times the aerating equipment is turned on, electricity consumption for controlling gates, etc. may be also taking into account when the total costs of different control strategies are considered.

7.4.2 Simulation results

The typical time scheduling of the BIO-DENIPHO process at the Aalborg West WWTP is similar to the scheme in Figure 3.4 with the exception of Phase C being omitted. The total operation cycle length is normally 4 hours and the duration of Phase A and Phase B are 20 minutes and 1 hour 40 minutes, respectively. Applying (7.4) to a ten days simulation of this BIO-DENIPHO operation mode results in a total cost of 53389 DKK. In Table 7.1 the total costs of simulated operations are given for the combination of the proposed control strategies of the oxygen setpoint concentration, (1)-(3), and the aerobic/anoxic phase lengths, (a)-(e). Below the cost values in the table, the total cost relative to the typical BIO-DENIPHO time scheduling given above, is listed. The operation of the plant in the simulations has been optimized with respect to the parameters of the control strategies. In most cases the optimization can only be done by hand, since the total cost function is not smooth due to the randomly generated innovations used in the simulations. Hence, a global optimum is not guaranteed in all cases, and the costs found in Table 7.1 act more as possible improvements.

Control strategies for Aalborg West WWTP	Oxygen setpoint concentration strategies		
Typical operation 53389 DKK 100%	(1) Constant oxygen setpoint	(2) Sinusoidal oxygen setpoint	(3) Oxygen set-point function of $\widehat{r}_{rnit,t}$
(a) Constant phase lengths	43171 DKK 80.9%	43025 DKK 80.6%	43056 DKK 80.7%
(b) Switching off aeration, $S_{NH_4^+,t}<\delta$	37607 DKK 70.4%	37602 DKK 70.4%	37580 DKK 70.4%
(c) Combined with switching, $S_{NO_3^-,t}<\kappa$	36399 DKK 68.2%	36349 DKK 68.1%	36389 DKK 68.2%
(d) Aerobic $\rightarrow$ anoxic $\widehat{r}_{nit,,,t} < \alpha$	36993 DKK 69.3%	36755 DKK 68.8%	36958 DKK 69.2%
(e) Strategy sketched in Figure 7.3	35776 DKK 67.0%	35701 DKK 66.9%	35701 DKK 66.9%

Table 7.1. *Lattice of control strategies evaluated by the cost function given in the previous subsection. The typical time-scheduling of the BIO-DENIPHO process results in a total cost of 53389 DKK.*

Comments to the simulation results in Table 7.1:

(a1): The time scheduling of the BIO-DENIPHO process is optimized with respect to the phase lengths and the oxygen setpoint concentration. In this case the length of the total operation cycle is 2 hours with 8 minutes for Phase A and 52 minutes for Phase B in Figure 3.4. The typical time-scheduling is 20 minutes for Phase A and 1 hour 40 minutes for Phase B. The optimal oxygen setpoint concentration is found to be 1.7 mg O_2/l, which is lower than the typical oxygen setpoint concentration. Thus, a significant improvement of the total cost is obtained compared to the typical BIO-DENIPHO operation mode, simply by optimizing the present plant operation.

(a2): Phase lengths are as in (a1). The oxygen setpoint concentration is controlled according to the ammonia load profile with an average of 1.6 mg O_2/l, and it varies within the range of 1.2-2.0 mg O_2/l. Compared to strategy (a1), this strategy yields a lower oxygen consumption for aeration and a slight improvement in the total cost.

(a3): Phase lengths are as in (a1). The oxygen setpoint concentration is optimized as a suggested linear function of the present nitrification rate, i.e. $O_{2,setpoint} = 1.4 + 0.80 \cdot \widehat{r}_{nit,NH_4^+,t}$. Hence, the oxygen setpoint concentration is approximately within 2.4-3.0 mg O_2/l in the beginning of the aerobic phase whereupon it decreases towards 1.4 mg O_2/l. Compared to strategy (a1) a small improvement of the total cost is found.

(b1): Phase lengths are as in (a1) with the aerating equipment being turned off in the aerobic phase once the measured ammonia concentration, $S_{NH_4^+,t} < 0.90$. The time delay on the ammonia concentration monitoring equipment is 16 minutes, and the optimal oxygen setpoint concentration is found to be 2.5 mg O_2/l. Hence, when the aeration is turned off the actual ammonia concentration in the aeration tank is approximately 0.5 mg NH_4^+-N/l. A significant improvement of the total cost compared to strategy (a1) is obtained. It should also be noted that the optimal oxygen setpoint concentration is increased.

(b2): Phase lengths are as in (a1) with the aerating equipment being turned off in the aerobic phase once the measured ammonia concentration, $S_{NH_4^+,t} < 0.85$. The optimal oxygen setpoint concentration is found to vary within the range of 2.4-2.6 mg O_2/l according to the diurnal profile of the ammonia load. However, the total cost of this strategy does not differ significantly from the value obtained in (b1).

(b3): Phase lengths are as in (a1) with the aerating equipment being turned off in the aerobic phase once the measured ammonia concentration, $S_{NH_4^+,t} < 0.90$. The oxygen setpoint concentration is optimized as a linear function of the present nitrification rate, $O_{2,setpoint} = 2.3 + 0.50 \cdot \widehat{r}_{nit,NH_4^+,t}$, but this does not give an improved total cost for this strategy compared to (b1).

(c1): A switch of operating conditions from the aerobic to anoxic phase is performed when $S_{NH_4^+,t} < 1.1$, and similarly from the anoxic to aerobic phase if $S_{NO_3^-,t} < 2.0$ or $S_{NH_4^+,t} > 1.5$. In the simulation of control strategy (c) a minimum aerobic phase of 36 minutes is always ensured. The time delay of the nitrate concentration monitoring equipment is 8 minutes and the optimal oxygen setpoint concentration is found to be 2.6 mg O_2/l. Compared to strategy (b1) a notable improvement in the total cost of operation is achieved.

(c2): A switch of operating conditions from the aerobic to anoxic phase is performed when $S_{NH_4^+,t} < 1.1$, and similarly from the anoxic to aerobic phase if $S_{NO_3^-,t} < 1.7$ or $S_{NH_4^+,t} > 1.5$. The optimal oxygen setpoint concentration is found to vary within the range 2.4-2.6 mg O_2/l according to the diurnal profile of the ammonia load. No significant further improvement of the total cost is obtained.

(c3): A switch of operating conditions from the aerobic to anoxic phase is performed when $S_{NH_4^+,t} < 1.2$, and similarly from the anoxic to aerobic phase if $S_{NO_3^-,t} < 1.7$ or $S_{NH_4^+,t} > 1.5$. The oxygen setpoint concentration is optimized as $O_{2,setpoint} = 2.6 + 0.30 \cdot \widehat{r}_{nit,NH_4^+,t}$. No significant improvement of the total cost is obtained.

(d1): Phase lengths are as in (a1) with the aerating equipment being turned off in the aerobic phase once the model-based estimate of the nitrification rate, $\widehat{r}_{nit,NH_4^+,t} < 1.10$. The optimal oxygen setpoint concentration is found to be 2.8 mg O_2/l. This strategy compares to (b1) in its operation behavior, and it is clearly recognized that the use of on-line estimates in the plant control improves the total cost of operation.

(d2): Phase lengths are as in (a1) with the aerating equipment being turned off in the aerobic phase once the model-based estimate of the nitrification rate, $\widehat{r}_{nit,NH_4^+,t} < 1.10$. The optimal oxygen setpoint concentration is found to vary within the range 2.4-2.6 mg O_2/l according to the diurnal profile of the ammonia load. The total cost of this strategy is somewhat lower than the costs of (d1) and (d3), though the reason is still unclear.

(d3): Phase lengths are as in (a1) with the aerating equipment being turned off in the aerobic phase once the model-based estimate of the nitrification rate, $\widehat{r}_{nit,NH_4^+,t} < 1.10$. The oxygen setpoint concentration is optimized as $O_{2,setpoint} = 2.5 + 0.30 \cdot \widehat{r}_{nit,NH_4^+,t}$. No significant improvement of the total cost is obtained.

(e1): The strategy is sketched in Figure 7.3 where switching from aerobic to anoxic conditions is performed when $\widehat{r}_{nit,NH_4^+,t} < 1.18 \cdot \widehat{r}_{denit,t}$, and where switching from anoxic to aerobic conditions is performed when $\widehat{r}_{denit,t} < 0.50 \cdot \widehat{r}_{nit,NH_4^+,t}$. The nitrification and denitrification rates used in this strategy are on-line estimates from the grey box models. The optimal oxygen setpoint concentration is found to be 2.8 mg O_2/l. This strategy compares to (c1) in its operation behavior, and for this type of strategy it is also clearly recognized that the use of on-line estimates in the control strategy improves the total cost of operation.

(e2): The strategy is sketched in Figure 7.3 where switching from aerobic to anoxic conditions is performed when $\widehat{r}_{nit,NH_4^+,t} < 1.16 \cdot \widehat{r}_{denit,t}$, and where switching from anoxic to aerobic conditions is performed when $\widehat{r}_{denit,t} < 0.51 \cdot \widehat{r}_{nit,NH_4^+,t}$. The optimal oxygen setpoint concentration is found to vary within the range 2.6-2.8 mg O_2/l according to the diurnal profile of the ammonia load. This control strategy yields the minimum total cost of operation in the table.

(e3): The strategy is sketched in Figure 7.3 where switching from aerobic to anoxic conditions is performed when $\widehat{r}_{nit,NH_4^+,t} < 1.15 \cdot \widehat{r}_{denit,t}$, and where switching from anoxic to aerobic conditions is performed when $\widehat{r}_{denit,t} < 0.51 \cdot \widehat{r}_{nit,NH_4^+,t}$. The oxygen setpoint concentration is optimized as $O_{2,setpoint} = 2.4 + 0.45 \cdot \widehat{r}_{nit,NH_4^+,t}$. No significant improvement of the total cost is obtained.

The optimal parameters of the control strategies above are found by simulating a finite number of parameter combinations in a discrete parameter space (e.g. combinations of 2.1-3.0 mg O_2/l with a step length of 0.1 mg O_2/l are performed for the oxygen setpoint concentration). Hence, the

strategies above may be further optimized with respect to the parameters, if the sensitivity of the parameter space is increased. However, this will also increase the number of simulations to be performed.

7.4.3 Discussion

The total cost of plant operation seems to be almost indifferent to the proposed strategies for control of the oxygen setpoint concentration as the level of complexity in the proposed strategies for control of aerobic/anoxic phase lengths increases. At the same time, the oxygen setpoint concentration is increased. Hence, according to this simulation example the plant should be operated at a high oxygen setpoint concentration with relative short aerobic periods. Actually, using different parameter values in the cost functions above (7.1-7.3), it is found that the optimal oxygen setpoint concentration is determined by the cost of aerating relative to the cost of discharging ammonia to the recipient (e.g. if the cost of discharging ammonia is increased/decreased, the optimal oxygen setpoint concentration is also increased/decreased).

The phase lengths of the aerobic and anoxic periods are mainly determined by the cost of discharging ammonia relative to discharging nitrate. However, the simulations show that at least 50% of the operation time should always be dedicated to denitrification in the more advanced control strategies ((b)-(e)) and aerobic periods should never coincide with periods of influent flow.

The strategy minimizing the total cost of operation in Table 7.1 is found to be (e2), which yields a slightly improved total cost compared to (e3). Comparing this strategy with the typical plant operation of Aalborg West WWTP the following average effluent concentrations are obtained for the ten days simulation:

	Typical operation	Strategy (e2)
$\overline{S}^E_{NH_4^+}$	0.67 mg NH_4^+-N/l	0.95 mg NH_4^+-N/l
$\overline{S}^E_{NO_3^-}$	4.75 mg NO_3^--N/l	2.97 mg NO_3^--N/l

While the average effluent ammonia concentration is slightly increased by applying strategy (e2), the average effluent nitrate concentration is almost reduced by 2 mg NO_3^--N/l. Furthermore, the simulation of the control strategy (e2) yields 37% aerobic operation time at an average oxygen concentration of 2.7 mg O_2/l and 63% anoxic operation time. The typical plant operation has 50% aerobic operation time at an oxygen concentration of 2.0 mg O_2/l. Thus, evaluating these two different plant operations only by the cost of aeration, it is found

	Typical operation	Strategy (e2)
$Cost_{O_2,total}$	20853 DKK	15398 DKK

Therefore, strategy (e2) reduces the total nitrogen discharge to the recipient as well as the cost of aerating. It should be stressed that the major improvement in the total cost function of the different strategies compared to the typical operation is obtained from the identification of the nitrogen removal processes, while the optimization of the parameters of the control strategy has a smaller effect on the total cost function.

If the cost function (7.4) is an adequate measure of plant performance, a plant operated according to the control strategy (e2) can be reduced in size. It is found that a reduction of the volumes of the aeration tanks in the simulation of control strategy (e2) to 5170 m^3 yields a total cost of operation similar to the typical plant operation. This is a reduction in volume of 20.5%. Thus, if control strategies for plant operation are taken into account when designing new plants, large savings on the cost of construction may be obtained.

7.5 Conclusion

In this chapter methods are proposed which use the grey box models of the previous chapter for control of the BIO-DENITRO and BIO-DENIPHO processes. Applying the grey box models to a WWTP requires, in general, that the flow rate, oxygen, ammonia, nitrate, phosphate, and suspended solids concentrations are monitored and used for estimating the parameters of the given plant. Lack of some of these measurements result in less appropriate models and a reduced operation performance. The grey box models may be used for control of the oxygen concentration setpoints in aerobic periods and phase lengths of aerobic and anoxic periods. Two different approaches to the application of the grey box models in control of WWTP's are suggested: off-line simulations of control strategies and on-line model-based predictive control.

In order to use the grey box models for control of plant operation, strategies for the given actuators needs to be developed. If these strategies and a cost function for evaluating the strategies are supplied, the grey box models may serve as an off-line simulator by means of which the effect of the different strategies can be assessed. The cost function may incorporate the costs of plant operation and a cost related to the discharge of nutrients to the recipient. Furthermore, the rates estimates of the grey box models may be used for assessing the effects of physical experiments related to the biomass activity.

Implementing the grey box models on-line in a SCADA-system provides on-line filtering of the monitored nutrient salts concentrations and on-line predictions of the nutrient concentrations. Applying model predictions to the controlling system enhances the operation performance because the measurement system is associated with noise and some time delay, and more advanced control strategies may be proposed based on estimates from the models in addition to strategies based on measured values. Furthermore, the implementation of the grey box models on-line serve as a surveillance system for inhibition and toxicity. Failures and mis-calibrations of the

measurement system can be detected, if some kind of rule-based procedures on the parameter estimates and model predictions are applied.

In a simulation study, strategies for control of the oxygen concentration setpoint and aerobic/anoxic phase lengths are evaluated by a cost function. The grey box models with parameters estimated on data from the Aalborg West WWTP are used for simulating the BIO-DENIPHO process. The simulations show that a reduction in both total nitrogen discharge and oxygen consumption is obtained by applying advanced control strategies to the plant operation. However, the major improvement in the total cost function of the different strategies compared to the typical operation is obtained from the identification and quantification of the ammonia load, nitrification, and denitrification processes. This may have a major impact on the plant operation of existing plants as well as the design of new plants.

Chapter 8

Conclusion

The present thesis is addressed to the formulation of operational models for control of wastewater treatment plants including nutrients removal. The proposed models are from a pragmatically point of view based on the available data of the given plant being modelled. Physical insight of the system is incorporated into the models by including terms of the hydraulic and biological processes which can be statistically identified. These terms are discrete time approximations to the deterministic differential equation formulations, which have been predominant in the modelling of wastewater processes in the last decades.

Measurements of ammonia, nitrate, and phosphate concentrations from plants of the BIO-DENITRO and BIO-DENIPHO type contain a great deal of dynamic due to the alternating operation mode. An excessive amount of information is extracted from the large variations of these measurements, making the statistical identification of rates from several hydraulic and biological processes possible. The models in the present context include rate expressions for

- Influent nutrient load.

- Nutrient transport of the aeration tanks.
- Hydrolysis and growth of biomass.
- The nitrification process.
- The denitrification process.
- Biological phosphate uptake in biomass.
- Stripping of phosphate.

The majority of parameters used for modelling these processes have the quality of interpretability relating to the deterministic theory of the processes. The alternating operation mode introduces natural break points in the time series of the measurements, which is used for modelling of three time-varying parameters in the operation cycle time domain.

- Influent load rate of ammonia.
- Maximum nitrification rate.
- Maximum denitrification rate.

Applying simple approximations to the three time-varying parameters above, estimates of these describe the variations of the influent ammonia concentration to the aeration tanks, the activity of the autotrophic biomass, and the activity of the heterotrophic biomass. The three time-varying parameters are essential to the nitrogen removal performance of a biological nutrient removal system. The models presented in this thesis are denoted grey box models, since they are not as detailed as the "white" deterministic models and still contain some physical insight of the system as opposed to the black box models. Data from two different wastewater treatment facilities have been used for the development of the grey box models.

Two data sets from the Lundtofte pilot scale plant have been employed for the estimation of the grey box models. In order to use the Kalman filter

on this data, a model for the correlation of the measurement noise has to be formulated. It is found, that the identification of Monod-kinetic expressions is practically feasible, if an extensive data set is available. The kinetic parameter estimates of the grey box models are consistent with the values found in the literature. The estimated influent ammonia concentrations reflect a major part of the dynamics of the measured influent ammonia concentrations, but the estimates are biased towards lower values. The variations of the influent ammonia concentrations are modelled according to human behavior in the operation cycle time domain, but the diurnal and weekly patterns are interrupted by periods of rainy weather. The activities of the autotrophic and the heterotrophic biomass are time-varying. However, lack of information on external variables describing some of this variation reduces the performance of the models in the operation cycle time domain.

At the Aalborg West wastewater treatment plant two sets of ammonia and nitrate concentrations are monitored from the alternating aeration tanks. The modelling of the influent ammonia load to the plant is divided into two distinct situations, dry weather periods and rainy weather periods. The latter is based on the assumption, that the dynamics of the sewerage, the primary clarifiers, and anaerobic pretreatment tanks can be modelled as two ideally mixed tanks in series with identical volume holdings. The estimates of the kinetic parameters are consistent with the suggested values of the literature, though several of these estimates are influenced by the mis-calibration of one of the ammonia sensors. The estimated influent ammonia concentrations show large variations which are partly due to many rainy weather periods. The estimated autotrophic biomass activity is found to be strongly correlated with past estimates of the ammonia load rate. This is modelled as a short-term dependency in the operation cycle time domain. However, the slow dynamics of the autotrophic and the heterotrophic biomass are not adequately described in the operation cycle time domain due to lack of information on the influence of external variables. A small number of irregularly samples measurements of temperature and sludge volume index may suggest a relationship between these two variables and the overall biomass activity.

The models are useful for on-line surveillance and control of a wastewater treatment plant of the BIO-DENITRO or BIO-DENIPHO type, because the states of the plant are quantified by the physically interpretable parameters of the grey box models. In order to use the grey box models for control, operational strategies need to be developed. These strategies are evaluated by a cost function which includes the cost of operation and discharge of nutrients. Primarily, the grey box models may be applied to off-line simulations of the developed strategies, and secondly, selected strategies may be practically implemented on the plant with or without an on-line implementation of the grey box models. A simulation study evaluating and optimizing several control strategies shows that a reduction in both total nitrogen discharge and oxygen consumption is obtained by applying on-line model-based predictive control to the plant operation. Though, the identification and quantification of the wastewater processes used in the control strategies has a larger effect on the plant operation than the optimization of the parameters of the control strategies. Thus, an improved operation by applying advanced control should be considered on existing plants as well as in the design of new plants.

Appendix A

Numerical considerations

The choice of numerical methods applied to the estimation of the grey box models presented in Chapter 4 is crucial. The increasing complexity of the parameterization of the structural models calls for the development of well-suited numerical methods in order to implement the estimation algorithms on a computer. The problems arise due to the finite arithmetic in a computer introducing rounding errors for every calculation with real numbers. The calculations of an algorithm may have several algebraically equivalent implementations with different numerical properties. Thus, for a given estimation algorithm the selection of the appropriate numerical implementation is very important. However, as a general rule, the computations should always be carried out using double precision. In the first section of this appendix methods for stabilizing the Kalman filter recursions given in Section 4.6 are described, and the second section deals with the numerical optimization.

A.1 Kalman filter data processing

Applying the Kalman filter recursions (4.71-4.77) to time series with many observations often give rises to numerical problems. This is due to the accumulation of rounding errors in the covariance matrix of the state vector, $\widehat{\boldsymbol{P}}_t$, and eventually the covariance matrix may become non-positive definite (i.e. at least one of the eigenvalues of $\widehat{\boldsymbol{P}}_t$ is non-positive). Unreliable estimates of the covariance matrix also affect the calculation of the Kalman gain (4.77) and the variance of the prediction error (4.74). In the end, all the parameter estimates become unreliable and the convergence of the estimation algorithm is endangered.

Bierman (1977) suggest replacing the covariance matrix update (4.76) by a stabilized covariance update

$$\widehat{\boldsymbol{P}}_{t|t} = \widehat{\boldsymbol{P}}_{t|t-1} - \boldsymbol{K}_t \widehat{R}_{t|t-1} \boldsymbol{K}_t^T + \boldsymbol{K}_t \boldsymbol{K}_t^T \tag{A.1}$$

which enhances the numerical stability. However, it does not guarantee numerical stability and positive definiteness of $\widehat{\boldsymbol{P}}_t$. Thus, methods for updating the square root of the covariance matrix have been proposed in order to ensure that $\widehat{\boldsymbol{P}}_t$ is positive definite. Since all covariance matrices should be symmetric and positive definite, it is desirable to use their Cholesky factorization, e.g. the LDL^T factorization (see Fletcher & Powell (1974)).

Assume that a $n \times n$ matrix $\boldsymbol{A}$ is known to be positive definite. Hence, $\boldsymbol{A}$ has a Cholesky decomposition form

$$\boldsymbol{A} = \boldsymbol{L}\boldsymbol{D}\boldsymbol{L}^T \tag{A.2}$$

where $\boldsymbol{L}$ is a lower triangular matrix and $\boldsymbol{D}$ is a diagonal matrix with the elements of the diagonal $d_i > 0$. Suppose $\boldsymbol{A}$ is modified as follows

$$\widetilde{\boldsymbol{A}} = \boldsymbol{A} + \boldsymbol{G}\boldsymbol{D}_g\boldsymbol{G}^T \tag{A.3}$$

where $\widetilde{\boldsymbol{A}}$ is known from other considerations to be positive definite, and $\boldsymbol{D}_g$ is a diagonal matrix. Thus, it is necessary to compute a unit lower triangular matrix $\widetilde{\boldsymbol{L}}$ and a diagonal matrix $\widetilde{\boldsymbol{D}}$ with $\widetilde{d}_i > 0$ such that

$$\widetilde{\boldsymbol{A}} = \widetilde{\boldsymbol{L}}\widetilde{\boldsymbol{D}}\widetilde{\boldsymbol{L}}^T \tag{A.4}$$

An algorithm for solving this problem is given in Thornton & Bierman (1980) based on modified Gram-Schmidt orthogonalization techniques (see e.g. Lawson & Hanson (1974)).

Hence, using the LDL^T-factorization of $\widehat{\boldsymbol{P}}_{t-1|t-1}$, the prediction of the covariance matrix in (4.73) implicitly apply to the transformation (A.3) and the LDL^T-factorization of $\widehat{\boldsymbol{P}}_{t|t-1}$ is found by applying the algorithm of Thornton & Bierman (1980).

The updating equation of the covariance matrix (4.76) is rewritten as

$$\begin{aligned}
&\widehat{\boldsymbol{P}}_{t|t} = \widehat{\boldsymbol{P}}_{t|t-1} - \boldsymbol{K}_t \widehat{R}_{t|t-1} \boldsymbol{K}_t^T \\
\Updownarrow \\
&\widehat{\boldsymbol{P}}_{t|t} = \widehat{\boldsymbol{P}}_{t|t-1} - \widehat{\boldsymbol{P}}_{t|t-1}\boldsymbol{c}^T \widehat{R}_{t|t-1}^{-1} \boldsymbol{c}\widehat{\boldsymbol{P}}_{t|t-1}{}^T \\
\Updownarrow \\
&\widetilde{\boldsymbol{L}}\widetilde{\boldsymbol{D}}\widetilde{\boldsymbol{L}}^T = \boldsymbol{L}\boldsymbol{D}\boldsymbol{L}^T - \boldsymbol{L}\boldsymbol{D}\boldsymbol{L}^T\boldsymbol{c}^T \widehat{R}_{t|t-1}^{-1} \boldsymbol{c}(\boldsymbol{L}\boldsymbol{D}\boldsymbol{L}^T)^T \\
\Updownarrow \\
&\widetilde{\boldsymbol{L}}\widetilde{\boldsymbol{D}}\widetilde{\boldsymbol{L}}^T = \boldsymbol{L}(\boldsymbol{D} - \boldsymbol{G}\widehat{R}_{t|t-1}^{-1}\boldsymbol{G}^T)\boldsymbol{L}^T
\end{aligned} \tag{A.5}$$

where

$$\boldsymbol{G} = \boldsymbol{D}\boldsymbol{L}^T\boldsymbol{c}^T \widehat{R}_{t|t-1}^{-1} \tag{A.6}$$

The expression $(\boldsymbol{D} - \boldsymbol{G}\widehat{R}_{t|t-1}^{-1}\boldsymbol{G}^T)$ in (A.5) is of the form (A.3) which can be solved by the previously mentioned algorithm for the factors $\overline{\boldsymbol{L}}\,\overline{\boldsymbol{D}}\,\overline{\boldsymbol{L}}$

Algorithm	Adds	Multiplies	Divides
Conventional Kalman	$1.5n^2 + 3.5n$	$1.5n^2 + 4.5n$	1
Stabilized Kalman	$4n^2 + 4n$	$4n^2 + 6n$	1
LDL^T-factorization	$2n^2 + n$	$2.5n^2 + 5n$	n

Table A.1. Operation counts for the Kalman recursions. Data from Thornton & Bierman (1980).

and as a result $\widetilde{\boldsymbol{L}}=\boldsymbol{L}\overline{\boldsymbol{L}}$ and $\widetilde{\boldsymbol{D}}=\overline{\boldsymbol{D}}$. Thus, with the LDL^T-factorization of the covariance matrix, $\boldsymbol{L}$ and $\boldsymbol{D}$ are used for updating and prediction such that the positive definiteness of $\widehat{\boldsymbol{P}}_t$ is preserved. The implementation of this algorithm for the Kalman recursions is facilitated by a routine developed by Madsen & Melgaard (1992).

Table A.1 lists the computation requirements of standard implementations of the conventional Kalman filter (4.71- 4.77), the stabilized Kalman filter ((4.76) substituted by (A.1)), and the LDL^T-factorization method (A.3-A.6), where n denotes the dimension of the state space vector $\boldsymbol{x}_t$. The LDL^T-factorization of the covariance matrix is very competitive with the other algorithms. For the extensive data sets in Chapter 5 and Chapter 6 used to estimate the grey box models of Section 4.4, numerical instability of the Kalman filter was observed using the conventional Kalman filter and the stabilized Kalman filter. Applying the LDL^T-factorization to the computations on the covariance matrix, the positive definiteness of $\widehat{\boldsymbol{P}}_t$ was ensured for these large data sets.

A.2 Numerical optimization

Estimating the parameters of the grey box models presented in Section 4.4 requires optimizing the maximum likelihood function (4.84). In the actual case, it is not possible to give a closed form expression for the estimates as a function of the sample values, and the maximization has to

be performed using a numerical procedure. The methods presented in this context also apply for non-linear least squares estimation and other optimization problems. Some parameters may be constrained to span only a part of the vector space, $\Re^n$, which, in practice, is implemented by adding a penalizing term around the constraints. However, only simple constraints on the parameters Ψ of the form $\psi_i > 0$ is needed for estimating the grey box models considered in the present context. Thus, the problem can be transformed into an unbounded optimization problem by estimating the logarithmic transform of the parameter, and hence, the estimation of the parameters of the grey box models is based on unconstrained optimization.

For practical reasons the negative logarithm of the likelihood (4.85) is considered. The object is to minimize this function, which will have the same properties as the likelihood function. Hence, the general problem considered is to find the minimizing point of a non-linear function $\mathcal{F}$: $\Re^n \rightarrow \Re$

$$\min_x \mathcal{F}(\boldsymbol{x}) \tag{A.7}$$

Several methods for minimizing $\mathcal{F}$ are proposed in Judge et al. (1985). Most of these methods are gradient methods characterized by a step length λ and a step direction $\boldsymbol{h}$ such that

$$\mathcal{F}(\boldsymbol{x} + \lambda\boldsymbol{h}) < \mathcal{F}(\boldsymbol{x}) \tag{A.8}$$

Among optimization methods, Newton-Raphson's method has shown to be exceptionally effective. The method uses the inverse of the Hessian to specify the step direction in each iteration. The method is based on a Taylor expansion of $\mathcal{F}$ at the search point $\boldsymbol{x}_k$ up to the quadratic terms

$$\mathcal{F}(\boldsymbol{x}) \simeq \mathcal{F}(\boldsymbol{x}_k) + \mathcal{G}(\boldsymbol{x}_k)^T(\boldsymbol{x} - \boldsymbol{x}_k) + \frac{1}{2}(\boldsymbol{x} - \boldsymbol{x}_k)^T\mathcal{H}(\boldsymbol{x}_k)(\boldsymbol{x} - \boldsymbol{x}_k) \tag{A.9}$$

where $\mathcal{G}(\boldsymbol{x})$ is the gradient and $\mathcal{H}(\boldsymbol{x})$ is the Hessian, which is always symmetric and positive definite in the minimum point of $\mathcal{F}(\boldsymbol{x})$.

The first-order condition of a minimum for $\mathcal{F}$ is found by differentiating (A.9) with respect to $\boldsymbol{x}$

$$\mathcal{G}(\boldsymbol{x}_k) + \mathcal{H}(\boldsymbol{x}_k)(\boldsymbol{x} - \boldsymbol{x}_k) = 0 \tag{A.10}$$

or

$$\boldsymbol{x} = \boldsymbol{x}_k - \mathcal{H}(\boldsymbol{x}_k)^{-1}\mathcal{G}(\boldsymbol{x}_k) \tag{A.11}$$

and the step size $\boldsymbol{h}$ is then given by

$$\boldsymbol{h}_k = -\mathcal{H}(\boldsymbol{x}_k)^{-1}\mathcal{G}(\boldsymbol{x}_k) \tag{A.12}$$

The procedure (A.11) requires the computation of the gradient and Hessian. However, analytical computations of the first and second derivative of $\mathcal{F}$ cannot be provided for the estimation method considered in this context. Thus, a finite-difference approximation $\boldsymbol{g}(\boldsymbol{x}_k)$ to the gradient $\mathcal{G}(\boldsymbol{x}_k)$ and a secant approximation $\boldsymbol{B}_k$ to the Hessian $\mathcal{H}(\boldsymbol{x}_k)$ is applied. The secant approximation is more effective and robust than a finite-difference Hessian approximation in the minimization. This class of secant methods are called quasi-Newton, and the most successful seems to be the BFGS method for iterative Hessian approximation combined with soft line search (see Dennis & Schnabel (1983)).

A.2.1 Finite-difference derivatives

An obvious finite-difference approximation to the gradient is the forward difference approximation

$$g_i(\boldsymbol{x}_k) \simeq \frac{\mathcal{F}(\boldsymbol{x}_k + h_i\boldsymbol{e}_i) - \mathcal{F}(\boldsymbol{x}_k)}{h_i}, \qquad i = 1, \ldots, n \tag{A.13}$$

where $\boldsymbol{e}_i$ is the i'th basis vector and h_i is the step-size used in the calculations. Although this forward difference approximation is generally accurate, the central difference approximation may be used for obtaining better estimates of the gradient.

$$g_i(\boldsymbol{x}_k) \simeq \frac{\mathcal{F}(\boldsymbol{x}_k + h_i\boldsymbol{e}_i) - \mathcal{F}(\boldsymbol{x}_k - h_i\boldsymbol{e}_i)}{2h_i}, \qquad i = 1, \ldots, n \tag{A.14}$$

However, one disadvantage of using the central difference approximation is, that is requires $2n$ rather than n evaluations of $\mathcal{F}$ assuming that $\mathcal{F}(\boldsymbol{x}_k)$ is already available.

According to Dennis & Schnabel (1983) the optimal choice of step size for the forward difference approximation is

$$h_i = \eta^{1/2} x_i \tag{A.15}$$

and for the central difference approximation

$$h_i = \eta^{1/3} x_i \tag{A.16}$$

where x_i is the i'th parameter of the $\boldsymbol{x}_k$-vector and η is a constant somewhat larger than the given machine precision (e.g. 100 times larger than the given machine precision). If $\mathcal{F}$ is calculated by an iterative procedure, η may be much larger than the machine precision. The forward difference approximation usually provides acceptable accuracy unless the gradient at the evaluation point is small. Thus, switching to the central difference approximation at a certain stage in the procedure is recommended as the gradient approaches zero in the neighborhood of the minimum. The switch should be effectuated when there is a failure to find a lower point during the linear search.

A.2.2 BFGS-update

The method used for updating the Hessian approximation $\boldsymbol{B}_k$ is the BFGS-update given in Dennis & Schnabel (1983)

$$\boldsymbol{B}_{k+1} = \boldsymbol{B}_k + \frac{\boldsymbol{y}_k \boldsymbol{y}_k^T}{\boldsymbol{y}_k^T \boldsymbol{s}_k} - \frac{\boldsymbol{B}_k \boldsymbol{s}_k \boldsymbol{s}_k^T \boldsymbol{B}_k}{\boldsymbol{s}_k^T \boldsymbol{B}_k \boldsymbol{s}_k} \tag{A.17}$$

where $\boldsymbol{y}_k$ is the difference between the present and the previous gradient (i.e. $\boldsymbol{y}_k = \boldsymbol{g}(\boldsymbol{x}_{k+1}) - \boldsymbol{g}(\boldsymbol{x}_k)$) and $\boldsymbol{s}_k$ is the difference between the present and previous parameter estimate (i.e. $\boldsymbol{s}_k = \boldsymbol{x}_{k+1} - \boldsymbol{x}_k$). A necessary and sufficient conditions for this formula to have a positive definite solution $\boldsymbol{B}_{k+1}$ is, that $\boldsymbol{B}_k$ is positive definite and

$$\boldsymbol{y}_k^T \boldsymbol{s}_k > 0 \tag{A.18}$$

The soft line search will meet this demand.

A.2.3 The soft line search

The parameter updating equation (A.11) is improved by applying a scalar $\lambda_k > 0$ to the search direction

$$\boldsymbol{x}_{k+1} = \boldsymbol{x}_k + \lambda_k \boldsymbol{h}_k \tag{A.19}$$

where $\boldsymbol{h}_k$ is the secant direction obtained from (A.12) with the BFGS-update of the Hessian. The parameter λ_k is chosen to assure that the next iterate decreases the function value of $\mathcal{F}$ and the condition (A.18) is fulfilled. Often $\lambda_k = 1$ will satisfy these demands such that the soft line search reduces to the secant method (A.11).

It can be shown that the line search will be globally convergent if each step satisfies two simple conditions. Firstly, the decrease in $\mathcal{F}$ is sufficiently large in relation to the length of the step $\boldsymbol{s}_k = \lambda_k \boldsymbol{h}_k$. The relation

$$\mathcal{F}(\boldsymbol{x}_{k+1}) < \mathcal{F}(\boldsymbol{x}_k) + \alpha \boldsymbol{g}(\boldsymbol{x}_k)^T \boldsymbol{s}_k \tag{A.20}$$

where α is a constant in the range between zero and one, is chosen to ensure this condition. Secondly, the step length must not be too short. The equation

$$\boldsymbol{g}(\boldsymbol{x}_{k+1})^T \boldsymbol{s}_k \geq \beta \boldsymbol{g}(\boldsymbol{x}_k)^T \boldsymbol{s}_k \tag{A.21}$$

will implement this condition, with β being a constant in the range between zero and one. This last expression and $\boldsymbol{g}(\boldsymbol{x}_k)^T \boldsymbol{s}_k < 0$ imply

$$\boldsymbol{y}_k^T \boldsymbol{s}_k = (\boldsymbol{g}(\boldsymbol{x}_{k+1}) - \boldsymbol{g}(\boldsymbol{x}_k))^T \boldsymbol{s}_k \geq (\beta - 1) \boldsymbol{g}(\boldsymbol{x}_k)^T \boldsymbol{s}_k > 0 \tag{A.22}$$

hence the condition (A.18) is fullfilled.

In practice, when using the soft line search the first guess is $\lambda_k = 1$. If this λ is not admissible because it fails (A.20) then it will be decreased. The new λ is found by a cubic interpolation that fits $\mathcal{F}(\boldsymbol{x}_k)$, $\boldsymbol{g}(\boldsymbol{x}_k)$, $\mathcal{F}(\boldsymbol{x}_k + \lambda_p \boldsymbol{h}_k)$, and $\boldsymbol{g}(\boldsymbol{x}_k + \lambda_p \boldsymbol{h}_k)$, where λ_p is the previous value of λ. Alternatively, if the λ value satisfies (A.20) and not (A.21), λ will be increased. The new λ is found by extrapolation. After one or more repetitions of the λ-transitions, an admissible λ_k is found, as it can be proved that there exists an interval of λ-values satisfying the condition (A.20) and (A.21), see Dennis & Schnabel (1983).

An important result when applying the algorithm described above to the maximum likelihood estimation is, that the $\boldsymbol{B}_k$ approximation of the Hessian matrix at minimum of $\mathcal{F}$ can be used as an estimate of Fisher's information matrix. Thus,

$$V[\hat{\boldsymbol{\Psi}}] \simeq -\boldsymbol{B}_*^{-1} \tag{A.23}$$

where $\boldsymbol{\Psi}$ is the parameter vector of length n. The covariance matrix of the parameter estimates is obtained from the BFGS-update of the Hessian at minimum, $\boldsymbol{B}_*$.

The implementation of this algorithm for optimization of a non-linear function given a parameter vector is facilitated by a routine developed by Madsen & Melgaard (1992). This routine has been investigated together with another quasi-Newton algorithm, the IMSL-routine DB2ONF (IMSL (1987)). The routine by Madsen & Melgaard (1992) is more robust in the convergence, but it also yields larger estimates in the diagonal of the Hessian, i.e. a smaller variance on the estimates, if the variances of the estimates are not well-conditioned.

A.3 Summary

The choice of the numerical implementation of an algorithm has a major impact on the result obtained due to the finite arithmetic of a computer. The practical implementation of two algorithms essential to the estimation of the grey box models of Section 4.4 is presented. Firstly, the application of the conventional Kalman filter algorithm on large data sets is unstable, potentially resulting in a non-positive definite covariance matrix of the state space vector. Using the LDL^T-factorization of the covariance matrix ensures that the covariance matrix is maintained positive definite throughout the Kalman filter recursions. Secondly, the optimization of the likelihood function with respect to the parameters is performed using a quasi-Newton algorithm with a finite-difference approximation to the gradient and BFGS-update of the Hessian. Combining the BFGS-update with a soft line search ensures that the Hessian is positive definite at optimum. A very important result is, that an estimate of the covariance matrix of the parameter vector estimate is obtained by evaluating the Hessian at the optimum.

Appendix B

Summary of grey box models

This appendix summarizes the grey box models of Section 4.4. In the first section the general form of the observation equation and the process equation for all the time series is listed. The following sections deal with the modelling of the mean process rate for the time series of ammonia, nitrate, and phosphate concentrations.

B.1 Observation and process equations

The following observation and process equations are valid for the time series of ammonia, nitrate, and phosphate.

Observation equation:

$$y_t = m_t + \boldsymbol{\kappa}^T \boldsymbol{u}_t + \nu_t \tag{B.1}$$

Process equation:

$$(1 + \phi_1 B + \ldots + \phi_p B^p)(\Delta m_t - \mu_{,t}) = \boldsymbol{\delta}^T \boldsymbol{u}_t + e_t \tag{B.2}$$

B.2 Mean process rate of ammonia

The mean process rate of (B.2) for the time series of ammonia concentrations is given by:

$$\mu_{NH_4^+,t} = r_{load,NH_4^+,t} + r_{transport,NH_4^+,t} + r_{hydrolysis,NH_4^+,t} + r_{nit,NH_4^+,t}, \tag{B.3}$$

where

$$r_{load,NH_4^+,t} = \begin{cases} k_{load,NH_4^+,f} \cdot Q_{t-1} & \text{inlet gate open} \\ 0 & \text{inlet gate closed} \end{cases} \tag{B.4}$$

$$r_{transport,NH_4^+,t} = \begin{cases} k_{transport,NH_4^+}(S^I_{NH_4^+,t-1} - S_{NH_4^+,t-1}) \cdot Q_{t-1} & \text{outlet gate open} \\ 0 & \text{outlet gate open} \end{cases} \tag{B.5}$$

$$r_{hydrolysis,NH_4^+,t} = k_{hydrolysis,NH_4^+} \cdot k_{load,NH_4^+} \cdot Q_{t-1} \tag{B.6}$$

$$r_{nit,NH_4^+,t} = \begin{cases} -k_{nit,max,NH_4^+,f} \cdot \frac{S_{NH_4^+,t-1}}{S_{NH_4^+,t-1}+K_{NH_4^+}} \cdot \frac{S_{O_2,t-1}}{S_{O_2,t-1}+K_{O_2}} \cdot X_{SS,t-1} & \text{aerobic conditions} \\ 0 & \text{anoxic/anaerobic conditions} \end{cases} \tag{B.7}$$

and the following models are given in the operation cycle time domain to describe the variations of some of the parameters above:

Influent ammonia load rate:

$$\Phi_{load}(B)(k_{load,NH_4^+,f} - \mu_{load,NH_4^+,t}) = e_{load,NH_4^+,f} \tag{B.8}$$

where

$$\mu_{load,NH_4^+,t} = \begin{cases} \mu_{weekday,NH_4^+} \cdot \rho_t & \text{if the samples of the operation cycle are on a weekday} \\ \mu_{weekend,NH_4^+} \cdot \rho_t & \text{if the samples of the operation cycle are on a weekend} \end{cases} \tag{B.9}$$

and

$$\rho_t = \sum_{i=0}^{s} (\alpha_i \cos \frac{2\pi i t}{T} + \beta_i \sin \frac{2\pi i t}{T}) \tag{B.10}$$

Maximum nitrification rate:

$$\Phi_{nit}(B)(k_{nit,max,NH_4^+,f} - \mu_{nit,max,NH_4^+,f}) = e_{nit,NH_4^+,f} \tag{B.11}$$

where

$$\mu_{nit,max,NH_4^+,f} = f(T, pH, k_{load,NH_4^+,f-1}, \ldots) \tag{B.12}$$

B.3 Mean process rate of nitrate

The mean process rate of (B.2) for the time series of nitrate concentrations is given by:

$$\mu_{NO_3^-,t} = r_{transport,NO_3^-,t} + r_{nit,NO_3^-,t} + r_{denit,t}, \tag{B.13}$$

where

$$r_{transport,NO_3^-,t} = \begin{cases} k_{transport,NO_3^-}(S^I_{NO_3^-,t-1} - S_{NO_3^-,t-1}) \cdot Q_{t-1} \\ \qquad \text{inlet gate closed and outlet gate open} \\ -k_{transport,NO_3^-} \cdot S_{NO_3^-,t-1} \cdot Q_{t-1} \\ \qquad \text{inlet gate open} \\ 0 \qquad \text{otherwise} \end{cases} \tag{B.14}$$

$$r_{nit,NO_3^-,t} = \begin{cases} k_{nit,max,NO_3^-,f} \cdot \frac{S_{NH_4^+,t-1}}{S_{NH_4^+,t-1}+K_{NH_4^+}} \cdot \frac{S_{O_2,t-1}}{S_{O_2,t-1}+K_{O_2}} \cdot X_{SS,t-1} \\ \qquad \text{aerobic conditions} \\ 0 \qquad \text{anoxic/anaerobic conditions} \end{cases} \tag{B.15}$$

$$r_{denit,t} = \begin{cases} -k_{denit,max,f} \frac{S_{NO_3^-,t-1}}{S_{NO_3^-,t-1}+K_{NO_3^-}} \frac{k_{load,NH_4^+} Q_{t-1}}{k_{load,NH_4^+} Q_{t-1}+K_{load,NH_4^+}} X_{SS,t-1} \\ \qquad \text{anoxic conditions} \\ 0 \qquad \text{aerobic/anaerobic conditions} \end{cases} \tag{B.16}$$

and the following models are given in the operation cycle time domain to describe the variations of some of the parameters above:

Maximum nitrification rate:

$$\Phi_{nit}(B)(k_{nit,max,NO_3^-,f} - \mu_{nit,max,NO_3^-,f}) = e_{nit,NO_3^-,f} \tag{B.17}$$

where

$$\mu_{nit,max,NO_3^-,f} = f(T, pH, k_{load,NH_4^+,f-1}, \ldots) \tag{B.18}$$

Maximum denitrification rate:

$$\Phi_{denit}(B)(k_{denit,max,f} - \mu_{denit,max,f}) = e_{denit,f} \tag{B.19}$$

where

$$\mu_{denit,max,f} = f(T, pH, k_{load,NH_4^+,f-1}, \ldots) \tag{B.20}$$

B.4 Mean process rate of phosphate

The mean process rate of (B.2) for the time series of phosphate concentrations is given by:

$$\mu_{PO_4^{3-},t} = r_{load,PO_4^{3-},t} + r_{transport,PO_4^{3-},t} + r_{hydrolysis,PO_4^{3-},t} + r_{P-uptake,t} + r_{P-strip,t} \quad \text{(B.21)}$$

where

$$r_{load,PO_4^{3-},t} = \begin{cases} k_{load,PO_4^{3-}} \cdot Q_{t-1} & \text{inlet gate open} \\ 0 & \text{inlet gate closed} \end{cases} \quad \text{(B.22)}$$

$$r_{transport,PO_4^{3-},t} = \begin{cases} k_{transport,PO_4^{3-}} (S^I_{PO_4^{3-},t-1} - S_{PO_4^{3-},t-1}) \cdot Q_{t-1} & \text{outlet gate open} \\ 0 & \text{outlet gate open} \end{cases} \quad \text{(B.23)}$$

$$r_{hydrolysis,PO_4^{3-},t} = k_{hydrolysis,PO_4^{3-}} \cdot k_{load,PO_4^{3-}} \cdot Q_{t-1} \quad \text{(B.24)}$$

$$r_{P-uptake,t} = \begin{cases} -k_{P-uptake,max} \cdot \frac{S_{PO_4^{3-},t-1}}{S_{PO_4^{3-},t-1} + K_{PO_4^{3-}}} \cdot X_{SS,t-1} & \text{aerobic conditions} \\ -k'_{P-uptake,max} \cdot \frac{S_{PO_4^{3-},t-1}}{S_{PO_4^{3-},t-1} + K_{PO_4^{3-}}} \cdot X_{SS,t-1} & \text{anoxic conditions} \\ 0 & \text{anaerobic conditions} \end{cases} \quad \text{(B.25)}$$

$$r_{P-strip,t} = \begin{cases} k_{P-strip} & \text{anaerobic conditions} \\ 0 & \text{aerobic/anoxic conditions} \end{cases} \quad \text{(B.26)}$$

Appendix C

The state space form of the grey box models

In this appendix the grey box models of Appendix A are put into the state space form, (4.65) and (4.66), to be accordingly handled by the Kalman filter.

Review of the state space form

Observation equation:

$$y_t = \boldsymbol{c}\boldsymbol{x}_t + \boldsymbol{\kappa}^T \boldsymbol{u}_t + \nu_t \tag{C.1}$$

Process equation:

$$\boldsymbol{x}_t = \boldsymbol{A}\boldsymbol{x}_{t-1} + \boldsymbol{D}\boldsymbol{u}_t + \boldsymbol{b}e_t \tag{C.2}$$

State space formulation

The state space form of (B.1) and (B.2) is obtained by defining the state vector $\boldsymbol{x}_t$ with the dimension $n = p + 2$, where p is the order of the autoregressive polynomial in (B.2).

$$\boldsymbol{x}_t = [\, m_{t-1} \;\; \Delta m_t \;\; \ldots \,]^T \tag{C.3}$$

Thus, the vectors of the observation equation (C.1) is given by

$$\boldsymbol{c} = [\, 1 \;\; 1 \;\; 0 \;\; \ldots \;\; 0 \,]^T \tag{C.4}$$

and

$$\boldsymbol{\kappa} = [\, \kappa_1 \;\; \kappa_2 \;\; \ldots \;\; \kappa_n \,]^T \tag{C.5}$$

Similarly, the vectors and matrices of process equation (C.2) is found by defining

$$\boldsymbol{A} = \begin{bmatrix} 1 & 1 & 0 & 0 & \cdots & 0 \\ 0 & \phi_1 & 1 & 0 & \cdots & 0 \\ 0 & \phi_2 & 0 & 1 & \cdots & 0 \\ \vdots & \vdots & \vdots & \vdots & \ddots & \vdots \\ 0 & \phi_p & 0 & 0 & \cdots & 1 \\ 0 & 0 & 0 & 0 & \cdots & 0 \end{bmatrix} \tag{C.6}$$

$$\boldsymbol{D} = \begin{bmatrix} 0 & 0 & 0 & \cdots & 0 \\ 1 & \delta_1 & \delta_2 & \cdots & \delta_l \\ -\phi_1 & 0 & 0 & \cdots & 0 \\ \vdots & \vdots & \vdots & \ddots & \vdots \\ -\phi_p & 0 & 0 & \cdots & 0 \end{bmatrix} \tag{C.7}$$

$$\boldsymbol{b} = [\, 1 \;\; 0 \;\; \ldots \;\; 0 \,]^T \tag{C.8}$$

where $\boldsymbol{u}_t$ in (C.1) and (C.2) is given by

$$\boldsymbol{u}_t = \begin{bmatrix} \mu_t \\ u_{1t} \\ \vdots \\ u_{lt} \end{bmatrix} \tag{C.9}$$

The vector of external variables is modified to also include μ_t, such that all the information available from previous samples is contained in $\boldsymbol{x}_t$ and μ_t.

References

Akaike, H. (1974). A new look at the statistical model identification. *IEEE Transactions on Automatic Control*, *21*, 716–723.

Anderson, B. & Moore, J. (1979). *Optimal Filtering*. Prentice Hall.

Andrews, J. (Ed.). (1992). *Dynamics and Control of Activated Sludge Processes*. Technomic. 275 pp.

Antoniou, P., Hamilton, J., Koopman, B., Jain, R., Holloway, B., Lyberatos, G., & Svoronos, S. (1990). Effect of temperature and pH on the effective maximum specific growth rate of nitrifying bacteria. *Water Research*, *24*(1), 97–101.

Aoki, M. (1987). *State Space Modeling of Time Series*. Springer-Verlag. 314 pp.

Barnard, J. (1973). Biological denitrification. *Journal of the Water Pollution and Control Federation*, *72*.

Barnard, J. (1975). Biological nutrient removal without the addition of chemicals. *Water Research*, *9*, 485–490.

Bhat, N. & McAvoy, T. (1990). Use of neural nets for dynamic modeling and control of chemical process systems. *Computer and Chemical Engineering*, *14*(5), 573–583.

Bierman, G. (1977). *Factorization Methods for Discrete Sequential Estimation*. Academic Press. 241 pp.

Box, G. & Jenkins, G. (1976). *Time Series Analysis, Forecasting and Control*. Holden-Day. 575 pp.

Box, G. & Tiao, G. (1975). Intervention analysis with applications to economic and environmental problems. *Journal of the American Statistical Association*, *70*(3), 70–79.

Bundgaard, E. (1988). Nitrogen and phosphorus removal by the BIO-DENITRO and BIO-DENIPHO processes. In *Proceedings of the International Workshop on Wastewater Treatment Technology*, Copenhagen.

Capodaglio, A., Novotny, V., & Fortina, L. (1992). Modelling wastewater treatment plants through time series analysis. *Environmetrics*, *3*(1), 99–120.

Carstensen, J., Madsen, H., Poulsen, N., & Nielsen, M. (1992). Identification of wastewater processes using nonlinear grey box models. Technical Report, Institute of Mathematical Statistics and Operations Research, Technical University of Denmark, Lyngby.

Carstensen, J., Madsen, H., Poulsen, N., & Nielsen, M. (1993). Grey box modelling in two time domains of a wastewater pilot scale plant. *Environmetrics*, *4*(2), 187–208.

Carstensen, J., Madsen, H., Poulsen, N., & Nielsen, M. (1994). Identification of wastewater treatment processes for nutrient removal on a full-scale WWTP by statistical methods. *Water Research*, *28*(10), 2055–2066.

Carstensen, J. (1992). Wastewater processes - controlling a sewage treatment plant. Technical Report, Institute of Mathematical Statistics and Operations Research, Technical University of Denmark, Lyngby.

Couillard, D. & Zhu, S. (1992). Control strategy for the activated sludge process under shock loading. *Water Research*, *26*(5), 649–655.

Dennis, J. & Schnabel, R. (Eds.). (1983). *Numerical Methods for Unconstrained Optimization and Nonlinear Equations*. Prentice Hall. 378 pp.

Durbin, J. (1969). Test for serial correlation in regression analysis based on the periodogram of least-squares residuals. *Biometrika*, *56*, 1–15.

Eckenfelder, W. & Grau, P. (Eds.). (1992). *Activated Sludge Process Design and Control: Theory and Practice*. Technomic. 266 pp.

Einfeldt, J. (1992). The implement of biological phosphorus and nitrogen removal with the BIO-DENIPHO process on a 265,000 PE treatment plant. *Water Science Technology*, *25*(4-5), 161–168.

Ekama, G. & Marais, G. (1984). *Theory, Design and Operation of Nutrient Removal Activated Sludge Processes (Biological Nutrient Removal)*. Water Research Commission, Pretoria.

Enbutsu, I., Baba, K., Hara, N., Waseda, K., & Nogita, S. (1993). Integration of multi AI paradigms for intelligent operation support systems - fuzzy rule extraction from a neural network. In Jank, B. (Ed.), *6th IAWQ Workshop on Instrumentation, Control, and Automation of Water & Wastewater Treatment and Transportation Systems*, pp. 171–180, Banff/Hamilton.

Fletcher, R. & Powell, J. (1974). On the modification of LDL^T factorizations. *Mathematical Computations*, *28*, 1067–1087.

Glass, G. (1972). Estimating the effects of intervention into a nonstationary time series. *American Educational Research Journal*, *9*(3), 463–477.

Goodwin, G. & Payne, R. (1977). *Dynamic System Identification - Experiment Design and Data Analysis*. Academic Press.

Granger, C. (1966). The typical shape of an econometric variable. *Econometrica*, *34*, 150–161.

Harremoës, P., Henze, H., Arvin, E., & Dahi, E. (1989). *Theoretical Water Sanitation*. Polyteknisk Forlag. In Danish: Teoretisk vand-hygiejne.

Harvey, A. (1981a). *The Econometric Analysis of Time Series*. Philip Allan Publishers Ltd.

Harvey, A. (1981b). *Time Series Models*. Philip Allan Publishers Ltd. 229 pp.

Harvey, A. (1989). *Forecasting, structural time series models and the Kalman filter*. Cambridge University Press. 554 pp.

Henze, M., Grady, C., Gujer, W., Marais, G., & Matsuo, T. (1987). Activated sludge model No. 1. Technical Report, IAWPRC Science and Technology Reports No. 1, London.

Henze, M., Harremoës, P., & la Cour Jansen, J. (1990). *Wastewater Treatment - Biological and Chemical*. Polyteknisk Forlag. In Danish: Spildevandsrensning - biologisk og kemisk. 299 pp.

Hiraoka, M., Tsumura, K., Fujitsa, I., & Kanaya, T. (1990). System identification and control of activated sludge process by use of autoregressive model. In Briggs, R. (Ed.), *Instrumentation, Control and Automation of Water and Wastewater Treatment and Transport Systems*, Advances in Water Polution Control, pp. 121–128. IAWPRC, Pergamon Press.

Holmberg, A. & Ranta, J. (1982). Procedures for parameter and state estimation of a microbial growth process model. *Automatica, 18*(2), 181–193.

IMSL (1987). *Fortran Subroutines for Mathematical Applications*. IMSL, Houston, Texas.

Isaacs, S., Søeberg, H., & Kümmel, M. (1992). Monitoring and control of a biological nutrient removal process; rate data as a source of information. In *Proceedings of the ICCAFT 5/IFAC-BIO 2 Conference, Keystone, Colorado*.

Jenkins, G. (1982). Some practical aspects of forecasting in organizations. *Journal of Forecasting, 1*(1), 3–21.

Judge, G., Griffiths, W., Hill, R. C., Lütkepohl, H., & Lee, T. (1985). *The Theory and Practice of Econometrics* (Second edition). Wiley. 1019 pp.

Kabouris, J. & Georgakakos, A. (1991). Stochastic control of the activated sludge process. *Water Science and Technology, 24*(6), 249–255.

Kalman, R. (1960). A new approach to linear filtering and prediction problems. *Transactions of ASME, Series D, Journal of Basic Engineering, 82*, 35–45.

Kerrn-Jespersen, J. & Henze, M. (1993). Biological phosphorus uptake under anoxic and aerobic conditions. *Water Research, 27*(4), 617–624.

Kitagawa, G. & Gersch, W. (1984). A smoothness priors-state space modeling of time series with trends and seasonalities. *Journal of the American Statistical Association, 79*, 378–389.

Knowles, G., Downing, A., & Barrett, M. (1965). Determination of kinetic constants for nitrifying bacteria in a mixed culture with the aid of a computer. *J.Gen.Microbiology, 38*.

Kulhavy, R. (1990). Recursive nonlinear estimation: A geometric approach. *Automatica, 26*, 545–555.

Lawson, C. & Hanson, R. (1974). *Solving Least Squares Problems*. Prentice Hall.

Levin, G. & Shapiro, J. (1965). Metabolic uptake of phosphorus by wastewater organisms. *Journal of the Water Pollution and Control Federation, 36*(6), 800–821.

Ljung, L. (1987). *System Identification - Theory for the User*. Prentice Hall. 519 pp.

Ludzack, F. & Ettinger, M. (1962). Controlling operation to minimize activated sludge effluent nitrogen. *Journal of the Water Pollution and Control Federation, 34*.

Lütkepohl, H. (1985). Comparison of criteria for estimating the order of a vector autoregressive process. *Journal of Time Series Analysis*, *6*(1), 35–52. Correction 8(1987), 373.

Madsen, H. & Melgaard, H. (1992). The mathematical and numerical methods used in CTLSM a program for ML-estimation in stochastic, continuous time dynamical models. Technical Report, Institute of Mathematical Statistics and Operations Research, Technical University of Denmark, Lyngby.

Madsen, H. (1989). *Time Series Analysis*. Institute of Mathematical Statistics and Operations Research, Technical University of Denmark, Lyngby. In Danish: Tidsrækkeanalyse.

Monod, J. (1949). The growth of bacterial cultures. *Annual Reviews in Microbiologi*, *3*, 371–394.

Nielsen, M. & Lynggaard-Jensen, A. (1993). Superior tuning and reporting (STAR) - a new concept for on-line process control of wastewater treatment plants. In Jank, B. (Ed.), *6th IAWQ Workshop on Instrumentation, Control, and Automation of Water & Wastewater Treatment and Transportation Systems*, pp. 560–574, Banff/Hamilton.

Novotny, V., Jones, H., Feng, X., & Capodaglio, A. (1991). Time series analysis models of activated sludge plants. *Water Science and Technology*, *23*(4-6), 1107–1116.

Olsson, G., Andersson, B., Hellström, B., Holmström, H., Reinius, L., & Vopatek, P. (1989). Measurements, data analysis and control methods in wastewater treatment plants - state of the art and future trends. *Water Science and Technology*, *21*(10/11), 1333–1345.

Parkum, J. (1992). *Recursive Identification of Time-varying Systems*. Ph.D. thesis, Institute of Mathematical Statistics and Operations Research, Technical University of Denmark, Lyngby. 212 pp.

Pattarkine, V. (1991). *The Role of Metals in Enhanced Biological Phosphorus Removal from Wastewater*. Ph.D. thesis, Virginia Polytechnic Institute and State University, Blacksburg, Virginia, USA. 328 pp.

Pedersen, K., Kümmel, M., & Søeberg, H. (1990). Monitoring and control of biological removal of phosphorus and nitrogen by flow injection analyzers in a municipal pilot scale waste water treatment plant. *Analytica Chimica Acta*, 191–199.

Randall, C., Barnard, J., & Stensel, H. (Eds.). (1992). *Design and Retrofit of Wastewater Treatment Plants for Biological Nutrient Removal*. Technomic. 415 pp.

Rao, C. (1965). *Linear Statistical Inference and its Applications*. John Wiley. 522 pp.

Schwarz, G. (1978). Estimating the dimension of a model. *Annals of Statistics*, *6*, 461–464.

Thomsen, H. & Nielsen, M. (1992). Practical experience with on-line measurements of NH4, NO3, PO4, redox, MLSS, and SS in advanced activated sludge plants. In *HYDROTOP92, The City and the Water*, Vol. 2, pp. 378–388, Marseilles, France.

Thornton, C. & Bierman, G. (1980). UDU^T covariance factorization for kalman filtering. In Leondes, C. (Ed.), *Control and Dynamic Systems*, Vol. 16. Academic Press. 415 pp.

Tong, H. (1990). *Non-linear Time Series - A Dynamical System Approach*. Clarendon Press, Oxford. 564 pp.

Watanabe, S., Baba, K., Yoda, M., Wu, W., Enbutsu, I., Hiraoka, M., & Tsumura, T. (1993). Intelligent operation support system for activated sludge process. In Jank, B. (Ed.), *6th IAWQ Workshop on Instrumentation, Control, and Automation of Water & Wastewater Treatment and Transportation Systems*, pp. 161–170, Banff/Hamilton.

Ph. D. theses from IMSOR

1. **Sigvaldason, Helgi.** (1963). *Beslutningsproblemer ved et hydrotermisk elforsyningssystem.* 92 pp.

2. **Nygaard, Jørgen.** (1966). *Behandling af et dimensionerings problem i telefonien* 157 pp.

3. **Krarup, Jakob.** (1967). *Fixed-cost and other network flow problems as related to plant location and to the design of transportation and computer systems.* 159 pp.

4. **Hansen, Niels Herman.** (1967). *Problemer ved forudsigelse af lydhastighed i danske farvande. Analyse af et stokastisk system. Del 1: Tekst. Del 2: Figurer og tabeller.* 104 pp. + 95 pp.

5. **Larsen, Mogens E.** (1968). *Statistisk analyse af elementære kybernetiske systemer.* 210 pp.

6. **Punhani, Amrit Lal.** (1968). *Decision problems in connection with atomic power plants.* 133 pp.

7. **Clausen, Svend.** (1969). *Kybernetik, systemer og modeller.* 205 pp.

8. **Vidal, R.V. Valqui.** (1970.) *Operations research in production planning. Interconnections between production and demand. Volume 1-2.* 321 pp.

9. **Bilde, Ole.** (1970). *Nonlinear and discrete programming in transportation, location and road design. Volumes 1-2.* 291 pp.

10. **Rasmusen, Hans Jørgen.** (1972). *En decentraliseret planlægningsmodel.* 185 pp.

11. **Dyrberg, Christian.** (1973). *Tilbudsgivning i en entreprenør virksomhed.* 158 pp.

12. **Madsen, Oli B.G.** (1973). *Dekomposition og matematisk programmering.* 271 pp.

13. **Dahlgaard, Peter.** (1973). *Statistical aspects of tide prediction. Volume 1. Volume 2: Figures and tables.* 202 pp. + 170 pp.

14. **Spliid, Henrik.** (1973). *En statistisk model for stormflodsvarsling.* 205 pp.

15. **Pinochet, Mario.** (1973). *Operations research in strategic transportation planning. The decision process in a multiharbour system.* 374 pp.

16. **Christensen, Torben.** (1973). *Om semi-markov processer. Udvidelser og anvendelser inden for den sociale sektor.* 239 pp.

17. **Jacobsen, Søren Kruse.** (1973). *Om lokaliseringsproblemer, modeller og løsninger.* 355 pp.

18. **Marqvardsen, Hans.** (1973). *Skemalægning ved numerisk simulation.* 222 pp.

19. **Mortensen, Jens Hald.** (1974). *Interregionale godstransporter. Teoridannelser og modeller.* 223 pp.

20. **Severin, Juan Melo.** (1974). *Introduction to operations research in systems synthesis. A chemical process design synthesis application.* 249 pp.

21. **Spliid, Iben & Uffe Bundgaard-Jørgensen.** (1974). *Skitse til en procedure for kommunalplanlægning.* 544 pp.
22.

23. **Mosgaard, Christian.** (1975). *International planning in disaster situations.* 187 pp.

24. **Holm, Jan.** (1975). *En optimeringsmodel for kollektiv trafik.* 246 pp.

25. **Jesson, Pall.** (1975). *Stokastisk programmering. Del 1: Modeller. Del 2: Metodologiske overvejelser og anvendelser.* 333 pp.

26. **Iversen, Villy Bæk.** (1976). *On the accuracy in measurements of time intervals and traffic intensities with application to teletraffic and simulation.* 202 pp.

27. **Drud Arne.** (1976). *Methods for control of complex dynamic systems. Illustrated by econometric models.* 209 pp.

28. **Togsverd, Tom.** (1976). *Koordinering af kommunernes ressourceforbrug.* 295 pp.

29. **Jensen, Olav Holst.** (1976). *Om planlægning af kollektiv trafik. Operationsanalytiske modeller og løsningsmetoder.* 321 pp.

30. **Beyer, Jan E.** (1976). *Ecosystems. An operational research approach.* 315 pp.

31. **Bille, Thomas Bastholm.** (1977). *Vurdering af Egnsudviklingsprojekter. Samspil mellem benifit-cost analyse og den politiske vurdering i en tid under forandring.*
260 pp.

32. **Holst, Erik.** (1979). *En statistisk undersøgelse af tabletserier.* 316 pp.

33. **Aagaard-Svendsen, Rolf.** (1979). *Econometric methods and Kalman filtering.*
300 pp.

34. **Hansen, Steen.** (1979). *Project control by quantitative methods.* 230 pp.

35. **Scheufens, Ernst Edvard.** (1980). *Statistisk analyse og kontrol af tidsafhængige vandkvalitetsdata.* 152 pp.

36. **Lyngvig, Jytte.** (1981). *Samfundsøkonimisk planægning.* 252 pp.

37. **Troelsgård, Birgitte.** (1981). *Statistisk bestemmelse af modeller for rumlufttemperatur.* 213 pp.

38. **Raft, Ole.** (1981). *Delivery planning by modular algorithms.* 220 pp.

39. **Jensen, Sigrid M.** (1981). *Analyse af interregionale togrejser. + Figurer og appendices.* 212 pp. + 174 pp.

40. **Ravn, Hans.** (1982). *Technology and underdevelopment. The case of Mexico.*
376 pp.

41. **Hansen, Sten.** (1983). *Phase-type distributions in queueing theory.* 209 pp.

42. **Ferreira, Jose A.S.** (1984). *Optimal control of discrete-time systems with applications.* 252 pp.

43. **Behrens, Jens Christian.** (1985). *Mathematical modelling of aquatic ecosystems applied to biological waste water treatment + Appendix 1-2.* 32 pp. + 389 pp. +
180 pp.

44. **Poulsen, Niels Kjølstad.** (1985). *Robust self tuning controllers.* 240 pp.

45. **Madsen, Henrik.** (1985). *Statistically determined dynamic models for climate processes. Part 1-2.* 428 pp.

46. **Sørensen, Bo.** (1986). *Interactive distribution planning.* 253 pp.

47. **Lethan, Helge B.** (1986). *Løsning af store kombimatoriske problemer.* 173 pp

48. **Boelskifte, Søren.** (1988). *Dispersion and current measurements. An investigation based on time series analysis and turbulence models.* Risø-M-2566. 154 pp.

49. **Nielsen, Bo Friis.** (1988). *Modelling of multiple access systems with phase type distributions.* 253 pp.

50. **Christensen, John M.** (1988). *Project planning and analysis. Methods for assessment of rural energy projects in deveoping countries.* Risø-M-2706. 158 pp.

51. **Olsen, Klaus Juel.** (1988). *Texture analysis of ultrasound images of livers.* 162 pp.

52. **Holst, Helle.** (1988). *Statistisk behandling af nærinfrarøde reflektionsmålinger.*
309 pp. + app.

53. **Knudsen, Torben.** (1989). *Start/stop strategier for vind-diesel systemer.* 275 pp.

54. **Ersbøll, Bjarne Kjær.** (1989). *Transformations and classifications of remotely sensed data. Theory and geological cases.* 297 pp.

55. **Kragh, Anders Laage.** (1990). *Kø-netværksmodeller til analyse af FMS anlæg.*
205 pp.

56. **Hansen, Christian Kornerup.** (1990). *Statistical methods in the analysis of repairable systems reliability.* 56 pp.

57. **Parkum, Jens Ejnar.** (1992). *Recursive identification of time-varying systems.*
206 pp.

58. **Bilbo, Carl M.** (1992). *Statistical analysis of multivariate degradation models.*
167 pp.

59. **Carstensen, Jens Michael.** (1992). *Description and simulation of visual texture.* 234 pp.

60. **Halse, Karsten.** (1992). *Modeling and solving complex vehicle routing problems.*
372 pp.

61. **Hendricks, Elbert.** (1992). *Identification and estimation of non-linear systems using physical modelling.* 273 pp.

62. **Windfeld, Kristian.** (l992). *Application of computer intensive data analysis methods to the analysis of digital images and spatial data.* 190 pp.

63. **Iwersen, Jørgen.** (1992). *Statistial control charts : Performance of Shewhart and Cusum charts.* 326 pp.

64. **Olsson, Carsten Kruse.** (1993). *Image processing methods in materials science.* 274 pp.

65. **Sejling, Ken.** (1993). *Modelling and prediction of load in heating systems.* 283 pp.

66. **Søgaard, Henning T.** (1993). *Stochastic systems with embedded parameter variations - applications to district heating.* 280 pp.

67. **Grunkin, Michael.** (1993). *On the analysis of image data using simultaneous interaction models.* 223 pp.

68. **Pálsson, Ólafur Pétur.** (1993). *Stochastic modeling, control and optimization of district heating systems.* 275 pp.

69. **Sørensen, Lene.** (1993). *Environmental planning and uncertainty.* Risø-R-709(EN). 226 pp.

70. **Thygesen, Bent Georg.** (1993). *Modelling and control of systems in the delta domain.* 207 pp.

71. **Jensen, Jens Arnth.** (1993). *Digital image processing designed for evaluation of MR-Examinations of the Cardiovascular system.* 256 pp.

72. **Jørgensen, Jan Friis.** (1993). *Scanning probe microscopy image restoration and analysis.* ATV Erhvervsforskerprojekt EF 349. l44 pp.

73. **Carstensen, Jacob.** (1994). *Identification of wastewater processes.* ATV Erhvervsforskerprojekt EF 354. 242 pp.